Alma Mater Studiorum · Università di Bologna

Dottorato di ricerca in Fisica

xxxiv ciclo

Settore concorsuale: 02/d1
Settore scientifico-disciplinare: fis/07

Shaping transverse beam distributions by means of adiabatic crossing of resonances

Presentata da:
Federico Capoani

Coordinatore Dottorato:
prof. Michele Cicoli

Supervisore:
prof. Armando Bazzani

Co-supervisore:
dott. Massimo Giovannozzi

Esame finale anno 2022

Le monde, chère Agnès, est une étrange chose.

Molière, *L'école des femmes*, Acte II, Scène 5.

Abstract

Non-linear effects are responsible for peculiar phenomena in the dynamics of charged particles in circular accelerators. Recently, they have been extensively used to propose novel beam manipulations where it is possible to modify the transverse beam distribution in a controlled way, with the goal to fulfil the constraints posed by new applications. One example is the resonant beam splitting used at CERN for the Multi-Turn Extraction (MTE), which is used to transfer proton beams from the PS to the SPS.

The theoretical description of these effects relies on the formulation of the particle's dynamics in terms of Hamiltonian systems and symplectic maps, and on the theory of adiabatic invariance and resonant separatrix crossing. Close to a resonance, new stable regions and new separatrices appear in the phase space. As non-linear effects do not preserve the linear Courant-Snyder invariant, it is possible for a particle to cross a separatrix, changing the value of its adiabatic invariant. This process opens the path to new possibilities in terms of beam manipulations.

This thesis deals with a variety of possible effects that can be used to shape, in a controlled fashion, the transverse beam dynamics, starting from 2D and then moving to 4D models of the particles' motion. We show the possibility of performing beam splitting using a resonant external exciter, as well as combining the action of an exciter with MTE-like tune modulation close to resonance. Non-linear effects can also be used to cool a beam by acting on its transverse beam distribution. We discuss the special case of a beam with an annular distribution, showing how its emittance can be reduced by means of modulating the amplitude and frequency of a resonant oscillating dipole.

We then consider 4D models where the motion in the two transverse planes is coupled when acting close to resonance. This fact can be exploited to operate on the transverse emittances by means of a controlled crossing of a 2D resonance. Depending on the resonance, the result is an emittance exchange between the two planes, or an emittance sharing. These phenomena are described and understood in terms of adiabatic invariance theory.

Contents

Introduction

*In nova fert animus mutatas dicere formas
corpora; di, coeptis (nam vos mutastis et illas)
adspirate meis primaque ab origine mundi
ad mea perpetuum deducite tempora carmen.*

OVID., *Met.* I, 1–4.

PARTICLE ACCELERATORS have played a fundamental role in many important discoveries in the field of fundamental particle physics. Large scale experiments, such as the ones carried out in the Large Hadron Collider at CERN, are immense, complex projects that require a wide variety of competences in many fields of physics and engineering. These experiments would never succeed if high-quality beams were not delivered to the collision points. This is the goal of accelerator physicists, who devote their research to understand and optimize many aspects of particles' motion inside the accelerating machine.

If the ultimate goal of particle physics experiments with accelerators is to answer fundamental questions on the Universe and its symmetries, testing predictions from quantum-field theory, the physical concepts that drive particles' dynamics are far more simple. Motion in an accelerator is reduced, in the end, to a charged, relativistic particle that moves under an electromagnetic field. We are therefore in the realm of classical mechanics, looking at problems that are best treated with a Lagrangian or Hamiltonian formulation of dynamics.

One could be tempted to class mechanics as "simple physics", far from the counter-intuitive nature of the quantum world. In reality, as soon as non-linear effects are introduced, and concepts like chaos, resonances, integrability etc. enter the game, things get far more complex. Research on these topics, halfway between mathematics and physics, is in constant development. For several decades, its interest was mainly rooted in orbital and celestial dynamics. The pioneers of non-linear dynamics — Poincaré, Birkhoff, Lyapunov, Moser... — considered astronomy as the main field of application of their theoretical ad-

vances. During the years, the interest in non-linear dynamics migrated to other domains of applied physics: climate science, geophysics, complex systems, plasma physics, and, last but not least, accelerator physics. It should come with no surprise, therefore, that one of the fundamental equations for particle motion in an accelerator was originally developed to describe the orbit of the Moon!

In this work, we look to new possible applications of "modern classical mechanics" to accelerator physics. Of course, as the field is immense, we need to restrict ourselves to a small class of problems. For this reason, we investigate some possibilities to employ non-linear effects to manipulate the transverse shape of a particle beam. It is the opposite approach to what is commonly done when operating accelerators, where non-linear dynamics is mainly studied to avoid, or at least mitigate its adverse effects.

How can a particle beam distribution be manipulated via non-linear effects? Under appropriate resonant conditions, in the particles' phase-space new stable regions and new separatrices are created. By slowly modulating the perturbation that creates the resonance, it is possible to make particles cross the separatrix and be trapped in another stable region. This results, in the end, in a beam distribution with a different transverse shape. To study these phenomena, one needs a mathematical toolbox that is composed by the theory of adiabatic invariance and its conservation accuracy, the knowledge of perturbation averaging at resonances, and the details about what happens when a separatrix is crossed. These concepts are provided by xx-century progresses in classical mechanics.

Particle accelerators represent privileged test beds for these theories, as their parameters can be accurately controlled at the operation level. Yet, we do not consider our beam manipulations as academic exercises and particle accelerators as a mere playground to test our predictions. In this thesis, we propose techniques which address some specific problems that have arisen in accelerator operation, and whose solutions would be useful for C<small>ERN</small> experiments, but, potentially, also for the many different applications of particle accelerators.

It is not the first time that non-linear resonances and stable islands are exploited to achieve a transformation of the transverse beam shape: our predecessor is the Multi-Turn Extraction (M<small>TE</small>) method which is used at C<small>ERN</small> to split a beam into five beamlets for the beam transfer between two accelerators, P<small>S</small> and S<small>PS</small>. Proposed in 2002 and officially become operational thirteen years later, it stands as the main inspiration for some of our proposed manipulations, and in general as a reminder that a long process is needed to transfer an idea that works in a mathematical model to the real world. In other words, in spite of the hurdles, it is indeed possible to successfully turn an idea into an operational method.

Our approach is the following: for each effect we analyse, we start from

a time-dependent Hamiltonian and/or Poincaré map which models a particle motion in the transverse phase space under some given conditions, when a parameter is modulated. We therefore continue with a theoretical analysis of the system attempting to capture its main properties in the adiabatic hypothesis, i.e. that the modulation is much slower than the velocity scale of the system. These results are then compared with the outcome of numerical simulations of the original system.

We could choose between two roads. In a "vertical" approach, we would have theoretically studied one or two models and, if proven feasible by mathematical analysis and numerical simulation, quickly transfer our efforts to build a machine configuration model to be fed to the accelerator simulation software, before attempting an experimental validation on a real machine. On the other hand, we opted for an "horizontal" philosophy, studying a variety of effects only in their mathematical models, leaving the technical and experimental issues to future research — we are reassured in this by the fact that the original, simple model of MTE made predictions that proved valid also in realistic simulations of accelerator dynamics and in an experimental context. We think that our approach was helpful for having a deeper understanding of the models' dynamics and gave us the occasion to widely explore the possibilities offered to us by non-linear phenomena in particle accelerators.

Structure of the work

The thesis is divided into two parts. In **Part I**, we set the foundations of our works: in the **first chapter**, we recall concepts and theorems of Hamiltonian mechanics which will be used in the following theoretical discussions; in the **second chapter** we introduce the mathematical modelling of a charged-particle dynamics in a circular accelerator, discussing linear and non-linear effects, while the **third chapter** is devoted to a brief description of the Multi-turn Extraction experience at CERN.

In **Part II** we discuss a beam manipulation proposal in each chapter. We first start with models with two degrees of freedom. In the **fourth chapter** we study the possibility of beam splitting using stable islands generated by the crossing of a resonance using an oscillating exciter. In the **fifth chapter** some preliminary results on the possibility to split a beam adding an oscillating exciter to the MTE method in a double-resonant condition are presented. In the **sixth chapter**, the effect of a resonant oscillating dipole is used to reduce the emittance of an annular beam distribution.

We then proceed with two chapters devoted to the study of models with four degrees of freedom. In the **seventh chapter**, the phenomenon of emittance ex-

change between the x and y direction when crossing the coupling resonance is discussed in terms of adiabatic invariant theory, deriving scaling laws for the adiabaticity. In the **eighth chapter**, this study is extended to higher-order resonances, showing how their crossing leads to an emittance sharing between the two coordinates.

We close the work with a **final chapter**, in which we draw conclusions and discuss some possible outlooks and future steps of the research presented in the thesis.

Part I

Foundations

1 | Mathematical concepts

In this chapter, a brief review of the main mathematical-physics methods and tools which are useful to describe non-linear transverse beam dynamics and manipulations in circular accelerators is presented. In general, the proposed beam shaping techniques start from an Hamiltonian model and rely on the existence of an *adiabatic invariant*. Close to resonance, fast and slow variables appear and one employs the averaging principle to reduce the degrees of freedom of the dynamics. As one parameter of the Hamiltonian is (slowly) changed, new separatrices and phase space regions are created, and a particle can "jump" to a different region with a change in value of the adiabatic invariant. Therefore, in the following, after a brief recap on Hamiltonian mechanics, we shall introduce the concept of adiabatic invariance, the averaging principle, the role of resonances with the Poincaré-Birkhoff theorem, the theory of separatrix crossing, and some notions on the error in the adiabatic jump due to non-adiabatic conditions.

Finally, Normal Form theory is introduced, due to its usefulness to derive Hamiltonian models for the dynamics close to resonance.

1.1 | Hamiltonian mechanics

First of all, we briefly review some basic concepts of Hamiltonian dynamics, mainly to introduce nomenclature and notation that will be used throughout the thesis. We mainly follow Refs. [3] and [4].

Given a set of co-ordinates $(p_i(t),\ q_i(t))$ and a function $\mathcal{H}(p_i,\ q_i,\ t)$, where $1 \leq i \leq n$, the system is said to be *Hamiltonian* if the following equations hold:

$$\dot{p}_i = -\frac{\partial \mathcal{H}}{\partial q_i}, \qquad \dot{q}_i = \frac{\partial \mathcal{H}}{\partial p_i}.\tag{1.1}$$

These equations are called *Hamilton equations* while $\mathcal{H}$ is the *Hamilton function*, or *Hamiltonian*. They are related to the Least Action Principle via the 1-form

$$\omega = p_i \mathrm{d}q_i - \mathcal{H}\,\mathrm{d}t\,.\tag{1.2}$$

In fact, the integral of the form on the trajectory $q_0 \rightarrow q_1$ which is described by the motion of a particle in the time interval $[t_0, t_1]$ yields

$$\int_{q_0=q(t_0)}^{q_1=q(t_1)} (p_i \mathrm{d}q_i - \mathcal{H}\,\mathrm{d}t) = \int_{t_0}^{t_1} \left(p_i \frac{\mathrm{d}q_i}{\mathrm{d}t} - \mathcal{H}\right)\mathrm{d}t = \int_{t_0}^{t_1} \mathcal{L}\,\mathrm{d}t \,. \qquad (1.3)$$

where $\mathcal{L} = p_i \dot{q}_i - \mathcal{H}$ is the Lagrangian, obtained by Legendre transformation of the Hamiltonian.

1.1.1 │ Canonical transformations

The power of the Hamiltonian formulation relies on the fact that it is independent on the co-ordinate choice. The choice of co-ordinates is fully unconstrained: positions and momenta are independent (differently from the Lagrangian formulation) and they can exchange their role, or being mixed in complete freedom, while the Hamilton equations maintain their form.

We can therefore find, for an Hamiltonian $\mathcal{H}(p, q, t)$ and a transformation $(p_i, q_i) \rightarrow (P_i, Q_i)$, a function $\mathcal{K}(P, Q, t)$ for which

$$\dot{P}_i = -\frac{\partial \mathcal{K}}{\partial Q_i}, \qquad \dot{Q}_i = \frac{\partial \mathcal{K}}{\partial P_i}\,. \qquad (1.4)$$

Both formulations needs to fulfil Least Action Principle:

$$\mathrm{d}(p_i \mathrm{d}q_i - \mathcal{H}\,\mathrm{d}t) = \mathrm{d}(P_i \mathrm{d}Q_i - \mathcal{K}\,\mathrm{d}t)\,. \qquad (1.5)$$

This means that that the form

$$\mathrm{d}F = p_i \mathrm{d}q_i - P_i \mathrm{d}Q_i + (\mathcal{K} - \mathcal{H})\mathrm{d}t\,, \qquad (1.6)$$

must be exact. This yields the transformation laws

$$p_i = \frac{\partial F}{\partial q_i}, \qquad P_i = -\frac{\partial F}{\partial Q_i}, \qquad \mathcal{K} = \mathcal{H} + \frac{\partial F}{\partial t}\,. \qquad (1.7)$$

The form of the Hamiltonian needs to be changed only if the transformations are time-dependent. The function $F(q, Q, t)$ is called *generating function*.

The full freedom in co-ordinate choice is also reflected in the role of time. Given that $\mathrm{d}F$ must be exact, it is possible to give the role of time to every co-ordinates of the system — the new Hamiltonian function will be the momentum conjugate to that variable, with a minus sign.

Let us express the k–th term of the form as $p_k = \tilde{p}$, $q_k = \tilde{q}$. Hence we can write

$$p_i \mathrm{d}q_i - \mathcal{H}\,\mathrm{d}t = \sum_{i \neq k} p_i \mathrm{d}q_i + (-\mathcal{H})\mathrm{d}t + (-\tilde{p})\mathrm{d}\tilde{q}\,. \qquad (1.8)$$

This form, which is formally equivalent to the previous one, makes it possible to express the motion as a function of $\tilde{q}$, whilst $-\tilde{p}$ plays the role of the Hamiltonian in the equivalent equations of motion

$$
\begin{aligned}
\frac{\mathrm{d}p_i}{\mathrm{d}\tilde{q}} &= -\frac{\partial \tilde{p}}{\partial q_i}, & \frac{\mathrm{d}q_i}{\mathrm{d}\tilde{q}} &= \frac{\partial \tilde{p}}{\partial p_i} & (i \neq k), \\
\frac{\mathrm{d}\mathcal{H}}{\mathrm{d}\tilde{q}} &= -\frac{\partial \tilde{p}}{\partial t}, & \frac{\mathrm{d}t}{\mathrm{d}\tilde{q}} &= \frac{\partial \tilde{p}}{\partial \mathcal{H}}.
\end{aligned}
\tag{1.9}
$$

Finally, the time evolution of an Hamiltonian system is a canonical transformation itself. This property justifies the construction of *symplectic integrators*, i.e. algorithms of numerical integration of Hamilton equations that preserve the Hamiltonian structure of the system.

1.1.2 | Action-angle variables

In a n-degree of freedom integrable Hamiltonian system, i.e. a $2n$−dimensional symplectic manifold described by the phase variables $(p_i,\, q_i)$, where n integrals of motion $I_i = k_i$ in involution are known, a theorem due to Liouville states that, if the set M_k of the points for which $I_i = k_i$, is compact, then it is diffeomorphic to the n−torus $\mathbb{T}^n$. We also find that for some functions ω_i which we will call *frequencies*, we have

$$
\dot{\phi}_i = \omega_i(k_1 \ldots, k_n).
\tag{1.10}
$$

This assures that, setting as the Hamiltonian one of the integrals, e.g. $\mathcal{H} = I_1$, we have the equations

$$
\dot{I}_i = 0, \qquad \dot{\phi}_i = \omega_i(I_1 \ldots, I_n)
\tag{1.11}
$$

which describe the phase flow relative to the chosen Hamiltonian.

Now we have the co-ordinates $(I_i,\, \phi_i)$ but nothing guarantees that they are symplectic, i.e. that the transformation $(p_i,\, q_i) \to (I_i,\, \phi_i)$ is canonical.

It is possible, however, to introduce different functions $J_i = J_i(I_1, \ldots, I_n)$ which fulfill

$$
\dot{J}_i = 0, \qquad \dot{\phi}_i = \omega_i(J_1 \ldots, J_n),
\tag{1.12}
$$

and keep the canonical change of variables.

These functions can be explicitly written. Let us start with the one-dimensional case, where the only integral is the Hamiltonian, and its conserved value h, and the set M_k reduces to M_h.

A canonical transformation is given by the generating function $S(J, q)$ and

$$
p = \frac{\partial S}{\partial q}, \qquad \phi = \frac{\partial S}{\partial J}, \qquad \mathcal{H}\left(p = \frac{\partial S}{\partial q}, q\right) = h(J).
\tag{1.13}
$$

The invariant torus reduces to the closed curves that are identified just from the value of the energy h, and, being $h = h(J)$, by that of J. The differential $\mathrm{d}S$, for constant J, reads

$$\mathrm{d}S = \frac{\partial S}{\partial q}\,\mathrm{d}q = p\,\mathrm{d}q\,,\tag{1.14}$$

therefore

$$S = \int p\,\mathrm{d}q\,,\tag{1.15}$$

which is the generating function.

The 1−form $p\,\mathrm{d}q$ is closed, and therefore locally exact on invariant surfaces. Thus, on a level curve of energy, the whole change of S is

$$\Delta S(J) = \oint_{M_{h(J)}} p\,\mathrm{d}q\tag{1.16}$$

that, thanks to Stokes' theorem, corresponds to the area inside the curve. From the second equation of (1.13),

$$\oint_{M_{h(J)}} \mathrm{d}\phi = 2\pi\,.\tag{1.17}$$

The periodicity of ϕ on the torus means that

$$\oint_{M_{h(J)}} \mathrm{d}\!\left(\frac{\partial S}{\partial J}\right) = \frac{\partial \Delta S(J)}{\partial J} = 2\pi\,,\tag{1.18}$$

from which we finally get

$$J = \frac{1}{2\pi}\oint_{M_h} p\,\mathrm{d}q\,.\tag{1.19}$$

On the other hand, differentiating (1.15) in J we retrieve, from the definition of ϕ

$$\phi = \frac{1}{2\pi}\frac{\partial}{\partial J}\int p\,\mathrm{d}q\,.\tag{1.20}$$

The generalization to systems with more degrees of freedom is straightforward, if we are working in a $\mathbb{R}^{2n}$ phase space. In fact, being $\gamma_1, \ldots, \gamma_n$ 1D cycles which form a basis on the torus M_{k_i}, which means that the variation of the angular variable ϕ_i on the cycle γ_j is equal to $2\pi\delta_{ij}$, δ_{ij} being the Kroenecker symbol.

The actions J_i are then defined to be

$$J_i(k_1, \ldots, k_n) = \frac{1}{2\pi} \int_{\gamma_i} p_j \, \mathrm{d}q_j \,. \qquad (1.21)$$

It can be shown that these integrals are independent from the choice of the γ_i. [4]

1.2 | Adiabatic invariance

We now introduce a fundamental concept on which all our work on transversal beam manipulation rely: adiabatic invariance. We consider an Hamiltonian system which is dependent on a varying parameter $\lambda = \varepsilon t$. When λ is constant (*frozen system*), we assume that the system is integrable and that there exist action variables J_i which are integrals of motion. However, if the variation is sufficiently *slow* (for small values of ε — we will discuss what this *slowness* actually means), it is possible to find variables which are *quasi*-invariant, i.e. which change slowlier than the varied parameter.

The canonical example of such a system is a pendulum whose leg is shortened during the oscillation. Quite interestingly, the first mention of such a problem is not in the works of Lagrange or Hamilton, but in a conversation, reported in the proceedings of the 1911 Solvay conference between Hendrik Lorentz and Albert Einstein [57]. We are in the first years of the quantum revolution, and the discussion revolves on which are the quantities that need to be quantized. If a pendulum with frequency ω has energy $\hbar\omega$, and its leg is shortened — argues Lorentz — its energy decreases: how is it possible if the energy is quantized? No, — Einstein replies — if the leg is varied infinitely slowly the frequency stays constant, and so the energy, as it is proportional to the frequency. This observation led Sommerfeld and Ehrenfest to assume that the discretely-quantized variables should be these quantities which are invariant if the parameter change is infinitely slow. It was Ehrenfest himself who coined the expression *adiabatic invariant* [33], in analogy with the adiabatic transformations in thermodynamics which do not exchange heat (with the curious fact that, on a gas, an adiabatic transformation has to be performed *fast*, while in mechanics the parameter change must be, ideally, infinitely slow). A student of Ehrenfest, Burgers [26] and, later Tullio Levi-Civita [63] went on to prove the adiabatic invariant of the action variable in mechanical systems. Levi-Civita notes how the Ehrenfest principle propose "for the still standing scholars of pure mechanics the abstract study of the adiabatic invariants, very interesting *per se* and for applications".

However, with the advent of Schrödinger quantum mechanics, the interest in adiabatic invariants faded, being rediscovered a few decades later in the field of celestial mechanics, mainly in Soviet Union (in the years of the space race). In 1963 Vladimir I. Arnol'd would write [5] that adiabatic invariance "has been little studied by mathematicians in spite of its importance and interest", in a paper where the relationship between adiabatic invariance and perturbation theory was established. From orbital dynamics, theory of adiabatic invariance then moved into other fields, such as plasma and accelerator physics, as the implications of such researches, being just technological or related to fundamental physics issues, contributed to maintain interest in this topic.

We can now give a formal definition of *adiabatic invariance* (essentially due to Mandel'shtam). [4, 68]

Adiabatic invariant. A variable $J(p, q, \lambda = \epsilon t)$ is said to be an *adiabatic invariant* if, for every $\varepsilon > 0$ there exists a $\delta_\varepsilon > 0$ so that, for every $\epsilon < \delta_\varepsilon$ and $t < 1/\epsilon$

$$|J(p(t), q(t), \epsilon t) - J(p(0), q(0), 0)| < \varepsilon \,. \tag{1.22}$$

In a less formal way, we want that the adiabatic invariant, over a time evolution of $t \sim \epsilon^{-1}$, only undergoes a change which is $\mathcal{O}(\epsilon)$. It should be emphasized that this definition holds independently for every disconnected region of the phase space.

Thus, the speed ϵ of parameter variation is related to the time in which our variable variation is constrained.

A stronger requirement of a variable is to be a *perpetual* adiabatic invariant: the variation of J should be $\mathcal{O}(\epsilon)$ for *every* time. A theorem, proven by Arnol'd, states that, for 1D Hamiltonians, if the parameter variation is periodic, adiabatic invariants are also perpetual. [5]

In one dimension, we have a simple example of adiabatic invariant: the action.

1.2.1 | Adiabatic invariance of the action

We now prove, following [56], that, in an 1D system, the action variable is actually an adiabatic invariant. Starting from the time-dependent Hamiltonian $\mathcal{H}(p, q, \lambda(t))$, we have, differentiating

$$\frac{\partial \mathcal{H}}{\partial t} = \dot{\lambda} \frac{\partial \mathcal{H}}{\partial \lambda} \,. \tag{1.23}$$

We can take the average of this equality. If $\dot{\lambda}$ is constant,

$$\left\langle \frac{\partial \mathcal{H}}{\partial t} \right\rangle = \dot{\lambda} \left\langle \frac{\partial \mathcal{H}}{\partial \lambda} \right\rangle = \frac{\dot{\lambda}}{T} \int_0^T \mathrm{d}t \, \frac{\partial \mathcal{H}}{\partial \lambda} \,, \tag{1.24}$$

according to the definition of λ.

It is convenient to rewrite

$$\mathrm{d}t = \frac{\mathrm{d}q}{\partial \mathcal{H}/\partial p} \,, \tag{1.25}$$

thanks to Hamilton equations. Moreover, the period T can be written as $\int_0^T \mathrm{d}t$, so

$$\left\langle \frac{\partial \mathcal{H}}{\partial t} \right\rangle \oint \frac{\mathrm{d}q}{\partial \mathcal{H}/\partial p} = \dot{\lambda} \oint \mathrm{d}q \, \frac{\partial \mathcal{H}/\partial \lambda}{\partial \mathcal{H}/\partial p} \,, \tag{1.26}$$

where the closed-line integral is extended to one orbit of the system in phase space.

We rewrite this expression in a single integral in the variable q:

$$\oint \mathrm{d}q \left[\left\langle \frac{\partial \mathcal{H}}{\partial t} \right\rangle \frac{\partial p}{\partial \mathcal{H}} - \dot{\lambda} \frac{\partial \mathcal{H}}{\partial \lambda} \left(\frac{\partial \mathcal{H}}{\partial p} \right)^{-1} \right] = 0 \,. \tag{1.27}$$

If λ variation is slow, during one orbit its value can be seen as constant, so the total derivative of $\mathcal{H}$ w.r.t. λ should be zero, i.e.

$$\frac{\partial \mathcal{H}}{\partial \lambda} = -\frac{\partial \mathcal{H}}{\partial p} \frac{\partial p}{\partial \lambda} \,. \tag{1.28}$$

Substituting this result into the Equation (1.27) we get

$$\oint \mathrm{d}q \left[\left\langle \frac{\partial \mathcal{H}}{\partial t} \right\rangle \frac{\partial p}{\partial \mathcal{H}} + \dot{\lambda} \frac{\partial p}{\partial \lambda} \right] = 0 \,, \tag{1.29}$$

which turns out to be equal to

$$\oint \mathrm{d}q \left[\left\langle \frac{\partial p}{\partial t} \right\rangle + \dot{\lambda} \frac{\partial p}{\partial \lambda} \right] = \frac{\mathrm{d}}{\mathrm{d}t} \left\langle \oint p, \mathrm{d}q \right\rangle = 0 \,. \tag{1.30}$$

This means that the average variation of the action

$$J = (2\pi)^{-1} \oint p \, \mathrm{d}q \tag{1.31}$$

over a orbit is zero, i.e. that the action integral is an adiabatic invariant.

1.2.2 | Conservation of the adiabatic invariant

We can now ask ourselves how good is the "quasi-"invariance of the action variable, i.e. : up to which order the action is conserved when we introduce our time-dependent modulation in the Hamiltonian? The answer is in an article by A.I. Neishtadt [75].

First of all, following this reference, we show that it is indeed possible, under some conditions, to find an adiabatic invariant at any accuracy. [62]

Let us consider the usual Hamiltonian $\mathcal{H}(q, p, \lambda = \epsilon t)$. We construct the action-angle co-ordinates (ϕ_0, J_0) for the unperturbed motion.

The perturbed Hamiltonian will read

$$\mathcal{H}(\phi_0, J_0, \lambda) = \mathcal{H}_0(J_0, \lambda) + \epsilon \mathcal{H}_1(\phi_0, J_0, \lambda), \tag{1.32}$$

where

$$\mathcal{H}_1 = \frac{1}{\partial H_0 / \partial J_0} \left[\frac{\phi_0}{2\pi} \int_0^{2\pi} \mathrm{d}\phi \, \frac{\partial \mathcal{H}}{\partial \lambda} - \int_0^\phi \frac{\partial \mathcal{H}}{\partial \lambda} \right]. \tag{1.33}$$

We can further generate new action-angle co-ordinates (ϕ_1, J_1) using perturbation theory with the generating function

$$F_1 = J_1 \phi_0 + \epsilon S_1(J_1, \phi_0, \lambda). \tag{1.34}$$

The new Hamiltonian $\mathcal{K}_1$ becomes

$$\mathcal{K}_1 = \mathcal{H}_0\left(J_1 + \epsilon \frac{\partial S_1}{\partial \phi_0}\right) + \epsilon \mathcal{H}_1\left(J_1 + \epsilon \frac{\partial S_1}{\partial \phi_0}, \phi_0, \lambda\right) + \epsilon^2 \frac{\partial S_1}{\partial \lambda}. \tag{1.35}$$

The equation for S_1 that kills the $\mathcal{O}(\epsilon)$ term in $\mathcal{K}_1$ is solved by

$$\begin{aligned} S_1 = \frac{1}{\partial \mathcal{H}_0 / \partial J_0} & \left[\int_0^{\phi_0} \mathrm{d}\phi'_0 \, \mathcal{H}_1(J_1, \phi'_0, \lambda) \right. \\ & \left. + \frac{1}{2\pi} \int_0^{2\pi} \mathrm{d}\phi_0 \int_0^{\phi_0} \mathrm{d}\phi'_0 \, \mathcal{H}_1(J_1, \phi'_0, \lambda) \right]. \end{aligned} \tag{1.36}$$

Note that writing $\mathcal{K}_1$ implies deriving S_1, and therefore $\mathcal{H}_1$ w.r.t. λ.

With this solution for S_1, $\mathcal{K}_1$ reads

$$\begin{aligned} \mathcal{K}_1 &= \mathcal{H}_0(J_1) + \epsilon^2 \mathcal{H}_2(J_1, \phi_1, \lambda) \\ &= [\mathcal{H}_0 + \epsilon^2 \langle \mathcal{H}_2 \rangle] + \epsilon^2 [\mathcal{H}_2 - \langle \mathcal{H}_2 \rangle] \\ &= \mathcal{K}_0^{(1)}(J_1, \lambda) + \epsilon^2 \mathcal{K}_2(\phi_1, J_1, \lambda). \end{aligned} \tag{1.37}$$

Now, we can apply the same process on $\mathcal{K}_1$, obtaining a new adiabatic invariant J_2 that is correct up to order ϵ^3, and so on, until an order n so that

$\mathcal{K}_n = \mathcal{K}_0^{(n)}(J_n) + \epsilon^{n+1}\mathcal{K}_n(\phi_n, J_n, \lambda)$, and with a variable J_n that is conserved up to $\mathcal{O}(\epsilon^{n+1})$. However, this improvement of adiabatic invariants can last as long as it is possible to perform the derivative $\partial H_1/\partial\lambda$, whose smoothness is decreased by an order at each iteration. Let us call N, if it exists, the maximum possible order, with J_N conserved up to $\mathcal{O}(\epsilon^{N+1})$.

However, our first question was about the accuracy of the original invariant J_0. Let a perturbation be limited in the interval $[\lambda_-, \lambda_+]$, i.e. it is zero with a number of its derivatives for $\lambda \leq \lambda_-$ and $\lambda \geq \lambda_+$. We are interested in the variation of $\Delta J_0 = |J_0(\lambda_-) - J_0(\lambda_+)|$ in this interval. Let us suppose that the smoothness of the perturbation allows us to write an invariant J_N.

The canonical change of variables $(\phi_0, J_0) \to (\phi_N, J_N) = (\phi_0, J_0) \to (\phi_1, J_1) \to \cdots \to (\phi_{N-1}, J_{N-1}) \to (\phi_N, J_N)$ is made through a generating function $F = J_N\phi_0 + \epsilon S(\phi_0, J_N, \lambda)$. The variation ΔJ_0 now reads

$$\Delta J_0 = \Delta J_N + \epsilon \left.\frac{\partial S(\phi_0, J_N, \lambda)}{\partial\phi}\right|_{\lambda_-}^{\lambda_+}. \tag{1.38}$$

The generating function S, originating from a combination of the N_1 functions S_k, on $\lambda_\pm$ where all the derivatives of $\mathcal{H}_1$ vanish except for the last one has order $\mathcal{O}(\epsilon^{N-1})$, while ΔJ_N is $\mathcal{O}(\epsilon^{N+1})$. Therefore, the accuracy of the unimproved invariant is $\Delta J_0 = \mathcal{O}(\epsilon^N)$.

This is true if the perturbation has finite smoothness. Should $\mathcal{H}_1$ be $\mathbb{C}^\infty$, ΔJ_0 is smaller than any polynomial, and is therefore exponentially accurate: $\Delta J_0 = \mathcal{O}(\exp(-c/\epsilon))$ with $c > 0$. A formal proof is found in [75].

1.3 | Fast and slow variables. Averaging principle

Some of our beam shaping techniques rely on time-periodic perturbations. Such systems present, of course, time-dependent equations of motion which are, in general, difficult to treat. If the time scale of the perturbation is far smaller than the time scale of the unperturbed system, one could be tempted to simplify the model averaging perturbations. Some details of the motions, whose effects are limited, are lost but the global "drift" impressed to the system by the perturbation still stands. This is the base of the averaging principle. A principle that — Arnol'd reminds — is "not a theorem, but a physical proposition, that is, a vaguely stated and, strictly speaking, false assertion". However — he concludes — "Such assertions often happen to be fruitful sources for mathematical theorems". [3]

When Hamiltonian systems are taken into account, however, more rigorous result can be drawn. In particular, for our applications, we are interested

in what happens when a resonant condition is met. We follow, in this brief exposition, Refs. [4] and [65].

Let us consider an Hamiltonian system with n degrees of freedom with a periodic perturbation (of period 2π)

$$\mathcal{H} = \mathcal{H}_0 + \epsilon \mathcal{H}_1 . \tag{1.39}$$

If $\mathcal{H}_0$ is integrable, we can write the equations of motion in terms of action-angle variables (I_j, ϕ_j):

$$\begin{cases} \dot{I}_j & = 0 \\ \dot{\phi}_j & = \dfrac{\partial \mathcal{H}_0}{\partial I_j} = \omega_j(I_1, \ldots, I_n) \end{cases} , \tag{1.40}$$

while the perturbed system, using the same co-ordinates, assumes the form

$$\begin{cases} \dot{I}_j & = \quad - \epsilon \dfrac{\partial \mathcal{H}_1}{\partial \phi_j} \\ \dot{\phi}_j & = \omega_j + \epsilon \dfrac{\partial \mathcal{H}_1}{\partial I_j} \end{cases} . \tag{1.41}$$

If the perturbation is periodical also in time (with frequency ω), it will suffice to extend the phase space to introduce two new degrees of freedom: the angle $\psi = \omega t$ and the conjugated momentum J_ψ.

The idea behind *averaging* is to transform the perturbed system into a simpler one, where the small oscillations induced by the periodic perturbation are neglected, but the drift on the solution caused by the extra part of the Hamiltonian is kept. Therefore, the fast variable dynamics is averaged, i.e., a new Hamiltonian $\langle \mathcal{H} \rangle$ is introduced so that

$$\langle \mathcal{H} \rangle (J) = \mathcal{H}_0(J) + \epsilon \langle \mathcal{H}_1(\phi_i, J_i, \epsilon = 0) \rangle . \tag{1.42}$$

The average of a generic function f is given by

$$\langle f \rangle = \frac{1}{(2\pi)^n} \oint_{\mathbb{T}^m} \mathrm{d}^m \phi \, f(\epsilon = 0) . \tag{1.43}$$

where $\mathbb{T}^n$ is the n-dimensional torus. If the frequencies ω_j (and, in case, the perturbation frequency ω) are not in any resonant conditions, it is immediate to observe that the action variables J_j, whose variation are $\mathcal{O}(\epsilon)$, are *slow variables*, while the angles ϕ_j, which vary $\mathcal{O}(1)$, are *fast*.

In the non-resonant case, the integration on the torus of $\partial \mathcal{H}_1/\partial \phi_j$ gives zero, therefore the dynamics of the slow variables is trivially $\dot{J}_j = 0$, i.e. the slow variables are integrals of the motion in the averaged system.

On the other hand, when the unperturbed frequencies ω_j satisfy resonance conditions things are more complicated. Let us suppose that the frequencies $\omega_1, \ldots, \omega_r$ $(r \leq n)$ are in a resonant relation, i.e. there exists a vector $k_j \in \mathbb{Z}^r$ for which $k_j \omega_j = \mathbb{O}(\epsilon)$. In that case, there exists a symplectic linear transformation in the resonant $r-$dimensional subspace which makes $r - 1$ angles slow variables, over which it is impossible to average.

Let us consider the simplest case (two frequencies, e.g. ω_1 and ω_2 in resonant condition $k_1 \omega_1 + k_2 \omega_2 \approx 0$). After the transformation

$$\begin{cases} \theta_1 & = k_1 \phi_1 + k_2 \phi_2 \\ \theta_j & = \phi_j \qquad (2 \leq j \leq n) \end{cases}, \tag{1.44}$$

which also linearly transforms the momenta J_j into $\tilde{J}_j$, in order to fulfill the symplectic condition, the equation for θ_1 is

$$\dot{\theta}_1 = k_1 \omega_1 + k_2 \omega_2 + \epsilon \frac{\partial \mathscr{H}_1}{\partial \tilde{J}_1} = \mathbb{O}(\epsilon). \tag{1.45}$$

Therefore, one cannot average over θ_1, as it is a slow variable, but can safely average over all the other $n - 1$ angles, which will result in the conservation of all the momenta $\tilde{J}_i$. Note that a new integral of motion arises, which is given by a linear combination of the momenta conjugated to the resonant angles.

1.4 | Poincaré-Birkhoff theorem

Let us now consider the evolution of a non-linear system described by an area-preserving map. This could be, of course, a genuine map model but also the solution of an integrable Hamiltonian system. When a perturbation is added, the interplay between the perturbation and the natural resonances present in the map results in the creation of a chain of stable regions ("islands") which appear in the phase space at given amplitudes. This is the core of a theorem, first stated by Henri Poincaré [82] whose complete proof was given by Birkhoff [23], which we now expose and prove, following Refs. [2] and [85].

We start from an area-preserving map T_k $(k \in \mathbb{Z})$, which could be, for instance, a Poincaré map of the symplectic evolution of an Hamiltonian system, whose equations have periodicity 1. If the system is integrable, it is possible to find action-angle co-ordinates (ϕ, J) where, for every J, an invariant curve Γ_J is defined, along which, at each turn, ϕ increases by an angle $\omega(J)$. The map T therefore becomes:

$$\begin{pmatrix} \phi_{k+1} \\ J_{k+1} \end{pmatrix} = \begin{pmatrix} \phi_k + \omega(J_k) \\ J_k \end{pmatrix}. \tag{1.46}$$

For every value of J, a different frequency of rotation of ϕ is found. There exist some initial condition $\mathbf{x}_J$ for which $\omega(J)/(2\pi) \in \mathbb{Q}$, let's say $\omega(J) = 2\pi m/n$. In that case, the n-th iterate T^n maps a point into itself, and $T^k \mathbf{x}_J$ is a finite set of n points. On the other hand, if $\omega(J)/(2\pi) \in \mathbb{R} \setminus \mathbb{Q}$, the orbit of the map is dense on Γ_J.

Now let us introduce a perturbation of the map $T_{k,\epsilon} = T_k + \epsilon T_k^{(1)}$. A theorem by Kolmogorov states that, if ϵ is small enough, the invariant curves Γ_ϵ of T_ϵ are close to the invariant curves Γ of T. We concentrate on the commensurable invariant curves, with $\omega(J) = 2\pi m/n$. Having introduced a perturbation, it is no more true that, on that curves, $T_\epsilon^n \mathbf{x} = \mathbf{x}$. However, T_ϵ^n has a chain of $2n$ fixed points close to the unperturbed commensurable invariant curve.

The proof relies on the fact that, if at action J^*, on the curve Γ_{J^*}, the map T^n transforms a point into itself, as the rotation is $n\omega(J^*) = 0 \pmod{2\pi}$, there will exist also a curve Γ_+, at $J_+ > J^*$, and Γ_-, at $J_- < J^*$, on which ϕ rotates, under the action of T^n, with opposite direction. We can assume, for example, that $n\omega(J_-) < n\omega(J^*) < n\omega(J_+)$ and therefore $\omega(J_-) < 0$ and $\omega(J_+) > 0$.

This is true also for a sufficiently small perturbation ϵ. For each angle ϕ, there exists a value of J, J_ϕ for which T_ϵ^n does not perform any rotation. We call R_ϵ the closed curve described by the pairs $(\phi, \ J_\phi)$ under T_ϵ^n. It will be close to the unperturbed invariant curve Γ. We defined as R_ϵ' the resulting curve having applied T_ϵ^n at each point of R_ϵ. As the map is area-preserving, the area enclosed by R_ϵ' cannot be nor greater nor smaller than the area enclosed by R_ϵ. Therefore, it is impossible that one of the two curves surround the other one: they must intersect in an even number of points, and the points of intersection are fixed points of T_ϵ^n. A picture of this situation is given in Fig. 1.1.

We still have to determine the nature of these fixed points. The construction of Fig. 1.1 helps us. We need to consider the flow of T^n in the vicinity of Γ^+ and Γ^- and look how it connects to the the dynamics of $R_\epsilon \to T^n R_\epsilon$. When the arrows move around the fixed point, it is an elliptic fixed point. When the arrows move *away*, the dynamic is hyperbolic. Going back to T_ϵ, we have a chain of n elliptic fixed points of period n, alternating with n hyperbolic fixed points of the same period. This gives origin to the Poincaré-Birkhoff islands.

1.5 | Separatrix crossing: standard theory

In the last section, we were able to show that resonance creates extra separatrices and stable regions in the phase space. For our transverse manipulation techniques, we need an extra step: the fact that, when a system perturbation is time-dependent separatrices are no more impassable barriers, as they can be crossed by particles. If the time modulation is adiabatic, the capture into one
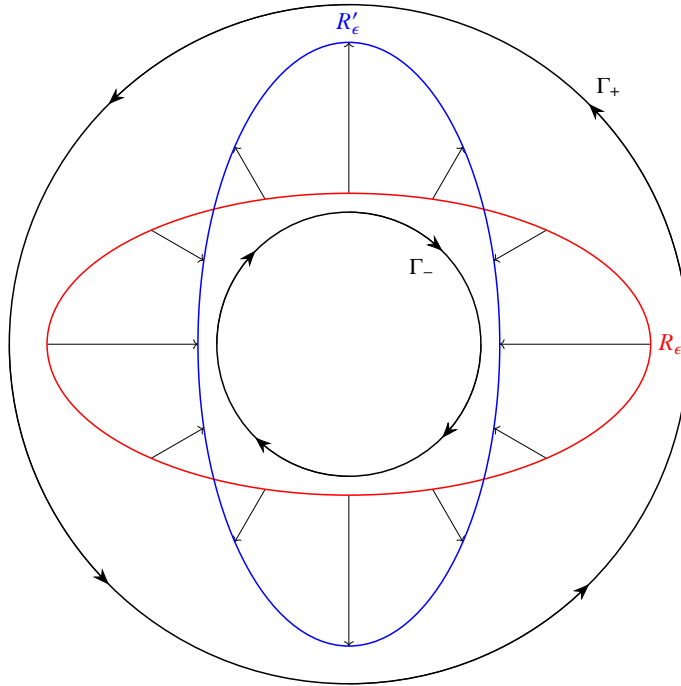
FIGURE 1.1 − The surfaces Γ_+, Γ_-, R_ϵ and R'_ϵ of the map T^n_ϵ. Arrows represent the action of the map. The intersections between R_ϵ and R'_ϵ are the fixed points.

stable region is inherently a random event [72], and the value of the adiabatic invariant after the capture changes dramatically [74, 77]. We now present the "standard" theory of separatrix crossing, i.e. with the hypothesis that the modulation is infinitely slow. The original source for these results is a work by A.I. Neishtadt [76], although for the argument which supports the probability formula for separatrix crossing we follow a review by J. Henrard (Ref. [45]). The leading order effects of non-adiabaticity will be discussed in the next section, as the "improved" separatrix crossing theory.

Let us consider an Hamiltonian $\mathcal{H}(q, p, \lambda)$ which is dependent on a parameter λ. A time variation on λ, namely $\lambda = \epsilon t$ is also introduced. If ϵ is sufficiently small, we can apply the adiabatic approximation to our system.

We now look at a phase space like the one in Fig. 1.2: the origin C ($x = 0$, $p = 0$) is an hyperbolic fixed point and, for each value of λ, the separatrix $H(x, p, \lambda) = H(0, 0, \lambda)$ divides the phase space in three regions: the two lobes G_1 and G_2 and the outer region G_3. We define $\ell_i = \partial G_i$ and A_i the areas enclosed by ℓ_i. Finally, we can add some constant value to the Hamiltonian so that $H(0, 0, \lambda) = 0$ (and $H > 0$ in the outer region and $H < 0$ inside G_1 and

G_2).

Initial conditions determine which region, at the beginning, a particle will orbit in. As long as adiabaticity is assured, for each value of λ the motion will follow the energy level curves for the Hamiltonian $\mathcal{H}_\lambda$, keeping the value of the orbit area almost constant. However, if the evolution of the separatrix causes the region where the particle is orbiting inside to shrink, eventually it will be impossible for the particle to stay inside that region. In that case, the trajectory will cross the separatrix and enter a different region, changing the value of the adiabatic invariant (i.e., the area of the orbit),

Let us assume that, in the system of Fig. 1.2, the regions enclosed by the separatrix increase their area when λ is increased. If a particle is orbiting in the outer region, at some point $\lambda = \lambda^*$ the orbit area $2\pi J_3^*$ will be equal to the area of the eight-shaped figure A_3 when $\lambda = \lambda^*$.

Considering the variation of λ in the Hamiltonian $\mathcal{H}(p, q, \lambda = \epsilon t)$ as a perturbation, and using the averaging principle, it is possible to estimate the change of the energy value H between two passages close to the hyperbolic point, while orbiting around the separatrix ℓ_3 in the external region.

$$\Delta H = \epsilon \int_0^T \frac{\partial \mathcal{H}}{\partial \lambda}\bigg|_{\lambda^*} \mathrm{d}t = -2\pi\epsilon \frac{\partial J}{\partial \lambda} = -\epsilon \frac{\mathrm{d}A_3(\lambda)}{\mathrm{d}\lambda}, \qquad (1.47)$$

where T is the time of the motion in the interval considered, and we used the fact that $\mathrm{d}J = p\mathrm{d}q = -\mathcal{H}\mathrm{d}t$.

Therefore, for each turn, H is decreased by a quantity which is proportional to ϵ (with an error $\mathcal{O}(\epsilon^{3/2})$). Therefore, there exist a value H^* (when $\lambda = \lambda^*$) for the last passage in the outer region, which is found in the interval $0 < H^* < |\Delta H_3|$ (in the outer region, H is positive). We define ΔH_3 the value of ΔH at
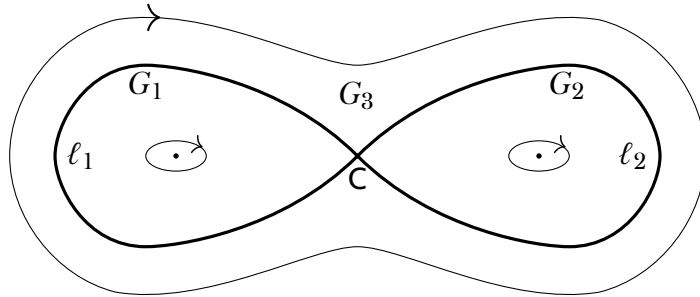
FIGURE 1.2 – Sketch of the phase diagram of the phase space for the separatrix crossing process. A particle orbiting in G_3 can either be trapped in G_1 or in G_2 as their area grow with time.

λ^*, i.e.

$$\Delta H_3 = \frac{\epsilon}{2\pi} \int_{\ell_3} p \mathrm{d}q = -2\pi\epsilon \left.\frac{\partial J_3^*}{\partial \lambda}\right|_{\lambda^*} = -\epsilon \left.\frac{\mathrm{d}A_3}{\mathrm{d}\lambda}\right|_{\lambda^*}. \tag{1.48}$$

Now, if the areas A_1 and A_2 increase with λ, defining, as in the previous equation $\Delta H_1 = -\epsilon A_1'(\lambda^*)$ and $\Delta H_2 = -\epsilon A_2'(\lambda^*)$, it is found that ΔH_1 and ΔH_2 are negative, too. Now, as $H^* < |\Delta H_3|$ we have two possibility: either $0 < H^* < |\Delta H_1|$ or $|\Delta H_1| < H^* < |\Delta H_3|$.

In the first case, the particle energy becomes negative while orbiting around ℓ_1, and therefore crosses the separatrix ℓ_1, being trapped into G_1. In the second case, the particle has still a positive energy (i.e. is in the outer region) when starting its orbit around ℓ_2, but this time the energy will become negative before finishing the lap, and the particle will inevitably fall into G_2. After trapping, the particle will orbit in G_1 or in G_2 along the isoenergetic line at the new, negative value of H, conserving hereinafter the value of its adiabatic invariant (the trajectory area). In adiabatic conditions, as $\epsilon \to 0$, the energy tends to 0^-, and the new value of the action is exactly the area of G_1 or G_2 at $\lambda = \lambda^*$, divided by 2π. A discussion of the error of this limit when finite adiabaticity is taken into account is carried out in the next section.

The value of H^* is unknown, but we can assume that, for an uniform ensemble of particles, it is uniformly distributed. The argument [76] relies on Liouville's theorem. We can therefore describe trapping into G_1 or G_2 as a random event, whose probability is given by the measure of the energy intervals in which H^* can be found. Let P_i ($i = 1, 2$) the probability of transition between G_3 and G_i. We have

$$P_i = \frac{\Delta H_i}{\Delta H_3} = \left.\frac{\mathrm{d}A_i/\mathrm{d}\lambda}{\mathrm{d}A_3/\mathrm{d}\lambda}\right|_{\lambda=\lambda^*}. \tag{1.49}$$

Here we assumed that A_1 and A_2 were increasing with λ. This of course is not always the case. A similar analysis on the energy difference between each transit close to the saddle point tells us the fact that, if only one region increases its area, a particle will be certainly trapped into it. Therefore the generalized transition probability between two regions, G_i and G_j reads

$$P_{i \to j} = \max\left\{0, \min\left\{\left.\frac{\mathrm{d}A_i/\mathrm{d}\lambda}{\mathrm{d}A_j/\mathrm{d}\lambda}\right|_{\lambda^*}, 1\right\}\right\}, \tag{1.50}$$

and after trapping, in adiabatic condition, the new value of the action is $J = A_j(\lambda^*)/2\pi$.

Taking into account the error $\mathcal{O}(\epsilon^{3/2})$ in the value of ΔH, it follows that there is an exceptional set of particles that do not follow Eq. (1.49). The measure of this set is proportional to $\sqrt{\epsilon}$ [73].

1.6 | Separatrix crossing: improved theory

The standard theory works in an adiabatic environment. It is nevertheless possible to correct it to take into account first-order effects of non-adiabaticity. When no separatrix crossing is present, the natural oscillations of the adiabatic invariant, once averaged, cancel each other and an accuracy in the conservation of the action variable, which depends on the smoothness of the perturbation, is obtained. Now, when a separatrix is crossed, oscillations before and after the crossing do not cancel each other anymore, and a residual effect is present and computable.

Of course, we expect this contribution to be at least of order $\mathcal{O}(\varepsilon)$, since it needs to disappear in the limit $\varepsilon \to 0$.

This phenomenon, first highlighted by Tennyson *et al.* [86], has been fully mathematically exploited in the seminal work of A. I. Neishtadt [73], whose general results we will now review, before applying the same method to the specific class of Hamiltonians we are interested in.

Let $\mathcal{H}$ be a 1D Hamiltonian, dependent on the parameter $\lambda = \varepsilon t$, whose phase space is described by Fig. 1.2, where C is the hyperbolic point where the separatrices cross. The space is thus divided into three regions, G_1, G_2 and G_3. We will also set, on a separatrix, $\mathcal{H} = 0$.

If $h \ll 1$ is the value of the energy close to our separatrix. The period of the motion depends logarithmically on h:

$$T_i = -a \log |h| + \mathcal{O}(h \log |h|) \,, \tag{1.51}$$

and the action, integrating (1.51), becomes

$$2\pi J = A_i - ah \log |h| + ah + \mathcal{O}(h^2 \log |h|) \tag{1.52}$$

where A_i is the area of the region i, and accounts for the value of J when the energy h is exactly zero. We can get the expression for $a = a(\lambda)$ via linearization of the motion in the vicinity of the hyperbolic point.

We also introduce the area derivatives $\Theta_i = \mathrm{d}A_i/\mathrm{d}t$. The change of value of the adiabatic invariant is given by three contributions: the one before crossing the separatrix, the one at the separatrix crossing and the one after having crossed.

As in the previous section, we look at a point which starts in the outer region, and revolves around the separatrix getting closer and closer. We call J_- the initial values of the action and J_* the value at separatrix crossing. At each passage (labelled with a number n which decreases to 0 when the separatrix is met), the energy evolution is

$$h_{n+1} = h_n + \varepsilon(\Theta_3 + \mathcal{O}(h_{n+1}^{1/2})) \,. \tag{1.53}$$

Then, the passage time τ_n is calculated, considering that a particle passes close to the saddle point three times (one at energy h_n, one at energy $h_n + \varepsilon\Theta_1$ and the final one at energy h_{n+1}) and, integrating, the action J_n, and the first-order improved action $\tilde{J}_n$ are found. We do not report all the calculations, but we only give the final result before crossing the separatrix:

$$2\pi(\Delta\tilde{J})_- = 2\varepsilon a\Theta_3\left[-\frac{1}{2}\ln\frac{2\pi}{\Gamma(\xi)\Gamma(\xi+\frac{\Theta_1}{\Theta_3})}+\xi+\left(\frac{\Theta_2}{2\Theta_3}-\xi\right)\ln\xi\right] \\ + \mathcal{O}(\varepsilon^{3/2}\ln\varepsilon)\,, \tag{1.54}$$

where $\xi = h/(\varepsilon\Theta_3)$.

This was only the first step. We need now to analyze what happens when the separatrix is crossed.

In this case, we need a better approximation for the crossing time t_*, which we will call $t_*^{(i)}$ where the index i denotes the final region G_1 or G_2.

We will use

$$t_*^{(i)} = t_* - \frac{a}{2}\ln h_0 - \frac{a}{2}\ln|h_*^i| + \mathcal{O}(\varepsilon\ln^2\varepsilon) \tag{1.55}$$

where

$$h_*^i = h_* - \varepsilon\Theta_i\,. \tag{1.56}$$

Then, denoting as $\tilde{J}_*^{(i)}$ the value for $\tilde{J}_*$ which comes from the integration of Eq. (1.55), we have, defining

$$\xi_i = \frac{|h_*^{(i)}|}{\varepsilon\Theta_i}\,, \tag{1.57}$$

and using the substitutions

$$h_* = \varepsilon\xi\Theta_3\,, \qquad h_*^i = \varepsilon\xi\Theta_i \tag{1.58}$$

the final result

$$2\pi(\Delta\tilde{J})_{*,i} = A_i(\lambda^*) + \frac{\Theta_i}{\Theta_3}(2\pi J - S_3(\tau_*)) + a\varepsilon\Theta_i\left(\xi_i - \frac{1}{2}\right)\ln(\xi_i\Theta_i\varepsilon) \\ - \left(2\frac{\Theta_i}{\Theta_3}\ln(\xi\Theta_3\varepsilon)\right) + a\varepsilon\frac{\Theta_i}{\Theta_3}(\Delta\Theta_i\xi_i - 2\Theta_i) \\ + \mathcal{O}(\varepsilon^{3/2}\ln\varepsilon)\,. \tag{1.59}$$

Finally, the point enters either in G_1 or in G_2. As done before, we use a map where every step coincides with the passage on the x axis, either at the left or at the right of the saddle point.

Here the calculations are almost the same of those we used to obtain (1.54), adapted to the fact that a particle, once inside G_i, passes close to the hyperbolic point twice, moving for half a separatrix when the energy is $h_n = h_0 - n\varepsilon\Theta_i$ and for another half with the increased energy step h_{n+1}.

This means that, having defined $\tilde{J}_+$ as the final value for the improved adiabatic invariant

$$2\pi(\Delta\tilde{J})_{+,i} = \varepsilon a\Theta_i\left[-\ln\frac{\sqrt{2\pi}}{\Gamma(\xi_i)} + \xi_i + \left(\frac{1}{2} - \xi_i\right)\log\xi_i\right] + \mathcal{O}(\varepsilon^{3/2}\log\varepsilon) \quad (1.60)$$

We can now add the three contributions (1.54, 1.59, 1.60) to get the value of the final improved action $\tilde{J}_+$. If the initial and final points are chosen where the perturbation is absent, we have $\tilde{J} = J$ and

$$2\pi\tilde{J}_+ = A_i(\lambda^*) + \varepsilon a\Theta_i\left(\xi_i - \frac{1}{2}\right)\left[\ln(\varepsilon\Theta_i) - \frac{2\Theta_i}{\Theta_3}\ln(\varepsilon\Theta_3)\right]$$
$$- \varepsilon a\Theta_i\ln\frac{(2\pi)^{3/2}}{\Gamma(\xi_i)\Gamma\left(\frac{\Theta_i}{\Theta_3}(1-\xi_i)\right)\Gamma\left(1-\frac{\Theta_i}{\Theta_3}\xi_i\right)} \quad (1.61)$$
$$+ \mathcal{O}(\varepsilon^{3/2}(\ln\varepsilon - (1-\xi_i)^{-1})) .$$

Now, the variables $\xi_i \in [0, 1]$, with an ε in the denominator, are strongly dependent on the initial conditions and can be regarded as random variables, which, in principle, are uniformly distributed. Therefore, for a distribution of initial conditions, one can average Eq. 1.61 over ξ_i to find the mean final value of the adiabatic invariant depending on the attainment region G_i. One finds, at the lowest order in ε,

$$2\pi\left\langle\tilde{J}_+\right\rangle = A_i(\lambda^*) + \varepsilon a\Theta_3 f(\Theta_i/\Theta_3) \quad (1.62)$$

where

$$f(\theta) = \theta\int_0^1 d\xi \ln\frac{(2\pi)^{3/2}}{\Gamma(\xi)\Gamma(\theta(1-\xi))\Gamma(1-\theta\xi)} . \quad (1.63)$$

1.7 | Normal Form approach to nonlinear maps

Let us consider a 4D nonlinear map **F**, where the origin is a stable fixed point and whose linear dynamics have been diagonalized, e.g.

$$\begin{pmatrix}x'\\p'_x\\y'\\p'_y\end{pmatrix} = \begin{pmatrix}\boldsymbol{R}(\omega_x) & \mathbf{0}\\\mathbf{0} & \boldsymbol{R}(\omega_y)\end{pmatrix}\begin{pmatrix}x + f_1(x, p_x, y, p_y)\\p_x + f_2(x, p_x, y, p_y)\\y + f_3(x, p_x, y, p_y)\\p_y + f_4(x, p_x, y, p_y)\end{pmatrix} \quad (1.64)$$

where $\boldsymbol{R}(\omega)$ are rotation matrices and f_i polynomial functions in the variables x, p_x, y, p_y. A convenient change of variables is done setting

$$z_1 = x - ip_x, \qquad z_1^* = x + ip_x, \qquad z_2 = y - ip_y, \qquad z_2^* = y + ip_y, \qquad (1.65)$$

yielding

$$\mathbf{F} = \boldsymbol{R}_\omega \left(\boldsymbol{z} + \sum_{n \geq 2} [\mathbf{F}]_n \right) \tag{1.66}$$

where

$$\begin{aligned} \boldsymbol{z} &= (z_1, z_1^*, z_2, z_2^*), \\ \boldsymbol{F} &= (F_1, F_1^*, F_2, F_2^*), \\ \boldsymbol{R}_\omega &= \mathrm{diag}(e^{i\omega_x}, e^{-i\omega_x}, e^{i\omega_y}, e^{-i\omega_y}), \end{aligned} \tag{1.67}$$

and the symbol $[\cdot]_n$ identifies the terms of the polynomial with degree n.

Close to the origin, the dynamic of **F** is elliptical. However, as the radius increases, the effect of the non-linearities f_i deforms the motion. The goal is to find another map, U, which has the property to respect the symmetries that are present in the linear part of $\boldsymbol{F}$. Let $\mathcal{G}_\omega$ the group $\mathcal{G}_\omega = \left\{ n \in \mathbb{Z} | e^{in\omega_x}, e^{in\omega_y} \right\}$. If there are no resonance conditions between ω_x, ω_y and 2π, it is dense on a 2-torus and therefore it is isomorphic to $U(1) \otimes U(1)$. In resonant conditions, it fixes the discrete rotational symmetries.

The map U is defined to be a *normal form* of F with respect to $\mathcal{G}_\omega$ if

$$[U, \boldsymbol{R}_\omega] = 0, \tag{1.68}$$

id est, U commutates with the action of the group $\mathcal{G}$. This means that the dynamics of U respects the symmetry given by $\mathcal{G}_\omega$. Far from resonance, the deformed dynamics of the nonlinear map reduce to circles, while on resonance a discrete symmetry is preserved.

We still need to construct U. In general, it is possible to act perturbatively, and obtain a truncation of U at any order.

We start defining the commutative diagram:

$$\begin{array}{ccc} \mathbf{z} & \xrightarrow{\ \mathbf{F}\ } & \mathbf{z}' \\ {\scriptstyle \Phi}\big\uparrow & & \big\downarrow{\scriptstyle \Psi} \\ \zeta & \xrightarrow[\ \mathbf{U}\ ]{} & \zeta' \end{array} \tag{1.69}$$

where the coupling functions $\boldsymbol{\Phi}$ and $\boldsymbol{\Psi} = \boldsymbol{\Phi}^{-1}$ have been introduced, to enact the change of co-ordinates $\boldsymbol{z} \to \boldsymbol{\zeta}$. Now, the functional equation

$$\boldsymbol{F} \circ \boldsymbol{\Phi} = \boldsymbol{\Phi} \circ U \tag{1.70}$$

must be solved in a order-by-order fashion.

If we define the operator

$$\mathbf{\Delta}_\omega(\mathbf{\Phi}) = [\mathbf{\Phi}, R_\omega] \,, \tag{1.71}$$

at order N, Eq. (1.70) can be recast as

$$\mathbf{\Delta}_\omega[\mathbf{\Phi}]_N + [U]_N = [[F]_{\leq N}([\mathbf{\Phi}]_{<N}]_N - [[\mathbf{\Phi}]_{<N}([U]_{<N}]_N \,. \tag{1.72}$$

Therefore, at order N, U contains all the monomials that are present in the right side of the equation but which are closed under the action of $\mathbf{\Delta}_\omega$, which depends on whether ω is resonant.

Equation (1.72) is then used recursively to determine U, $\mathbf{\Phi}$ and $\mathbf{\Psi}$ at any order. However, the term-to-term comparison of Eq. (1.72) does not fully determine U and $\mathbf{\Phi}$. For the remaining terms, one wants to impose that the co-ordinate transformation $\mathbf{\Phi}$ is symplectic at any truncation order (i.e. , its Jacobian matrix, up to order N, is a symplectic matrix). The symplectic condition is given by the Poisson brackets $\{\Phi_i, \Phi_j^*\} = \delta_{ij}$, $\{\Phi_i, \Phi_j\} = 0$.

From the expression of U, truncated at some convenient order, it is then possible to build an interpolating Hamiltonian. First of all, we introduce the action-angle co-ordinates $(J_x, \phi_x, J_y, \phi_y)$ according to the relations

$$\zeta_1 = \sqrt{2J_x}e^{i\phi_x}, \qquad \zeta_2 = \sqrt{2J_y}e^{i\phi_y} \,. \tag{1.73}$$

In non-resonant conditions, the interpolating Hamiltonian will be given by

$$\mathcal{H} = \mathcal{H}_0 = \omega_x J_x + \omega_y J_y + \sum_{m+n\geq 2} \Omega_{m,n} J_x^m J_y^n \,, \tag{1.74}$$

where the coefficients $\Omega_{m,n}$ are obtained from U.

In resonant conditions $\mathbf{k}\cdot\tilde{\omega} = 0$, where $\mathbf{k} = (k_x, k_y, 1)$ is a vector of integers and $\tilde{\omega} = (\omega_x, \omega_y, 2\pi)$ the Hamiltonian will also contain an angular part:

$$\mathcal{H}_{\text{res}} = \sum_{\mathbf{k}\cdot\tilde{\omega}=0} h_{\mathbf{k}} J_x^{k_x/2} J_y^{k_y/2} \cos(\mathbf{k}\cdot\tilde{\boldsymbol{\phi}}) \,, \tag{1.75}$$

where $\tilde{\boldsymbol{\phi}} = (\phi_x, \phi_y, 0)$.

Finally, it is possible to write a normal form in quasi-resonant conditions, i.e. with $\mathbf{k}\cdot\tilde{\omega} = \delta$, and considering the normal form with respect to the symmetry group in resonant conditions. At first order in δ, one has

$$\mathcal{H} = \delta J_x + \Omega(J_x, J_y) + \mathcal{H}_{\text{res}}(\phi_x, \phi_y, J_x, J_y) \,. \tag{1.76}$$

The computation of Normal Form approximation for polynomial maps is made easy by software like [15], which implement polynomial manipulations, solving, at each order, Eq. (1.72). Given the coefficients of F, they return, up to a given order, the coefficients of $\boldsymbol{\Phi}$ and $\boldsymbol{\Psi}$, as long as the interpolating Hamiltonian, in non-resonant, resonant or quasi-resonant conditions.

If we restrict ourselves to a 2D map, some results are simpler to obtain. We represent the function $U(\zeta, \zeta^*)$ and $\Phi(\zeta, \zeta^*)$ as

$$U(\zeta, \zeta^*) = e^{i\omega}\zeta + \sum_{n\geq 2}\sum_{k} u_{k,n-k}\zeta^k \zeta^* n - k \,,$$

$$\Phi(\zeta, \zeta^*) = \zeta + \sum_{n\geq 2}\sum_{k} \phi_{k,n-k}\zeta^k \zeta^* n - k \,. \tag{1.77}$$

The action of Δ_ω, close to resonance q (i.e. $\omega \approx 2\pi/q$) gives a condition on the coefficients of U: $u_{k,n-k} = 0$ if $2k - n - 1 \neq \ell q$, with $\ell \in \mathbb{Z}$. Therefore, even in non-resonant conditions, the coefficients $u_{\frac{n+1}{2},\frac{n-1}{2}}$ are always non-zero. The truncated Normal Form U up to order N is the exponential of its interpolating Hamiltonian flow, therefore, defining Ω as $U = e^{i\Omega(\zeta\zeta^*)}\zeta)$, with $\Omega = \omega + \sum_{n>1}\Omega_{2n}(\zeta\zeta^*)^n$, one has, expanding

$$U(\zeta, \zeta^*) = e^{i\omega}\left[1 + i\Omega_2\zeta\zeta^* + i\left(\Omega_4 - \frac{\Omega_2^2}{2}\right)(\zeta\zeta^*)^2 + \cdots\right]\zeta \,, \tag{1.78}$$

whence it can be seen that each term $u_{\frac{n+1}{2},\frac{n-1}{2}}$ can be used to find the value of Ω_{n-1}. The Hamiltonian is given by the integration of the flow. If $\zeta\zeta^* = 2J$

$$\mathscr{H}(J) = -i\int \mathrm{d}J\,\Omega(J) = \omega J + \sum \frac{\Omega_{2n}}{n+1}(2J)^{n+1} \,. \tag{1.79}$$

In the resonant case, the expansion up to the order $q - 2$ is the same, as no resonant term appears in the expression of U before that order. The first resonant term in U is given by $u_{0,q-1}\zeta^{*q-1}$. At first order, $\Omega = e^{-i\omega}U$ and

$$\Omega = \Omega_{2n}(\zeta^*\zeta)^n\zeta + e^{-i\omega}u_{0,q-1}\zeta^{*q-1} \,. \tag{1.80}$$

The computation of the Hamiltonian is more involved (one has to make hypothesis on the polynomial structure of the flow), but in the end it gives the result

$$\mathscr{H}(\zeta, \zeta^*) = i\sum_{n} \frac{\Omega_{2n}}{n+1}(\zeta\zeta^*)^{n+1} + \left(\frac{e^{-i\omega}u_{0,q-1}}{q} - \text{c.c.}\right) \tag{1.81}$$

which, in action-angle co-ordinates, gives

$$\mathscr{H}(\phi, J) = \sum_{n} \frac{\Omega_{2n}}{n+1}J^{n+1} + \frac{2|u_{0,q-1}|}{q}J^{q/2}\cos(q\phi) \,. \tag{1.82}$$

Finally, in the quasi-resonant approach one has the Hamiltonian

$$\mathcal{H}(\phi, J) = \delta J + \sum_n \frac{\Omega_{2n}}{n+1} J^{n+1} - (2J)^{q/2}\left(\frac{\delta e^{i\omega}}{e^{-i\delta q} - 1}u_{0,q-1}e^{iq\phi} + \text{c.c.}\right); \quad (1.83)$$

as $\delta \to 0$, the resonant term tends to the exactly-resonant one.

We remark that the formal series which results from the order-by-order solution of Eq. (1.72) is an asymptotic series which, in general, is divergent. However, for any disk of radius R, it is possible to show that there exists an optimal truncation order $\hat{N} \sim 1/R$ which, in the disk, minimizes the error $E_N = U - U_N$, which, at $N = \hat{N}$, is $\mathcal{O}(\exp(-1/R))$. A theorem by Nekhoroshev ensures that, given R, the evolution of the map F is limited inside the disk for a number of iterates $T \sim \exp[(R^*/R)^\alpha]$, with R^*, α constants, ensuring that, for any iterate $t < T$, the estimate on the error of U_N holds [16]. Further details are found in Ref. [17].

2 | Elements of accelerator physics

After the mathematical introduction of Chapter 1, we now devote our attention to some concepts on the description of the motion of charged particles in accelerators. The scope of this chapter is two-fold. First of all, we want to introduce the nomenclature, co-ordinates, common approximations and assumptions, and main results, which are needed to understand motivations and consequences of the beam manipulation techniques which are the "core" of novel results of this thesis, and to justify from first principles the mathematical models (based on Hamiltonians and symplectic maps) which are employed to describe these effects. Secondly, this is the possibility to apply some of the tools introduced in the previous chapter to the description of some physical systems.

We remark that this is not, and is not meant to be, a brief summary of a textbook in accelerator physics. Books like Refs. [59] and [92] provide excellent introductions to the field, which we also use as a reference for our discussion. Here, we limit ourselves to cover, from a theoretical point of view, only the topics that have some intersection with the beam manipulations we will analyse in Part II of the thesis.

<p style="text-align:center">❖</p>

A particle accelerator is a machine in which a beam of charged particles is accelerated using electromagnetic fields, in order to increase their energy and have them colliding with a fixed target or another particle beam, for performing physical experiments, but also for medical and industrial applications. Depending on their topology, we distinguish between *linear* or *circular* accelerators. In this thesis, we will always refer to circular machines.

Another important distinction is given by the type of particles that are accelerated. When a charged particle moves along a curved trajectory, it loses part of its energy due to synchrotron radiation. However, this effect, as it depends on the particle mass as m^{-4}, is negligible for hadron (protons or ions) beams. Electron beams therefore should account for dissipative effects, making the Hamiltonian description of the motion more difficult. In this thesis,

we will consider all effects to happen in hadron machines, and at energy scale where one can safely discard synchrotron radiation.

The third assumption we make in our description of accelerators is to reduce to study "single-particle dynamics". This means that we assume the motion of each particle of the beam to be independent: we therefore neglect the repulsive Coulomb force which acts between the same-signed charges which are in the beam. These collective effects are object of dedicated studies, and can in any case be treated as perturbations of the single-particle dynamics.

Then, we decouple the motion in two components. We therefore distinguish between two types of dynamics:

- *longitudinal*, along the accelerator circumference (*reference trajectory*);

- *transverse*, in the plane normal to the longitudinal motion.

To understand transverse motion, one could imagine that a piece of paper is placed between the particle and the center of the accelerator, normally to the accelerator plane, and co-rotates with the particle orbit. At each time instant, the particle "draws" its position on the paper. The resulting line is the transverse trajectory. The manipulations proposed in Part II of this thesis all refer to the shape of the beam in the transverse plane.

The Chapter is organized as follows. In Section 2.1 we introduce the co-ordinate system and we write the Hamiltonian of a charged particle in an electromagnetic field. In Section 2.2 we solve the equations of motion in the transverse plane when only linear magnetic fields are considered. Then, in Section 2.3, we introduce the theory of adiabatic invariants in the linear motion, defining the Courant-Snyder variables and the concept of emittance. In Section 2.4, we briefly describe the main effects that arise when also non-linear magnetic elements are considered, with specific importance given to the theory of non-linear resonances. Finally, in Section 2.5, we discuss the relationship between Hamiltonian description of transverse dynamics and the one given by Poincaré maps, which will both be employed in Part II to model non-linear manipulations.

2.1 | Co-ordinate system and equations of motion

To describe the motion of particles inside accelerators, a convenient choice of co-ordinates needs to be performed, taking advantage of the toroidal symmetry of the system.

We can introduce the Frenet-Serret co-ordinate system. It should be natural to choose one curvilinear co-ordinate s along the longitudinal motion and two Cartesian co-ordinates x, y for the transverse one (Fig. 2.1).
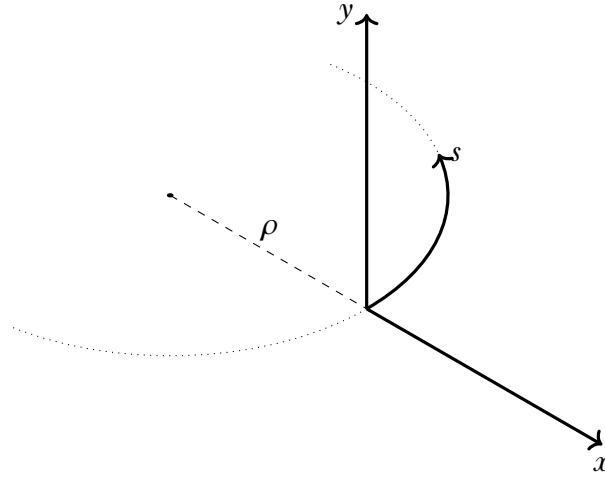
Figure 2.1 – The Frenet-Serret co-ordinate system which we will use throughout this work. The dotted line is the particle trajectory, whose curvature radius is ρ. The s co-ordinate is measured along the trajectory while x and y are orthogonal to it.

Let ρ be the accelerator radius. The Cartesian system (X, Y, Z), centered in the accelerator centre can be mapped into the Frenet-Serret system via the following transformations:

$$X = (x + \rho) \cos\left(\frac{s}{\rho}\right), \qquad Y = y, \qquad Z = (x + \rho) \sin\left(\frac{s}{\rho}\right). \qquad (2.1)$$

Our goal now is to write the Hamiltonian for a particle in an accelerator in this co-ordinate system.

It actually turns out that it is convenient to regard s as the time co-ordinate (due to canonical coupling, the conjugated moment p_s will work as the Hamiltonian function).

The Hamiltonian we will apply to particles in circular accelerators is the one of a charged particle under the effect of an electromagnetic field, which acts with Lorentz force. Particles are accelerated in modulus by the action of an electric field **E** (or by the scalar potential Φ), and their trajectories are bent, in order to keep them in a circular orbit, by a magnetic field **B**, which will be more conveniently expressed by the vector potential **A** (**B** = $\nabla \times$ **A**).

A linear electromagnetic field keeps particles on a planar circular motion with radius ρ, where ρ is given by the equilibrium between magnetic and centrifugal force.

The quantity $B\rho$ is called *beam rigidity* and corresponds to

$$B\rho = \frac{p}{e} \qquad (2.2)$$

where p is the particle momentum while e is its charge.

Now, Hamiltonian for a relativistic particle under Lorentz force is

$$\mathscr{H} = e\Phi + \sqrt{m^2c^4 + (c\mathbf{p} - e\mathbf{A})^2}\,. \tag{2.3}$$

We should express the square norm of $(c\mathbf{p} - e\mathbf{A})$ in the Frenet-Serret system of co-ordinates $(x,\ y,\ s)$, whose metric tensor is

$$g_{ij} = \mathrm{diag}\!\left(1,\ 1,\ 1 + \frac{x}{\rho}\right). \tag{2.4}$$

Thus,

$$\mathscr{H} = e\Phi + \sqrt{m^2c^4 + \frac{(cp_s - eA_s)^2}{(1 + x/\rho)^2} + (cp_x - eA_x)^2 + (cp_y - eA_y)^2}\,. \tag{2.5}$$

Now we substitute time variable with the longitudinal co-ordinate s. In this way, the conjugated momentum $-p_s$ will become the new Hamiltonian $\tilde{\mathscr{H}}$. Solving the latter equation for p_s, we obtain

$$\tilde{\mathscr{H}} = -\left(1 - \frac{x}{\rho}\right)\sqrt{\frac{E^2}{c^2} - m^2c^2 - (p_x - eA_x)^2 - (p_y - eA_y)^2} - eA_s\,, \tag{2.6}$$

where $E = \mathscr{H} - e\Phi$. From special relativity, $E^2/c^2 = p^2 + m^2c^2$ and our Hamiltonian reduces to

$$\tilde{\mathscr{H}} = -\left(1 - \frac{x}{\rho}\right)\sqrt{p^2 - (p_x - eA_x)^2 - (p_y - eA_y)^2} - eA_s\,. \tag{2.7}$$

Because (at least in the accelerators that we consider for our studies) the motion in the longitudinal direction is far faster than in the transverse ones, we have $p \gg p_x$ and $p \gg p_y$ and the Hamiltonian can be expanded as $\sqrt{1 + x} \approx 1 + x/2$, as

$$\tilde{\mathscr{H}} = \left(1 + \frac{x}{\rho}\right)\left[-p + \frac{1}{2p}\left(p_x^2 + p_y^2\right)\right] - eA_s\,, \tag{2.8}$$

where, as far as we are taking into account only transverse effects, we can assume there is no magnetic field in the longitudinal direction, thus the only contribution to the vector potential is along s, and $A_x = A_y = 0$, i.e. $\mathbf{B} = (B_x,\ B_y,\ 0)$.

It is convenient to write the magnetic field contribution to the Hamiltonian, eA_s, using the multipole expansion of the magnetic field.

From Maxwell's equation $\boldsymbol{\nabla} \times \mathbf{B} = 0$, one gets the Laplace equation $\nabla^2 \mathbf{A}$, which, for A_s has the general solution

$$A_s = \mathrm{Re} \sum_n \left[\frac{k_n + i j_n}{(n+1)!} (x + iy)^{n+1} \right], \tag{2.9}$$

and the corresponding expansion of the magnetic field reads

$$B_y + i B_x = \sum_n \frac{k_n + i j_n}{n!} (x + iy)^n . \tag{2.10}$$

The coefficients

$$k_n = \left. \frac{\partial^n B_y}{\partial x^n} \right|_{x=y=0}, \qquad j_n = \left. \frac{\partial^n B_x}{\partial y^n} \right|_{x=y=0} \tag{2.11}$$

are called, respectively, the *normal* and *skew* $2(n+1)$-polar coefficients of the magnetic field. Usually, in accelerators, magnetic elements generate fields with only one multipolar component: we therefore talk about normal or skew dipoles, quadrupoles, sextupoles, octupoles and so on.

2.2 | Transverse motion. Hill's equation

Hamiltonian (2.8) serves as as a basis to derive the equations of motion of the particle in the transverse plane. We have

$$x' = \left(1 + \frac{x}{\rho} \right) \frac{p_x}{p} , \qquad p'_x = \frac{p}{\rho} \left(1 + \frac{x}{\rho} \right) + e \frac{\partial A_s}{\partial x} ,$$
$$y' = \left(1 + \frac{x}{\rho} \right) \frac{p_y}{p} , \qquad p'_y = e \frac{\partial A_s}{\partial y} . \tag{2.12}$$

Now, we can express the partial derivatives of A_s as a function of the x and y components of the magnetic field $\mathbf{B}$. Expressing the curl in Frenet-Serret co-ordinates, we have

$$\boldsymbol{\nabla} \times \mathbf{A} = -\frac{\hat{x}}{1 + x/\rho} \frac{\partial A_s}{\partial y} + \frac{\hat{z}}{1 + x/\rho} \frac{\partial A_s}{\partial x} = B_x \hat{x} + B_z \hat{y} \tag{2.13}$$

which yields

$$\frac{\partial A_s}{\partial x} = -\left(1 + \frac{x}{\rho} \right) B_y , \qquad \frac{\partial A_s}{\partial y} = \left(1 + \frac{x}{\rho} \right) B_x , \tag{2.14}$$

which, substituted in the equations of motion gives

$$x' = \left(1 + \frac{x}{\rho}\right)\frac{p_x}{p}\,, \qquad p'_x = \left(1 + \frac{x}{\rho}\right)\left[\frac{p}{\rho} - eB_y\right]$$
$$y' = \left(1 + \frac{x}{\rho}\right)\frac{p_x}{p}\,, \qquad p'_y = e\left(1 + \frac{x}{\rho}\right)B_x\,. \tag{2.15}$$

Using $p = eB\rho$, and rewriting the equations as second order differential equations one gets

$$x'' = \frac{1}{\rho} + \frac{x}{\rho^2} + \frac{B_z}{B\rho}\left(1 + \frac{x}{\rho}\right)^2\,,$$
$$y'' = \frac{B_x}{B\rho}\left(1 + \frac{x}{\rho}\right)^2\,. \tag{2.16}$$

Considering only linear terms, these equation assume the form

$$z'' + K_z(s)z = 0\,, \tag{2.17}$$

where z stands for either x or y, and the function $K(s)$ is in general the effect of the linear magnetic fields (which, in multipole expansion, is given by dipolar and quadrupolar elements) the particle is subject to in the accelerator. Now, if a circular accelerator of length L is considered, we have the periodic condition $K_z(s) = K_z(s+L)$. This equation with the periodic condition, which was introduced to study the motion of the Moon, is called *Hill's equation* [47]. An Ansatz for the solution of Hill's equation is in the form

$$z(s) = A\sqrt{\beta_z(s)}\cos\psi_z(s)\,, \tag{2.18}$$

which, substituted into Hill's equation results in a relation between $\psi_z(s)$ and $\beta_z(s)$,

$$\frac{1}{\sqrt{\beta_z(s)}}\frac{\mathrm{d}}{\mathrm{d}s}(\beta_z(s)\psi_z(s)) = 0\,, \tag{2.19}$$

which can be solved as

$$\psi_z = \int_0^s \frac{\mathrm{d}s'}{\beta_z(s')} \tag{2.20}$$

and a non-linear equation for $\beta_z(s)$:

$$\frac{1}{2}\beta_z\beta_z'' - \frac{1}{4}\beta_z'^2 + K_z(s)\beta_z^2 = 1\,. \tag{2.21}$$

The phase advance over the ring is called *tune*:

$$\nu_z = \frac{1}{2\pi}\oint \frac{\mathrm{d}s'}{\beta_z(s')}\,. \tag{2.22}$$

Now, the solution of the equation for $\beta_z(s)$ only determines a scaling of the solution $z(s)$ at each value s. We are interested in the transverse motion, i.e. to the evolution of the particle at each passage at some value $s = s_0$, where the phase ψ_z will have advanced by a quantity $2\pi\nu_z$. A co-ordinate transformation can now be employed to normalize the solution to decouple the envelope dynamics, described by $\beta_z(s)$, and the "pure" transverse motion.

2.3 | Courant-Snyder ellipse. Adiabatic invariants. Emittance

Let us start from Hill's equation solution $z(s)$ from Eq. (2.18). The momentum $z'(s)$ reads

$$z'(s) = -\frac{z}{\beta_z(s)}(\alpha_z(s) + \tan\psi_z(s)) \tag{2.23}$$

where $\alpha_z = -\beta_z'/2$. We introduce the angular variable $\phi_z = \psi_z$. The first kind generating function

$$F = \int \mathrm{d}z\, z' = -\frac{z^2}{2\beta_z}(\alpha + \tan\phi) \tag{2.24}$$

and the other canonical variable J_z is given by

$$J_z = \frac{\partial F}{\partial\phi_z} = \frac{z^2}{2\beta_z}(1 + \tan^2\phi) = \frac{1}{2\beta_z}\left[z^2 + (\beta z' + \alpha z)^2\right]. \tag{2.25}$$

In the new variables, Hill's Hamiltonian $\mathscr{H} = z'^2/2 + K_z z^2/2$, taking into account the derivative $\partial F/\partial s$, reduces to the simple expression

$$\mathscr{H}(\phi, J, s) = \frac{J}{\beta(s)}. \tag{2.26}$$

Now, the equation for the variable ϕ_z is $\phi_z' = 1/\beta(s)$. Another transformation can be made to make ϕ_z proportional to s (and remove any dependence on the β function from the equations of motion).

Introducing the frequency $\omega_z = 2\pi\nu_z/L$, the transformation $(\phi_z, J_z) \to (\tilde{\phi}_z, \tilde{J}_z)$ is given by the generating function

$$G(\phi_z, \tilde{J}_z) = \tilde{J}_z\left(\omega_z s - \int_0^s \frac{\mathrm{d}s'}{\beta(s')}\right) + \phi\tilde{J}, \tag{2.27}$$
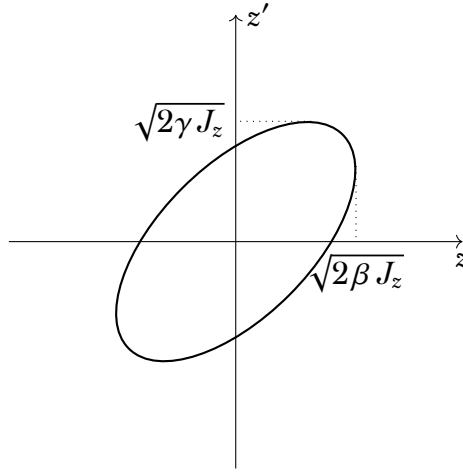
FIGURE 2.2 – The Courant-Snyder ellipse $\gamma z^2 + 2\alpha z z' + \beta z'^2 = 2J_z$. The area enclosed by the ellipse is equal to $2\pi J_z$.

which results in the Hamiltonian

$$\mathcal{H}(\tilde{\phi}_z, \tilde{J}_z) = \omega_z \tilde{J}_z \,, \tag{2.28}$$

which is the Hamiltonian of an harmonic oscillator. Cartesian co-ordinates $\hat{z} = \sqrt{2J_z} \cos \phi_z$, $\hat{p}_z = \sqrt{2J_z} \sin \phi_z$ can also be introduced.

In general, the transverse linear motion can therefore be modeled using the Hamiltonian

$$\mathcal{H}(\hat{x}, \hat{p}_x, \hat{y}, \hat{p}_y) = \frac{\omega_x}{2}(\hat{x}^2 + \hat{p}_x^2) + \frac{\omega_y}{2}(\hat{y}^2 + \hat{p}_y^2) \,. \tag{2.29}$$

Under the Hamiltonian of Eq. (2.29), the trajectories are circles in the decoupled phase spaces $(\hat{x}, \hat{p}_x)$ and $(\hat{y}, \hat{p}_y)$. Furthermore, the actions $J_x = (\hat{x}^2 + \hat{p}_x^2)/2$ and $J_y = (\hat{y}^2 + \hat{p}_y^2)/2$, which correspond to the trajectory area divided by 2π are conserved. For historical reasons, the value $2J_z$ is called the Courant-Snyder invariant. From its definition in the physical co-ordinates (z, z') given in Eq. (2.25), it is possible to draw the constant-J surfaces in the (z, z') phase space, as in Fig. 2.2, which correspond to concentric ellipses, described by the equation

$$J_z = \frac{1}{2\beta_z}\left[z^2 + (\alpha z + \beta z'))^2\right] = \frac{1}{2}\left(\gamma z^2 + 2\alpha z z' + \beta z^2\right), \tag{2.30}$$

having defined $\gamma = (1 + \alpha^2)/\beta$. The area of the ellipse is still equal to $2\pi J_z$, and is conserved at any value of s. In short, the $(z, z') \rightarrow (\hat{z}, \hat{p}_z)$ transformation

makes the physical co-ordinates ellipses into circles with the same area in the normalized co-ordinates.

The definition of the Courant-Snyder invariant applies to a single particle. For a beam, a quantity, called *emittance* is defined as the average of the Courant-Snyder invariant: $\varepsilon_z = \langle J_z \rangle$, which is related to the second moments of the beam distribution in $(\hat{z}, \hat{p}_z)$. Now, averaging over J_z and ϕ_z in the definitions of $\hat{z}$ and $\hat{p}_z$ one gets

$$\langle \hat{z}^2 \rangle = \beta_z \varepsilon_z, \qquad \langle \hat{p}_z^2 \rangle = \gamma_z \varepsilon_z, \qquad \langle \hat{z}\,\hat{p}_z \rangle = -\alpha_z \varepsilon_z, \qquad (2.31)$$

whence, using the definition of J_z,

$$\varepsilon_z = \sqrt{\langle \hat{z}^2 \rangle \langle \hat{p}_z^2 \rangle - \langle \hat{z}\,\hat{p}_z \rangle^2}. \qquad (2.32)$$

The beam emittance corresponds therefore to the average Courant-Snyder invariant of a distribution, or to the area (up to a 2π factor) of the orbit of the rms particle of the beam. This is useful when dealing with Gaussian beam distribution: in (ϕ_z, J_z) co-ordinate a normal particle distributions assumes the form

$$\rho_z = \frac{1}{\varepsilon_z} \exp\left(-\frac{J_z}{\varepsilon_z}\right). \qquad (2.33)$$

2.4 | Non-linear beam dynamics

Hill's equation description of transverse dynamics deals only with linear effects, i.e. the ones generated by dipole and quadrupole magnets.

Non-linear effects are introduced adding non-linear terms in the electromagnetic potential that appears in Hill's Hamiltonian. In an accelerator, they can represent either unwanted non-linear effects of linear magnets or specifically added non-linear magnetic elements, such as sextupoles and octupoles. Sextupoles, for example, are needed to correct *chromaticity*, i.e. the fact that particles with different momentum are differently focused by quadrupoles. Other sources of non-linearities are the space charge and the beam-beam effects, caused by the electromagnetic interaction of charged particles with other charged particles, in the same or in another beam (for colliding machines).

Non-linear effects due to higher-order magnets can be simply introduced in the Hamiltonian as anharmonic perturbation to the harmonic oscillators. The non-linear magnetic contribution to the Hamiltonian is given by the terms of A_s, as in Eq. (2.9), for $n \geq 2$, having transformed (x, y) into $(\hat{x}, \hat{y})$. The non-linear part of the Hamiltonian is therefore given by

$$\mathcal{H}_{\text{nlin}}(\hat{x}, \hat{p}_x, s) = \text{Re} \sum_{n \geq 2} \left[\frac{k_n(s) + i j_n(s)}{(n+1)!} (\sqrt{\beta}_x \hat{x} + i \sqrt{\beta}_y \hat{y})^n \right]. \qquad (2.34)$$

The strengths $k_n(s)$ and $j_n(s)$ due to the effect of a normal or a skew $(2n + 2)$-polar magnetic field are substituted by integrated coefficients K_n, J_n, which express the overall effect of a field on an accelerator turn, scaled by the value of β_x and β_y where the magnetic elements are placed. We also introduce the quantity $\beta(s) = \beta_y(s)/\beta_x(s)$, and its averaged value $\bar{\beta}$. We have

$$K_n = \oint ds\, k_n(s)\beta_x^{\frac{n+1}{2}}(s), \qquad J_n = \oint ds\, j_n(s)\beta_x^{\frac{n+1}{2}}(s), \qquad \bar{\beta} = \oint ds\, \frac{\beta_y(s)}{\beta_x(s)},$$
$$(2.35)$$

where the integrations are extended over the accelerator turn. With the new averaged coefficients, the non-linear Hamiltonian becomes

$$\mathcal{H}_{\mathrm{nlin}}(\hat{x}, \hat{p}_x) = \mathrm{Re} \sum_{n \geq 2} \left[\frac{K_n + i J_n}{(n+1)!}(\hat{x} + i\bar{\beta}^{1/2}\hat{y})^n \right]. \qquad (2.36)$$

For a 1D (flat) beam model with normal multipoles, the Hamiltonian reduces to

$$\mathcal{H}(\hat{x}, \hat{p}) = \omega\frac{\hat{x}^2 + \hat{p}^2}{2} + \sum_{n > 2} K_n \frac{x^{n+1}}{(n+1)!}. \qquad (2.37)$$

The introduction of non-linear elements in a circular accelerator results in three main effects: the reduction of the dynamic aperture, an amplitude-dependent detuning, and the excitation of non-linear resonances. [46]

Dynamic aperture

Hamiltonian (2.29), which describes the linear transverse motion, corresponds to the Hamiltonian of an harmonic oscillator with two degrees of freedom, which is always stable. When a non-linearity is introduced, the stability region is reduced. For instance, introducing a normal sextupole in Hamiltonian (2.37), one has the potential

$$V(\hat{x}) = \omega\frac{\hat{x}^2}{2} + K_2\frac{\hat{x}^3}{3} \qquad (2.38)$$

which has an hyperbolic point at $\hat{x} = -\omega/K_2$, and the separatrix delimits the stability region, which is further reduced by a stronger sextupole.

Due to unavoidable high-order resonance effects, close to the unstable fixed points the phase space is populated by tiny-scale island chains: this means that particles getting too close to the border of the stability region enter in a chaotic region where the motion is stochastic, and can get lost. *Dynamic aperture* is defined as the volume of the region of stability of the phase space. Usually, it is computed via extremely long time particle tracking simulations, while studies are on-going to predict the dynamic aperture using less computing resources. [19]

Amplitude-dependent detuning

The second effect of non-linear elements on transverse motion is the fact that the rotation frequency — the tune — becomes a function of the amplitude, i.e. the value of the action J. In the linear Hamiltonian (2.29), the frequency Ω is given by

$$\Omega = \frac{\partial \mathscr{H}}{\partial J} = \omega \,, \tag{2.39}$$

being $J = (\hat{x}^2 + \hat{p}^2)/2$. The tune is constant at any action, all particles have the same rotation frequency.

Let us add now an octupolar contribution to the Hamiltonian, i.e., with a $n = 3$ element in Eq. 2.37. In action-angle co-ordinates $(\phi, \, J)$ we have

$$\mathscr{H} = \omega J + K_3 J^2 \cos^4 \phi \,. \tag{2.40}$$

Averaging over the angular variable ϕ, one gets

$$\langle \mathscr{H} \rangle = \omega J + \frac{3}{8} K_3 J^2 \,, \tag{2.41}$$

and

$$\Omega(J) = \frac{\partial \langle \mathscr{H} \rangle}{\partial J} = \omega + \frac{3K_3}{4} J \,. \tag{2.42}$$

Now we have a linear dependence of the tune on the action: each particle, at a given amplitude, will have a different rotation frequency.

Note that the averaging approach we used in the simple example of a detuning driven by octupoles only captures first-order effects in the frequency. When an Hamiltonian is written using the Normal Form approach, contributions from higher orders of K_n due to lower-order magnets can also be found. For instance, a sextupole strength K_2 will have an effect on $\Omega(J)$ proportional to K_2^2.

In general, amplitude-dependent detuning can be measured performing a Fast Fourier Transform of the transverse orbit of a particle as function of the initial amplitude. Some techniques are proposed in [8, 9, 83]. Indeed, it is possible to use high-accuracy tune measurements as a probe of the underlying dynamics, as the tune values give information on the chaoticity of the motion and on the presence of resonant effects. [80]

Non-linear resonances

Let us start from the linear Hamiltonian (2.28) using one degree of freedom, and we add a non-linear perturbation U with a small parameter ϵ. The Hamiltonian reads

$$\mathscr{H}(\phi, J, \theta) = \omega J + \epsilon U(\phi, J, \theta) \,. \tag{2.43}$$

We follow the perturbation-theoretical approach of Ref. [93]. A transformation into new variables $(\tilde{\phi}, \tilde{J})$ is done via a generating function

$$F(\phi, \tilde{J}) = \tilde{J}\phi + \epsilon\,\chi(\phi, \tilde{J}, \theta) \qquad (2.44)$$

and reads

$$\tilde{J} = J - \epsilon\frac{\partial\chi}{\partial\phi}, \qquad \tilde{\phi} = \phi + \epsilon\frac{\partial\chi}{\partial\tilde{J}}, \qquad \tilde{\mathcal{H}} = \mathcal{H} + \epsilon\frac{\partial\chi}{\partial\theta}. \qquad (2.45)$$

The new Hamiltonian, up to first order in ϵ, reads

$$\tilde{\mathcal{H}} = \omega\tilde{J} + \epsilon\left[\omega\frac{\partial\chi}{\partial\phi} + \frac{\partial\chi}{\partial\theta} + U(\phi, \tilde{J}, \theta)\right]. \qquad (2.46)$$

Setting the ϵ-proportional term equal to zero makes the Hamiltonian independent on the pseudo-time variable θ. The resulting differential equation is solved for χ after expanding in Fourier series. The perturbation potential U becomes

$$U(\phi, \tilde{J}, \theta) = \sum_{m,n} U_{m,n}(\tilde{J})e^{i(n\phi - m\theta)} \qquad (2.47)$$

where

$$U_{m,n} = \frac{1}{4\pi^2}\int \mathrm{d}\theta\mathrm{d}\phi\, U(\phi, \tilde{J}, \theta)e^{-i(n\phi - m\theta)}, \qquad (2.48)$$

and the differential equation has the solution

$$\chi(\phi, \tilde{J}, \theta) = i\sum_{m,n}\frac{U_{m,n}(\tilde{J})}{n(\omega - \omega_{\mathrm{r}})}e^{i(n\phi - m\theta)}, \qquad (2.49)$$

where we introduced the resonant frequency $\omega_{\mathrm{r}} = m/n$, resulting in the Hamiltonian

$$\tilde{\mathcal{H}} = \omega\tilde{J} + \sum_{m,n} U_{m,n}(\tilde{J})e^{i(n\phi - m\theta)}. \qquad (2.50)$$

If the frequency ω is close to ω_{r}, χ is divergent. However, in resonant conditions, it is possible to write an averaged Hamiltonian where all non-resonant terms in the sum become zero, only resonant terms appear, i.e.

$$\mathcal{H} = \omega\tilde{J} + U_{0,0}(\tilde{J}) + U_{m,n}e^{i(n\phi - m\theta)}, \qquad (2.51)$$

where $\omega \approx \omega_{\mathrm{r}} = m/n$.

Introducing a rotating frame, with the new angle $\gamma = \phi - \omega_r\theta$, the Hamiltonian becomes

$$\mathcal{H}(\gamma, J) = (\omega - \omega_{\mathrm{r}})J + \alpha(J) + \mathrm{Re}[U_{m,n}e^{in\gamma}]. \qquad (2.52)$$

This Hamiltonian has a peculiar phase space close to resonance. For example, let us introduce a non-linear magnetic potential $U = K_3 x^4/4$, which can be driven by an octupole, or, at an higher perturbation order, also by a sextupole). In action-angle co-ordinates, the potential becomes $U = K_3 J^2 \cos^4 \phi$. Writing $\cos^4 \phi = (\cos 4\phi + 4 \cos 2\phi + 3/2)/16$, and averaging close to resonance, using $\omega_r = 1/4$, one gets the Hamiltonian

$$\mathcal{H}(\gamma, J) = (\omega - \omega_r)J + \frac{3}{8}K_3 J^2 + \frac{K_3}{16}J^2 \cos 4\gamma . \qquad (2.53)$$

When the frequency ω is close to $1/4 \times 2\pi$, a chain of islands, with their extra fixed points, appear, consistently with Poincaré-Birkhoff theorem.

In normal accelerator operations, these islands reduce the dynamic aperture and, close to separatrices, cause the onset of chaotic motion. When a resonance is crossed due to small, undesired variations of the magnetic field, a beam amplitude growth is observed [42], impacting beam lifetime.

We can also consider systems with two degrees of freedom, where a resonant condition is found between the x and y frequency, i.e. $m\omega_x - n\omega_y \approx \ell$. In that case, the Hamiltonian assumes the form

$$\mathcal{H}(\phi_x, \phi_y, J_x, J_y) = \omega_x J_x + \omega_y J_y + \alpha(J_x, J_y) + U_{m,n} \cos(m\phi_x - n\omega_y + \ell\theta) . \qquad (2.54)$$

Only difference resonances ($m > 0$, $n > 0$) are stable, although they couple the motion between the two planes (it is possible to reduce the Hamiltonian to one degree of freedom), while sum resonances (when m and n have different signs) result in unstable motion. We will discuss the non-linear difference resonances more deeply, using Normal Form Hamiltonians in Chapter 8.

In general, the possible 1D and 2D resonances (up to order 4) are represented by lines in the (ω_x, ω_y) diagram of Fig. 2.3, where different colors show the resonance order. As higher-order resonances are generally weaker, one should select the accelerator working point quite far from the main resonances. Furthermore, it is possible to cancel the effect of some resonances by introducing super-periodicities in the accelerator magnetic lattice.

<p style="text-align:center">⋯⊛⋯</p>

Transverse non-linear effects in accelerator, whose theoretical description we did briefly report, have been experimentally observed and measured at Fermilab Tevatron [31] and at the Indiana university IUCF cooler ring [60]. However, the focus of these studies was the *observation* of these effects — they detected amplitude detuning and were able to distinguish stable resonant islands
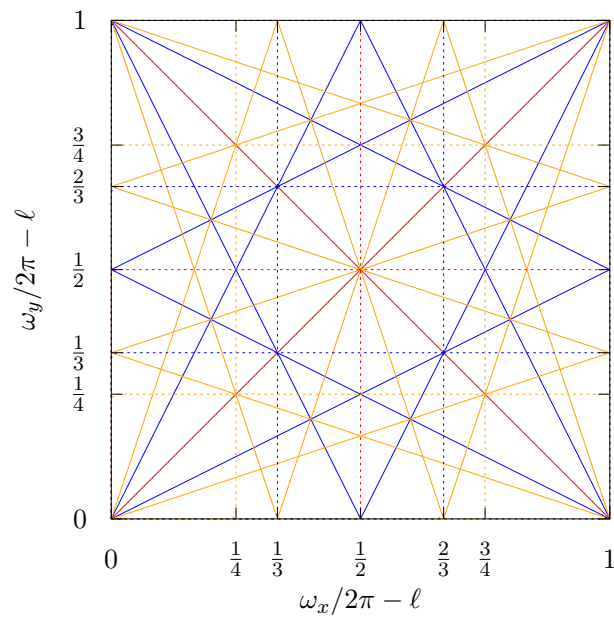
FIGURE 2.3 – Resonance diagram in the (ω_x, ω_y) space up to order 4. The same scheme is repeated for every integer ℓ. Dashed lines represent 1D resonances while continuous lines are for 2D resonances. Colours encode resonance order: red for order 2, blue for order 3 and orange for order 4.

in the particles' phase space. We want to go further: we want to *exploit* non-linear effects, as we will discuss in the next chapter. But first, we need to open a digression on the two possible methods to describe transverse motion, both in the linear and in the non-linear case: the Hamiltonian approach and the method of symplectic transfer maps.

2.5 | Hamiltonian models and transfer maps

An alternative way to look at transverse motion in an accelerator is using transfer maps. In general, the effect of each magnetic element on the phase co-ordinates (x, x', y, y') of the beam can be written, in an analogy with geometrical optics, as the action of a 4×4 matrix on the co-ordinate vector. This matrix, of course, corresponds to the symplectic flow of the Hamiltonian for a given magnetic field. When considering non-linear fields, the one-kick approximation is employed (i.e. it is assumed that the magnetic element located at $s = s_0$ act with a $\delta(s - s_0)$ potential). Of course, this method simplifies the numerical tracking of particles, reducing it to matrix multiplication instead of integrating differential equations.

When interested in the Poincaré map at each passage of the particle at a given value of s, the one-turn map is computed. When only linear effects are present, in the normalized co-ordinates $\hat{\mathbf{z}} = (\hat{x}, \hat{p}_x, \hat{y}, \hat{p}_y)$ the Hamiltonian is just an harmonic oscillator and its phase flow from turn n to turn $n + 1$ is given by

$$\begin{pmatrix} \hat{x} \\ \hat{p}_x \\ \hat{y} \\ \hat{p}_y \end{pmatrix}_{n+1} = \begin{pmatrix} \cos \omega_x & \sin \omega_x & 0 & 0 \\ -\sin \omega_x & \cos \omega_x & 0 & 0 \\ 0 & 0 & \cos \omega_y & \sin \omega_y \\ 0 & 0 & -\sin \omega_y & \cos \omega_y \end{pmatrix} \begin{pmatrix} \hat{x} \\ \hat{p}_x \\ \hat{y} \\ \hat{p}_y \end{pmatrix}_{n} . \tag{2.55}$$

Now, it is straightforward to extend this linear evolution $\hat{\mathbf{z}}' = R(\omega)\mathbf{z}$ to the case when a single non-linear element in the one-kick approximation in $s = s_0$, which results in the addition of a non-linear contribution $\mathbf{f}(\hat{\mathbf{z}})$ to the rotation. Now, the magnetic force is given by the gradient of the potential A_s. This results in the map

$$\begin{pmatrix} \hat{x} \\ \hat{p}_x \\ \hat{y} \\ \hat{p}_y \end{pmatrix}_{n+1} = R(\omega_x, \omega_y) \begin{pmatrix} \hat{x} \\ \hat{p}_x + \operatorname{Re} \sum_r \frac{K_r + i J_r}{r!} (\hat{x} + i\sqrt{\beta}\hat{y})^r \\ \hat{y} \\ \hat{p}_y - \operatorname{Im} \sum_r \frac{K_r + i J_r}{r!} (\hat{x} + i\sqrt{\beta}\hat{y})^r \end{pmatrix}_{n} . \tag{2.56}$$

where the values of the β functions (which also appear in the definitions of K_r, J_r) are evaluated at $s = s_0$.
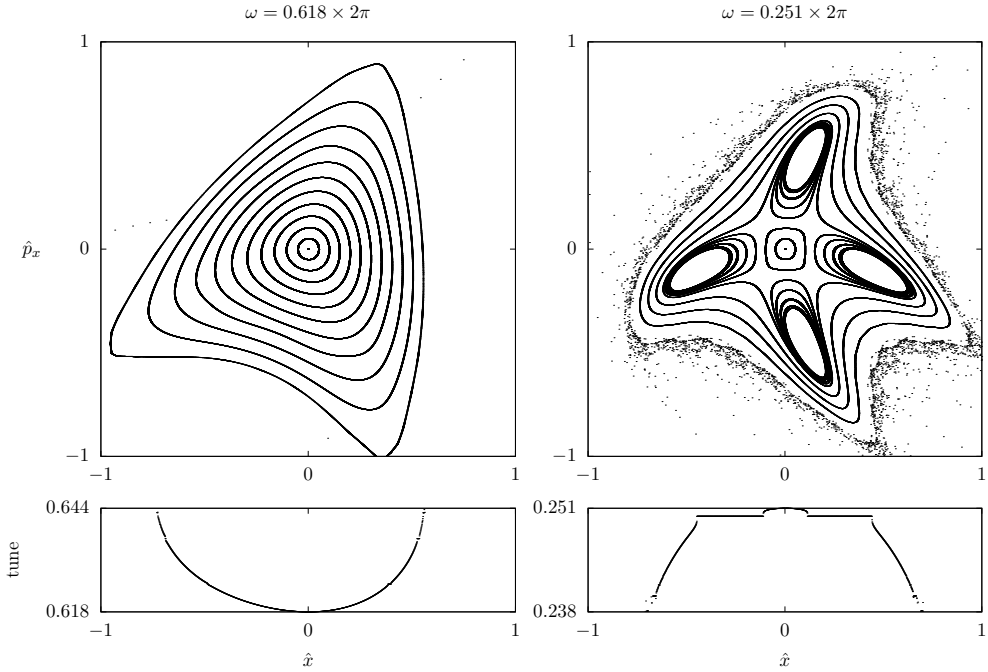
FIGURE 2.4 – Up: Phase space portrait $(\hat{x}, \hat{p}_x)$ of the map in Eq. 2.58 for two values of ω. Bottom: tune evaluated by FFT for particles at initial conditions $(\hat{x}_0 = \hat{x}, \hat{p}_{x,0} = 0)$.

We define, in general, maps of the form

$$\begin{pmatrix} \hat{\mathbf{x}} \\ \hat{\mathbf{p}} \end{pmatrix}_{n+1} = R(\omega) \begin{pmatrix} \hat{\mathbf{x}} \\ \hat{\mathbf{p}} + \mathbf{f}(\hat{\mathbf{x}}) \end{pmatrix}_n \tag{2.57}$$

to be *Hénon-like maps*, after the well-known map introduced in Ref. [44]:

$$\begin{pmatrix} \hat{x} \\ \hat{p}_x \end{pmatrix}_{n+1} = R(\omega) \begin{pmatrix} \hat{x} \\ \hat{p}_x + \hat{x}^2 \end{pmatrix}_n . \tag{2.58}$$

In the accelerator language this map would model a flat beam under a linear lattice with frequency ω with a normal sextupolar kick with normalised strength $K_2 = 2$. This model, although very simple, already shows all the peculiar effects that are suffered by a beam under non-linear magnetic fields: a finite dynamical aperture (with the onset of chaotic motion close to separatrices), an amplitude-dependent detuning and the presence of island chains close to resonance, such as shown in Fig. 2.4, where two phase spaces for Hénon map are shown at two different frequencies: far from resonance ($\omega = 0.618 \times 2\pi$), and close to resonance ($\omega = 0.251 \times 2\pi$), together with the tune measured on a line of initial

condition at the given value of x and $p_x = 0$. From the plots close to resonance 4, it is possible to observe that the tune inside islands is "locked" at the resonant value.

It should be noted that first-order perturbation-averaged Hamiltonians with a sextupolar term did not capture the amplitude-detuning effect nor the islands' chains at resonance of order other than 3. When dealing with maps, the perturbation theory is done via Normal Forms. Using this formalism, it is possible to obtain non-resonant, resonant or quasi-resonant interpolating Hamiltonians which capture all non-linear properties of the motion. The theory of Normal Forms applied to Hénon-like maps is presented in [17].

The description of beam manipulations using separatrix crossing in modulated map models requires that the adiabatic theory is applied to discrete mapping where the varying parameters are dependent on the turn number n. The presence of non-linear resonances in the map results in the existence of a cutoff value of the adiabatic parameter under which the adiabatic invariance of the action does not hold any more (details are found in the Appendix of Ref. [14]). These extra conditions on the adiabatic invariance justifies the interest we put in Part II when dealing with non-linear manipulation in performing numerical simulations using models of transverse dynamics in terms of Hénon-like maps.

3 | Multi-Turn Extraction

A number of undesired phenomena due to to non-linear effects in the transverse dynamics were listed in the previous chapter (Section 2.4). The diagram in Fig. 2.3 is useful as a reference to choose the accelerator tunes to be far enough from strong resonances. Yet it is not true that non-linear resonances are always unwanted effects in transverse motion: they indeed can serve useful purposes.

Exploiting resonant effects to manipulate beam geometry is exactly the topic of this thesis. However, employing stable resonant islands to obtain peculiar effects on the beam geometry is not a complete novelty.

The predecessor we are referring to is the Multi-Turn Extraction (MTE) method used to extract beams from the Proton Synchrotron (PS) machine to the Super Proton Synchrotron (SPS) in the CERN accelerator chain, in which for the first time non-linear stable islands are used to split the beam into five beamlets.

The MTE process has undergone all the stages, from the theoretical formulation to the experimental evidence, until becoming a routine operation in PS/SPS. We shall therefore spend some pages describing its motivation, the theory behind it, and some of its experimental and operational history.

3.1 | From PS to SPS. Continuous transfer.

Despite the widespread popularity of the Large Hadron Collider and its grand-scale particle physics experiments, the LHC is not the only accelerator present at CERN. Other circular machines, which have historically been the flagships of CERN, are now employed as pre-acceleration stages leading beams to LHC, or to dedicated experimental areas. This is the case of the Proton Synchrotron, the 628 m, 26 GeV first synchrotron built in 1959 at CERN, and the 6.9 km, 450 GeV Super Proton Synchrotron, which entered into service in 1976.

Beams for fixed-target experiments at the SPS are extracted from the PS
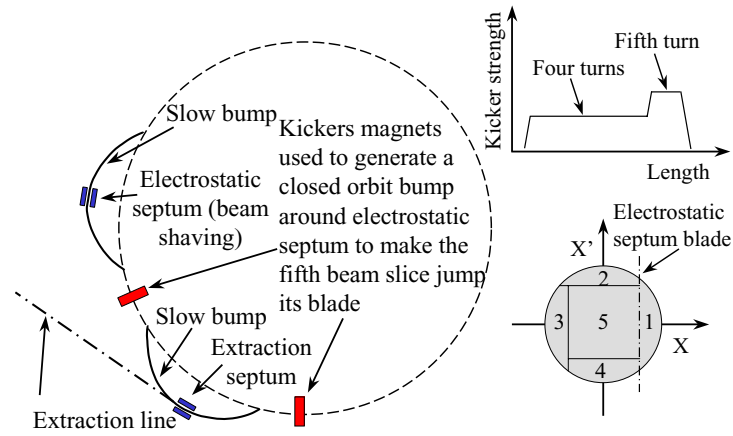
FIGURE 3.1 – Left: schematic layout of PS configuration for Continuous Transfer. Top right: kicker strength as function of time. Bottom right: phase space diagram with beam slicing. Image courtesy of M. Giovannozzi.

when they reach a momentum $14\,\text{GeV}\,c^{-1}$, and are then injected into the SPS. Now, to extract a beam from an accelerator, there exist, essentially, two methods:

(a) *fast extraction*, when the beam is completely ejected during one turn using a fast dipole magnet (kicker) and a magnetic septum, and subsequently transferred into the subsequent machine;

(b) *slow extraction*, when an unstable third-order resonant condition is employed to cause particles to increase amplitude, and follow the hyperbolic dynamic to be collected outside the machine.

With slow extraction one can extract the beam over million of machine turns, and it is used to deliver a precise amount of particles to targets for physics experiments or medical applications.

However, in some cases, a *multi-turn* extraction method can be used. This is the solution which has always been employed in PS→SPS transfer for fixed-target experiments. In fact, SPS is longer 11 times PS, which means that it can be filled using ten pulses of PS, each one extracted by fast extraction — with an empty slot which is reserved for the injection kicker rising time. But if the goal is to reduce the SPS filling time a different method can be devised. If the PS beam is divided into five beamlets, two PS pulses could fill SPS. This is the idea behind the Continuous Transfer (CT) scheme [25]. The continuous transfer scheme was used to deliver the high-intensity proton beam needed for the CERN to Gran Sasso neutrinos experiment.

In this scheme (see Fig. 3.1), two bumps in the closed orbit are generated by slow dipoles with the goal to move the beam close to the foil of the electrostatic septum and the blade of the magnetic one. After this, kicker magnets are employed to generate a bump which, at each turn, moves the beam close to the septum. Setting the kicker strength appropriately, a 20% fraction of the beam is shaved off by the septum, and, after moving around 3/4 of the PS ring, it enters the magnetic septum that deflects it into the transfer line. During one turn, as the PS horizontal tune is set at $\omega_x = 6.25 \times 2\pi$, the beam rotates by $\pi/2$, and a second section of the beam is shaved off and extracted. This is repeated four times, until, at the fifth turn, with a higher-strength kick, the remaining beam in the core is extracted from the accelerator. Although convenient for a fast PS→SPS transfer, the CT scheme had some important drawbacks. First of all, beam losses, especially close to the septum, are unavoidable, and they can account up to $\approx 15\%$ of the beam and are spread around a large fraction of the PS circumference, thus posing serious issues of irradiation. [7] Furthermore, the extracted slices have different optical parameters from the core beam, causing, once injected into SPS what is called as a *betatronic mismatch*, which results in an emittance blow-up. Finally, the transverse emittance is not the same in each extracted slice.

3.2 | Resonant MTE: theory

A method to overcome these issues was proposed in 2002 [29] by R. Cappi and M. Giovannozzi. The initial observation is that, in an Hénon map with a frequency close to resonance $\omega \approx 2\pi (p/q)$, a chain of q Poincaré-Birkhoff islands appears. While adiabatically changing ω, the area and position of the islands are changed and separatrix crossing theory allows for certain particles to be trapped into the islands. At the end of the process, starting with a Gaussian beam distribution in the center of the phase space, a consistent fraction of particles will be moved into the islands, and transported far from the centre, resulting in a transverse beam splitting between the core and the islands. If resonance 4 is used, the beam can be split into five different beamlets (four islands and the core) to be extracted as in CT, but without employing any mechanical action.

The model taken into consideration in the original MTE paper is an Hénon-like map which models the horizontal transverse motion in a circular accelerator with tune ω with a non-linear contribution in the single-kick approximation of a sextupole and a octupole (with coefficients K_2 and K_3):

$$\begin{pmatrix} \hat{x} \\ \hat{p}_x \end{pmatrix}_{n+1} = R(\omega) \begin{pmatrix} \hat{x} \\ \hat{p}_x + \frac{K_2}{2}\hat{x}^2 + \frac{K_3}{3}\hat{x}^3 \end{pmatrix}_n . \tag{3.1}$$
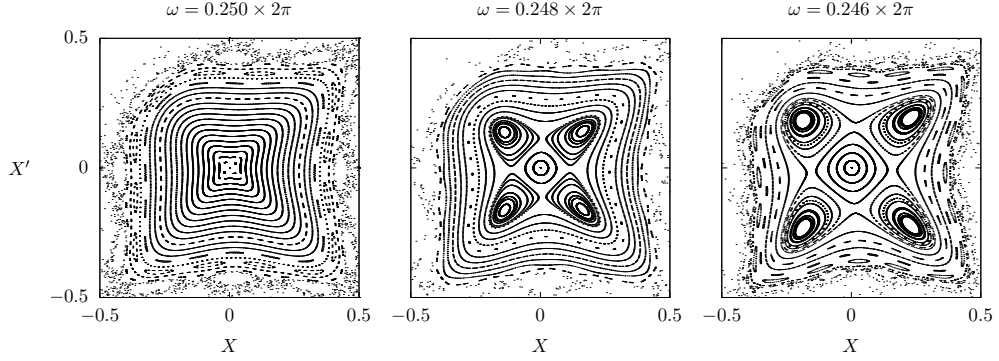
FIGURE 3.2 – Phase space portraits of Eq. 3.3 with $\kappa = -2$ at three values of ω. Note that the islands grow as ω moves further from resonance.

It is convenient to recast the map in rescaled co-ordinates $(X,\, X') = \lambda\,(\hat{x},\, \hat{p}_x)$ introducing

$$\lambda = \frac{K_2}{2}\,, \qquad \kappa = \frac{2K_3}{3K_2^2}\,. \tag{3.2}$$

The map becomes

$$\begin{pmatrix} X \\ X' \end{pmatrix}_{n+1} = R(\omega) \begin{pmatrix} X \\ X' + X^2 + \kappa X^3 \end{pmatrix}_n\,. \tag{3.3}$$

Close to the fourth-order resonance, the phase space presents the characteristic four-island structure (Fig. 3.2). The main parameters of the islands are found from Normal Form analysis [17] and they are: the estimates of the fixed points action J_+, the distance between separatrices Δ, the island surface A_{isl} and the secondary frequency inside islands ω_{sec}. Having defined the distance from resonance $\delta = \omega - \pi/2$, we have

$$\rho_+ = \frac{\delta}{\Omega_2 + 2\delta|u_{0,3}|}\,, \qquad \Delta = 4\sqrt{\left|\frac{\delta u_{0,3}}{\Omega_2}\right| J_+^2}\,, \tag{3.4}$$

$$A_{\mathrm{isl}} = 4\Delta\,, \qquad\qquad \omega_{\mathrm{sec}} = 4|\Omega_2|\Delta\,,$$

where

$$\Omega_2 = -\frac{1}{16}\left(3\cot\frac{\omega}{2} + \cot\frac{3\omega}{2}\right) - \frac{3}{8}\kappa\,, \qquad u_{0,3} = \frac{ie^{i\omega}}{16}\left(\cot\frac{\omega}{2} - \cot\frac{3\omega}{2} - 2\kappa\right). \tag{3.5}$$

and the equation for the separatrices in action-angle variables

$$J_{\text{sep}}^{\pm}(\phi, \delta) = \frac{-\lambda \pm 2\sqrt{\dfrac{|u_{0,3}|\delta^3 \cos^2 2\phi}{2\delta|u_{0,3}| - \Omega_2}}}{\Omega_2 + 2\delta|u_{0,3}|\cos 4\phi} \; . \tag{3.6}$$

It is easily seen from these formulae that, as δ increases, the islands' area grows proportionally, at first order, to δ and they are transported out from the center, as their distance from the origin is also proportional to δ (one should remember while expanding for δ that the values of Ω_2 and $u_{0,3}$ in Eq. (3.5) are also dependent on δ through ω). According to separatrix crossing theory, the islands will trap particles. A simulation of the evolution of a beam distribution under the action of Eq. 3.3 is shown in Fig. 3.3.

In this model, beam losses are reduced to zero. Furthermore, the islands have all the same optical parameters, this resulting in a better betatronic matching and in the four island beamlets having all the same emittance.

A discussion on the adiabatic trapping in islands and their relation with the adiabaticity parameter $\epsilon = \delta/N$ for the MTE map is found in Ref. [14].

Given a generic stable resonance q, with the quasi-resonant Normal Form Hamiltonian

$$\mathcal{H} = \delta J + \frac{\Omega_2}{2}J^2 + A(\delta)J^{q/2}\cos q\phi \, , \tag{3.7}$$

it can be proven that the adiabatic condition holds if $\epsilon \ll \omega_{\text{sec}}^2$. As the secondary frequency ω_{sec} reads

$$\omega_{\text{sec}} = \left(\frac{A}{\Omega_2}\right)^{1/2}\left(\frac{\delta}{\Omega_2}\right)^{q/4} \tag{3.8}$$

and the distance of the fixed point from center is $\rho_0 \sim \sqrt{\delta/\Omega_2}$, it follows that the quasi-resonant conditions is met if $\epsilon \ll \rho_0^q/\Omega_2$. This results in the existence of a minimum trapping radius R_{min} which must be proportional to $\varepsilon^{1/q}$.

Moreover, we can take into account the exceptional set of particles that, being too close to the hyperbolic point, do not experience separatrix crossing. Its measure is given by $K\sqrt{\epsilon/\omega_{\text{sec}}^2}$. Therefore, if the tune modulation is performed between $\delta = \delta_0$ and $\delta = \delta_1$, particle will be trapped into islands only in the range $[\delta_{\text{min}}, \delta_1]$, where

$$\pi R_{\text{min}}^2 = \int_0^{2\pi} \mathrm{d}\phi \, J_{\text{sep}}^+(\delta_{\text{min}}, \phi) \, , \tag{3.9}$$

which, approximating for small values of R_{min}, gives $\delta_{\text{min}} \sim \epsilon^{2/q}$.
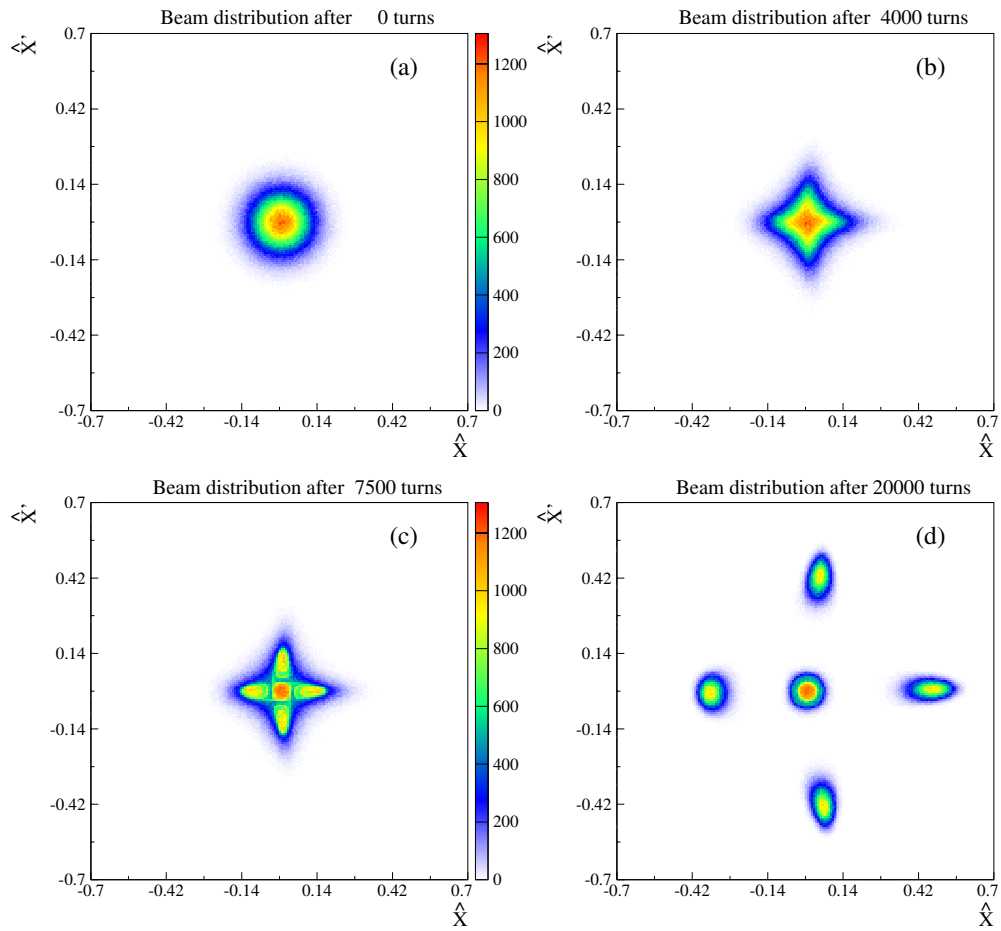
FIGURE 3.3 – Simulation of the Multi-turn extraction process of Eq. (3.3) with $\kappa = -2$. Image from [28] licensed under CC-BY 3.0. The complete animation is available at URL https://ab-project-mte.web.cern.ch/Documentation/Movies/ct5t.gif.

The fraction τ of particles trapped into islands reads

$$\tau = \int_{\delta_{\min}}^{\delta_1} d\delta \, \rho(J(\delta)) \frac{\Theta_{\text{isl}}}{\Theta_{\text{cen}}} \left[1 - K \frac{\sqrt{\epsilon}}{\omega_{\text{sec}}} \right], \qquad (3.10)$$

where $\rho(J(\delta))$ is the normalized distribution of particles' trapping action, $\Theta_{\text{isl}} = dA_{\text{isl}}/d\delta$ and Θ_{cen} the same for the area of the central region. As $\omega_{\text{sec}} \sim \delta^{3/2}$, the dependency of the integral on ϵ can be written as

$$\tau = c_0 + c_1 \epsilon^{1/2} + c_2 \epsilon^{1/2 - 1/q} . \qquad (3.11)$$

For resonance $q = 4$, the expression for τ becomes

$$\tau = c_0 + c_1 \epsilon^{1/2} + c_2 \epsilon^{1/4} . \qquad (3.12)$$

The parameters c_0, c_1 and c_2 can be used to fit the simulated data from Eq. (3.3).

3.3 | MTE from experiment to operational routine and beyond

In 2006 [37] the resonant MTE beam splitting method received its first experimental confirmation in PS. The employed machine scheme is shown in Fig. 3.4, where a sextupole and a octupole are used to generate the kick while tune is controlled modulating quadrupole strengths. The evidence of splitting is obtained with a wire scanner. This device, used to measure the transverse beam profile, consists in a thin ($\approx 50\,\mu\text{m}$) carbon wire which is moved through the beam. Secondary particles which are generated from the interaction between the beam and the wire therefore generate a current in the wire which is measured, and is proportional to the number of particles present in the beam at a given position.

The beam profile measured by the wire scanner is then fitted as the sum of five Gaussian distributions, one for the core and for each island. The result is shown in Fig. 3.5.

Optimizing over the octupole strength, the best results of the 2006 experiment showed a 18% trapping fraction in each of the island beamlets (to be confronted with the desired 20% for perfect 5-fold splitting) and with losses accounting only to 2%–3% of the beam intensity, mainly due to longitudinal effects, with a great improvement w.r.t. CT.

In 2008, new experiments were made to evaluate the feasibility of splitting crossing resonances 3 and 5 in the PS [34]. In the same time, MTE started

Section 54

Section 55

Flying wires

Section 64

Sextupole magnets

Section 71

Kicker magnet

Octupole magnets

Section 21

Section 20

Slow bump

Extraction
septum

Extraction line

Section 16
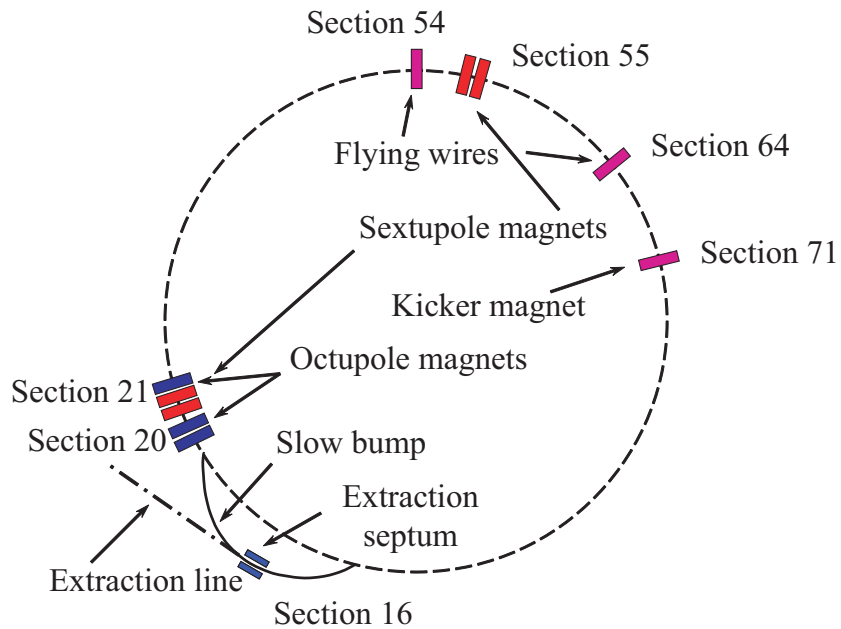
FIGURE 3.4 – Schematic diagram of PS configuration for Multi-turn Extraction experiments. Image from [37], licensed under CC-BY 3.0.
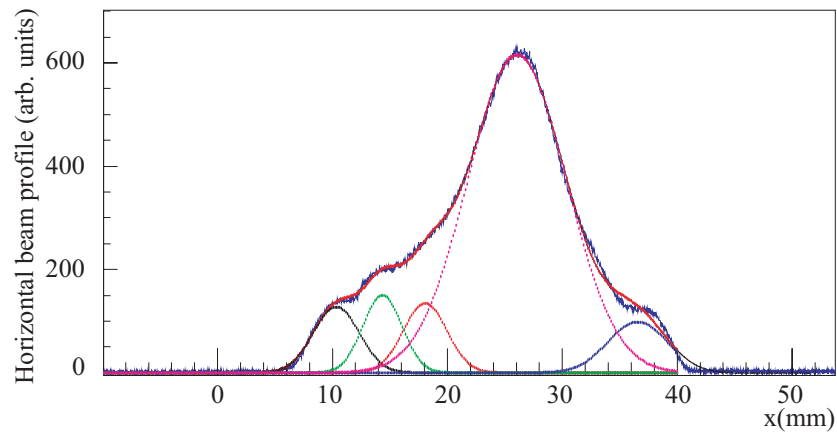
FIGURE 3.5 – Measured beam profile in PS after MTE resonant beam splitting. A fit of the data is presented using the sum of five normal distributions, one for the core and one for each of the islands. Image from [37], licensed under CC-BY 3.0.

commissioning phase. Bunched beams were used and, in some cases, sent to SPS.

In 2010, a short MTE operational period followed. Some issues appeared, as the irradiation increase in the extraction region (due to the longitudinal beam structure), and in general the trapping efficiency and extraction trajectories result showed poor reproducibility. Therefore, in the two following years, studies continued to find physical observables which were correlated with the trapping. Intensity-dependent effects were observed [38]. The irradiation increase problem was solved using a dummy septum, and MTE entered the final commission stage.

In 2015, thirteen years after the first theoretical formulation, MTE was officially made operational, replacing the old extraction scheme and became the operational beam manipulation at the Proton Synchrotron [24, 48, 50] for beams to be used in fixed-targets experiments at the SPS.

Some proposals of extending the MTE principle to other manipulations have also been made. For example, one could time-reverse MTE to perform a multi-turn *injection*, coalescing the islands into the core. [29, 39] Another possibility is to perform a 4-fold splitting using resonance 4 in an unstable condition to completely deplete the core. [40]

This thesis, in Chapter 4, will deal with some new proposed extension of Multi-turn extraction to achieve beam splitting, exploring the possibility of islands trapping in an Hénon-like map, where the tune is kept fixed, and an oscillating kick is inserted, whose frequency is modulated to cross a resonance with the tune. Furthermore, some preliminary results are shown in a double-resonant condition, with a MTE-like scheme in which the tune crosses resonance and an oscillating external exciter is itself in resonance with the main frequency.

It is clear that MTE is the main source of inspiration for the transverse beam shaping effects investigated in the present work, as it represents a successful example of moving the study of non-linear effects from the simple world of mathematical models to the harsh reality of accelerator operations.

Before ending this chapter, we would like to mention another possibility for extending MTE beyond its current domain. So far, the non-linear effects have been considered in the framework of Hamiltonian theory, which corresponds to considering the motion of protons in a circular accelerator. As it is well known, protons do not suffer from dissipative phenomena such as radiation damping or quantum excitation (at least if the beam energy does not exceed few TeV). On the other hand, the dynamics of lepton rings is intrinsically dependent on such dissipative effects. In spite of this intrinsic difficulty, exporting the non-linear techniques is an interesting and fruitful domain of research. Not only, some performance improvements could be brought by these novel techniques, but even the theory would need some new developments. Although

this field is still in rapid development, we would like to mention the work on theoretical and numerical aspects [35, 66], as well as experimental studies [41, 55, 67, 79] that have been carried out so far.

Part II

Beam manipulations

4 | Resonant beam splitting with oscillating exciters

The first beam manipulation we explore is the possibility to achieve beam splitting trapping into resonance islands, as done in MTE, without changing the accelerator tune. Instead of exciting a "natural" resonance of the accelerator (i.e., a frequency commensurable to 2π), an oscillating magnetic device whose frequency is modulated close to a resonant condition with the tune still generates, according to Poincaré-Birkhoff theorem, an island chain into which it is possible to control beam trapping. The oscillating magnet is, in general, a multipole magnet (a dipole, a quadrupole, a sextupole...) which is fed with AC current, generating an oscillating magnetic field.

This would be useful to extend the possibility to perform an efficient beam trapping into stable islands even when the unperturbed frequencies of the system cannot be modulated, e.g. in the case of a circular particle accelerator where the presence of space charge effects imposes a special choice of linear tunes, making MTE "exportable" also to machines different from PS.

Therefore, in this Chapter, we consider the problem of obtaining an accurate estimate of the resonance-trapping efficiency and of the phase-space transport for a given distribution of initial conditions in the case of polynomial symplectic maps when a time-dependent periodic perturbation is present. The perturbation frequency and amplitude are adiabatically changed. We show that the concept of interpolating Hamiltonian can be applied to derive the scaling laws of the main parameters of the map, i.e. the perturbation amplitude, and the non-linearity coefficients. In this way, we obtain explicit analytical estimates for the trapping and transport efficiencies, thus generalizing the analytical results obtained for Hamiltonian systems. The accuracy of the proposed estimates has been verified by means of extensive numerical simulations of different study cases. Furthermore, we study the limits of the adiabatic approximation for the observed phenomena, and of the validity of our results. The modulation of the external perturbation parameters is realized according to procedures that could be feasible on accelerator elements, opening the way to novel transverse

beam manipulations experiments.

The Chapter is organized as follows: after having recalled some theoretical results of the adiabatic theory that are needed to measure the resonance-trapping phenomenon, we introduce the map- and Hamiltonian-based models in Section 4.1. In Section 4.2 we perform a detailed analysis of the phase-space evolution during the trapping process, whereas in Section 4.3 we discuss the results of detailed numerical simulations about the evolution of a particle distribution, comparing the dynamics of the interpolating Hamiltonian with that of the corresponding symplectic maps. In Section 4.4, a more complex model is presented and discussed to show that in spite of its features, the theory works well in generic systems. Finally, some conclusions are drawn in Section 4.5, and some detailed computations of the the perturbation-theory calculations for a Hamiltonian system with a time-dependent exciter and the minimum action for which trapping occurs are reported in Appendix 4.A, and 4.B, respectively.

<p style="text-align:center">⟡</p>

The possibility to extend beam splitting using an oscillating exciter reduces to the study of the adiabatic trapping in area-preserving maps when a time-modulated external sinusoidal term is introduced in the dynamics. We consider a forcing term with amplitude proportional to q^m, $m \in \mathbb{N}$, $m \geq 1$, and a frequency which is adiabatically changed to cross a resonance with the unperturbed frequency of the system. This external forcing mimics the effect of a transverse kicker on the charged particle dynamics in a circular accelerator (see, e.g. [22, 71, 87–89, 91] and references therein).

We recall the results on slowly modulated Hamiltonian systems that have been resumed in Sections 1.5 and 1.6. As the modulation of the Hamiltonian changes the shape of the separatrices in phase space, the trajectories can cross separatrices and enter into different stable regions that are associated with non-linear resonances. The probability of the separatrix crossing, which is described by a random process in the adiabatic limit, can be computed as well as the change of adiabatic invariant due to the crossing. [73, 76].

The adiabatic trapping into resonances has been studied in a number of different works [76, 78] to show the possibility of transport in phase space when some system's parameters are slowly modulated. In this case, Poincaré–Birkhoff theorem (Section 1.4) can be applied to prove the existence of stable islands in phase space. On the other hand, an extension of the results of adiabatic theory to quasi-integrable area-preserving maps needs to be considered, where probabilities of Eq. (1.49) still describe the capture of particles which lie in the center of the phase space into the resonance islands [14]. Properties of islands for polynomial Hénon-like maps are found in [17].

4.1 | Models: Map and Hamiltonian

We consider a Hénon-like symplectic map of the form

$$\mathcal{M}_{\ell,m} : \begin{pmatrix} q_{n+1} \\ p_{n+1} \end{pmatrix} = R(\omega_0) \begin{pmatrix} q_n \\ p_n - \sum_{j>2} k_j q_n^{j-1} - q_n^{\ell-1} \varepsilon_{\mathrm{m}} \cos \omega n \end{pmatrix}, \qquad (4.1)$$

where $R(\omega_0)$ is a rotation matrix of an angle ω_0, n is the iteration number, $\ell \in \mathbb{N}$, and the dynamics is perturbed by a modulated kick of amplitude ε_{m} whose frequency ω is close to a resonance condition $\omega = m\omega_0 + \delta$, $\delta \ll 1$. We remark that when $\ell = 1$, the fixed point at the origin of the unperturbed system becomes an elliptic periodic orbit of period $2\pi/\omega$, and the linearized frequencies depend on the perturbation strength, so that they are adiabatically modulated. This is not the case when $\ell \geq 2$, which is also interesting for applications. We shall consider explicitly these two cases.

The Birkhoff Normal Form theory allows to establish a relationship between the map of Eq. (4.1) and the Hamiltonian [17]

$$\mathcal{H}_{\ell,m}(p, q, t) = \omega_0 \frac{q^2 + p^2}{2} + \sum_{j>2} \hat{k}_j \frac{q^j}{j} + \varepsilon_{\mathrm{h}} \frac{q^\ell}{\ell} \cos \omega t \qquad (4.2)$$

In particular, from Eq. (4.1) we can derive the Normal Form Hamiltonian

$$\hat{\mathcal{H}}_{\ell,m}(\hat{J}, \hat{\theta}) = \omega_0 \hat{J} + \sum_{j>2} \Omega_{j-1}(k_j) \hat{J}^{\frac{j-1}{2}} + \varepsilon_{\mathrm{m}} c_{\ell,m} \hat{J}^{m/2} \cos(m\hat{\theta} - \omega t), \quad (4.3)$$

where $\Omega_j(k_j)$ are detuning terms, obtained from the non-resonant Normal Form, while $c_{\ell,m}$ is the Fourier component of the mth harmonic, which is the only one remaining when $\omega \approx m\omega_0$. We remark that the dependence of Ω_{j-1} on the k_j is in the form of a polynomial, and the scaling laws have been derived in [17]. For instance, in the case of Ω_2 one has $\Omega_2 = a k_3^2 + b k_4$, where

$$a = -\frac{1}{16} \left[3 \cot\left(\frac{\omega_0}{2}\right) + \cot\left(\frac{3\omega_0}{2}\right) \right]. \qquad (4.4)$$

If the Hamiltonian (4.2) is averaged on the resonance, one obtains an expression of the same form as Eq. (4.3), i.e.

$$\mathcal{H}_{\ell,m}(J, \theta) = \omega_0 J + \sum_{j>2} \frac{\omega_{j-1}(\hat{k}_j)}{2} J^{\frac{j-1}{2}} + \varepsilon_{\mathrm{h}} c_{\ell,m} J^{m/2} \cos(m\theta - \omega t), \quad (4.5)$$

where we have the same $c_{\ell,m}$ Fourier coefficient that appears from the expansion of $\cos^\ell \theta \cos \omega t$ on the resonant harmonic, and ω_J is a polynomial function of the k_j.

From these two expressions, it is possible to evaluate the relation between the corresponding parameters, i.e. k_j, $\hat{k}_j$ and ε_{m}, ε_{h}, which enables applying the analytical results valid for the Hamiltonian system to the corresponding polynomial symplectic map of the form (4.1).

Let $(\hat{J}, \hat{\theta})$ be the action-angle variables for the map defined by the perturbation series. The frequency of the angle dynamics can be written in the form [17]

$$\Omega(\hat{J}) = \omega_0 + \sum_{j>2} \Omega_{j-1}(k_j)\, \hat{J}^{\frac{j-1}{2}} \,, \tag{4.6}$$

while from the Hamiltonian (4.2), which is expressed in terms of the action-angle variables (J, θ), we obtain

$$\left\langle \frac{\partial \mathcal{H}_{\ell,m}}{\partial J} \right\rangle_\theta = \omega_0 + \sum_{j>2} \omega_{j-1}(\hat{k}_j)\, J^{\frac{j-1}{2}} \,, \tag{4.7}$$

where $\langle \ \rangle_\theta$ stands for the average over the variable θ.

If a single detuning term of order j is considered and a single term k_l is present in the system under study, and $\Omega_{j-1} = \Omega_{j-1,0}k_l^r$ (and similarly for ω_{j-1}), then one can assume that $k_l = \hat{k}_l$ and only the action variables need to be re-scaled to ensure the same frequency variation with action for the two systems under consideration. If $\hat{J} = \kappa\, J$, then from the expression

$$\omega_0 + k_l^r\, \Omega_{j-1,0}\, \kappa^{\frac{j-1}{2}}\, J^{\frac{j-1}{2}} = \omega_0 + k_l^r\, \omega_{j-1,0}\, J^{\frac{j-1}{2}} \tag{4.8}$$

we derive

$$\kappa = \left(\frac{\omega_{j-1,0}}{\Omega_{j-1,0}} \right)^{\frac{2}{j-1}} \,. \tag{4.9}$$

In the more general case in which several detuning terms are considered, but a single term k_l is present, we have $\Omega_{j-1}(k_l) = k_l^{r_{l,j}}\Omega_{j-1,0}$ (and similarly for $\omega_{j-1}(k_l)$). The approach consists of re-scaling $\hat{k}_l = \kappa_{l,j}k_l$ instead of the action, which would then give the solution

$$\kappa_{l,j} = \left(\frac{\omega_{j-1,0}}{\Omega_{j-1,0}} \right)^{1/r_{l,j}} \,, \tag{4.10}$$

thus making the frequency variation the same for both systems also in this case.

For $\ell = 1$ and $m = 3$, the outlined approach gives

$$\kappa = \frac{\omega_{2,0}}{\Omega_{2,0}} \,, \tag{4.11}$$

and we still need to match the strength of the time-dependent perturbation, which is proportional to $\varepsilon_{\mathrm{m}} c_{1,3} \hat{J}^{3/2} = \varepsilon_{\mathrm{m}} c_{1,3} \kappa^{3/2} J^{3/2} = \varepsilon_{\mathrm{h}} c_{1,3} J^{3/2}$, so that

$$\frac{\varepsilon_{\mathrm{h}}}{\varepsilon_{\mathrm{m}}} = \left(\frac{\omega_{2,0}}{\Omega_{2,0}}\right)^{3/2}. \tag{4.12}$$

In the numerical simulations, we set $k_3 = 1$ and $\omega_0/(2\pi) = 0.1713$, finding $\varepsilon_{\mathrm{h}}/\varepsilon_{\mathrm{m}} \approx 3.92$ from the computation of the Fourier coefficient $c_{1,3}$ by means of the perturbation theory, which is found in Appendix 4.A).

Performing analogous computations for $\ell = 2$ and $m = 3$ (see Appendix 4.A), the coefficient $c_{2,3}$ can be computed and by comparing it with the corresponding coefficient $c_{1,3}$ for the case $\ell = 1$ one determines the different scale of the perturbation strength in the two cases, namely

$$\frac{c_{1,3}}{c_{2,3}} = \frac{19}{62}\frac{k_3^2}{\omega_0}. \tag{4.13}$$

According to the parameters used in the simulations ($k_3 = 1$ and $\omega_0/2\pi = 0.1713$) we obtain $c_{1,3}/c_{2,3} = 0.284$, and the values of ε_{h} are the same order of magnitude for the two cases. We thus expect comparable results for the resonance-trapping phenomenon.

4.2 | Analysis of the trapping process

The numerical studies carried out to analyze the phenomenology of the trapping process have been performed with the map model of Eq. (4.1) as well as the Hamiltonian of Eq. (4.2) in order to establish conditions under which the adiabatic resonance trapping for the modulated symplectic map can be described by the analytical results for Hamiltonian systems in a neighborhood of the elliptic fixed point.

The main aspect relevant for applications is to investigate which initial conditions are trapped in the resonance and transported in phase space. For this purpose, we determine whether a trajectory is in the resonance islands of the frozen map, relying on the result that the main Fourier component of an orbit in a $n-$resonance island corresponds to the resonant tune $1/n$. We used high-accuracy algorithms for the computation of the main Fourier component [8, 58] to perform the correct identification of the trapped orbits. In Fig. 4.1 (left) we show an example of the main frequency for a set of orbits with initial conditions of the form $(q_0, 0)$ whose evolution under the Hamiltonian model (4.2) is evaluated by freezing the time dependence of the system parameters (the corresponding phase-space portrait is shown in the right plot of Fig. 4.1). A
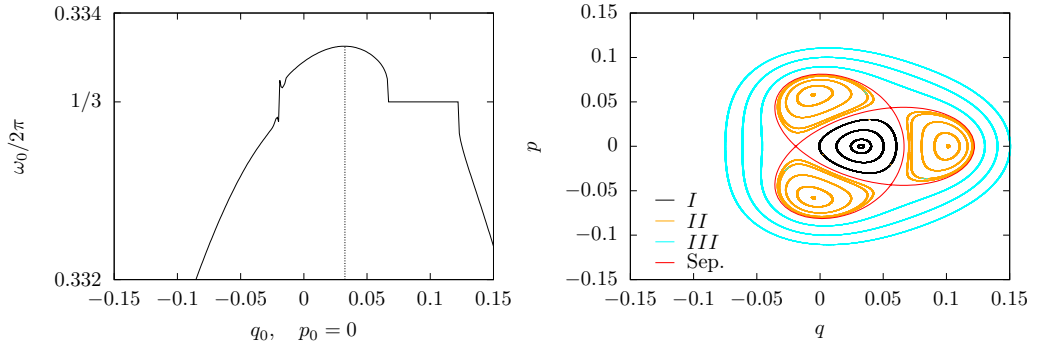
FIGURE 4.1 – Left: Frequency $\omega_0/(2\pi)$ evaluated with a high-accuracy FFT algorithm [8, 58] for an ensemble of orbits with initial conditions $(q_0, 0)$ whose orbits are computed using the same model and parameters of the right plot. When the initial conditions are inside the resonance islands, the frequency is locked to the value $1/3$. Right: Phase-space portrait of the Poincaré map of the Hamiltonian $\mathcal{H}_{1,3}$ (4.2) evaluated at $\omega t = 2k\pi$, $k \in \mathbb{N}$, for $\omega_0/(2\pi) = 0.1713$, $k_3 = 1$, $\varepsilon_h = 0.28$, $\omega = 2.995\,\omega_0$.

dependence of the main frequency as a function of q_0 is clearly visible. Note also that the region of constant frequency corresponds to the so-called phase-locking, which occurs when the dynamics is inside a stable island. A sudden jump in frequency can be observed at $q_0 = 0.066$, which corresponds to an initial condition on the hyperbolic fixed point.

In the following, the concept of trapping fraction will be used in view of studying and qualifying the efficiency of trapping protocols. Given a distribution of initial conditions, the trapping fraction is defined as the ratio of the trapped particles to those in the initial distribution. It is clear that the definition depends on the distribution selected for the initial conditions. For our analysis, it is important to record the original and final regions of the particles: this is made by defining the symbol $\tau_{a \to b}$, where a stands for the region (or regions) from which the initial conditions are taken and b stands for the region in which they are trapped. We remark that the definition of the region from which particles are taken or trapped is based on the phase-space topology (such as that visible in Fig. 4.1), at the end of the first stage of the trapping protocol described in the next section.

4.2.1 | Hamiltonian models

To study the phase space of the Hamiltonian of Eq. (4.2), it is convenient to use the Poincaré map (see the right plot of Fig. 4.1 for an example of phase-space portrait). When either ε_h or ω are changed, the separatrices move in

phase space changing the enclosed area, while keeping the same topology for ε_h sufficiently small and ω sufficiently close to the resonance. To describe the phenomenology, the third-order resonance is selected, but the concepts used can be generalized to any resonance order.

According to [76], when the system parameters are adiabatically modulated, the trapping of the orbits into the stable islands and the adiabatic transport are possible. To optimize the trapping probability, we propose a protocol divided into two steps. In the first one, the perturbation frequency ω is kept constant at a value $\omega_i < m\,\omega_0$, near the mth-order resonance, while the exciter is slowly switched on, increasing its strength ε_h from 0 to the final value $\varepsilon_{h,f}$. In the second stage, the exciter strength is kept fixed at $\varepsilon_{h,f}$, and the frequency is modulated from ω_i to ω_f. Both modulations are performed by means of a linear variation in N time steps.

In the first step, as ε_h increases, the area of the resonance islands increases, thus trapping all orbits that cross the separatrix according to Eq. (1.49). The phase space can be divided in three regions (see Fig. 4.1, right): the inner region (Region I) encloses the origin and is limited by the inner part of the separatrices, the resonance region (Region II) made of the stable islands, and the outer region (Region III) from the outer part of the separatrix to infinity. The areas of Region I and II are shown in Fig. 4.2 as a function of the exciter strength ε_h (left) and the distance from the resonance $\delta = 3\,\omega_0 - \omega$ (right).
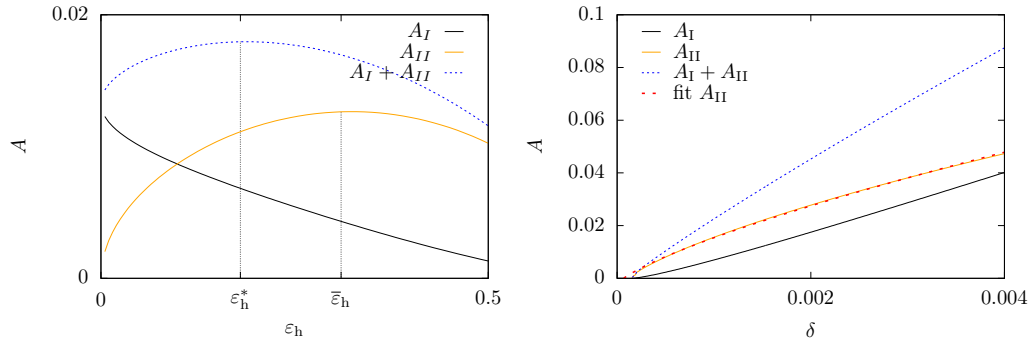
FIGURE 4.2 − Left: Areas of Region I (black), Region II (orange) and of their sum (blue, dotted) as a function of the exciter strength ε_h, for $k_3 = 1$, $\omega_0/(2\pi) = 0.17133$, $\omega = 2.995\,\omega_0$ for $\mathscr{H}_{1,3}$. The sum of the areas has a maximum at ε_h^* whereas A_{II} has a maximum at a different point $\overline{\varepsilon}_h$. Right: Areas of Region I (black), Region II (orange) and of their sum (blue, dotted) as a function of the distance from the resonance $\delta = 3\,\omega_0 - \omega$ with $k_3 = 1$, $\omega_0/(2\pi) = 0.17133$, $\varepsilon_h = 0.28$ for the Hamiltonian $\mathscr{H}_{1,3}$. A_{II} is fitted as $\alpha\delta^{3/4} + \beta$ (red, dashed line) according to the predictions in [17].

We remark that A_I is always decreasing with ε_h, whereas A_{II} is increasing up
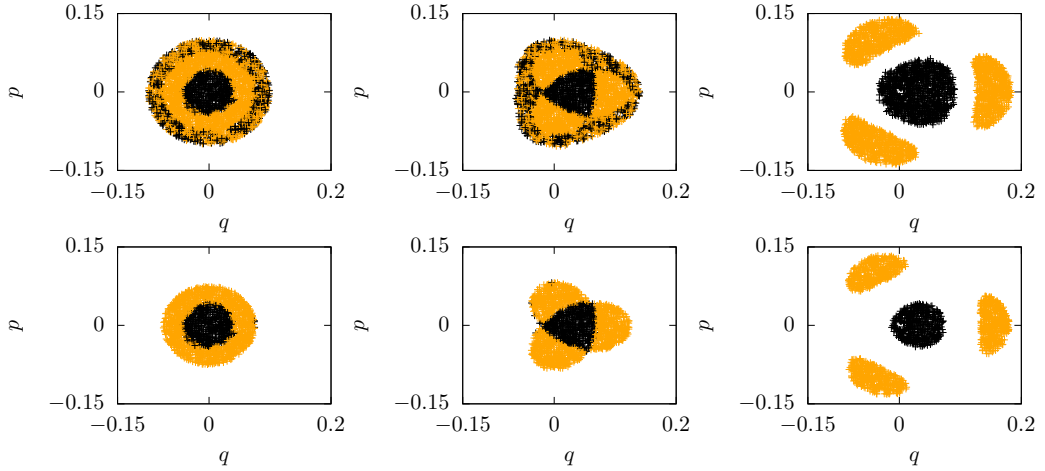
FIGURE 4.3 — Evolution of an ensemble of particles in phase space with the colours used to identify in which region each initial condition has been trapped into (Region I, black, and Region II, orange) for the Hamiltonian model (4.2) with $\ell = 1$, $m = 3$ at the beginning of the process (left column), at the end of the ε_h variation (mid column) and at the end of the frequency variation (right column). The difference between the top and bottom cases is the extent of the distribution of initial conditions: in the top case, some initial conditions are in Region III, while this is not the case for the bottom case. At large amplitudes, initial conditions can be either trapped in Region I or II in the top case, while this is absent in the bottom case. Parameters: $k_3 = 1$, $\omega_0/(2\pi) = 0.17133$, $\omega_i = 2.995\,\omega_0$, $\omega_f = 2.983\,\omega_0$, $\varepsilon_{h,f} = 0.28$.

to $\varepsilon_h = \overline{\varepsilon}_h$. Therefore, since $A_I + A_{II}$ has a maximum at $\varepsilon_h^* < \overline{\varepsilon}_h$, the Region III area is increasing when $\varepsilon_h > \varepsilon_h^*$.

In the case of an ensemble of initial conditions chosen in Region I, for $\varepsilon_h < \varepsilon_h^*$ adiabatic theory ensures that every orbit crossing the inner separatrix is trapped in the resonance, i.e. in Region II. When $\varepsilon_h^* < \varepsilon_h < \overline{\varepsilon}_h$, as both Region II and III areas are increasing, a fraction of orbits will enter into Region III according to Eq. (1.49). These observations are essential for engineering the variation of the system parameters in order to control the trapping and transport phenomena, which is essential for devising successful applications. An example of the behavior described above is shown in Fig. 4.3 in which the evolution of a set of initial conditions under the dynamics generated by $\mathcal{H}_{1,3}$ using the protocol for trapping and transport described above is shown.

Both rows show the evolution of an ensemble of initial conditions under the same dynamics generated by $\mathcal{H}_{1,3}$ and the colors are used to indicate which region the initial conditions are trapped into. The trapping and transport phe-

nomena are clearly visible, thus indicating that the proposed protocol works efficiently. Between the two rows, the distribution of initial conditions is changed. In the top row, the larger amplitude of the initial conditions is such that an annulus exists in which the initial conditions can be trapped either in Region I or II. On the other hand, the smaller extent of the initial distribution in the bottom row removes this phenomenon and there is a clear separation between particles that will be trapped in Region I or II. We remark also that the initial conditions at large amplitude in the top row contribute to a larger surface of the transported islands and core.
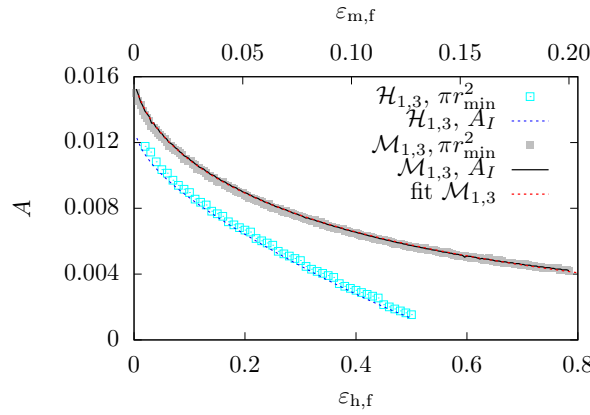
FIGURE 4.4 – Comparison of the minimum enclosed area of trapped orbits and A_{I} at the end of the first stage, i.e. the linear variation of the exciter strength, as a function of $\varepsilon_{\mathrm{h,f}}$, for $\mathscr{H}_{1,3}$ with $k_3 = 1$, $\omega_0/(2\pi) = 0.17133$, $\omega = 2.995\,\omega_0$, and for the corresponding map $\mathscr{M}_{1,3}$. A model o $A_I(\varepsilon_{\mathrm{m}}) = a + f(\varepsilon_{\mathrm{m}}, b, \varepsilon_0)\varepsilon_{\mathrm{m}}^{-2/3}$ fit for $\mathscr{M}_{1,3}$ is presented, where $f(\varepsilon_{\mathrm{m}}, b, \varepsilon_0)$ is a form factor $(f(\varepsilon_{\mathrm{m}}, b, \varepsilon_0) = b/[1 + (\varepsilon_0/\varepsilon_{\mathrm{m}})^{2/3}])$. The dynamics of $\mathscr{H}_{1,3}$ has been simulated using $N = 10^6$ time steps.

According to adiabatic theory [76], all particles whose orbit encloses an area A at the end of the first stage satisfying $A_{\mathrm{I}}(\varepsilon_{\mathrm{h,f}}) < A < A_{\mathrm{II}}(\min(\varepsilon_{\mathrm{h}}^*, \varepsilon_{\mathrm{h,f}}))$ will be trapped in the resonance, whereas the particles with $A < A_{\mathrm{I}}(\varepsilon_{\mathrm{h,f}})$ will remain in Region I. Furthermore, assuming that the orbits in the excluded region are very close to the origin, we can estimate the average distance from the origin at which the resonance trapping occurs by $r_{\min} = \sqrt{A_{\mathrm{I}}(\varepsilon_{\mathrm{h,f}})/\pi}$. Figure 4.4 shows the remarkable agreement between the minimum enclosed area of the trapped orbits and the final area A_{I} as function of $\varepsilon_{\mathrm{h,f}}$.

If $\varepsilon_{\mathrm{h,f}} > \varepsilon_{\mathrm{h}}^*$, the particles that enclose an area A satisfying $A_{\mathrm{II}}(\varepsilon_{\mathrm{h,f}}) < A < A_{\mathrm{II}}(\varepsilon_{\mathrm{h}}^*)$ will be found in the external Region III at the end of the first stage. Therefore, the distribution of initial conditions around the origin can be di-

vided in three parts: the part close to the origin that remains in Region I, the part trapped in the resonance i.e. in Region II, and the part that is or enters into Region III.

During the second phase, the exciter's frequency is varied to move the resonance in phase space and thus performing the adiabatic transport of the trapped initial conditions. As shown in Fig. 4.2 (right), both Region I and II increase their area so that no further trapping of orbits close to the origin nor any detrapping from the resonance region are expected. Conversely, the orbits in Region III will enter either Region II or I according to the probabilities of Eq. (1.49) that are calculated at the time when the separatrix crossing occurs [76].

We remark that for the systems under consideration, the dependence of A_i on the system parameters is so smooth that approximating the λ derivatives of A_i at the time of the actual separatrix crossing, which is needed to compute the trapping probabilities, with a finite difference is an excellent approximation.

The situation is radically different when one considers $\mathcal{H}_{2,3}$ as it can be seen in Fig. 4.5, where the areas of the center (Region I) and of the islands (Region II) are shown as a function of ε_{h}.
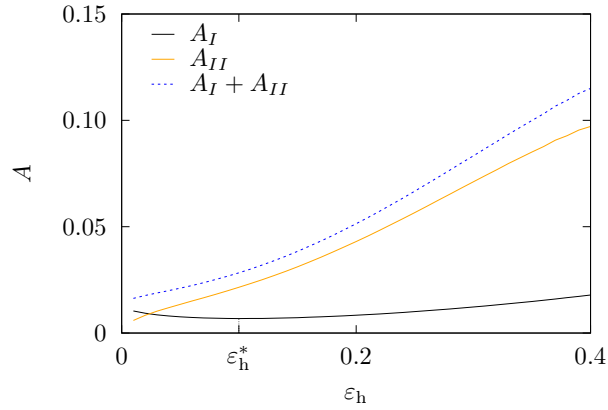
FIGURE 4.5 – Areas of the center (black), islands (orange) areas, and their sum (blue, dotted) as a function of ε_{h} with $k_3 = 1$, $\omega_0/(2\pi) = 0.17133$, $\omega = 2.995\,\omega_0$ for $\mathcal{H}_{2,3}$.

Indeed, in this case, A_{I} is decreasing only for a small interval of ε_{h} around zero, and then it increases, while A_{II} increases monotonically, similarly to the sum of the two areas. This implies that there is no possibility for trapping in Region III. Furthermore, the initial conditions in Region III will be trapped either in Region I or II according to Eq. (1.49).
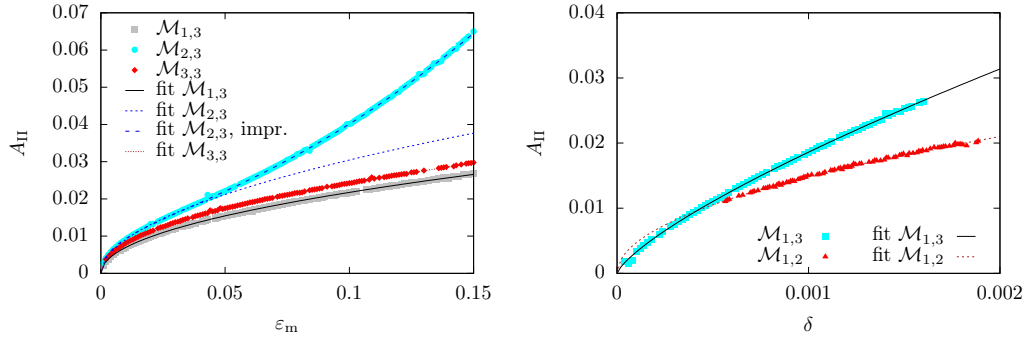
FIGURE 4.6 – Values of A_{II} for $\mathcal{M}_{\ell,m}$ as a function of ε_m (left) and δ (right) and their power-law fits, $A_{II} \propto \varepsilon_m^{1/2}\delta^{m/4}$, to compare with the prediction in [17]. For $\mathcal{M}_{2,3}$, the improved fit from Eq. (4.21) is also shown (left).

4.2.2 | Map models

To investigate the same phenomena using the map (4.1) we need to provide an appropriate framework that allows determining the areas of the various regions as done for the Hamiltonian models.

We remark that A_{II}, inspected for different models $\mathcal{M}_{\ell,m}$ follows the scaling laws $A_{II} \propto \varepsilon^{1/2}$ and $A_{II} \propto \delta^{n/4}$ outlined in [17]. In fact, if we assume that close to a hyperbolic fixed point with action-angle coordinates (J_h, θ_h), we can approximate the motion using the pendulum-like Hamiltonian

$$\mathcal{H}_{\ell,m}(\overline{J}, \theta) = \frac{\partial^2 \mathcal{H}_{\ell,m}}{\partial J^2}\bigg|_{J=J_h} \frac{\overline{J}^2}{2} + b J_h^{m/2} \cos m\theta \,, \tag{4.14}$$

where b is proportional to ε_m, $\overline{J} = J - J_h$, and A_{II} reads

$$A_{II} = \frac{8}{\left|[\partial^2 \mathcal{H}_{\ell,m}/\partial J^2]_{J=J_h}\right|^{1/2}} b^{1/2} J_h^{m/4} \,, \tag{4.15}$$

and since $J_h \propto \delta$, we obtain

$$A_{II} \propto \varepsilon_m^{1/2}\delta^{m/4} \,. \tag{4.16}$$

This scaling law is shown in Fig. 4.6, where the numerical evaluation of A_{II} is compared with the scaling law (4.16) as a function of ε_m (left) and δ (right).

Figure 4.6 (left) shows clearly that the fit $A_{II} = \alpha\varepsilon_m^{1/2}$ fails for large values of ε_m for $\mathcal{M}_{2,3}$. We remark that the Hamiltonian of Eq. (4.14) is approxi-

mated, hence a better estimate of A_{II} can be found by starting from the following Hamiltonian i.e.

$$\mathscr{H}_{\ell,m}(\overline{J}, \theta) = \left.\frac{\partial^2 \mathscr{H}_{\ell,m}}{\partial J^2}\right|_{J=J_{\mathrm{h}}} \frac{\overline{J}^2}{2} + \varepsilon_{\mathrm{m}}(J_{\mathrm{h}} + \overline{J})^{3/2} \cos 3\theta\,, \qquad (4.17)$$

and approximating the coefficient of the resonant term with the first-order series expansion in $\overline{J}$, which gives

$$\mathscr{H}_{\ell,m}(\overline{J}, \theta) = \left.\frac{\partial^2 \mathscr{H}_{\ell,m}}{\partial J^2}\right|_{J=J_{\mathrm{h}}} \frac{\overline{J}^2}{2} + b J_{\mathrm{h}}^{3/2} + \frac{3}{2} b J_{\mathrm{h}}^{1/2} \overline{J} \cos 3\theta\,. \qquad (4.18)$$

The area enclosed by the separatrix is then given by the integral

$$A_{\mathrm{II}} = A_{\mathrm{II},0} \int_0^{2\pi} \mathrm{d}\theta \, \sqrt{k^2 \cos^2 \theta - \cos \theta + 1}\,, \qquad (4.19)$$

where $A_{\mathrm{II},0}$ is the value of A_{II} given in Eq. (4.15), while $k^2 = 2b/\left(9\,\Omega_2\,J_h^{1/2}\right)$, i.e. $k \propto \varepsilon_{\mathrm{m}}^{1/2}$. The expansion of (4.19) reads [69]

$$A_{\mathrm{II}} = A_{\mathrm{II},0}\left(1 + \frac{15\sqrt{2} - 5}{24} k^2 - \frac{1}{4} k^2 \log k\right) + O(k^2)\,, \qquad (4.20)$$

which corresponds to a dependence, in ε_{m}

$$A_{\mathrm{II}} = c_0 \varepsilon_{\mathrm{m}}^{1/2} (1 + c_1 \varepsilon_{\mathrm{m}} + c_2 \varepsilon_m \log \varepsilon_m)\,, \qquad (4.21)$$

where c_0, c_1 and c_2 can be determined via a fitting process. This estimate, shown in Fig. 4.6 (left) as "improved fit", is in good agreement with the $\mathscr{M}_{2,3}$ data.

In Fig. 4.4, we see the excellent agreement between the minimum radius for which the trapping occurs, and the area of Region I at the end of the first phase of the modulation for the map model, which is a further indication of the validity of the proposed approach. This is also confirmed by the results shown in Fig. 4.7, where the fraction of particles trapped in Region II from Region III is shown for different $\mathscr{M}_{\ell,m}$ models as a function of $\varepsilon_{\mathrm{m,f}}$. The predictions from Eq. (1.49) are also shown and a very good agreement is observed. Moreover, in Fig. 4.4 we show that a fit function of the form $A_I(\varepsilon_{\mathrm{m}}) = a + f(\varepsilon_{\mathrm{m}}, b, \varepsilon_0)\varepsilon_{\mathrm{m}}^{-2/3}$ fits well the data for A_I, where $f(\varepsilon_{\mathrm{m}}, b, \varepsilon_0)$ is a form factor that tends to a constant value for large values of ε_{m}, and that reads

$$f(\varepsilon_{\mathrm{m}}, b, \varepsilon_0) = \frac{b}{1 + (\varepsilon_0/\varepsilon_{\mathrm{m}})^{2/3}}\,. \qquad (4.22)$$

This model is fully consistent with the analysis of the minimum trapping action presented in Appendix 4.B. We remark that the approach presented in the Appendix finds, as estimate of the minimum trapping action, the action of the hyperbolic fixed point. This is proportional to the area of the central region only when it is small i.e. at large values of the perturbation parameter ε. For smaller values, the relationship between action of the fixed point and area of the central region is no longer linear, which explains the form of the fit function used.
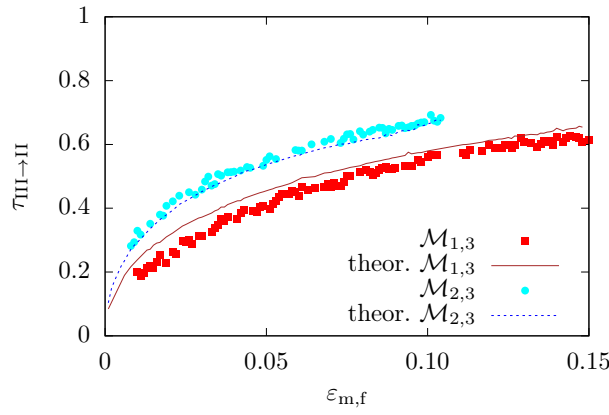
FIGURE 4.7 – Comparison between the fraction of initial conditions in Region III and trapped in Region II as a function of $\varepsilon_{\mathrm{m,f}}$, as computed with numerical simulations (markers) or using Eq. (1.49) (lines) for $\mathcal{M}_{1,3}$ and $\mathcal{M}_{2,3}$. Note that the derivatives of the areas are estimated considering the finite difference for $\omega_{\mathrm{i}} = 2.995\,\omega_0$ and $\omega_{\mathrm{f}} = 2.983\,\omega_0$ having set $k_3 = 1$, $\omega_0/(2\pi) = 0.1713$.

4.3 | Comparison of Hamiltonian and map models

Extensive numerical simulations have been performed to evaluate the fraction τ of initial conditions trapped into islands as a function of various parameters both for the map and Hamiltonian models, for various types of exciters and resonances. The sets of initial conditions are uniformly distributed and are characterized by a maximum radius R, i.e. with a p.d.f.

$$\rho_R(q_0, p_0) = \frac{1}{\pi R^2} \qquad \text{with } q_0^2 + p_0^2 \le R^2 \,. \tag{4.23}$$

4.3.1 | Case $\ell = 1, m = 3$

We compare the Hamiltonian dynamics generated by $\mathcal{H}_{1,3}$, whose equations of motion are numerically integrated via the 4th-order symplectic Candy algorithm [27], and the map $\mathcal{M}_{1,3}$, for the same scenario where perturbation amplitude and frequency are changed one at a time. For all our simulations, $k_3 = 1$, $\omega_0/(2\pi) = 0.1713$. For simplicity, the same number of iterations has been selected to increase linearly the strength of the exciter and its frequency during the modulation stages. The process is implemented with $\omega/(2\pi) = \omega_{\rm i}/(2\pi) = 0.5132 = 2.995\,\omega_0/(2\pi)$ and $\omega_{\rm f}/(2\pi) = 0.5112 = 2.983\,\omega_0/(2\pi)$. When not differently stated, we set the number of integration time steps for the Hamiltonian at $N_{\rm h} = 1.2 \times 10^6$, as this value ensures that the modulation is slow enough to achieve adiabatic conditions.

In Fig. 4.8 we show the dependence of trapping on the adiabatic parameter $\epsilon = 1/N_{\rm m}$, where $N_{\rm m}$ is the number of iterations of the map, for the $\mathcal{M}_{1,3}$ and $\mathcal{H}_{1,3}$ models. For the Hamiltonian case, the number $N_{\rm h}$ of time steps has been rescaled according to $N_{\rm m} = N_{\rm h}/\nu$, where ν is the number of time steps, for $\varepsilon_{\rm h} = 0$, needed to rotate an initial condition by an angle ω_0 in phase space.
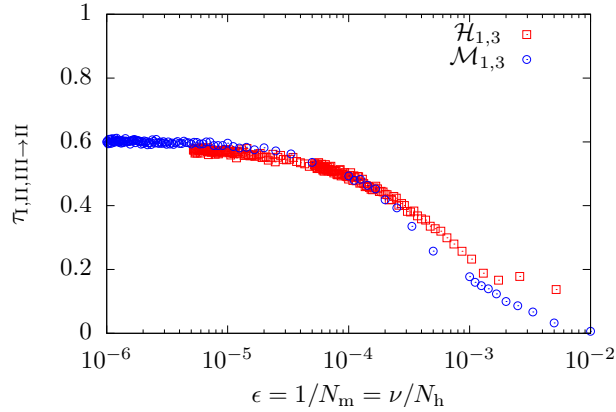
FIGURE 4.8 − Trapping fraction as a function of the adiabatic parameter ϵ for the Hamiltonian $\mathcal{M}_{1,3}$ and $\mathcal{H}_{2,3}$ for $\omega_0/(2\pi) = 0.1713$. As initial condition, a uniform distribution with $R = 0.1$ has been used, having set $\varepsilon_{\rm m,f} = 0.05$ and $\varepsilon_{\rm h,f} = \kappa^{3/2}\varepsilon_{\rm m,f} = 0.196$. The excellent agreement between map and Hamiltonian models in the adiabatic regime is clearly visible.

There is a visible excellent agreement in terms of trapping fraction for the map and Hamiltonian models in the adiabatic regime, i.e. when $\epsilon \ll 1$, with a slight worsening when ϵ increases.

In Fig. 4.9 we plot the trapping fraction as a function of $\varepsilon_{\rm h,f}$ for the Hamil-
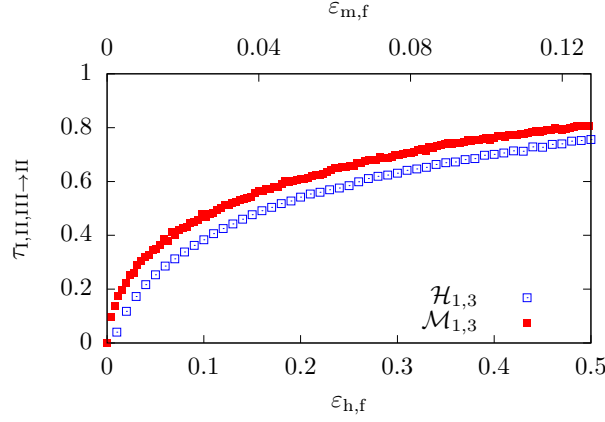
FIGURE 4.9 – Trapping fraction of the Hamiltonian $\mathcal{H}_{1,3}$ as a function of $\varepsilon_{h,f}$ (red markers) and map $\mathcal{M}_{1,3}$ as a function of $\varepsilon_{m,f}$ (blue markers), for initial uniform distribution with $R = 0.1$. The two perturbation strengths are compared via the scaling $\varepsilon_{m,f} = \kappa^{3/2}\varepsilon_{h,f}$ according to Eq. (4.12). Note the same functional behavior of the trapping for the two models, which feature only an offset.

tonian model and for the map, both for a uniform circular initial distribution with $R = 0.1$. The two models can be compared in re-scaling the two perturbation strengths via the ratio $(\omega_2/\Omega_2)^{3/2}$ according to Eq. (4.12). The graphs describing the evolution of the trapping function are showing the same function dependence on the strength of the exciter, with only an offset between the two curves.

4.3.2 │ Case $\ell = 2, m = 3$

Similar studies have been carried out using a quadratic perturbation q^2 in the Hamiltonian, namely

$$\mathcal{H}_{2,3} = \omega_0\left(\frac{p^2}{2} + \frac{q^2}{2}\right) + \frac{k_3}{3}q^3 + \varepsilon_h\frac{q^2}{2}\cos\omega t \qquad (4.24)$$

and the corresponding map

$$\mathcal{M}_{2,3}: \quad \begin{pmatrix} q_{n+1} \\ p_{n+1} \end{pmatrix} = R(\omega_0)\begin{pmatrix} q_n \\ p_n + k_3 q_n^2 + \varepsilon_m q\cos\omega n \end{pmatrix}. \qquad (4.25)$$

In this case the mechanism of adiabatic trapping is the same, but the behavior of the areas of phase-space regions are quite different (as discussed previously) so that there are important consequences for applications.

In Fig. 4.10 the dependence of the trapping fraction on $\varepsilon_{h,f}$ is shown for two values of the radius of the initial uniform distribution. The impact on the trapping fraction is clearly visible. Indeed, if $\varepsilon_{h,f}$ is not too small, A_I and A_{II} are both increasing. Hence, if the radius of the initial distribution is reduced, the fraction of particles that remains in Region I is high. Moreover, after the central area starts growing, trapping into resonance is not possible anymore, and the trapping fraction saturates. The saturation value depends on the radius of the initial distribution and increases for larger values of R. Conversely, when ε_h is small, since the resonance islands are created at the origin, an initial distribution with larger radius will place more initial conditions outside of the area swept by the island structure, which prevents them from being trapped. This explains why, for lower values of ε_h, we observe a better trapping efficiency for smaller initial distributions. In the same Figure, we show that the map model presents a qualitatively similar behavior (the scaling of the perturbation strength allows to compare the two models), with a good quantitative agreement observed in the saturation region.
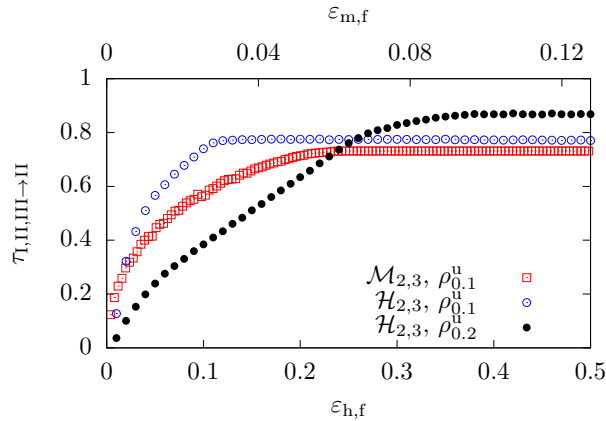
FIGURE 4.10 – Trapping fraction for $\mathscr{H}_{2,3}$ as a function of $\varepsilon_{h,f}$ (blue and black markers) and $\mathscr{M}_{2,3}$ as a function of $\varepsilon_{m,f}$ (red), for initial uniform distributions with $R = 0.1$ and $R = 0.2$. The two perturbation strengths are compared via the scaling $\varepsilon_{m,f} = \kappa^{3/2}\varepsilon_{h,f}$ according to Eq. (4.12).

We have performed numerical studies of the trapping efficiency as a function of $\varepsilon_{m,f}$ for a set of initial conditions, selected in Region I and II, whose distribution is given by ρ_R with $R = \sqrt{[A_I(\varepsilon_{m,f}) + A_{II}(\varepsilon_{m,f})]/\pi}$. In Fig. 4.11 we present a comparison between the trapping fraction computed by means of numerical simulations and the models derived for expressing the surface of

Region I and II, i.e.

$$\tau_{\text{I,II}\rightarrow\text{II}} = \frac{A_{\text{II}}(\varepsilon_{\text{m}})}{A_{\text{I}}(\varepsilon_{\text{m}}) + A_{\text{II}}(\varepsilon_{\text{m}})} \,, \tag{4.26}$$

where $A_{\text{I}} = a + f(\varepsilon_{\text{m}}, b, \varepsilon_0)\varepsilon_{\text{m}}^{-2/3}$, the factor $f(\varepsilon_{\text{m}}, b, \varepsilon_0)$ having been introduced in Eq. (4.22), and $A_{\text{II}} = c\,\varepsilon_{\text{m}}^{1/2}$. Note that the model presented in Eq. (4.26) is only valid for a uniform initial distribution. For a different radial initial distribution with p.d.f. $\rho(r)$ (the angular distribution is assumed to be uniform) we would have

$$\tau_{\text{I,II}\rightarrow\text{II}} = \frac{\displaystyle\int_{r_{\text{I}}}^{r_{\text{II}}} \mathrm{d}r\,\rho(r)}{\displaystyle\int_{0}^{r_{\text{II}}} \mathrm{d}r\,\rho(r)} \,, \tag{4.27}$$

where $r_i = \sqrt{A_i(\varepsilon_{\text{m}})/\pi}$, $i = \text{I, II}$.
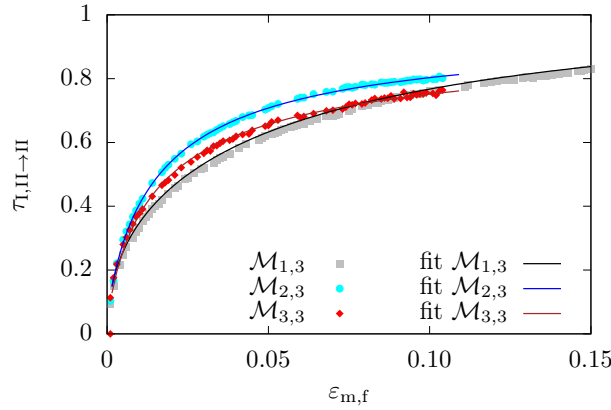
FIGURE 4.11 – Trapping fraction for the models $\mathcal{M}_{\ell,3}$, $\ell = 1, 2, 3$. Fits are presented based on Eq. (4.26), with $A_{\text{I}}(\varepsilon_{\text{m}}) = a + f(\varepsilon_{\text{m}}, b, \varepsilon_0)\varepsilon_{\text{m}}^{-2/3}$ and $A_{\text{II}}(\varepsilon_{\text{m}}) = c\varepsilon_{\text{m}}^{1/2}$, in agreement with the models reported in Figs. 4.4 and 4.6.

4.4 | A more complex model

As a last point, we have considered a more complex model in which an additional parameter has been added, namely a k_4 term in the Hamiltonian of Eq. (4.2) as well as in the map of Eq. (4.1).
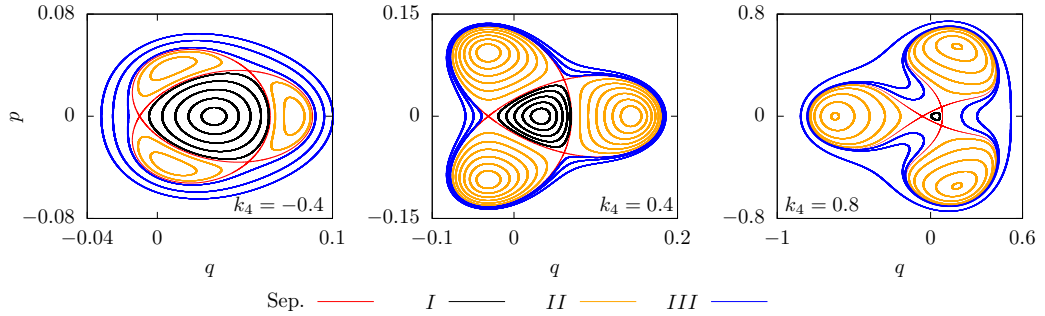
FIGURE 4.12 – Phase-space portraits for $\mathscr{H}_{1,3}$ in presence of different quartic nonlinearities k_4, having set $\omega_0/(2\pi) = 0.1713$, $\omega = 2.995\,\omega_0$, $\varepsilon = 0.28$. The portrait for $k_4 = 0$ is shown in Fig. 4.1 (right). Note the difference in scale of the three figures.

The reason for considering this case is that the phase-space topology changes considerably for different values of k_4, as can be seen in Fig. 4.12, where three phase-space portraits are shown, corresponding to three values of k_4.

Although the global topology is equivalent for all three cases, the detail is not, implying that the surface variation with time of the resonance islands might be rather different between the three considered cases. This would have an important impact on the trapping and transport phenomena.

The impact of the k_4 term on the trapping fraction has been studied by means of numerical simulations that have been performed on a model of type $\mathscr{M}_{1,3}$ and a second one of type $\mathscr{H}_{2,3}$ to assess the behavior for different types of time-dependent perturbations. The results are shown in Fig. 4.13, for the $\mathscr{M}_{1,3}$ (left) and the $\mathscr{H}_{2,3}$ (right) cases.
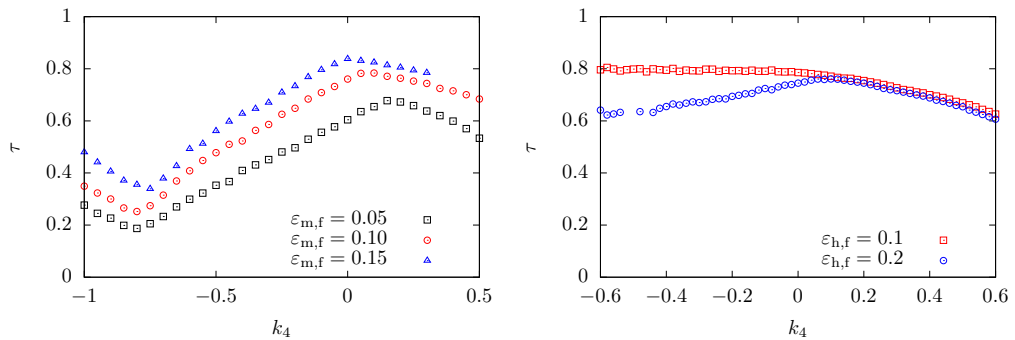
FIGURE 4.13 – Left: trapping fraction for the model $\mathscr{M}_{1,3}$ as a function of k_4. Three cases with different values of $\varepsilon_{\mathrm{m,f}}$ are shown. Right: trapping for the model $\mathscr{H}_{2,3}$ as a function of k_4. Two cases with different values of $\varepsilon_{\mathrm{h,f}}$ are shown. In all cases, the initial distribution is uniform with $R = 0.1$.

For the $\mathcal{M}_{1,3}$ model, three cases corresponding to different values of $\varepsilon_{\mathrm{m,f}}$ have been considered. A strong dependence of the trapping fraction on k_4 is clearly visible, with ε_{m} being also a parameter with a strong impact on trapping.

For the $\mathcal{H}_{2,3}$ model, a mild dependence of the trapping fraction on k_4 is observed. However, the two cases corresponding to different values of $\varepsilon_{2,3}$ behave differently as a function of k_4. For $k_4 > 0$ the two cases feature equal values of the trapping fraction, whereas for $k_4 < 0$ differences are visible.

It is worth stressing that even for this more complex model, which shows peculiar features, the trapping and transport processes have been designed using the criteria presented and discussed for the simpler models. This is an indication that the theory, developed for the basic models can also be used to interpret more general cases.

4.5 | Conclusions

In this chapter, a class of dynamical systems has been considered, in which nonlinear effects are combined with a time-dependent external exciter. This class of systems has been studied both in terms of Hamiltonian as well as using a nonlinear symplectic map. The goals of our analyses were to assess the possibility of deriving effective scaling laws for the efficiency of resonance trapping for adiabatically perturbed symplectic maps using the analytical results of adiabatic theory for Hamiltonian systems, and to identify the application of this class of systems to perform trapping and transport in phase space. Both aspects have been successfully carried out.

The comparison between Hamiltonian and symplectic map systems has been considered in detail. It has been shown that the adiabatic theory for Hamiltonian systems provides the appropriate framework to describe the trapping and transport phenomena for nonlinear symplectic maps, too. We have shown that adiabatic trapping into stable resonance islands while modulating a periodic, time-dependent perturbation, is an efficient mechanism for phase-space particle transport. A protocol to vary the two system parameters, namely, the strength and frequency of the time-dependent perturbation, has been proposed, which successfully addresses this aspect. The dynamic mechanisms occurring during the separatrix change in phase space have been understood for different models, highlighting the phase-space structure, and comparing the results of the numerical simulations with the theoretical predictions. Several scaling laws have been studied, and extensive simulations have been performed to probe the dependence of trapping and transport features as a function of the systems' parameters.

The extension of these results to realistic models, as required by physical

applications, implies considering multidimensional systems, for which the theory still needs to be fully developed. Nonetheless, the results presented in this Chapter open a road-map for a feasibility study to apply the resonance trapping induced by an external periodic perturbation in the field of particle accelerators, as a possible improvement of the novel beam manipulations that have been developed to trap beams of charged particles in a circular accelerator.

Appendices

4.A | Perturbative analysis of an Hamiltonian system with a time-dependent exciter

It is convenient to introduce the linear action-angle variables (I, ϕ) using $q = \sqrt{2I} \cos \phi$, $p = \sqrt{2I} \sin \phi$, and the Hamiltonian (4.2) reads

$$
\mathcal{H}_{\ell,m}(I, \phi) = \omega_0 I + \frac{2^{3/2} k_3}{3} I^{3/2} \sin^3 \phi \\
+ 2^{\ell/2} \varepsilon_{\mathrm{h}} I^{\ell/2} \sin^\ell \phi \cos \omega t \, . \tag{4.28}
$$

We denote by (J, θ) the action-angle variables of the unperturbed Hamiltonian, i.e. for $\varepsilon_{\mathrm{h}} = 0$, and J turns out to be the adiabatic invariant of the system when no resonance condition is fulfilled.

To study the adiabatic trapping, we compute the parametric dependence of (J, θ) from the nonlinear terms using a perturbative approach [90]. We apply the Lie transformation $\exp\big(D_{F(J, \theta)}\big)$ using a generating function

$$
F(J, \theta) = k_3^2 \sum_{m>2} J^{m/2} f_m(\theta) \tag{4.29}
$$

and we obtain a Normal Form Hamiltonian

$$
\mathcal{H}_0(J) = \omega_0 J + \sum_{m>1} \frac{\omega_m(k_3)}{m} J^m \, . \tag{4.30}
$$

The perturbative equation for $f_3(\theta)$ reads

$$f_3'(\theta) = \frac{2^{3/2}}{3\,\omega_0} \sin^3\theta \,, \qquad (4.31)$$

and it can be integrated, yielding

$$f_3(\theta) = \frac{2^{3/2}}{3\,\omega_0}\left(\frac{1}{3}\cos^3\theta - \cos\theta\right). \qquad (4.32)$$

At first order, the change of variables reads

$$
\begin{aligned}
I &= J - \frac{\partial F}{\partial\theta} + \mathcal{O}(J^2) = J - J^{3/2}k_3^2\,f_3'(\theta) + \mathcal{O}(J^2)\\
\phi &= \theta + \frac{\partial F}{\partial J} + \mathcal{O}(J) = \theta + \frac{3}{2}J^{1/2}k_3^2\,f_3(\theta) + \mathcal{O}(J)\,,
\end{aligned}
\qquad (4.33)
$$

and the ω_2 coefficient of the Normal Form Hamiltonian is the average value

$$\omega_2 = -\frac{3\omega_0}{2\pi}\int_0^{2\pi} \mathrm{d}\theta\, f_3'^2(\theta) = -\frac{5\,k_3^2}{6\,\omega_0}\,. \qquad (4.34)$$

The strength of the mth-order resonance, $\omega_0 + m\,\omega = 0$, is given by the mth Fourier coefficient of q^ℓ/ℓ, i.e.

$$c_{\ell,m} = \frac{1}{2\pi\ell}\int_0^{2\pi} \mathrm{d}\theta\, e^{im\theta}q^\ell \,, \qquad (4.35)$$

so that to study the third-order resonance ($m = 3$) with a linear forcing ($\ell = 1$), we can truncate the expansion at $J^{3/2}$, because higher-order terms in J will not have a projection on the Fourier coefficient of $\exp(\pm i3\theta)$.

The perturbation term is proportional to $q = \sqrt{2I}\sin\phi$ and setting $\eta = 2^{3/2}k_3^2/(3\,\omega_0)$ and expanding up to $J^{3/2}$, we obtain

$$
\begin{aligned}
q &= \sqrt{2I}\sin\phi\\
&= \sqrt{2}J^{1/2}(1 - J^{1/2}k_3^2\,f_3'(\theta))^{1/2}\sin\left(\theta + \frac{3}{2}J^{1/2}k_3^2 f_3(\theta)\right) + \mathcal{O}(J^2)\\
&= \sqrt{2}J^{1/2}(1 - 4\eta\,J^{1/2}\sin^3\theta - \frac{\eta^2}{8}J\sin^6\theta)\times\\
&\quad \times\left[\sin\theta + \frac{J^{1/2}\eta}{2}(\cos^4\theta - 3\cos^2\theta) +\right.\\
&\quad \left. -\frac{\eta^2 J}{8}\sin\theta(\cos^6\theta - 6\cos^4\theta + 9\cos^2\theta)\right] + \mathcal{O}(J^2)\,.
\end{aligned}
\qquad (4.36)
$$

The coefficient $[q]_{3/2}$ of the $J^{3/2}$ term reads

$$[q]_{3/2} = -\frac{\sqrt{2}\eta^2}{8} \sin\theta \left(2\cos^4\theta\sin^2\theta + \sin^6\theta - 5\cos^6\theta + 9\cos^2\theta\right), \quad (4.37)$$

and its Fourier coefficient of order 3 is

$$c_{1,3} = \frac{1}{2\pi} \int_0^{2\pi} d\theta\, e^{3i\theta} [q]_{3/2} = i\frac{57\sqrt{2}}{256}\eta^2 = i\frac{19\sqrt{2}}{96}\frac{k_3^4}{\omega_0^2}. \quad (4.38)$$

Performing analogous computations for the case $\ell = 2$ and $m = 3$, the term $q^2(\theta, J)$ can be written in the form

$$\frac{q^2}{2} = I\sin^2\phi = J\sin^2\theta + \frac{1}{2}J^{3/2}[q^2]_{3/2}(\theta) + \mathcal{O}(J^2), \quad (4.39)$$

and the Fourier coefficient of $[q^2]_{3/2}(\theta)$ is given by

$$c_{2,3} = \frac{1}{2\pi} \int_0^{2\pi} d\theta\, e^{3i\theta} \frac{[q^2]_{3/2}}{2} = i\frac{31}{32}\eta = i\frac{31\sqrt{2}}{48}\frac{k_3^2}{\omega_0}. \quad (4.40)$$

By comparing the coefficient $c_{2,3}$ with the corresponding coefficient $c_{1,3}$, one determines the different scale of the perturbation strength in the two cases, namely

$$\frac{c_{1,3}}{c_{2,3}} = \frac{19}{62}\frac{k_3^2}{\omega_0} \quad (4.41)$$

Finally, we observe that the expansion of $q(J, \theta)$ starts at $J^{1/2}$, whereas the one of $q^2(J, \theta)$ starts at J. In general, given a q^ℓ perturbation, the lowest-order term is given by $J^{\ell/2}\sin^\ell\theta$. This means that resonances with $m < \ell$ are excited by higher-order perturbation terms, so that the expected relevance for applications is considerably reduced.

We remark, that the Hamiltonian (4.28) can be analyzed using a different approach. In the new variables one obtains an approximate Hamiltonian of the form

$$\mathcal{H}_{1,3}(J, \theta) = \omega_0 J + \frac{\omega_2}{2}J^2 + \varepsilon_{\mathrm{h}} c_{1,3} J^{3/2} \cos(3\theta - \omega t), \quad (4.42)$$

and we can introduce the slow phase $\gamma = 3\theta - \omega t$ via a time-dependent generating function $G(\tilde{J}, \theta) = \tilde{J}(3\theta - \omega t)$. Setting $\delta = 3\omega_0 - \omega$ as the distance from the resonance, we have

$$\mathcal{H}_{1,3}(J,\theta) = \delta\tilde{J} + \frac{9\omega_2}{2}\tilde{J}^2 + \varepsilon_{\mathrm{h}}c_{1,3}\,3^{3/2}\,\tilde{J}^{3/2}\cos\gamma \tag{4.43}$$

and defining the parameters

$$\lambda = -\frac{4\delta}{9\,\omega_2}\,, \qquad \mu = \sqrt{\frac{2}{3}}\frac{\varepsilon_{\mathrm{h}}\,c_{1,3}}{\omega_2} \tag{4.44}$$

one obtains by rescaling the Hamiltonian

$$\mathcal{H}_{1,3}(\tilde{J},\gamma) = (2\tilde{J})^2 - \lambda\,(2\tilde{J}) + \mu(2\tilde{J})^{3/2}\cos\gamma\,. \tag{4.45}$$

The dynamics generated by this Hamiltonian can be studied, for what concerns trapping via separatrix crossing, with the methods exposed in [76, 78]. Its phase space, in fact, features, depending on λ and μ, an hyperbolic point at the crossing of separatrices, which enclose an inner and an outer region.

4.B | Analysis of the minimum trapping action

From the observations reported in the main body of the chapter, for any value of ε_{m} or ε_{h} the phase-space islands appear at some amplitude, which determines the smallest radius for which particles are trapped into the islands. A simplified approach to determine an estimate for the minimum action starts from the Hamiltonian

$$H(I,\theta,\lambda) = H_0(I,\lambda) + \varepsilon\,I^{m/2}\cos(m\,\theta - \omega\,t) \tag{4.46}$$

that corresponds to a forced nonlinear oscillator with a resonance condition

$$m\frac{\partial H_0}{\partial I}(I_{\mathrm{r}},\lambda) - \omega_{\mathrm{r}} = 0 \tag{4.47}$$

that defines the resonant action $I_{\mathrm{r}}(\lambda)$ (when it is real). Note that it is always possible to introduce the angle $m\,\theta = \phi$ and the re-scaling of the action $J = I/k$, so that the Hamiltonian reads

$$H(J,\phi,\lambda) = H_0(kJ,\lambda) + \varepsilon\,k^{m/2}J^{m/2}\cos(\phi - \omega\,t)\,. \tag{4.48}$$

The resonant phase $\gamma = \phi - \omega_{\mathrm{r}}t$ can be introduced by using the generating function

$$G(J,\phi) = J(\phi - \omega_{\mathrm{r}}\,t) \tag{4.49}$$

and one obtains the pendulum-like system

$$H(J,\phi,\lambda) = H_0(kJ,\lambda) - \omega_{\mathrm{r}}\,J + \varepsilon\,k^{m/2}J^{m/2}\cos\gamma\,. \tag{4.50}$$

To study the nonlinear resonance crossing, we assume

$$\frac{\partial H_0}{\partial J} - \omega_r = \Delta\omega_0(\lambda) + \Omega J \qquad (4.51)$$

so that the resonance amplitude in phase space is given by

$$J_r(\lambda) = -\frac{\Delta\omega_0(\lambda)}{\Omega} \geq 0 . \qquad (4.52)$$

We can further reduce the Hamiltonian to that of a forced pendulum by using the generating function

$$F(\hat{J}, \gamma, \lambda) = \gamma(\hat{J} + J_r(\lambda)) , \qquad (4.53)$$

and the new Hamiltonian has the form

$$H(\hat{J}, \gamma, \lambda) = \frac{\Omega}{2}\hat{J}^2 + \varepsilon\, k^{m/2}(\hat{J} + J_r(\lambda))^{m/2} \cos\gamma + \gamma\,\epsilon J_r'(\lambda) \qquad (4.54)$$

where $\lambda = \epsilon t$ ($\epsilon \ll 1$) and $J_r' = \mathrm{d}J_r/\mathrm{d}\lambda$. The condition for the existence of fixed points is

$$\begin{cases} \dfrac{\partial H}{\partial \hat{J}} &= \Omega\hat{J} + \varepsilon\, k^{m/2}\dfrac{m}{2}(\hat{J} + J_r(\lambda))^{m/2-1} \cos\gamma = 0 \\[2mm] \dfrac{\partial H}{\partial \gamma} &= -\varepsilon\, k^{m/2}(\hat{J} + J_r(\lambda))^{m/2} \sin\gamma + \epsilon J_r'(\lambda) = 0 . \end{cases} \qquad (4.55)$$

The first equation provides the resonance position in phase space, whereas the second one provides a condition on the existence of the resonance since we obtain

$$|\sin\gamma| = \frac{\epsilon}{\varepsilon}\frac{|J_r'(\lambda)|}{k^{m/2}J_r(\lambda)^{m/2}} \qquad (4.56)$$

and $|\sin\gamma| \leq 1$. We observe that for $\epsilon \ll 1$ (adiabatic parameter) we have the existence of the resonance for small values of the actions $J_r(\lambda)$. However, for fixed ϵ/ε ratio we obtain a condition for the resonance as

$$J_r(\lambda)^{m/2} \geq C\frac{\epsilon}{\varepsilon} , \qquad (4.57)$$

where C is a suitable constant, which means the existence of a minimal trapping action $J_{\min}$ that scales as

$$J_{\min} \propto \left(\frac{\epsilon}{\varepsilon}\right)^{2/m} \qquad (4.58)$$

and, e.g. for $m = 3$ then $J_{\min} \propto \varepsilon^{-2/3}$.

5 | Double-resonance beam splitting

This short chapter is devoted to another possibility to extend MTE, combining the usual beam splitting varying the accelerator tune as in MTE with the effect of an external AC kicker, whose frequency is kept in a second resonance condition with the principal tune, as discussed in Chapter 4.

The studies discussed in this chapter are still in their embryonic phase; nevertheless, interesting preliminary results have been drawn. We start, in Section 5.1 from a simple map model (an Hénon map with an oscillating dipole). Operating with a main frequency close to resonance 4 and setting the exciter frequency exactly at the resonant value, "frozen" phase-space portraits of the map dynamics are analyzed, observing a breaking of the symmetry group of the map. We perform numerical simulations of tune modulations to observe how trapping into islands changes in the presence of the dipolar time-dependent excitation, depending on the phase of the kicker and on its amplitude. The symmetry breaking visible in the phase-space portrait is reflected in the trapping data.

In Section 5.2, we derive, using Normal Form expansion, an interpolating Hamiltonian for our map model. Observing the generated phase-space portraits, we conclude hinting that this is the model on which further analytical studies on trapping in double-resonance conditions should be based on. We then conclude giving an outlook for future double-resonance trapping studies.

5.1 | Map model and trapping simulations

The model employed is a simple Hénon map to which a dipolar exciter is added:

$$\begin{pmatrix} x_{n+1} \\ p_{n+1} \end{pmatrix} = R(\omega_{0,n}) \begin{pmatrix} x_n \\ p_n + x_n^2 + \varepsilon \cos(\omega_n n + \psi_0) , \end{pmatrix} \tag{5.1}$$

where, being ω_r the resonant frequency, we set $\omega_{0,n} = \omega_r + \delta_n$, $\omega_n = \omega_r + \Delta_n$, therefore keeping the resonance conditions $\omega_n \approx \omega_{0,n} \approx \omega_r$. Now, ω_n is modulated as in MTE varying δ_n in some neighborhood of zero.

If $\Delta_n = 0$, i.e. the exciter frequency is kept fixed to $\omega_r = 2\pi/q$, it is possible to directly study the phase space of the qth iterate of the map of Eq. (5.1) at frozen values of ω_n. Some phase-space portraits of this iterated map for $q = 4$, obtained with GIOTTO [84], using different values of the exciter phase ψ_0 and amplitude ε are shown in Fig. 5.1.

Two interesting properties are visible: depending on the phase ψ_0, one island becomes larger than the others (or two islands, if an intermediate phase is chosen). For $\psi_0 = 0$, the "west" island is bigger (we use cardinal points w.r.t. the origin to identify to each island, i.e. north is up, east right and so on). For $\psi_0 = \pi/4$ the effect is shared between the west and the north island, at $\psi_0 = \pi/2$ it is the northern island which has a larger area, and so on. Secondly, as ε increases, this effect is more evident, until the center and some other islands disappear completely for large enough values of the exciter amplitude.

We therefore expect that an initial particle distribution that undergoes the double-resonance crossing will be mainly trapped in one of the islands, depending on the exciter phase, and that the core could be mostly depleted.

We simulate a trapping process using the map of Eq. (5.1) with a protocol similar to the one employed in Chapter 4. First we set $\omega_0/(2\pi) = 0.249$, lower than the resonant value, when no islands are present, and then we ramp up ε from zero to $\varepsilon = 1 \times 10^{-3}$ (in $N = 10^5$ steps). This is performed to avoid mismatching the initial distribution when the elliptic fixed point is shifted from the origin due to the effect of the exciter. Then, in other N steps, we vary linearly $\omega_0/(2\pi)$ from 0.249 to 0.251, while keeping constant $\omega_1 = \pi/2$ and ε. The initial distribution is an ensemble of 10^3 particles normally distributed in x and p with zero average and $\sigma_x = \sigma_p = 0.1$. The final distributions for three values of the initial phase ($\psi_0 = 0$, $\pi/4$ and $\pi/2$) are shown in Fig. 5.2.

It is possible to count the number of trapped particles in each island (by the usual tune-evaluation method, particles with final tune exactly equal to 0.25 are considered as trapped, and counted in each island depending on their final angle: from $-\pi/4$ to $\pi/4$ it is considered in the east island, from $\pi/4$ to $3\pi/4$ in the northern one and so on). Depending on ψ_0, we have a different "privileged" island that captures most of the beam. The captured fraction in each island depending on ψ_0 is shown in Fig. 5.3, where the symmetry of this behaviour is apparent. This effect, as seen in Fig. 5.4, increases as a function of the exciter amplitude ε. When the dipole amplitude is very small, the four islands trap a similar fraction of particles. As ε increases, not only one island (in our case, the northern one) captures most of the beam: the trapping fraction of the two adjacent islands (east and west) decreases with the same rate, while the opposite island (south) depletes faster.

The observed phase-dependent trapping in one privileged island suggests some interesting possible applications for double-resonance MTE in accelera-
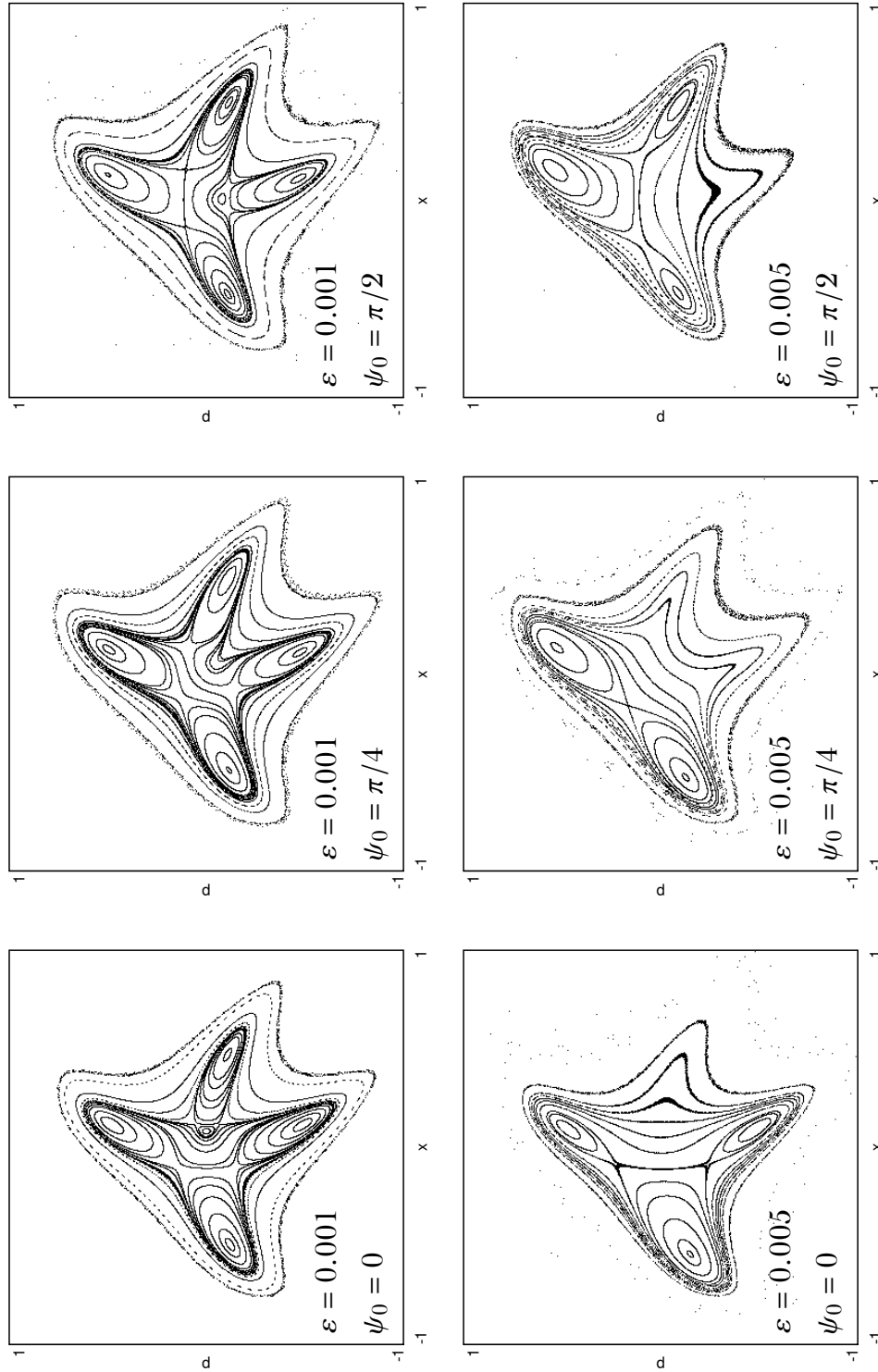
FIGURE 5.1 – Phase-space portraits of the 4th iterate of the map of Eq. (5.1) with $\omega_{0,n} = \pi/2$ for different values of ε and ψ_0.
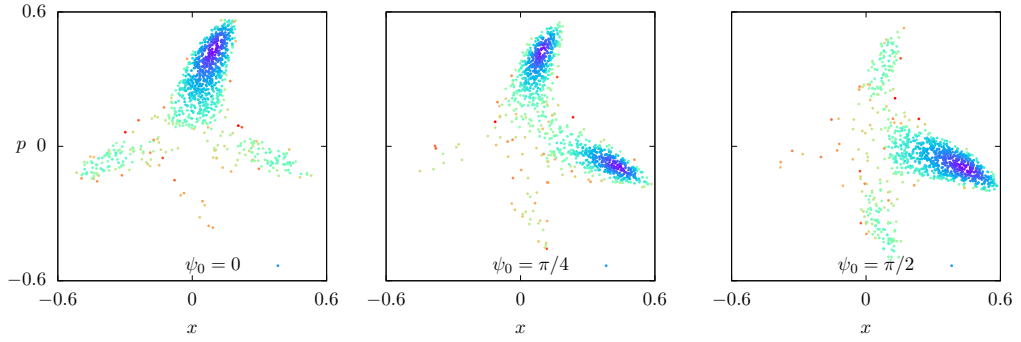
FIGURE 5.2 – Final distribution after the double-resonance trapping for three values of the exciter phase ψ_0. Initial distribution is Gaussian in (x, p) with $\sigma = 0.1$. Colors (from blue to red) encode the initial radius $\sqrt{x^2 + p^2}$. Map model of Eq. (5.1) has been used, with $\omega_r = \pi/2$, $\delta_n \in [-0.001, 0.001]$, $\varepsilon = 1 \times 10^{-3}$, $\Delta_n = 0$.
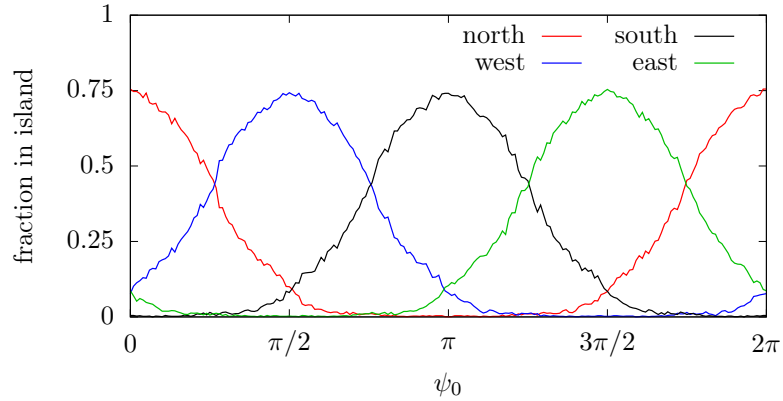
FIGURE 5.3 – Trapping fraction in each island in a double-resonance simulation, as function of the exciter phase ψ_0. Initial distribution is Gaussian in (x, p) with $\sigma = 0.1$. Map model of Eq. (5.1) has been used, with $\omega_r = \pi/2$, $\delta_n \in [-0.001, 0.001]$, $\varepsilon = 1 \times 10^{-3}$, $\Delta_n = 0$.
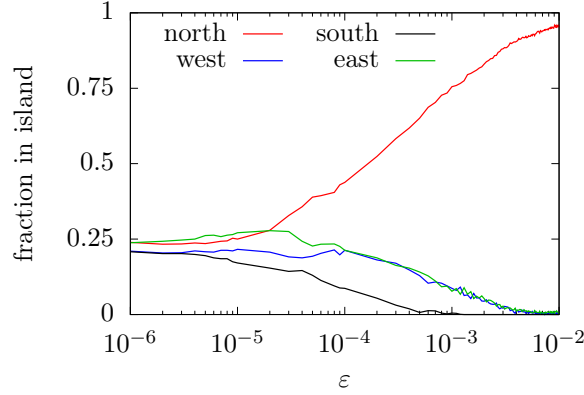
FIGURE 5.4 – Trapping fraction in each island in a double-resonance simulation, as function of the exciter amplitude ε (log scale) with the initial phase $\psi_0 = 0$. Initial distribution is Gaussian in (x, p) with $\sigma = 0.1$. Map model of Eq. (5.1) has been used, with $\omega_{\mathrm{r}} = \pi/2$, $\delta_n \in [-0.001, 0.001]$, $\varepsilon = 1 \times 10^{-3}$, $\Delta_n = 0$.

tors. A circular accelerator, longitudinally, contains a number of bunches distributed around its circumference in the RF buckets. In a situation akin to this double-resonance model, an AC dipole — the oscillating exciter — is inserted at the longitudinal co-ordinate $s = s_0$, generating a kick proportional to $\cos(\omega_{\mathrm{r}}t)$. At each turn, every bunch passes through the exciter at a different time, experiencing the dipolar kick with a different phase. Therefore, engineering the number and the phase distribution of the bunches, it might be possible to manipulate the trapping properties for each bunch.

5.2 | Interpolating Hamiltonian

To study this peculiar trapping phenomenon, it is convenient to write an interpolating Hamiltonian for Eq. (5.1). Due to the presence of an external element, we should proceed with some care before introducing the quasi-resonant approximation.

We start from the quasi-resonant Normal Form Hamiltonian of the Hénon map [17] close to resonance $1/4$ truncated at order J^3, but we stop before making the co-rotating change of variable that cancels the time dependence:

$$
\begin{aligned}
\mathscr{H}(\phi, J) = \omega_0(\lambda) J + J^2 \left[\frac{\Omega_2}{2} + A \cos(4\phi - 2\pi t) + B \sin(4\phi - 2\pi t) \right] + \\
+ J^3 \left[\frac{\Omega_4}{3} + C \cos(4\phi - 2\pi t) + D \sin(4\phi - 2\pi t) \right],
\end{aligned} \tag{5.2}
$$

where $\omega_0(\lambda) = \pi/2 + \delta(\lambda)$, $\lambda = \epsilon t$.

We want to add a resonant exciter $\varepsilon x \cos(\omega t + \psi_0)$, with $\omega(\lambda) = \pi/2 + \Delta(\lambda)$, and $\delta, \Delta \ll 1$, while ψ_0 is a phase that can be time-dependent. For the physical application, we are interested in the following two scenarios:

- Δ constant and δ time dependent;

- $\Delta = \alpha \delta + \beta$, with δ time dependent.

The coefficients of the Hamiltonian can be retrieved by the Normal Form computation of the Hénon map and are given by

$$
\begin{aligned}
\Omega_2 &= -\frac{1}{8} + \mathcal{O}(\delta), \quad \Omega_4 = -\frac{1}{128} + \mathcal{O}(\delta), \\
A &= \frac{1}{16} + \mathcal{O}(\delta), \quad B = \mathcal{O}(\delta), \\
C &= -\frac{1}{64} + \mathcal{O}(\delta), \quad D = \mathcal{O}(\delta).
\end{aligned}
\tag{5.3}
$$

Introducing the complex variables $z = x - ip$, $z^* = x + ip$, the conjugating function of the Normal Form $\mathbf{\Phi}(\zeta, \zeta^*)$ (see Section 1.7), and the action $2J = \zeta\zeta^*$, one has that at order J the expansion of x is

$$
x = \frac{z + z^*}{2} = \frac{\zeta + \zeta^*}{2} + \frac{\Phi(\zeta, \zeta^*) + \Phi^*(\zeta, \zeta^*)}{2},
\tag{5.4}
$$

with

$$
\Phi(\zeta, \zeta^*) = \sum_{n \geq 2} \sum_{k=0}^{n} \phi_{k,n-k} \zeta^k \zeta^{*n-k}.
\tag{5.5}
$$

In action-angle variables, Eq. (5.4) becomes

$$
\begin{aligned}
x(\phi, J) &= \sqrt{2J} \cos\phi + \sum_{n \geq 2} (2J)^{n/2} \sum_{k \leq n} \operatorname{Re}(\phi_{k,n-k}) \cos((2k-n)\phi) \\
&= \sum_{\ell \geq 1} x_\ell(J) \cos(\ell\phi),
\end{aligned}
\tag{5.6}
$$

where

$$
\begin{aligned}
x_1(J) &= \sqrt{2J}\left[1 + \sum_{n \geq 1} (2J)^n \operatorname{Re}(\phi_{n+1,n} + \phi_{n,n+1})\right], \\
x_\ell(J) &= \sum_n (2J)^{n/2} \operatorname{Re}\left(\phi_{\frac{n+\ell}{2}, \frac{n-\ell}{2}} + \phi_{\frac{n-\ell}{2}, \frac{n+\ell}{2}}\right) \qquad \text{for } \ell > 1.
\end{aligned}
\tag{5.7}
$$

The Hamiltonian of Eq. (5.2), with the extra contribution of a dipolar exciter, can be written as

$$\mathcal{H} = \omega_0(\lambda)J + J^2\left[\frac{\Omega_2}{2} + A\cos(4\phi - 2\pi t) + B\sin(4\phi - 2\pi t)\right]$$
$$+ J^3\left[\frac{\Omega_4}{3} + C\cos(4\phi - 2\pi t) + D\sin(4\phi - 2\pi t)\right] \qquad (5.8)$$
$$+ \varepsilon \sum_\ell x_\ell(J)\cos(\ell\phi)\cos(\omega t + \psi_0)\,.$$

We now introduce the coordinate change $J \to J$, $\phi \to \theta + \pi/2\,t$, which gives the new Hamiltonian via the generating function $F = \theta J = J(\phi - \pi t/2)$. In the new coordinates, the argument of the trigonometric functions $(4\phi - 2\pi t)$ reduces to 4θ. On the other hand, writing ω as $\pi/2 + \Delta$, for the term $\cos(\ell\phi)\cos(\omega t + \psi_0)$ we have

$$\cos(\ell\phi)\cos(\omega t + \psi_0) =$$
$$= \frac{1}{2}\left[\cos\left(\ell\theta + \frac{\ell+1}{2}\pi t + \Delta t + \psi_0\right) + \cos\left(\ell\theta + \frac{\ell-1}{2}\pi t - \Delta t - \psi_0\right)\right]\,.$$
$$(5.9)$$

In the simple case with $\Delta = 0$ (i.e. the exciter always works at the resonant frequency $\pi/2$), Eq. (5.9) averages over time to $\cos(\theta - \psi_0)/2$ only for $\ell = 1$, and zero otherwise. The averaged expansion of q, up to order J^3, becomes

$$\langle q(J)\rangle = \sqrt{2J}\left[1 + 2J\,\mathrm{Re}(\phi_{21} + \phi_{12}) + 4J^2\,\mathrm{Re}(\phi_{32} + \phi_{23})\right]$$
$$= \sqrt{2J}\left(1 + c_1\,J + c_2\,J^2\right)\,, \qquad (5.10)$$

where the coefficients c_1, c_2 can be calculated expanding the Normal Form of the Hénon map up to order 5, yielding $c_1 = 3/8 + \mathcal{O}(\delta^2)$ and $c_2 = 7/32 + \mathcal{O}(\delta)$.

Neglecting terms of order δ in the resonant term, we have the Hamiltonian

$$\mathcal{H} = \delta(\lambda)J + J^2\left[\frac{\Omega_2}{2} + A\cos(4\theta)\right] + J^3\left[\frac{\Omega_4}{3} + C\cos(4\theta)\right]$$
$$+ \frac{1}{2}\varepsilon\sqrt{2J}(1 + c_1\,J + c_2\,J^2)\cos(\theta - \psi_0)\,. \qquad (5.11)$$

In Fig. 5.5 we consider phase-space portraits of Eq. (5.11) for different values of ψ_0, reproducing the structures seen in Fig. 5.1, such as the increase of the area of a specific island depending on the exciter phase. This is due to the ε-proportional term in $\cos\theta$ that breaks the 4th order symmetry of the resonant Hénon map.
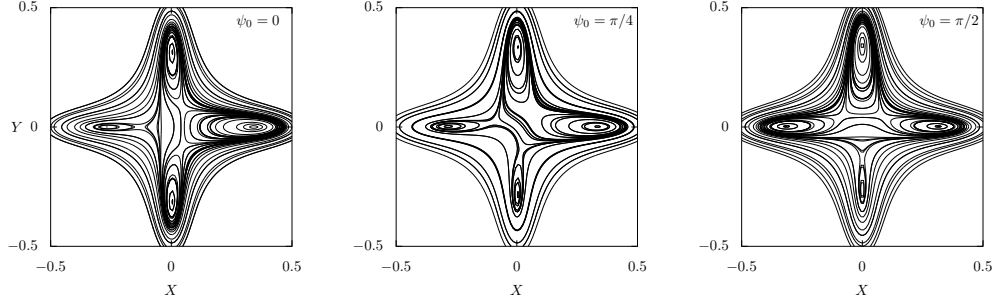
FIGURE 5.5 – Phase-space portraits of Hamiltonian of Eq. (5.11) in ($X = \sqrt{2J}\cos\theta$, $Y = \sqrt{2J}\sin\theta$) co-ordinates, with $\delta = 0.001$, $\varepsilon = 5 \times 10^{-4}$, for different values of ψ_0.

The similar island topology visible in portraits of the map model of Eq. (5.1) and of Hamiltonian of Eq. (5.11) suggests us the possibility to analyze trapping in a double-resonance MTE model from Eq. (5.11), using the same principles of the analysis of trapping with an oscillating exciter.

⁂

In conclusion, our preliminary studies show that including a double-resonance effect in MTE results in a symmetry breaking of the trapping, when, depending on the initial phase of the exciter, one island captures most of the beam. This fact is supported by the form of the interpolating Hamiltonian (5.11) that we derived. Future efforts on this subject will deal with a more systematic analysis of the trapping process both using the map and the Hamiltonian models, to establish — as in Chapter 4 — scaling laws and parametric dependencies. Furthermore, generalizations to other resonances shall be investigated (for example with resonance 3, once made stable with the introduction of an octupole term, as the normal form expansion of x introduces a non-zero contribution to the $J^{3/2}$ resonant term), or considering $\Delta \neq 0$ (one possibility would be to consider a coupled modulation $\omega_0 = \omega \approx \omega_r$).

Furthermore, observations from the operational implementation of MTE show that the addition of a transverse exciter enhances the fraction of the beam trapped in the beamlets [48–50]. The theoretical approach to understand this fact could be based upon these initial results on beam splitting in double resonance conditions.

6 | Nonlinear cooling of an annular beam distribution

The content of this chapter, with the due adaptations, has resulted in the article by A. Bazzani, F. C., M. Giovannozzi, R. Tomás *"Nonlinear cooling of an annular beam distribution"*, which has been made available as a preprint on arXiv in May 2022 (Ref. [13]) and submitted for publication to Phys. Rev. Acc. Beams.

In the last two chapters, we proposed and analyzed beam manipulation techniques that permit us to split a beam by trapping parts of it into resonance islands created by oscillating devices. However, beam splitting is not the only possible transverse beam geometry modification that can be proposed using our toolbox of resonances and separatrix crossing. In general, we observe that non-linear effects do not preserve the linear invariant, i.e. the linear action, or the so-called Courant-Snyder invariant. Is it therefore possible to exploit them to provide a reduction of the linear invariant? This would generate what is called a *cooling* of the transverse beam emittance, without violating the symplectic character of the Hamiltonian dynamics.

6.1 | Introduction

In this chapter, the initial step towards the development of a nonlinear cooling of a particle distribution is presented and discussed. We present a framework to cool an annular beam distribution, i.e. a distribution with nonzero density in an interval of radii $r_1 < r < r_2$, $r_1 > 0$ in the normalized phase space. It is well-known that the annular beam distributions are generated as the result of applying a single transverse kick to a centered beam in the presence of decoherence. Hence, a potential application of the cooling of annular beams might be the restoration of the initial centered distribution after the transverse kick.

The main idea is to create, using a resonant AC dipole, an island in the phase

space. Tuning the amplitude and the frequency of the exciter, it is possible to control the area of the island, and the probability it has to capture a particle at a given amplitude. It is therefore possible to optimize the trapping of particles in an annular distribution and to transport them to the center of the phase space, resulting in the end in a consistent emittance reduction.

The plan of the Chapter is the following: a general discussion of the systems that can be used to devise a cooling method for an annular beam distribution is presented in Section 6.2. The considered models are presented in Section 6.3 together with some results of the theory of adiabatic trapping applied to the models. In the same section, several cooling protocols are defined, whereas their performance is analyzed in detail by means of extensive numerical simulations, whose results are presented and discussed in Section 6.4. Finally, some conclusions are drawn in Section 6.5, whereas some mathematical details are reported in the Appendices.

6.2 | General considerations on the chosen model

The general idea underlying the approach developed to achieve cooling of the emittance of an annular beam distribution relies on creating stable islands in phase space by slowly modulating the parameters to vary the islands' area to cause the particles to cross the separatrices. Moving the resonance islands in the phase space, their action can be changed and eventually reduced.

To create stable phase-space islands, a resonance needs to be excited. The MTE experience suggests to use, as a model, a Hénon-like map close to stable low-order resonances, e.g. 1/4, 1/5. If the initial annulus lies outside the islands' chain, by changing the linear frequency, one can act on the areas of the central region and of the islands to trap particles in the center, thus reducing the action by a quantity equivalent to the islands' area divided by 2π, according to the theory of separatrix crossing.

A simple analysis of the scaling laws of the islands' parameters found in [17] suggests that this approach is feasible only for the resonance of order $n = 4$. However, to get the best cooling results, one needs two parameters to control the position and the area of the resonance islands. Acting on the sextupolar coefficient is not efficient since this acts as a global-scale parameter [17] and hence changes the dynamic aperture of the map. Therefore, we can introduce an octupolar kick. The estimates for the island area and the center can be derived using the results of [17] and [40]. However, the main drawback of this approach is the thick stochastic layer generated by the octupolar kick around the outer part of the separatrix of the four stable islands. This feature has the main downsize of inducing loss of particles, thus making the method unreliable.

These observations make the approach based on Hénon-like maps unsuitable to the application under consideration.

On the other hand, ongoing studies suggest that trapping into islands and transport from within the islands could also be efficiently achieved by means of AC-modulated magnets [10]. The most straightforward option consists in creating one island using an AC dipole in a 1 : 1 resonance condition, i.e. with the oscillation frequency close to the linear tune of the system. It is worth reminding that AC dipoles have been widely studied in the field of accelerator physics, with essential applications to beam diagnostics (see, e.g. [6, 22, 30, 71, 81, 87, 88, 91], for an overview on AC dipole studies and applications). A cooling method for annular beams will be devised using stable islands to perform the adiabatic trapping and transport using a Hamiltonian system modeling the transverse motion under the influence of an AC dipole.

6.3 | Theory

6.3.1 | The Hamiltonian model

Horizontal betatronic motion in the presence of an AC dipole can be described by the Hamiltonian of a generic oscillator with a sextupolar non-linearity and a dipolar time-dependent excitation [6, 81, 88], namely

$$\mathcal{H}(x, p_x, t) = \omega_0 \frac{x^2 + p_x^2}{2} + \frac{K_2}{3} x^3 + \varepsilon x \cos \omega t . \tag{6.1}$$

Using the action-angle coordinates (ϕ, J) of the unperturbed ($\varepsilon = 0$) system and averaging on the fast Fourier components, the Hamiltonian reads

$$\mathcal{H}(\phi, J, t) = \omega_0 J + \frac{\Omega_2}{2} J^2 + \varepsilon \sqrt{2J} \cos \phi \cos \omega t , \tag{6.2}$$

where we introduce an amplitude detuning term $\Omega_2 = g(\omega_0) K_2^2$ [17]. We recall that $J(x, p_x)$ is an adiabatic invariant of the unperturbed system if the frequency ω_0 is slowly modulated.

If we change the coordinates to refer the system to a rotating reference frame with slow angle $\gamma = \phi - \omega t$, taking into account the time derivative of the generating function F, i.e. $\partial F / \partial t = -\omega J$, the transformation gives

$$\mathcal{H}(\gamma, J, \psi) = (\omega_0 - \omega) J + \frac{\Omega_2}{2} J^2 + \varepsilon \sqrt{2J} \cos(\gamma + \psi) \cos \psi , \tag{6.3}$$

where $\psi = \omega t$.

One can average the fast variable ψ, using

$$\frac{1}{2\pi} \int_0^{2\pi} \mathrm{d}\psi \; \cos(\gamma + \psi) \cos\psi = \frac{1}{2} \cos\gamma \,, \qquad (6.4)$$

yielding the new averaged Hamiltonian

$$\mathcal{H}(\gamma, J) = (\omega_0 - \omega)J + \frac{\Omega_2}{2} J^2 + \frac{\varepsilon}{2} \sqrt{2J} \cos\gamma \,, \qquad (6.5)$$

which, after a rescaling, can be written in the following form

$$\mathcal{H}(\gamma, J) = 4J^2 - 2\lambda J + \mu\sqrt{2J} \cos\gamma \,, \qquad (6.6)$$

where

$$\lambda = \frac{4}{\Omega_2}(\omega - \omega_0) \,, \qquad \mu = \frac{4\varepsilon}{\Omega_2} \,. \qquad (6.7)$$

Equation (6.6) represents a well-known Hamiltonian [76, 78] that can be conveniently written in the form

$$\mathcal{H}(X, Y) = (X^2 + Y^2)^2 - \lambda(X^2 + Y^2) + \mu X \qquad (6.8)$$

using the Cartesian coordinates $X = \sqrt{2J} \cos\gamma$, $Y = \sqrt{2J} \sin\gamma$. When $\lambda > (3/2)\mu^{2/3}$, a hyperbolic fixed point exists only for $Y = 0$ and

$$X = x_{\mathrm{c}} = \frac{\sqrt{6\lambda}}{3} \cos\!\left(\frac{\pi}{6} + \alpha\right) \,, \qquad (6.9)$$

where

$$\alpha = \frac{1}{3} \operatorname{asin}\!\left(\frac{3\sqrt{6}}{4} \frac{\mu}{\lambda^{3/2}}\right) \,. \qquad (6.10)$$

The phase-space portrait of the Hamiltonian (6.8) is shown in Fig. 6.1, and it can be divided into three regions: the inner regions G_1 and G_2 (and $G_3 = G_1 \cup G_2$) and the region outside them.

Let us compute the area A_i of any region G_i. If $\mathcal{H}_c$ is the value of the Hamiltonian in $(X = x_{\mathrm{c}}, Y = 0)$, the equation $\mathcal{H}(\gamma, J) = \mathcal{H}_c$ has the solution

$$J(\gamma) = \frac{\lambda - 2x_{\mathrm{c}}^2}{2} - 2x_{\mathrm{c}}\sqrt{\lambda - 2x_{\mathrm{c}}^2} \sin\gamma + 2x_{\mathrm{c}}^2 \sin^2\gamma \,, \qquad (6.11)$$

and $J(\gamma) = 0$ for $\gamma = \gamma_0$ with

$$\gamma_0 = \operatorname{asin} \frac{\sqrt{\lambda - 2x_{\mathrm{c}}^2}}{2x_{\mathrm{c}}} \,. \qquad (6.12)$$
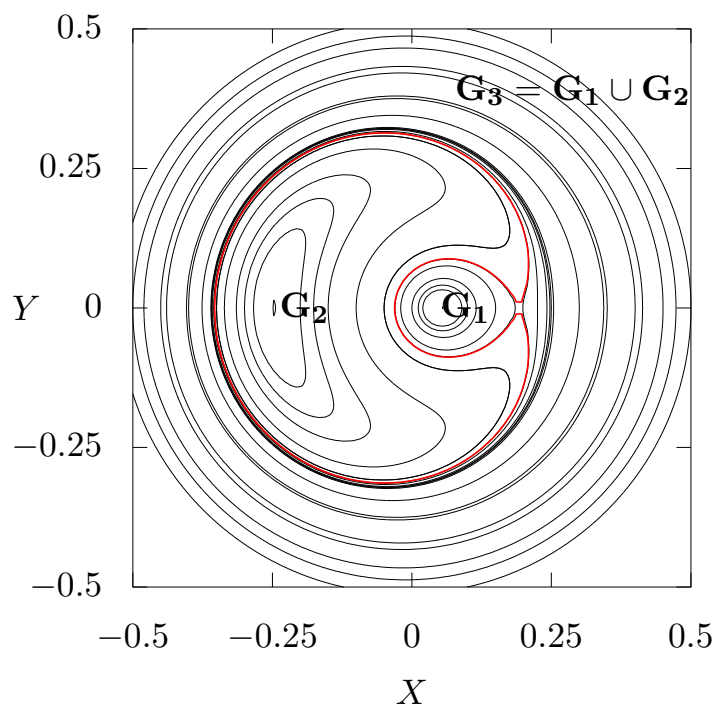
FIGURE 6.1 – Phase-space portrait of the Hamiltonian (6.8) with parameters $\lambda = 0.1$, $\mu = 0.01$. The red line represents the separatrix.

The area of G_1 in polar coordinates is thus given by

$$A_1 = \int_{-\gamma_0}^{\pi - \gamma_0} \mathrm{d}\gamma \, J(\gamma) = \frac{\pi \lambda}{2} - K_1 - K_2 \,, \qquad (6.13)$$

while the area of G_3 is given by

$$A_3 = \int_{-\pi - \gamma_0}^{\gamma_0} \mathrm{d}\gamma \, J(\gamma) = \frac{\pi \lambda}{2} + K_1 + K_2 \qquad (6.14)$$

so that

$$A_2 = A_3 - A_1 = 2(K_1 + K_2) \,, \qquad (6.15)$$

where

$$K_1 = \lambda \, \mathrm{asin}\left(\frac{\sqrt{\lambda - 2x_\mathrm{c}^2}}{2x_\mathrm{c}} \right), \qquad (6.16)$$

$$K_2 = \frac{3}{2} \sqrt{\lambda - 2x_\mathrm{c}^2} \sqrt{6x_\mathrm{c}^2 - \lambda} \,. \qquad (6.17)$$

Let us now consider a particle which lies in the outer region with an action $J_0 > A_3/(2\pi)$. The area enclosed by its orbit will be $A_0 = 2\pi J_0$. If we start a slow modulation of the parameters $\lambda = \lambda(t)$, $\mu = \mu(t)$, according to the theory of adiabatic separatrix crossing [4, 76], at $t = t^*$, when the condition $A_3 = A_0$ is met for $\lambda = \lambda^*$, $\mu = \mu^*$, the particle is captured into G_1 or G_2 as a random event. Defining (as in Eq. 1.49)

$$\xi_i = \frac{\mathrm{d}A_i/\mathrm{d}t}{\mathrm{d}A_3/\mathrm{d}t} \qquad i = 1,\, 2\,, \qquad (6.18)$$

the probability P_i of trapping into G_i, $i = 1,\, 2$ is given by

$$P_i = \begin{cases} 1 & \text{if } \xi_i > 1 \\ \xi_i & \text{if } 0 < \xi_i < 1 \,, \\ 0 & \text{if } \xi_i < 0 \end{cases} \qquad (6.19)$$

and after trapping, the resulting action J is given by $A_i/(2\pi)$, where A_i is computed when trapping occurs, namely for $\lambda = \lambda^*$, $\mu = \mu^*$.

Given an initial distribution of particles, all of which have an initial action in a small neighborhood of J_0, the expectation value of their final action is

$$\langle J \rangle = \left. \frac{P_1 A_1 + P_2 A_2}{2\pi} \right|_{\lambda^*, \mu^*}, \qquad (6.20)$$

and we have $\langle J \rangle \leq J_0$, since $P_1 + P_2 = 1$, $A_1 + A_2 = A_3 = 2\pi J_0$, and $A_i > 0$, $P_i > 0$. Hence, the final expected action is smaller than the initial one, i.e. , the emittance of the particle has been reduced. For a distribution of particles with action J_0, this results in a cooling of the beam.

Furthermore, when trapping occurs at (λ^*, μ^*) we have $A_3 = 2\pi J_0$ and using $A_3 = \pi\lambda^*/2 + K_1 + K_2 = 2\pi J_0$, we obtain the expression

$$K_1 + K_2 = \pi\left(2J_0 - \frac{\lambda^*}{2}\right) \tag{6.21}$$

and, substituting $K_1 + K_2$ in the expressions for A_1 and A_2, one obtains

$$A_1(\lambda^*, \mu^*) = \pi(\lambda^* - 2J_0) \qquad A_2(\lambda^*, \mu^*) = \pi(4J_0 - \lambda^*). \tag{6.22}$$

We remark that the values of A_1 and A_2 at the crossing time do not depend on μ^*.

We then rewrite $\langle J \rangle$ using $P_2 = 1 - P_1$, which gives

$$\langle J \rangle = 2J_0 - \frac{\lambda^*}{2} + P_1(\lambda^* - 3J_0) \tag{6.23}$$

having computed P_1 at $\lambda = \lambda^*$, $\mu = \mu^*$.

6.3.2 | Cooling protocols

We envisage three possible protocols to achieve beam cooling, as we can trap particles varying $\lambda(t)$ only, $\mu(t)$ only, or both parameters. We will present the three possible processes in this order, referring to them as Protocol A, B and C, respectively.

Variation of λ (Protocol A)

If we keep μ constant, $\mathrm{d}A_i/\mathrm{d}t = \partial A_i/\partial\lambda \cdot \mathrm{d}\lambda/\mathrm{d}t$, and the probabilities are thus given by

$$\xi_i = \frac{\mathrm{d}A_i/\mathrm{d}\lambda}{\mathrm{d}A_3/\mathrm{d}\lambda}\bigg|_{\lambda=\lambda^*} \qquad i = 1, 2. \tag{6.24}$$

Their expressions have been computed in [76, 78] and read

$$\frac{\partial A_1}{\partial\lambda} = \frac{\Theta}{2}, \qquad\qquad \frac{\partial A_2}{\partial\lambda} = \pi - \Theta,$$

$$P_1 = \frac{\Theta/2}{\pi - \Theta/2}, \qquad\qquad P_2 = \frac{\pi - \Theta}{\pi - \Theta/2}, \tag{6.25}$$
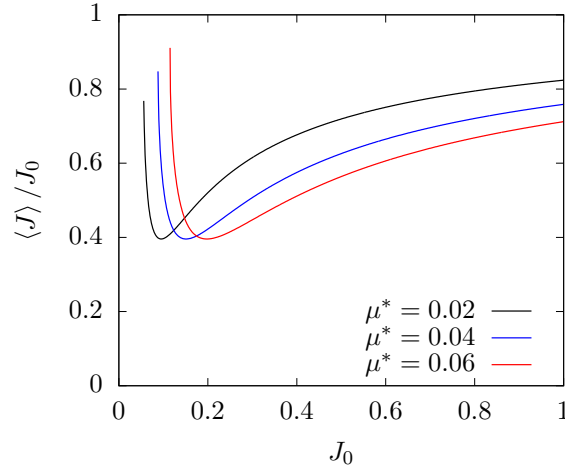
FIGURE 6.2 – Cooling ratio $\langle J \rangle / J_0$ for trapping in G_1 and G_2 with the variation λ according to Eq. (6.23), for some values of μ^*.

where

$$\Theta = \mathrm{acos}\left(\frac{\lambda}{2x_{\mathrm{c}}^2} - 2\right). \tag{6.26}$$

For different values of μ^*, $\langle J \rangle / J_0$ is shown as a function of J_0 in Fig. 6.2. Furthermore, we find that the value of $\langle J \rangle / J_0$ at the minimum point w.r.t. J_0 is independent on μ^* (the proof is given in Appendix 6.A).

A numerical computation of the minimum value of $\langle J \rangle / J_0$ gives 0.3957. Given J_0, we can always find a value μ that optimizes the cooling, and the final action is reduced to $\approx 40\%$ of the initial one.

We remark that this observation does not imply that the final *emittance* ϵ is also reduced to 40%. Indeed, when $\varepsilon \neq 0$, as in the final state of this protocol, the emittance is not equal to the average value of the adiabatic invariant. In the unperturbed motion (i.e. when $\varepsilon = 0$), we have $\epsilon = \langle J \rangle = \langle x^2 + p_x^2 \rangle / 2$. However, when $\varepsilon \neq 0$, and especially when particles are trapped both in G_1 and in G_2, as in the final state of this protocol, the average final action computed from Eq. (6.23) is proportional to the average orbit area either in G_1 or in G_2, and is not related to the average distance from the origin $x = 0$, $p_x = 0$, which is what characterizes the definition of the r.m.s. emittance. Particles trapped in G_2, being far from the center, have an average amplitude that is larger than their orbit area. Thus, the cooling ratio $\langle J \rangle / J_0$ computed from Eq. (6.23) is a lower bound to the actual ratio between the final and initial emittance values.

This effect could be solved or at least mitigated if we were able to develop an adiabatic transport protocol which, after the trapping phase, would preserve

the particles' actions while reducing μ to zero. However, such a method is not particularly efficient, since at best, when trapping is achieved by means of a variation of λ, only, the cooling ratio is $\approx 60\%$, whereas the methods that we are going to present in the following sections are, in theory, capable to achieve total cooling.

Variation of μ and complete trapping in G_2 (Protocol B)

For the protocol based on the variation of μ, the area derivatives ($i = 1, 2$) are given by

$$\frac{\mathrm{d}A_i}{\mathrm{d}\mu} = \frac{\mathrm{d}\alpha}{\mathrm{d}\mu} \frac{\mathrm{d}x_c}{\mathrm{d}\alpha} \frac{\mathrm{d}A_i}{\mathrm{d}x_c} , \qquad (6.27)$$

where

$$\frac{\mathrm{d}\alpha}{\mathrm{d}\mu} = \frac{1}{2}\sqrt{\frac{12}{8\lambda^3 - 27\mu^2}}, \qquad \frac{\mathrm{d}x_c}{\mathrm{d}\alpha} = -\frac{\sqrt{6\lambda}}{3}\sin\left(\frac{\pi}{6} + \alpha\right),$$

$$\frac{\mathrm{d}A_1}{\mathrm{d}x_c} = -2\frac{(6x_c^2 - \lambda)^{3/2}}{x_c\sqrt{2x_c^2 - \lambda}}, \qquad \frac{\mathrm{d}A_2}{\mathrm{d}x_c} = 4\frac{(6x_c^2 - \lambda)^{3/2}}{x_c\sqrt{2x_c^2 - \lambda}} . \qquad (6.28)$$

Thus, we have $\xi_1 = -1$ and $\xi_2 = 2$, which means that $P_1 = 0$ and $P_2 = 1$, i.e. all particles are going to be trapped in G_2, with an action value

$$J = \frac{A_2}{2\pi} = 2J_0 - \frac{\lambda^*}{2} \qquad (6.29)$$

and cooling is possible in the interval $\lambda^*/4 \leq J_0 \leq \lambda^*/2$, i.e. $2J_0 \leq \lambda^* \leq 4J_0$, which corresponds to the existence of the square roots $\sqrt{\lambda^* - 2x_c^2}$ and $\sqrt{6x_c^2 - \lambda^*}$.

On the other hand, for $\lambda^* > 4J_0$, the initial condition does not belong to the outer region, but to the inner one, G_1. In that case, the separatrix crossing occurs when $A_1 = 2\pi J_0$ and the particle is trapped into G_2 at an action $A_2(\lambda^*, \mu^*)/(2\pi)$. Using the expressions of A_1 and A_2, we find that the resulting expected final action is

$$J = \frac{\lambda^*}{2} - 2J_0 , \qquad (6.30)$$

which means that cooling is also possible for $4J_0 \leq \lambda^* \leq 6J_0$, i.e. $\lambda^*/6 \leq J_0 \leq \lambda^*/2$.

After trapping in G_2, the particle distribution has an action smaller than the initial one, but, as before, the definition of the adiabatic invariant, being $\mu \neq 0$, is not related to $(x^2 + p_x^2)/2$. Thus, a transport process to reduce μ to

zero without losing particles from G_2 needs to be designed. Since particles are trapped in G_2, we need to keep its area constant, i.e. $\mathrm{d}A_2/\mathrm{d}t = 0$, or

$$\frac{\mathrm{d}A_2}{\mathrm{d}t} = \frac{\mathrm{d}\lambda}{\mathrm{d}t}\left(\frac{\partial A_2}{\partial \lambda} + \frac{\mathrm{d}x_c}{\mathrm{d}\lambda}\frac{\partial A_2}{\partial x_c}\right) = 0\,, \tag{6.31}$$

which can be used to derive a differential equation for $\mu(\lambda)$

$$\frac{\mathrm{d}\mu}{\mathrm{d}\lambda} = -2x_c\sqrt{\frac{\lambda - 2x_c^2}{6x_c^2 - \lambda}}\,\mathrm{asin}\,\frac{\sqrt{\lambda - 2x_c^2}}{2x_c}\,. \tag{6.32}$$

Following this equation, as λ is reduced, μ is increased, and while A_2 is kept constant A_1 is reduced to zero, which happens when $\mu = (2\lambda/3)^{3/2}$. Thence, we can safely reduce both μ and λ to zero, switching off the perturbation, keeping, in general, $\mu < (2\lambda/3)^{3/2}$, which ensures that no island is present in the phase space.

Coupled variation of λ and μ and complete trapping in G_1 (Protocol C)

One could also devise a protocol in which both λ and μ are modulated at the same time. We can express μ as a function of λ and the expression of the capture probabilities becomes

$$P_i = \frac{\partial A_i/\partial \lambda + \mu'\,\partial A_i/\partial \mu}{\partial A_3/\partial \lambda + \mu'\,\partial A_3/\partial \mu}\bigg|_{\lambda=\lambda^*,\,\mu=\mu^*} \quad i = 1,\,2\,, \tag{6.33}$$

where the prime symbol denotes the derivative w.r.t. λ.

The trapping probability is calculated at the jumping point $(\lambda^*,\,\mu^*)$. Therefore, we can define an implicit function $\lambda^*(\mu)$ that resolves the equation $A_3 = A_0$ (see Fig. 6.3, left). Then, we optimize the probability by imposing that: (a) all particles are trapped in region G_1; (b) the area A_1 is minimized at the trapping point. For the first condition, the equation $P_1 = 1$, i.e. $P_2 = 0$ gives the following condition on μ'

$$\mu' = -\frac{\partial A_2/\partial \lambda}{\partial A_2/\partial \mu}\bigg|_{\lambda^*,\,\mu^*}\,. \tag{6.34}$$

Note that the signs of the partial derivatives of A_2 w.r.t. λ and μ ensure that $\mu' < 0$.

When $P_1 = 1$ and $P_2 = 0$, $2\pi\langle J\rangle = A_1 = \lambda^* - 2J_0$, we can minimize $\langle J\rangle$ choosing the minimum λ^* for which trapping is possible. This corresponds to $A_1 = 0$, whence $\lambda^* = 2J_0$, and the equation $A_3 = 2\pi J_0$ becomes

$$K_1 + K_2 = \pi J_0\,, \tag{6.35}$$
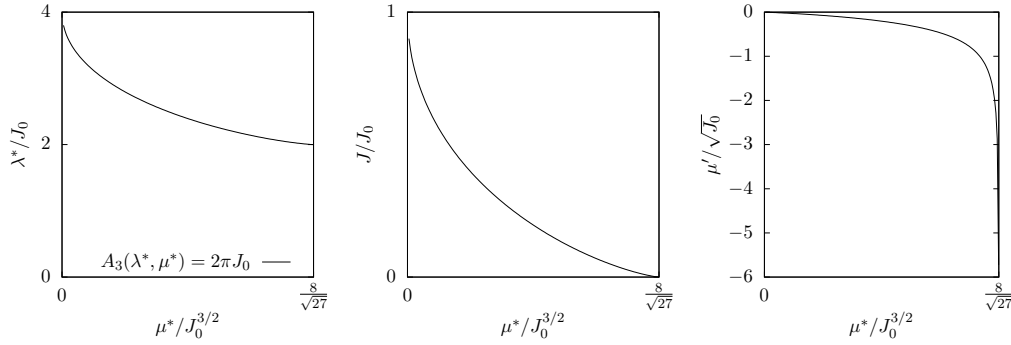
FIGURE 6.3 – Left: implicit solution $\lambda^*(\mu^*)$ of the equation $A_3(\lambda^*, \mu^*) = 2\pi J_0$. Center: expected cooling ratio J/J_0 for trapping particles via the coupled variation of λ and μ, as a function of μ^*. Right: required value of μ' to achieve the cooling efficiency shown in the center plot, as a function of μ^*. Thanks to the ratios of variables reported on the axes, the plotted functions are unique and independent from the value of J_0.

that can be solved by setting $K_1 = \pi J_0$ and $K_2 = 0$. From $K_1 = \pi J_0$ we have the equation

$$\mathrm{asin}\left(\frac{\sqrt{2J_0 - 2x_\mathrm{c}^2}}{2x_\mathrm{c}}\right) = \frac{\pi}{2} \, , \tag{6.36}$$

which is solved when the argument of the arc-sine is 1, so

$$\sqrt{2J_0 - 2x_\mathrm{c}^2} = 2x_\mathrm{c} \implies 6x_\mathrm{c}^2 - 2J_0 = 6x_\mathrm{c}^2 - \lambda = 0 \, . \tag{6.37}$$

It is straightforward to verify that this implies $K_2 = 0$. Additionally, this condition induces $\partial A_2/\partial \mu = 0$, and μ' diverges. Thus, a perfect cooling, i.e. in which the final value of the action is zero, would require to change μ infinitely fast, which contradicts the adiabatic condition we made to apply the theoretical results.

Although it is not possible to provide an analytic expression for the implicit solution $\lambda^*(\mu^*)$ of the equation $A_3 = 2\pi J_0$, we can prove that the plots shown in Fig. 6.3 represent the unique solution, after having properly scaled the axes. In particular, we find (the details are reported in Appendix 6.A and 6.B), that the graph of the implicit solution of the equation $A_3 = 2\pi J_0$ is independent on J_0 if we rescale $\lambda^* \to \lambda^*/J_0$ and $\mu^* \to \mu^*/J_0^{3/2}$ (see Fig. 6.3, left). Similar laws hold for the expected cooling J/J_0, which is a function of the only variable $\mu^*/J_0^{3/2}$ (see Fig. 6.3, center), and for the required μ', which fulfills the functional relation $\mu'/\sqrt{J_0} = f(\mu^*/J_0^{3/2})$ holds (see Fig. 6.3, right).

6.4 | Simulation results

We perform numerical simulations of the dynamics generated by the Hamiltonian of Eq. (6.1) varying λ and μ according to the protocols previously described. In these simulations, we set $\omega_0/(2\pi) = 0.414$, $K_2 = 1$, and the relations of Eq. (6.7) have been inverted to obtain the values of ω and ε as a function of λ and μ at each time step. The amplitude detuning parameter Ω_2 has been evaluated, for the unperturbed Hamiltonian at $\varepsilon = 0$, by using the algorithm to evaluate the tune described in [8], as $\Omega_2 = -0.3196$.

The initial distributions used in the simulations are an infinitely thin annular distribution with initial action $J_0 = (x_0^2 + p_{x,0}^2)/2$, while uniformly distributed according to the angle variable $\phi_0 = \text{atan}(p_{x,0}/x_0)$, i.e. with the p.d.f.

$$\rho_{J_0}(\phi, J) = \frac{\delta(J - J_0)}{2\pi} .$$ (6.38)

Examples of the initial annular distribution are shown in the left plots of Fig. 6.11 (for $J_0 = 0.05$).

6.4.1 | Protocol A: Cooling by varying λ

This protocol is divided in two phases. The first one is a matching phase, to adapt slowly the initial distribution to the phase-space topology, as when $\mu \neq 0$ the elliptic fixed point is shifted. We will increase μ until the chosen value μ^* while keeping $\lambda = 0$.

In the first phase, for time $t \in [0, t_1]$, we set

$$\begin{cases} \lambda(t) &= 0 \\ \mu(t) &= \mu^* \dfrac{t}{t_1} . \end{cases}$$ (6.39)

whereas the actual trapping occurs in the second phase. The parameter λ is linearly increased from 0 to a value $\Delta\lambda$. In order to trap particles at J_0, one needs $\Delta\lambda > \lambda^*$, being $\lambda^* = \lambda^*(\mu^*, J_0)$). We then set, for time $t \in [t_1, 2t_1]$

$$\begin{cases} \lambda(t) &= \Delta\lambda \left(\dfrac{t - t_1}{t_1} \right) \\ \mu(t) &= \mu^* . \end{cases}$$ (6.40)

We remark that although the proposed protocol, for the sake of simplicity, envisages two phases of the same duration, it is certainly possible to remove this constraint to adapt the duration of each phase to make it as adiabatic as possible.
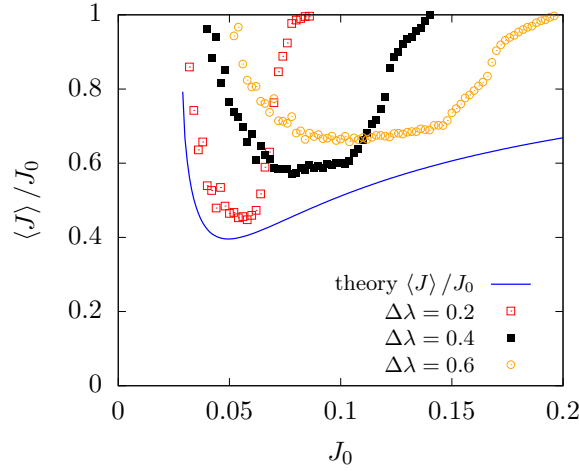
FIGURE 6.4 – Simulated cooling ratio obtained by applying Protocol A, for different values of $\Delta\lambda$, as function of the initial annular distribution action J_0. A comparison with the theoretical bound on the cooling efficiency given by Eq. (6.23) is presented. The Hamiltonian (6.1) has been used, with $K_2 = 1$, $\omega_0/(2\pi) = 0.414$, $\Omega_2 = -0.3196$, $\mu^* = 7.5 \times 10^{-3}$, $t_1 = 5 \times 10^4$.

Figure 6.4 shows the simulated $\langle J \rangle / J_0$ for different annular distributions ρ_{J_0}, as a function of the initial action J_0, using three values of $\Delta\lambda$ (with $\mu^* = 7.5 \times 10^{-3}$), and compares it to the theoretical estimate given by Eq. (6.23).

We observe two effects, which concur to the difference between the theoretical reduction of $\langle J \rangle / J_0$ and the observed behavior. For larger values of $\Delta\lambda$, the cooling range is increased at the expense of the minimum cooling ratio that becomes larger, while this is reversed for small values of $\Delta\lambda$. In fact, given $\Delta\lambda$ and μ^*, for large values of J_0, λ is never big enough to achieve trapping, since the λ^* value that solves $A_3(\lambda^*, \mu^*)$ is larger than $\Delta\lambda$. In addition, increasing $\Delta\lambda$ to trap more particles moves the center of G_2 far from the origin of the phase space (all fixed points of Eq. (6.8), from the solution of the resulting cubic equation, are $\mathbb{O}(\sqrt{\lambda})$ for large values of λ), thus decreasing the effective cooling ratio.

6.4.2 | Protocol B: Cooling by varying μ

This protocol consists in three phases: the first one is used to perform particle trapping, whereas the second and the third ones are needed to transport back the particles close to the center of the phase space, by reducing progressively the strength of the AC dipole.

In the first phase, for times $t \in [0, t_1]$, we have

$$
\begin{cases}
\lambda(t) & = \lambda^* \\
\mu(t) & = \mu_1 \dfrac{t}{t_1} \, ,
\end{cases}
\tag{6.41}
$$

and the condition $\mu_1 > \mu^*$, where μ^* solves the equation $A_3(\lambda^*, \mu^*) = 2\pi J_0$.

In the second phase, the differential equation (6.31) is solved. For $t \in [t_1, t_2]$, we set $\lambda(t) = \lambda^* - \dot\lambda \, (t - t_1)$ and we obtain $\mu(t)$ by numerically integrating the Cauchy problem

$$
\begin{cases}
\dfrac{d\mu}{dt} & = \dfrac{d\lambda}{dt} \dfrac{d\mu}{d\lambda} = -\dot\lambda \dfrac{d\mu}{d\lambda} \\
\mu(t_1) & = \mu_1 \, ,
\end{cases}
\tag{6.42}
$$

where $d\mu/d\lambda$ is given by Eq. (6.31). The second phase is stopped at time t_2 once the condition $\mu(t_2) = \mu_2 = (2\lambda(t_2)/3)^{3/2}$ is met. Then, the third phase follows for times $t \in [t_2, t_2 + t_1]$, with

$$
\begin{cases}
\lambda(t) & = \lambda(t_2) \left[1 - \left(\dfrac{t - t_2}{t_1} \right) \right] \\
\mu(t) & = \left(\dfrac{2}{3} \lambda(t) \right)^{3/2} \, .
\end{cases}
\tag{6.43}
$$

Plots of the time evolution of λ and μ are shown in Fig. 6.5.

In Fig. 6.6 we show the simulated cooling ratio $\langle J \rangle / J_0$, as a function of λ^*, for an initial annular distribution $\rho_{J_0}(\phi, J)$ with $J_0 = 0.05$, together with the theoretical expected value given by Eqs. (6.29) and (6.30).

We remark that the theory presented earlier describes accurately the simulated cooling ratio unless in the close vicinity of $\lambda^* = 4 J_0 = 0.2$, where theory predicts total cooling, while, in simulation, $\langle J \rangle / J_0 \approx 10\%$. This is due to the angular dependence we averaged upon in our analysis, as it can be inferred from Fig. 6.7. This Figure shows the distributions at the end of each of the three phases of Protocol B for an initial annular distribution for three values of λ^*. We observe that, at the end of each phase, the particles' actions, which were all the same at the beginning, are spread according to their initial phase. For example, red particles, which correspond to initial phase π, result in the innermost position when $\lambda^* = 0.15$ and in the outermost one when $\lambda = 0.25$ — this behavior is reversed for cyan particles, which have $\phi_0 = 0$. This means that initial conditions with different angles are trapped at slightly different values of J. Some particles are trapped earlier or later than expected, with a larger or smaller value of J than the theoretical one. In the plots it is also visible that
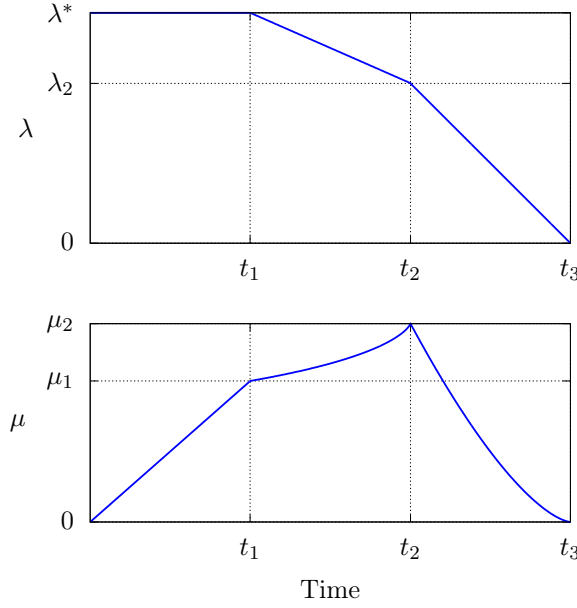
FIGURE 6.5 – Evolution of $\lambda(t)$ and $\mu(t)$ during the three phases of Protocol B.

the inner and outer particles are reversed depending on whether $\lambda^* < 4J_0$ or $\lambda^* > 4J_0$. When $\lambda \approx 4J_0$, however, all particles are trapped at a higher value than expected no matter when they cross the separatrix, thus increasing $\langle J \rangle$. In our simulations, we were able to reach $\langle J \rangle / J_0 = 0.078$, for a 92% cooling efficiency.

Moreover, in Fig. 6.8 we show the dependence of the cooling ratio on the value of the initial action J_0 for three values of λ^*. The range in which $\langle J \rangle / J_0 < 1$ represents the possible interval of actions of a thick annular distribution that it would be feasible to cool by using Protocol B. Note that, according to the theoretical predictions, the cooling is possible in the range $\lambda^*/6 \leq J_0 \leq \lambda^*/2$ and the optimal cooling ratio is found at $J_0 = \lambda^*/4$.

An animation of the trapping process under Protocol B for a thick annular distribution is available online. [1]

6.4.3 | Protocol C: Cooling by varying λ and μ

This protocol requires two phases: the first one is used to adapt the phase space; the second one is devoted to trapping and transport. Our goal, besides trapping the particles inside G_1, is to ensure that both at the beginning and at

---

[1]https://gitlab.cern.ch/fcapoani/nonlinear-cooling-animations/-/raw/master/
animation_protocol_B.mp4
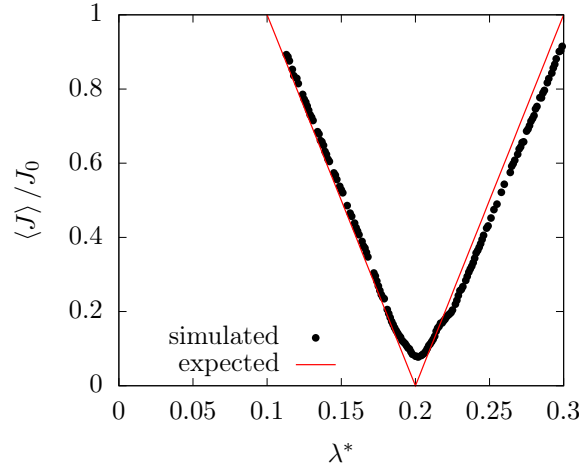
FIGURE 6.6 – Expected and simulated cooling ratio for trapping in G_2 using Protocol B as a function of λ^*. Initial distribution is $\rho_{0.05}$. The Hamiltonian (6.1) has been used, with $K_2 = 1$, $\omega_0/(2\pi) = 0.414$, $\Omega_2 = -0.3196$, $\mu_1 = 0.02$, $t_1 = 1/\dot{\lambda} = 5 \times 10^4$.

the end of the process the adiabatic invariant is as close as possible to the linear action variable $J = (x^2 + p_x^2)/2$, which is true if the AC dipole is switched off, i.e. when $\mu = 0$. Thus, in the first phase, μ is slowly increased, while keeping $\lambda = 0$ (i.e. , $\omega = \omega_0$), until it reaches the value needed to initiate the trapping process. In the second phase, the derivative of $\mu(\lambda)$ is kept at a value μ' while increasing λ, and, taking advantage of the fact that $\mu' < 0$, we slowly reduce μ until it reaches zero to recover the equivalence between the adiabatic invariant and J.

In the first phase, for times $t \in [0, t_1]$, we set

$$\begin{cases} \lambda(t) & = 0 \\ \mu(t) & = \mu_{\max} \dfrac{t}{t_1} \, , \end{cases} \tag{6.44}$$

where $\mu_{\max} = \mu^* + \lambda^* |\mu'|$. This ensures that, during the second phase, when $\lambda = \lambda^*$, μ is exactly μ^* and its derivative μ' has the appropriate value. The values of μ^* and λ^* are obtained by choosing a solution of the implicit equation $A_3 = A_0$ for the chosen value of J_0, which corresponds to the desired cooling. From Eq. (6.34), the desired value of μ' is also computed.

In the second phase, being $t \in [t_1, 2t_1]$, we have

$$\begin{cases} \lambda(t) & = \dfrac{\mu_{\max}}{|\mu'|} \left(\dfrac{t - t_1}{t_1} \right) \\ \mu(t) & = \mu_{\max} - |\mu'| \lambda(t) \, . \end{cases} \tag{6.45}$$
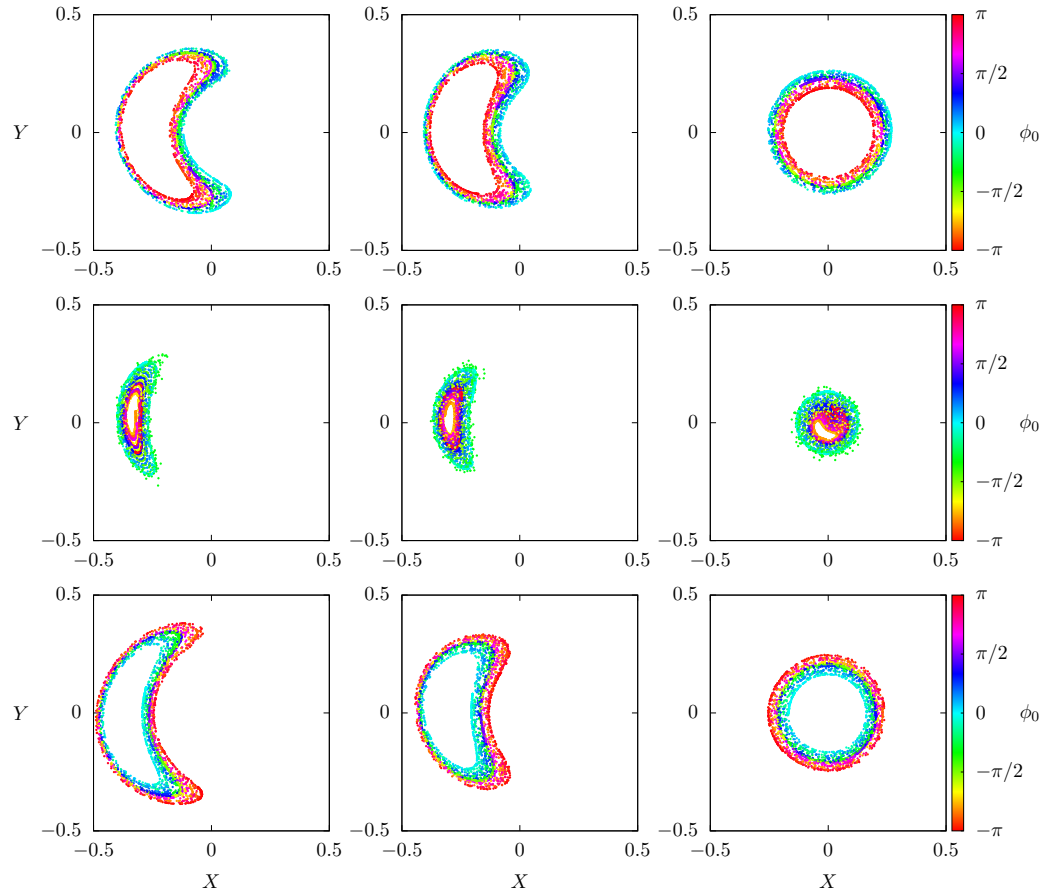
FIGURE 6.7 – Distributions at the end of the first (left), second (center), and third phase (right) for an initial distribution $\rho_{0.05}$ for Protocol B, with $\lambda^* = 0.15$ (top), $\lambda^* = 0.20$ (center) and $\lambda^* = 0.25$ (bottom). The hue represents the initial angle ϕ_0 and the color scale and initial distribution are the same as in Fig. 6.11 (left plot). Note that for $\lambda^* > 4J_0$ the angular dependence of the final action is reversed w.r.t. $\lambda^* < 4J_0$. The Hamiltonian of Eq. (6.1) has been used, with $K_2 = 1$, $\omega_0/(2\pi) = 0.414$, $\Omega_2 = -0.3196$, $\mu_1 = 0.02$, $t_1 = 1/\dot{\lambda} = 5 \times 10^4$
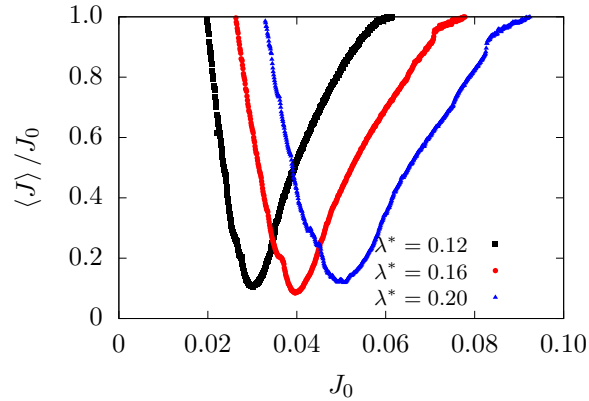
FIGURE 6.8 – Cooling ratio for trapping in G_2 using Protocol B, at different values of λ^*, as a function of the initial action of the annular distribution J_0. The Hamiltonian (6.1) has been used, with $K_2 = 1$, $\omega_0/(2\pi) = 0.414$, $\Omega_2 = -0.3196$, $\mu_1 = 0.02$, $t_1 = 1/\dot{\lambda} = 5 \times 10^4$.

When the process ends, $\mu = 0$ is reached, and G_2 disappears, as the perturbation provided by the AC dipole has been switched off, and the particles trapped in G_1 have been transported to the center of the phase space. The values of λ and μ during the whole procedure are plotted in Fig. 6.9.

We remark that although the proposed protocol envisages, for the sake of simplicity, two phases of the same duration, it is certainly possible to remove this constraint to adapt the duration of each phase to make it as adiabatic as possible.

In Fig. 6.10 we show the simulated cooling ratio $\langle J \rangle / J_0$ for an initial annular distribution $\rho_{0.05}(\phi, J)$, as a function of μ^*, and its comparison with the theoretical expected value $\langle J \rangle = (\lambda^*(\mu^*) - 2J_0)/(2\pi)$. It can be seen that the agreement between theory and simulations is remarkable until a break-down value of μ^*. This is due to the angular dynamics that has been neglected in the averaging process. In Fig. 6.11 we show the initial distribution, the situation at the end of the first phase, and the final distribution of particles for two different values of μ^*, using the hue to represent the initial angle ϕ_0. For both values of μ^*, we observe that the distribution after the first phase is no more infinitely thin, and the action of each particle at the end of the first phase depends on the initial angle. As a result, at the end of the second phase, each particle crosses the separatrix at a different time, resulting in different values of the final action. For μ^* smaller than the break-down threshold, all particles are still trapped into G_1, and this angular dependence is averaged out. On the other hand, for larger values of μ^*, particles that at the end of the first phase are in the outer part of
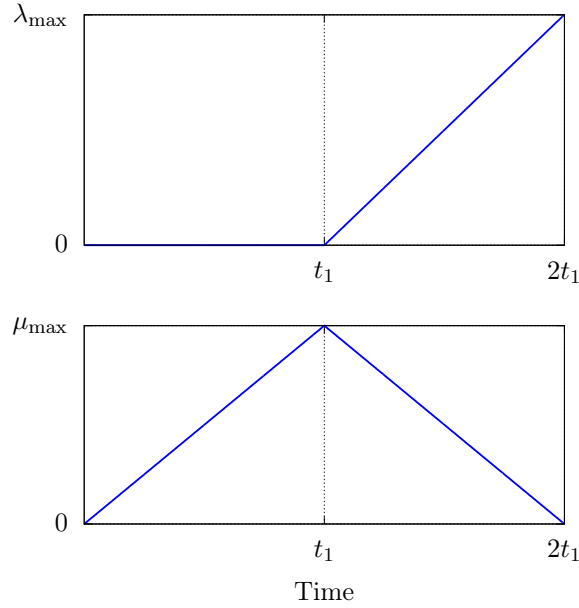
FIGURE 6.9 – Evolution of $\lambda(t)$ and $\mu(t)$ during the two phases of Protocol C. The two values $\lambda_{\max}$ and $\mu_{\max}$ have expressions in function of the computed λ^*, μ^*, and μ', i.e. $\mu_{\max} = \mu^* + \lambda|\mu'|$, $\lambda_{\max} = \lambda^* + \mu^*/|\mu'|$.

the distribution, can also be trapped into G_2 at large amplitude, thus dramatically increasing the value of the final action. Once more, we stress that in any case we cannot expect to reach total cooling, because, as discussed before, we would need $|\mu'|$ and $\mu_{\max}$ to reach unlimited values. The best cooling that we could achieve in our numerical simulations was 92%, at $\langle J \rangle / J_0 = 0.08$.

Finally, to study the applicability of the cooling protocol to a more realistic particle distribution, its effect on an ensemble of infinitely thin annular distributions ρ_{J_0} covering an certain interval in J_0 has been studied, having chosen the values of μ' and $\mu_{\max}$ to optimize the trapping for one value of J_0, called $\hat{J}_0$, and in this case we have $\hat{J}_0 = 0.05$. The results are shown in Fig. 6.12, where it is clearly visible that for different values of μ^*, which translates into different cooling targets for particles at $\hat{J}_0$, a significant range of action values is actually cooled. The width of this "cooling well" (the range of J_0 where $\langle J \rangle / J_0 < 1$) is the thickness of the annular distribution that the protocol can handle successfully.

We remark that, contrary to theoretical expectations, the minimum value of $\langle J \rangle / J_0$ does not occur at $\hat{J}_0$, although such a difference tends to reduce as μ^* increases. This is due, once more, to the angular dynamics. Using the same parameters of Fig. 6.12, in Fig. 6.13 two final distributions are shown using
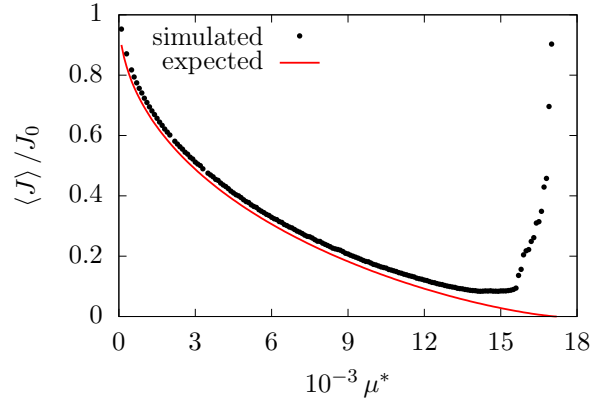
FIGURE 6.10 – Expected and simulated cooling ratio for trapping in G_1 using Protocol C as a function of μ^*. Initial distribution is $\rho_{0.05}$. The Hamiltonian (6.1) has been used, with $K_2 = 1, \omega_0/(2\pi) = 0.414, \Omega_2 = -0.3196, t_1 = 1 \times 10^5$.

color hue to identify the initial phase. The right plot shows the case in which the initial distribution is $\rho_{0.05}$, i.e. the initial conditions are selected at $\hat{J}_0$, while in the left plot we choose the distribution $\rho_{0.045}$, where the initial actions has a value $J_0 < \hat{J}_0$, but close to the minimum. In the left plot, a gap in the final distribution is clearly visible and it can be explained by observing that not all particles were trapped into G_1, as some, due to the action spread after the first phase, are trapped earlier (the red dots in the plots). These can end up either in G_2 or in G_1, according to the probability law, but when their area is smaller. Therefore, the average final action is reduced more by this effect than by the increase induced by the particles in G_2.

An animation of the trapping process with protocol C for a thick annular distribution is available online. [2]

6.5 | Conclusions

In this chapter, beam manipulations based on nonlinear beam dynamics have been devised with the goal of achieving cooling for annular transverse beam distributions. Such a peculiar beam distribution might be generated after kicking the beam in the transverse direction. The possibility of reaching cooling by means of crossing stable resonances generated by static magnetic elements has been ruled out, whereas the use of an AC dipole proved to be very

---

[2]https://gitlab.cern.ch/fcapoani/nonlinear-cooling-animations/-/raw/master/animation_protocol_C.mp4
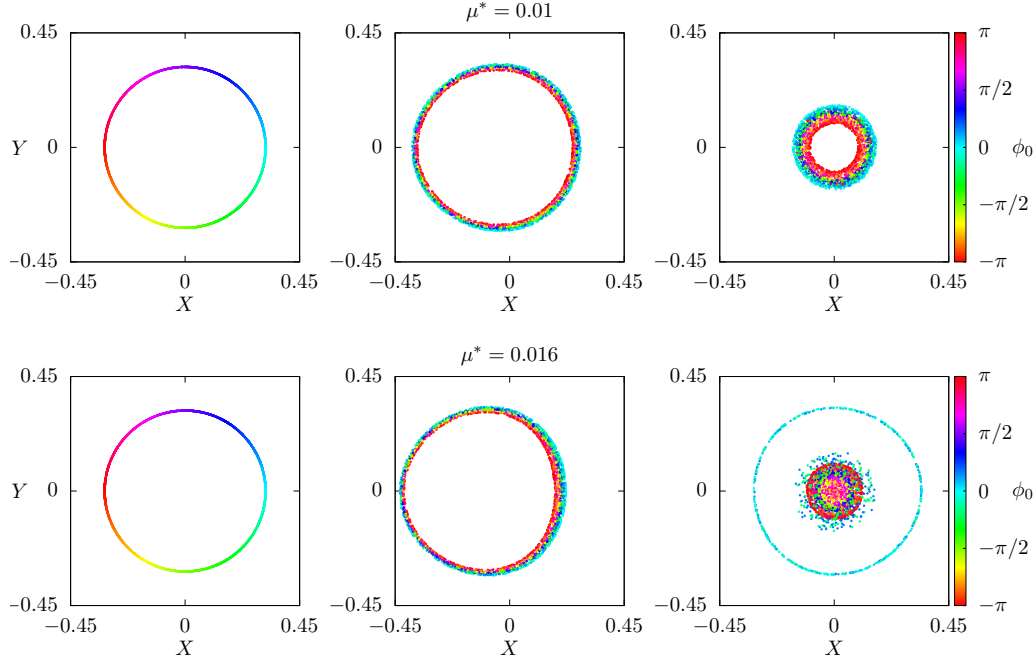
FIGURE 6.11 – Particle distributions when applying Protocol C at the beginning (left), after the first phase (middle), and at the end of the second phase (right), for two values of μ^*. The hue encodes the initial angle of the action distribution. The Hamiltonian (6.1) has been used, with $K_2 = 1$, $\omega_0/(2\pi) = 0.414$, $\Omega_2 = -0.3196$, $t_1 = 1 \times 10^5$.
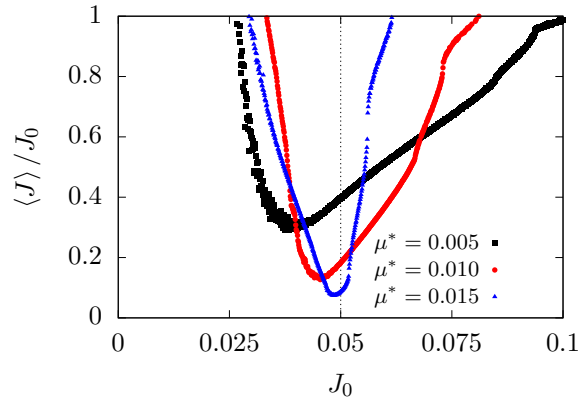
FIGURE 6.12 – Simulated cooling ratio $\langle J \rangle / J_0$ for initial distributions ρ_{J_0} using Protocol C at different values of μ^*, having computed μ' and $\mu_{\max}$ for $J_0 = \hat{J}_0 = 0.05$ (indicated by a vertical dotted line in the plot). The Hamiltonian (6.1) has been used, with $K_2 = 1$, $\omega_0/(2\pi) = 0.414$, $\Omega_2 = -0.3196$, $t_1 = 1 \times 10^5$
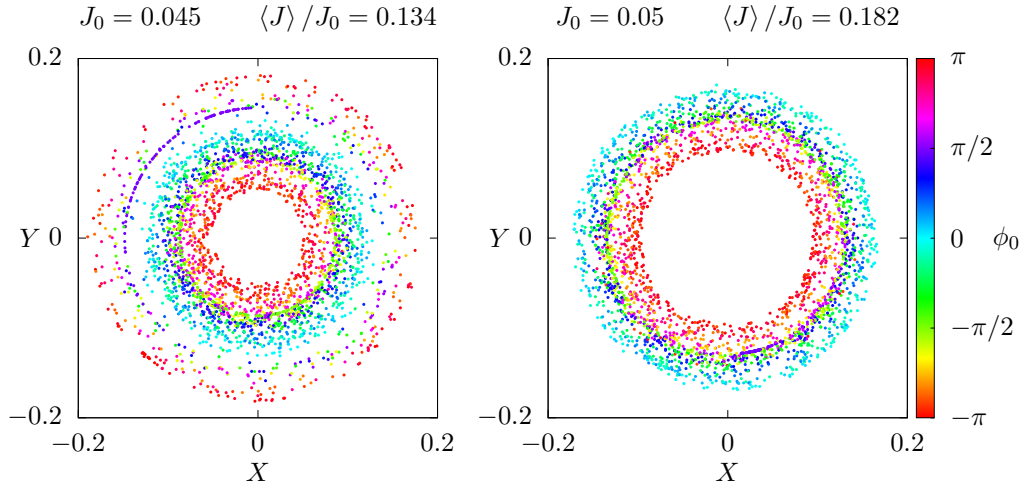
FIGURE 6.13 – Final particle distributions after applying Protocol C, for initial distributions $\rho_{0.045}$ (left) and $\rho_{0.05}$ (right), having computed μ' for $\hat{J}_0 = 0.05$. The hue indicates the initial angle ϕ_0. We see that, although the process has been optimized for $\hat{J}_0 = 0.05$, for $J_0 < \hat{J}_0$ (and close to the minimum shown in Fig. 6.12) the resulting cooling is better. The Hamiltonian (6.1) has been used, with $K_2 = 1$, $\omega_0/(2\pi) = 0.414$, $\Omega_2 = -0.3196$, $t_1 = 1 \times 10^5$, $\mu^* = 0.01$.

successful.

A Hamiltonian model describing the transverse dynamics in the presence of an AC dipole has been studied using the concepts from the adiabatic theory for Hamiltonian systems. This allowed designing three cooling protocols, two of which proved to be extremely effective, with a simulated best performance of $\approx 90\%$ cooling.

Detailed numerical simulations carried out on the considered Hamiltonian system have revealed a rich phenomenology that could be explained in detail by using the adiabatic theory for Hamiltonian systems. It is worth noting that although initially an infinitely thin annular distribution has been used, the two best protocols have a significant cooling range. It seems therefore possible to use them to cool a transverse annular beam distribution of finite thickness. Numerical studies on more realistic accelerator models will be considered in the future, also in view of possible experimental tests on a real machine.

Finally, it is worth mentioning that the annular beam distribution considered in these studies can be representative of the beam halo only. Therefore, in the future, applications to halo manipulation will be considered, possibly including experimental tests at the LHC.

Appendices

Some interesting and useful properties of the theoretical laws that describe the parameters of the cooling protocols described in this chapter can be derived by reasoning on the functional dependencies. Note that in the following, $f(x)$, $g(x)$, $A(x)$, $B(x)$ etc. represent generic functions of the only variable x, and the same occurs for their product, i.e. $f(x)g(x) = h(x)$.

6.A | Uniqueness of the minimum of $\langle J \rangle / J_0$ for Protocol A

From the expressions of x_c, K_1, K_2 and Θ (see Eqs. (6.9), (6.10), (6.16), (6.17), (6.26)), we define $\chi = \mu/\lambda^{3/2}$, and we can express these quantities as $x_c = \sqrt{\lambda}\, \tilde{x}_c(\chi)$, $K_i = \lambda \tilde{K}_i(\chi)$, and $\Theta = \Theta(\chi)$.

From the relation $A_3 = 2\pi J_0$, we have $J_0 = \lambda^* f(\chi^*)$, while from Eq. (6.23) one finds that $\langle J \rangle = \lambda^* g(\chi^*)$. Hence, setting $h(\chi) = g(\chi)/f(\chi)$, we finally

have $\langle J \rangle / J_0 = h(\chi^*)$. From the expression of $f(\chi^*) = \langle J \rangle / \lambda^*$, and noting that $g(\chi^*) = J_0 / \lambda^*$ is monotone (see Fig. 6.3, left) it is possible to show that the function $h(\chi^*)$ has a minimum for a value $\hat{\chi}^*$.

Then, there exists only one pair (λ^*, μ^*) that solves $A_3 = 2\pi J_0$ and for which $\mu^* / \lambda^{*3/2} = \hat{\chi}^*$. Thus, for each J_0 there exists only one value $\hat{\chi}^*$ and therefore an unique value of $h(\hat{\chi}^*)$, which does not depend on μ^*. This proves what has been observed in Section 6.3.2.

6.B | Scaling laws for Protocol C

A similar approach can be used to derive the scaling laws of Section 6.3.2. As $A_3 = \lambda^* \tilde{A}_3(\chi^*)$, the equation defining the invariant after the trapping reads

$$\lambda^* \tilde{A}_3(\chi^*) = \lambda^* \tilde{A}_3 \left(\frac{\mu^*}{\lambda^{*3/2}} \right) = 2\pi J_0 . \tag{6.46}$$

The functional equation

$$x f \left(\frac{y}{x^\alpha} \right) = 2\pi z \tag{6.47}$$

under the transformations $\overline{x} = x/z, \overline{y} = y/z^\alpha$ becomes

$$\overline{x} f \left(\frac{\overline{y}}{\overline{x}^\alpha} \right) = 2\pi . \tag{6.48}$$

This implicit equation is solved by the function $\overline{x} = g(\overline{y})$, whence we infer that, after the rescaling $\lambda^* \to \lambda^*/J_0$ and $\mu^* \to \mu^*/J_0^{3/2}$, the function

$$\frac{\lambda^*}{J_0} = A \left(\frac{\mu^*}{J_0^{3/2}} \right) \tag{6.49}$$

represents the unique solution to Eq. (6.46). This explains the scaling shown in Fig. 6.3 (left).

Moreover, inverting Eq. 6.46 one finds that χ^* can be written as a function of λ^*/J_0, and therefore of $\mu^*/J_0^{3/2}$:

$$\chi^* = \chi^* \left(\frac{\lambda^*}{J_0} \right) = \chi^* \left(A \left(\frac{\mu^*}{J_0^{3/2}} \right) \right) = \chi^* \left(\frac{\mu^*}{J_0^{3/2}} \right) . \tag{6.50}$$

We can therefore find a scaling law for the expected cooling ratio, as $2\pi J = A_1 = \lambda^* \tilde{A}_1(\chi^*)$, and using Eq. (6.49) and Eq. (6.50) one obtains

$$
\frac{J}{J_0} = \frac{\lambda^*}{J_0} \tilde{J}(\chi^*) = A\left(\frac{\mu^*}{J_0^{3/2}}\right) \tilde{J}\left(\chi\left(\frac{\mu^*}{J_0^{3/2}}\right)\right) =
$$
$$
= B\left(\frac{\mu^*}{J_0^{3/2}}\right),
$$
(6.51)

which explains the scaling shown in Fig. 6.3 (center).

In the same way, the coefficient μ', from the expressions of $\partial A_2/\partial\lambda$ and $\partial A_2/\partial\mu$ in Eqs. (6.25) and (6.26), can be written as

$$
\mu' = \sqrt{\lambda}\,\tilde{\mu}'(\chi)\,,
$$
(6.52)

and, dividing by $\sqrt{J_0}$ and using the functional dependencies from Eqs. (6.49) and (6.50) one obtains

$$
\frac{\mu'}{\sqrt{J_0}} = \sqrt{\frac{\lambda^*}{J_0}}\,\tilde{\mu}'(\chi^*) = C\left(\frac{\mu^*}{J_0^{3/2}}\right),
$$
(6.53)

whence the scaling for the plot shown in Fig. 6.3 (right).

7 | Emittance exchange: coupling resonance

This chapter is a slightly adapted version of the article by A. Bazzani, F. C., M. Giovannozzi, A.I. Neishtadt *"Adiabaticity of emittance exchange due to crossing of the coupling resonance"*, published in Phys. Rev. Accel. Beams 24 in September 2021 (Ref. [12]) by the American Physical Society under the terms of the Creative Commons Attribution 4.0 International license[1].

7.1 | Introduction

The previous three chapters were devoted to study general beam manipulation techniques that permit to employ a resonance to capture particles inside one island. There, a two-dimensional model was used, implying that motion in the other transverse direction has negligible effect on the evolution of the beam distribution. In this chapter, however, we extend our study to systems with four degrees of freedom, where we work close to a resonance condition between the tunes ω_x and ω_y. If the employed resonance is a difference resonance, i.e. $m\omega_x - n\omega_y = \ell$, with $m, n \in \mathbb{N}$, $\ell \in \mathbb{Z}$, then – using a standard technique for two-frequency systems – it is possible to find an invariant and reduce the system to two degrees of freedom, therefore coupling the x and y motion. From there, the usual steps apply: the phase space close to the resonance has some peculiar properties, and theory of adiabatic invariant conservation and separatrix crossing can be applied, when the tune is slowly varied to cross the resonance. First and foremost, we start with the study of the *coupling* resonance $\omega_x \approx \omega_y$, excited by the presence of a skew quadrupole. This is what is known as *linear coupling*.
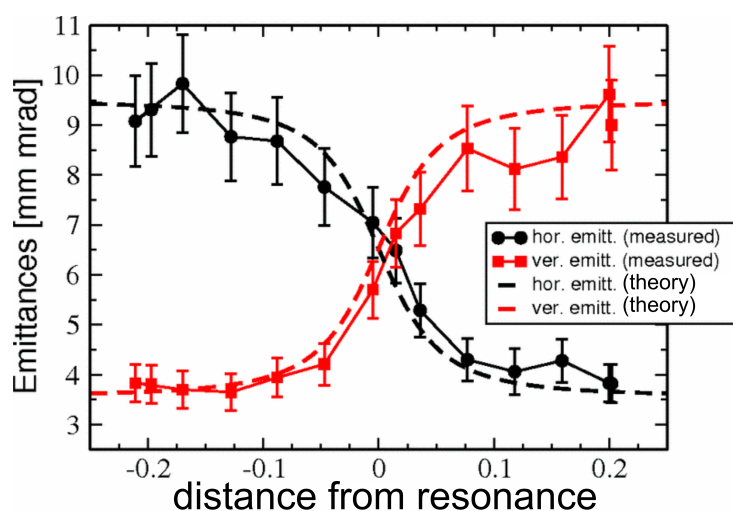
FIGURE 7.1 – Experimental measurement of coupling resonant emittance exchange at PS. Image from [36], with adapted labels, released under CC-BY 3.0.

The impact of linear coupling on transverse betatron motion has been extensively studied, as it has a peculiar impact already on the linear dynamics. In 2001, an interesting phenomenon of dynamic crossing of the difference coupling resonance was studied [70], noting that it results in an *emittance exchange* between the x and the y coordinate. If the initial beam distribution has emittances $\varepsilon_x = \varepsilon_{x,0}$ and $\varepsilon_y = \varepsilon_{y_0}$, after crossing the resonance, the final emittances are $\varepsilon_x = \varepsilon_{y,0}$ and $\varepsilon_y = \varepsilon_{x,0}$.

Further results were reported in 2007 [36], with an experimental measurement of the phenomenon in PS (Fig. 7.1). In the same article, it is mentioned that the full emittance exchange happens if the resonance crossing is adiabatic and an adiabatic condition is given. This research has opened a new domain of investigation. A paper by M. Aiba and J. Kallestrup [1] addressed the same topic with the goal to develop a complete theory to describe the emittance exchange process, where two properties were observed: the exponential dependence of the exchange efficiency on the adiabaticity of the tune modulation, and the quadratical scaling between the skew quadrupole strength and the adiabaticity parameter.

The framework of adiabatic invariance theory for Hamiltonian systems [4, 75], and especially the results on the conservation of the adiabatic invariant (see Section 1.2.2), which proved essential to understand non-linear beam manipulations, also provides a natural way of addressing the analysis of the resonance

crossing in the presence of linear coupling. In this chapter, we show how all observations reported in previous works, such as [1, 36], find a clear explanation using the results of adiabatic theory. Furthermore, we extend the analysis to the case in which nonlinear amplitude detuning is present in the considered system.

The plan of the Chapter is the following: in Section 7.2, the coupling Hamiltonian model is introduced and discussed in detail (Section 7.2.1), including an original view of the phase space on a sphere (Section 7.2.2). In Section 7.3, the same Hamiltonian system is analyzed using the normal modes and the main results on the properties of the dynamics are derived, whereas in Section 7.4, the analysis of the effect of amplitude detuning on the original Hamiltonian is carried out. A digression is made in Section 7.5, where the problem of two-way crossing of the coupling resonance is considered. In Section 7.6, the map model is introduced and, in Section 7.7, the results of the numerical simulations are presented and discussed in detail. Finally, conclusions are drawn in Section 7.8, while some mathematical details are reported in the Appendices.

7.2 | The Hamiltonian model and its dynamics

Following the treatment used in Chapter 2 and in Refs. [59, 61, 64], we consider a Hamiltonian written in physical coordinates in the following form

$$H(p_x, p_y, x, y, s) = \frac{p_x^2 + p_y^2}{2} + K_x(s)x^2 + K_y(s)y^2 - q\,xy\,, \qquad (7.1)$$

which represents the transverse dynamics in a focusing channel with properties that are *s*-dependent. The momenta are in fact normalized with respect to the total momentum, and the coefficient q is defined as

$$q = \frac{1}{2B\rho}\left(\frac{\partial B_y}{\partial y} - \frac{\partial B_x}{\partial x}\right) \qquad (7.2)$$

and represents the effect of a skew quadrupole on the betatron dynamics of a beam with magnetic rigidity $B\rho$. In the following, as in Chapter 2, the notation z will be used to denote x or y.

The Hamiltonian (7.1) is periodic with period L, the accelerator's circumference, and its dynamics can be studied after transforming it by means of the

standard Floquet transformation [59]

$$z = \sqrt{2\beta_z(s)J_z}\cos\Phi_z$$

$$p_z = -\sqrt{\frac{2J_z}{\beta_z(s)}}\sin\Phi_z \tag{7.3}$$

$$\Phi_z = \phi_z + \chi_z(s) - \omega_z s \quad \text{with} \quad \chi_z(s) = \int_0^s \frac{d\hat{s}}{\beta_z(\hat{s})}$$

and

$$\omega_z = \int_0^L \frac{ds}{\beta_z(s)}\,. \tag{7.4}$$

By introducing the corresponding Cartesian coordinates defined as

$$J_z = \frac{1}{2}\left(\omega_z \hat{z}^2 + \frac{\hat{p}_z^2}{\omega_z}\right)$$

$$\Phi_z = \operatorname{atan}\frac{\omega_z \hat{z}}{\hat{p}_z} \tag{7.5}$$

we obtain the new Hamiltonian

$$H(\hat{p}_x, \hat{p}_y, \hat{x}, \hat{y}) = \frac{\hat{p}_x^2 + \hat{p}_y^2}{2} + \frac{1}{2}\left(\omega_x^2 \hat{x}^2 + \omega_y^2 \hat{y}^2 + 2\hat{q}\,\hat{x}\hat{y}\right)\,, \tag{7.6}$$

where $\hat{q} = -\sqrt{\beta_x \beta_y \omega_x \omega_y}\, q$. This Hamiltonian will be studied in detail in the following, where the hats will be removed from all variables and symbols for simplifying the notation.

7.2.1 | Analysis of the dynamics in the presence of a skew quadrupole

We consider the adiabatic crossing of the linear coupling resonance, namely $\omega_x - \omega_y = 0$, when the frequencies are slowly modulated, and we define

$$\delta(\lambda) = \omega_x(\lambda) - \omega_y(\lambda) \tag{7.7}$$

with $\lambda = \epsilon t$, $\epsilon \ll 1$, and ϵ is the adiabatic parameter that describes the resonance-crossing process. Without loss of generality, $\delta(\lambda)$ is defined by a linear function that varies from positive to negative values (or vice versa) crossing zero.

The eigenvalues $\omega_{1,2}^2(\lambda)$ of the matrix associated with the quadratic potential matrix are given by

$$\omega_{1,2}^2(\lambda) = \frac{\omega_x^2(\lambda) + \omega_y^2(\lambda) \pm \sqrt{\left[\omega_x^2(\lambda) - \omega_y^2(\lambda)\right]^2 + 4q^2}}{2} \tag{7.8}$$

and it is convenient to define

$$\delta_2(\lambda) = \omega_x^2(\lambda) - \omega_y^2(\lambda) = \delta(\lambda)\left(\omega_x(\lambda) + \omega_y(\lambda)\right) \tag{7.9}$$

so that

$$\omega_1^2(\lambda) = \omega_x^2(\lambda) - \frac{\delta_2(\lambda) - \sqrt{\delta_2^2(\lambda) + 4q^2}}{2}$$

$$\omega_2^2(\lambda) = \omega_y^2(\lambda) + \frac{\delta_2(\lambda) - \sqrt{\delta_2^2(\lambda) + 4q^2}}{2} \, . \tag{7.10}$$

The corresponding eigenvectors are

$$\boldsymbol{v}_1(\lambda) = c_1\left(\frac{\delta_2(\lambda) + \sqrt{\delta_2^2(\lambda) + 4q^2}}{2}, q\right)$$

$$\boldsymbol{v}_2(\lambda) = c_2\left(-q, \frac{\delta_2(\lambda) + \sqrt{\delta_2^2(\lambda) + 4q^2}}{2}\right), \tag{7.11}$$

where c_i are the normalising constants. Note that for $q \ll 1$ and $\delta_2(\lambda) > 0$ one has $\boldsymbol{v}_1 \to \boldsymbol{e}_x$ and $\boldsymbol{v}_2 \to \boldsymbol{e}_y$, where $\boldsymbol{e}_x, \boldsymbol{e}_y$ are the unit vectors defining the horizontal and vertical planes. When $\delta_2(\lambda) = 0$, i.e. $\omega_x(\lambda) = \omega_y(\lambda)$, then $\boldsymbol{v}_1$ and $\boldsymbol{v}_2$ define the two bisectors of the two angles defined by the horizontal axis and the positive vertical axis, whereas when $|q| \ll 1$ and $\delta_2(\lambda) < 0$, then $\boldsymbol{v}_1 \to \boldsymbol{e}_y$ and $\boldsymbol{v}_2 \to -\boldsymbol{e}_x$. Therefore, the passage through the resonance $\omega_x - \omega_y$ implies an exchange of the direction of the eigenvectors.

The value of q is constrained by the conditions that $\omega_{1,2}$ are both real, i.e.

$$|q| \le \omega_x \, \omega_y \, , \tag{7.12}$$

otherwise, the closed orbit corresponding to the fixed point at the origin becomes unstable.

It is also worth noting that the following relations hold

$$\omega_1^2 + \omega_2^2 = \omega_x^2 + \omega_y^2$$

$$\omega_1^2 - \omega_2^2 = \sqrt{\left(\omega_x^2 - \omega_y^2\right)^2 + 4q^2} \tag{7.13}$$

$$\omega_1 \omega_2 = \sqrt{\omega_x^2 \omega_y^2 - q^2}$$

from which one remarks that the eigenvalues $\omega_{1,2}$ do not cross the linear resonance as their difference cannot get closer than $(\omega_1^2 - \omega_2^2)_{\min} = 2|q|$ as it is well known (see, e.g. Refs. [1, 36] and references therein). This observation leads to an essential conclusion: in the physical coordinates, the coupling resonance can be crossed, but the tunes are not the eigenvalues of the system. On the other hand, in the co-ordinate system of eigenvalues, the resonance cannot be crossed, although the eigenvalues are the proper quantities to describe the dynamics. For this reason, the term pseudo-resonance crossing will be also used in the following.

We introduce the linear normal form for the Hamiltonian (7.6) and the dependence of the symplectic transformation on time (via the parameter λ) introduces a further term in the original Hamiltonian. If we indicate with $G(\lambda)$ the matrix of the transformation $Z = z \sqrt{\omega_z(\lambda)}$, it induces the transformation

$$x = G(\lambda)\, X \,, \tag{7.14}$$

where X are the new co-ordinates. A generating function $F_2(x, P, \lambda)$ for the symplectic transformation can be written in the form

$$F_2(x, P, \lambda) = P^\top G^{-1}(\lambda)\, x \tag{7.15}$$

and the new Hamiltonian reads

$$\begin{aligned}
H(X, P, \lambda) = {}& \omega_x(\lambda)\frac{X^2 + P_x^2}{2} + \omega_y(\lambda)\frac{Y^2 + P_y^2}{2} + \\
& + \frac{q}{\sqrt{\omega_x(\lambda)\omega_y(\lambda)}}XY + \epsilon\, P^\top \frac{\partial G^{-1}}{\partial \lambda}GX \,,
\end{aligned} \tag{7.16}$$

where the last term is the time derivative of the generating function. The final form of the Hamiltonian reads

$$\begin{aligned}
H(X, P, \lambda) = {}& \omega_x(\lambda)\frac{X^2 + P_x^2}{2} + \omega_y(\lambda)\frac{Y^2 + P_y^2}{2} + \\
& + \frac{q}{\sqrt{\omega_x(\lambda)\omega_y(\lambda)}}XY + \\
& + \frac{\epsilon}{2}\left[\frac{\omega_x'(\lambda)}{\omega_x(\lambda)}XP_x + \frac{\omega_y'(\lambda)}{\omega_y(\lambda)}YP_y\right] \,,
\end{aligned} \tag{7.17}$$

where $\omega' = \mathrm{d}\omega/\mathrm{d}\lambda$. The linear action-angle variables (θ, I) can be used to recast the Hamiltonian (7.17) in the form

$$\begin{aligned}
H(\theta, I, \lambda) = {}& \omega_x(\lambda)I_x + \omega_y(\lambda)I_y + \frac{2q\sqrt{I_xI_y}}{\sqrt{\omega_x(\lambda)\omega_y(\lambda)}}\sin\theta_x\sin\theta_y + \\
& + \epsilon\left[\frac{\omega_x'(\lambda)}{\omega_x(\lambda)}I_x\sin\theta_x\cos\theta_x + \frac{\omega_y'(\lambda)}{\omega_y(\lambda)}I_y\sin\theta_y\cos\theta_y\right] \,.
\end{aligned} \tag{7.18}$$

We remark that the Hamiltonian dynamics is singular [2] at $I_x = I_y = 0$ and the frequencies $\omega_{x,y}$ are not the linear frequencies around the elliptic fixed point due to the presence of the linear coupling term. Hence, the condition $\omega_x(\lambda) = \omega_y(\lambda)$ is not a true dynamical resonance condition.

The Hamiltonian contains two small parameters, namely ϵ that tends to zero in the adiabatic limit, and q that measures the strength of the linear coupling: the main issue is how to determine and control the interplay between the two small parameters in the limit $\epsilon \to 0$.

The introduction of a slow phase $\phi_a = \theta_x - \theta_y$ in the generating function

$$F_2(\boldsymbol{\theta}, \boldsymbol{J}) = \begin{pmatrix} J_a, & J_b \end{pmatrix} \begin{pmatrix} 1 & -1 \\ 0 & 1 \end{pmatrix} \begin{pmatrix} \theta_x \\ \theta_y \end{pmatrix} \tag{7.19}$$

transforms the Hamiltonian to the form

$$\begin{aligned} H(\boldsymbol{\phi}, \boldsymbol{J}, \lambda) = \delta(\lambda) J_a + \omega_y J_b + \frac{2q\sqrt{J_a(J_b - J_a)}}{\sqrt{\omega_x(\lambda)\omega_y(\lambda)}} \sin(\phi_a + \phi_b) \sin\phi_b + \\ + \epsilon \left[\frac{\omega_x'(\lambda)}{\omega_x(\lambda)} J_a \sin(\phi_a + \phi_b) \cos(\phi_a + \phi_b) + \right. \\ \left. + \frac{\omega_y'(\lambda)}{\omega_y(\lambda)} (J_b - J_a) \sin\phi_b \cos\phi_b \right] \end{aligned} \tag{7.20}$$

and since we focus on the analysis when $\delta(\lambda) \to 0$, it is possible to apply a perturbative approach averaging over the fast-evolving angle ϕ_b to obtain the Hamiltonian

$$\begin{aligned} H(\boldsymbol{\phi}, \boldsymbol{J}, \lambda) = \delta(\lambda) J_a + \omega_y J_b + \frac{q}{\sqrt{\omega_x(\lambda)\omega_y(\lambda)}} \sqrt{J_a(J_b - J_a)} \cos\phi_a \\ + \mathcal{O}(\epsilon^2) + \mathcal{O}(q^2) . \end{aligned} \tag{7.21}$$

As ϕ_b is not present in the Hamiltonian, it follows that J_b is constant up to an error $\mathcal{O}(q^2) + \mathcal{O}(\epsilon^2)$ for a time interval of order $\mathcal{O}(\epsilon^{-1})$. The perturbative approach is possible only if this error is small, so that J_b can be considered constant during the resonance-crossing process. We remark that the term $\omega_y J_b$ can be dropped as it affects only the dynamics of ϕ_b, which is irrelevant in the case under consideration. In such a case, the action of the 1DoF Hamiltonian

$$H(\boldsymbol{\phi}, \boldsymbol{J}, \lambda) = \delta(\lambda) J_a + \frac{q}{\sqrt{\omega_x(\lambda)\omega_y(\lambda)}} \sqrt{J_a(J_b - J_a)} \cos\phi_a \tag{7.22}$$

---

[2]Here and in the following, *singular dynamics* means that the corresponding equations of motion are singular.

can be considered an adiabatic invariant up to an error $\mathcal{O}(q^2 \epsilon^{-1})$ for a time interval $\mathcal{O}(\epsilon^{-1})$, and we can study the change of J_a when $\delta(\lambda)$ passes through zero. In the end, it is possible to restrict the problem of studying the resonance-crossing process for the original Hamiltonian (7.6) by considering the dynamics generated by H in Eq. (7.22) that can be recast in the following form

$$H(\phi, J, \lambda) = \delta(\lambda)J + q\sqrt{(1-J)J}\sin\phi, \tag{7.23}$$

where, without loss of generality, we have re-scaled the action according to $J = J_a/J_b$ so that $J = 0$ and $J = 1$ are singular lines for the Hamiltonian (7.23). We also defined $\phi = \phi_a + \pi/2$, and then replaced $\delta(\lambda) \to \delta(\lambda)\sqrt{\omega_x(\lambda)\omega_y(\lambda)}/J_b$, which corresponds to a global re-scaling of the Hamiltonian. We remark that

$$\delta(\lambda)\frac{\sqrt{\omega_x(\lambda)\omega_y(\lambda)}}{J_b} = \delta(\lambda)\frac{\sqrt{\omega_x(0)\omega_y(0)}}{J_b} + \mathcal{O}(\epsilon^2) \tag{7.24}$$

and the higher-order terms can be dropped as they are part of the error considered in Eq. (7.21).

Note that the Hamiltonian (7.23) has the form

$$H(\phi, J, \lambda) = \epsilon t J + q H_1(J, \phi), \tag{7.25}$$

for which the equations of motion are

$$\begin{aligned}
\frac{\mathrm{d}J}{\mathrm{d}t} &= -q\frac{\partial H_1}{\partial \phi} \\
\frac{\mathrm{d}\phi}{\mathrm{d}t} &= \epsilon t + q\frac{\partial H_1}{\partial J}.
\end{aligned} \tag{7.26}$$

By introducing a new time $\bar{t} = q\,t$, Eq. (7.26) can be recast in the following form

$$\begin{aligned}
\frac{\mathrm{d}J}{\mathrm{d}\bar{t}} &= -\frac{\partial H_1}{\partial \phi} \\
\frac{\mathrm{d}\phi}{\mathrm{d}\bar{t}} &= +\frac{\epsilon}{q^2}\bar{t} + \frac{\partial H_1}{\partial J}.
\end{aligned} \tag{7.27}$$

Thus, the small parameter characterizing the adiabaticity is $\bar{\epsilon} = \epsilon/q^2$, and the new slow time is $\bar{\lambda} = \epsilon/q^2\,\bar{t}$. We remark that the reasoning can be extended to the case in which $\delta(\lambda)$ is a nonlinear function of λ, e.g. $\delta(\lambda) \approx 1/(2n+1)(\lambda - \lambda_c)^{2n+1}$, where λ_c represents the time of the resonance crossing. This option might be useful in applications in order to improve the overall adiabaticity of the process, as it was found in Ref. [28]. In this case, it is easy

to show that the small parameter characterizing the adiabaticity is $\bar{\epsilon} = \epsilon/q^{\frac{2n+2}{2n+1}}$, and the exponent tends to 1 when $n \to \infty$.

The Hamiltonian (7.23) is symmetric with respect to the transformation $\tilde{J} = 1 - J$ and $\tilde{\phi} = -\phi$, as

$$H(\tilde{\phi}, \tilde{J}, \lambda) = \delta(\lambda)(1 - \tilde{J}) - q\sqrt{(1 - \tilde{J})\tilde{J}} \sin \tilde{\phi}$$
$$= \delta(\lambda) - H(\phi, J, \lambda) \qquad (7.28)$$

so that we have the same dynamics by reverting the time arrow and the behavior for $J \to 0$ is the same as $J \to 1$.

The level curve that reaches $J = 1$ at $\phi = 0$ and $\phi = \pi$ is a critical one. It fulfills the equation

$$H(\phi, J, \lambda) = H(0, 1, \lambda) \qquad (7.29)$$

id est

$$q\sqrt{(1 - J)J} \sin \phi - \delta(\lambda)(1 - J) = 0 \qquad (7.30)$$

and thus

$$J(\phi) = \frac{\delta^2}{\delta^2 + q^2 \sin^2 \phi} \to 1 \quad \text{for} \quad \phi \to 0 \qquad (7.31)$$

that shows how the level curve $J(\phi)$ is tangent to the $J = 1$ curve. It is worth stressing that, in spite of being a critical curve, this special level curve of the Hamiltonian H is not a singularity of the dynamics and, in particular, the time spent on this curve is finite (see Appendix 7.A).

In Fig. 7.2, the phase-space portraits of the Hamiltonian (7.23) (assumed to be frozen, i.e. with λ constant) are shown in the first column, for $q = 1$ [3] and three values of δ, namely $1, 0, -1$ for the top, center, and bottom plot, respectively.

The red lines represent the critical curve, which is also called *coupling arc* in Refs. [59, 61]. In the top plot ($\delta = 1$), two separated islands are visible, whose areas increase as δ decreases to zero. Furthermore, there exists a region of *separatrix curves* around the islands, tangent to the singular lines $J = 0$ and $J = 1$. When $\delta = 0$ (center plot), the islands have maximal area, with a sort of separatrix that connects the singular line through the vertical line $\phi = \pi$. Finally, a symmetric situation when $\delta < 0$ is visible in the bottom plot.

The dynamics can also be studied by using the variables

$$\mathcal{X} = \sqrt{2J} \sin \phi \qquad \mathcal{Y} = \sqrt{2J} \cos \phi \qquad (7.32)$$

---

[3]The artificially large value of q, together with large values of δ and of the action, is used to make more visible the key features of the phase-space portrait.
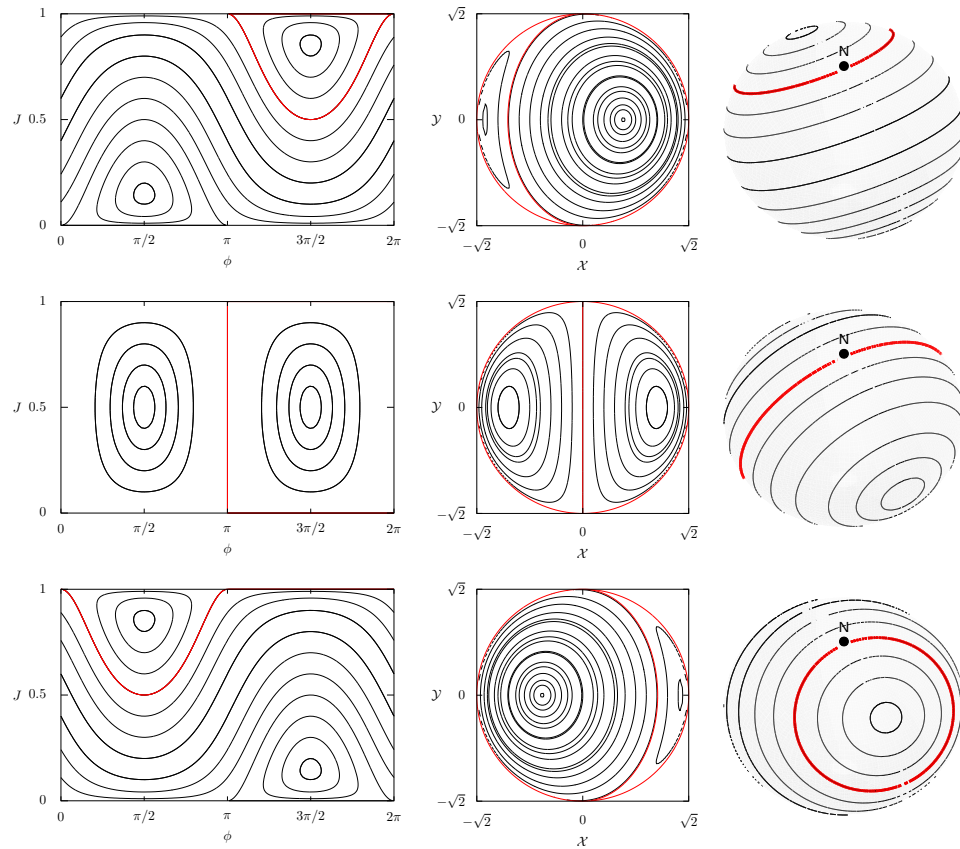
FIGURE 7.2 – Phase-space portraits of the Hamiltonian (7.23) for $q = 1$ and $\delta = 1$ (top), $\delta = 0$ (center), and $\delta = -1$ (bottom) in three different representations: action-angle co-ordinates (ϕ, J) on the left column, Cartesian co-ordinates $(\mathcal{X} = \sqrt{2J} \sin \phi, \mathcal{Y} = \sqrt{2J} \cos \phi)$ in the central column, and on a spherical surface (as described in Section 7.2.2) on the right column, where the coordinate ϕ is the polar angle while the azimuthal angle is given by $\theta = \mathrm{asin}(2J - 1)$. The red line represents the critical curve (the so-called *coupling arc* in Refs. [59, 61]). The plots on the left column are the equirectangular projections of the spherical surface, the poles being represented by the $J = 0$ and $J = 1$ lines while the plots on the central column are the azimuthal representations centered around the south pole. Note that the artificially-large value of q, together with large values of δ and of J, is used to make more visible the key features of the phase-space portrait.

so that the Hamiltonian reads as

$$H(\mathcal{X}, \mathcal{Y}, \lambda) = \frac{\delta(\lambda)}{2}(\mathcal{X}^2 + \mathcal{Y}^2) + \frac{q}{2}\sqrt{2 - (\mathcal{X}^2 + \mathcal{Y}^2)}\,\mathcal{X}\,. \tag{7.33}$$

A limiting circle $\mathcal{X}^2 + \mathcal{Y}^2 = 2$ appears and the dynamics is confined within it, due to the presence of the square root. Moreover, the *coupling arc* is the solution of

$$\delta^2(\lambda)(\mathcal{X}^2 + \mathcal{Y}^2) + q^2\mathcal{X}^2 = 2\delta^2(\lambda) \tag{7.34}$$

that separates the accessible domain of the phase space into two regions of different sizes, depending on the value of $\delta(\lambda)$. A sketch of the phase-space portrait is depicted in the central column of Fig. 7.2.

7.2.2 | Visualization of the dynamics on a sphere

In the previous section, the dynamics of the Hamiltonian (7.23) has been analyzed by means of two different co-ordinate systems. However, the essential features of the dynamics can be best appreciated by looking at the dynamics generated on a sphere, since we have two singular lines, namely, $J = 0$ and $J = 1$.

The north pole can be identified with $J = 1$ and the south pole with $J = 0$. Two charts have to be defined: one describing the southern and one the northern hemisphere, with a non-zero overlap at the equator to provide the necessary compatibility between the two charts. The co-ordinates (7.32) can be used to describe the chart of the northern hemisphere.

There are two symmetrically-located elliptic fixed points on the sphere, whereas the poles are singular lines, i.e. the phase dynamics $\phi(t)$ is not defined on the poles, but we observe that the phase velocity $\dot{\phi}$ increases as one approaches the poles as $1/\sqrt{(1 - J)J}$ so that the time spent in the part of the energy-level curves near the lines $J = 0$ and $J = 1$ tends to 0. We remark that the level curves tend to be parallel to these singular lines, whereas the angle ϕ varies in a neighborhood of $\pi/2$ or $3\pi/2$.

The level line $H(\mathcal{X}, \mathcal{Y}, \lambda) = 0$ close to the origin is given by

$$\delta(\lambda)(\mathcal{X}^2 + \mathcal{Y}^2) + \sqrt{2}q\,\mathcal{X} = \mathbb{O}(3)\,, \tag{7.35}$$

where $\mathbb{O}(3)$ stands for third-order terms in $\mathcal{X}$ and $\mathcal{Y}$. Such a curve is smooth and represents a circle passing through the origin. In the limit $\delta \rightarrow 0$, the radius of curvature diverges and the same is true near the south pole $J = 1$, where the variables are given by

$$\tilde{\mathcal{X}} = \sqrt{2(1 - J)}\sin\phi \qquad \tilde{\mathcal{Y}} = \sqrt{2(1 - J)}\cos\phi \tag{7.36}$$

and the Hamiltonian is

$$H(\tilde{\mathcal{X}}, \tilde{\mathcal{Y}}, \lambda) = -\frac{\delta(\lambda)}{2}(\tilde{\mathcal{X}}^2 + \tilde{\mathcal{Y}}^2) + \frac{q}{2}\sqrt{2 - \tilde{\mathcal{X}}^2 + \tilde{\mathcal{Y}}^2}\,\tilde{\mathcal{X}} + \delta(\lambda)\,. \qquad (7.37)$$

Both Hamiltonians (7.33) and (7.37) are analytic at their origin, and they have a singularity at

$$\frac{\tilde{\mathcal{X}}^2 + \tilde{\mathcal{Y}}^2}{2} = \frac{\mathcal{X}^2 + \mathcal{Y}^2}{2} = 1 \qquad (7.38)$$

corresponding to the points $J = 1$ and $J = 0$, respectively. However, the singularity is not in the dynamics, but only in the coordinates. Hence, the dynamics on the sphere has no singularity, although it cannot be described by a single chart and this is an essential point for our analyses. The dynamics on the sphere is represented in the plots on the third column of Fig. 7.2.

When the time dependence is considered, and in particular the limit $\delta(\lambda) \to 0$ is analyzed, then one can introduce the action-angle variables (θ, I) for each chart of the 1DoF frozen Hamiltonian (7.33).

7.2.3 | Analysis of the pseudo-resonance-crossing process

Let us assume that $\delta(\lambda) = \delta_{\max} \epsilon t$ where $-1/\epsilon \le t \le 1/\epsilon$ and $-\delta_{\max} \le \delta(\lambda) \le \delta_{\max}$. The fixed points of the Hamiltonian (7.23) correspond to $\phi_x^* = \pi/2, 3\pi/2$ and their action J^* is given by

$$\frac{2\delta_{\max}}{q}\lambda = \pm\frac{1 - 2J^*}{\sqrt{J^*(1 - J^*)}}\,, \qquad (7.39)$$

where the plus sign refers to $\phi^* = \pi/2$.

The applicability of the adiabatic theory for a resonance crossing relies on the control of a slow phase change during the variation of the parameter $\delta(\lambda)$. When $\lambda = 0$, $J^* = 1/2$ and

$$\frac{\mathrm{d}J^*(0)}{\mathrm{d}t} \simeq -\frac{\delta_{\max}}{q}\epsilon \qquad (7.40)$$

and this quantity has to be small, i.e. $\ll 1$, to apply the adiabatic theory.

The two fixed points move to opposite directions during the resonance-crossing stage, and the corresponding resonance islands have an amplitude J_{ri} estimated by

$$J_{\mathrm{ri}}(\lambda) = \frac{1}{\left(\frac{\delta(\lambda)}{q}\right)^2 + 1}\,. \qquad (7.41)$$

$J_{\text{ri}}(\lambda)$ is maximum when $\delta(\lambda) = 0$, but at the boundary values, i.e. $\pm\delta_{\max}$, it can be small if $\delta_{\max}/q \gg 1$. In such a case, trapping inside the island can occur near one of the borders, whereas detrapping occurs near the other one and such a phenomenon happens in a symmetric fashion with respect to the horizontal line $J = 1/2$, so that the values I_x and I_y (i.e. the Courant-Snyder invariants and then also the beam emittances) are exchanged by keeping approximately fixed their sum.

7.3 | Analysis of the dynamics using normal modes

By following the approach described in detail in Appendix 7.B, the prototype Hamiltonian to study the emittance exchange process can be written in the normal-modes space in the following form

$$H(\phi, J, \lambda) = \gamma(\lambda) J + \epsilon \sqrt{(1 - J)J} \sin \phi, \tag{7.42}$$

where, without loss of generality, we assume $J_2 = 1$, so that $J = 0$ and $J = 1$ are singular lines for the Hamiltonian. Although the geometrical properties of the dynamics generated by the Hamiltonian (7.42) coincide with those of (7.23), the two descriptions are carried out in different spaces, namely that of physical co-ordinates for Eq. (7.23) or that of the normal modes for Eq. (7.42). Hence, the exchange of the invariants occurs in different spaces.

The Hamiltonian (7.42) allows to study the effect of adiabaticity in the angular frequency modulation on the preservation of the action variables (J_1, J_2) and of their approximations (J_a, J_b) in the physical planes.

The Hamiltonian (7.42), being of the same form as (7.23), has two elliptic fixed points at $\phi^* = \pi/2, \ 3\pi/2$ and

$$\gamma(\lambda) = \pm\epsilon \frac{1 - 2J^*}{\sqrt{J^*(1 - J^*)}} \tag{7.43}$$

so that if $\gamma \gg \epsilon$ they are very close to boundaries $J = 0$ and $J = 1$, which means that the resonance trapping is not possible, and we have simply the invariance of J for $\epsilon \to 0$. The maximum resonance amplitude J_{ra} occurs at the minimum value of γ

$$J_{\text{ra}} = \frac{1}{O\left(\left(\frac{q}{\epsilon}\right)^2\right) + 1} \tag{7.44}$$

so that $J_{\text{ra}} = \mathcal{O}(1)$ only if $q = \mathcal{O}(\epsilon)$ whereas if $q \gg \epsilon$, then J_{ra} is negligible, which clearly describes the interplay between the two small parameters q and ϵ.

Even for $q = \mathcal{O}(\epsilon)$, I_1 and I_2 are adiabatic invariants, which are referred to the phase planes defined by the eigenvectors. At the beginning of the crossing process, given that q is small, the two planes are close to the original phase planes (X, P_X) and (Y, P_Y), and the same holds for the initial actions so that $I_1 \simeq I_x(0)$ and $I_2 \simeq I_y(0)$. With an error $\mathcal{O}(q)$, at the end of the process the two planes are exchanged, and the same is true for the emittances with the same approximation $\mathcal{O}(q)$. Hence, q defines the maximum possible emittance exchange whereas $\epsilon \ll 1$ allows a conservation of the adiabatic invariants.

Furthermore, the action-angle variables are analytic for $\gamma(\lambda) \to 0$ and the Hamiltonian reduces to the form

$$H(\phi, J, \lambda) = H(J, \lambda) + \epsilon H_1(\phi, J, \lambda), \qquad (7.45)$$

which is analytic on the sphere. It is then possible to apply the theorem reported in Ref. [75] to the Hamiltonian $H(\phi, J, \lambda)$ to state that the change of the action ΔJ for a given orbit of the system is exponentially small, i.e.

$$\Delta J = O(\exp(-c/\epsilon)) \qquad (7.46)$$

with c a positive constant, when λ varies, which corresponds to the crossing of the original difference resonance.

It is worth stressing that the same remarks made for the Hamiltonian (7.23) about the rescaled adiabaticity parameter hold also for the Hamiltonian (7.42). Therefore, one can state that

$$\Delta J = O\left(\exp\left(-c\,q^2/\epsilon\right)\right) \qquad (7.47)$$

in case of a resonance crossing linear in λ, or

$$\Delta J = O\left(\exp\left(-cq^{\frac{2n+2}{2n+1}}/\epsilon\right)\right) \qquad (7.48)$$

in case of a crossing of the resonance that is nonlinear in λ. Note that a nonlinear resonance crossing is more advantageous in terms of the adiabaticity of the process with respect to a linear one.

7.4 | Impact of amplitude detuning

In the presence of amplitude detuning generated by nonlinearities, the dynamics is governed by the Hamiltonian (7.6) plus the terms [64]

$$H_{\text{det}}(p_x, p_y, x, y) =$$

$$\alpha_{xx}\left(\frac{x^2 + p_x^2}{2}\right)^2 + 2\alpha_{xy}\left(\frac{x^2 + p_x^2}{2}\right)\left(\frac{y^2 + p_y^2}{2}\right) + \alpha_{yy}\left(\frac{y^2 + p_y^2}{2}\right)^2. \qquad (7.49)$$

This approach assumes that either nonlinear resonances are not excited by the nonlinearities, otherwise, additional terms should be included in the model studied, or that the resonances excited are far from the difference resonance we are considering. By performing the same substitutions that led to the Hamiltonian (7.23) starting from (7.6), H_{det} becomes

$$H_{\text{det}}(\phi_a, J_a) = \alpha_{aa} J_a^2 + \alpha_{ab} J_a J_b \,, \tag{7.50}$$

where a constant term in J_b has been discarded as J_b is a constant of motion and hence the constant term is irrelevant for the dynamics of J_a and ϕ_a, and

$$\alpha_{aa} = \alpha_{xx} - 2\alpha_{xy} - \alpha_{yy} \qquad \alpha_{ab} = 2\alpha_{xy} - \alpha_{yy} \tag{7.51}$$

and the complete Hamiltonian becomes

$$
\begin{aligned}
H(\phi_a, J_a, \lambda) = (\delta(\lambda) + \alpha_{ab} J_b) J_a + \alpha_{aa}\sqrt{\omega_x(\lambda)\omega_y(\lambda)}\, J_a^2 + \\
+ q\sqrt{J_a(J_b - J_a)} \cos\phi \,.
\end{aligned} \tag{7.52}
$$

It is obvious that α_{ab} can be reabsorbed in the definition of δ, which effectively would correspond to shifting the resonant condition to $\omega_x - \omega_y + \alpha_{ab} J_b = 0$ or, equivalently, to shifting the time at which the resonance is crossed. It is also evident that by acting on the three physical quantities α_{xx}, α_{xy}, α_{yy} it is possible to control the values of α_{aa} and α_{ab} independently on each other. As it was done for the Hamiltonian (7.23), it is possible to shift the phase of ϕ and set $J_b = 1$ to cast (7.52) in the following form

$$H(\phi, J, \lambda) = \tilde{\delta}(\lambda) J + \alpha(\lambda) J^2 + q\sqrt{J(1 - J)} \sin\phi \,. \tag{7.53}$$

Whenever the analysis would be carried out in the normal modes' coordinates, then it would be immediate to find that the amplitude detuning would lead to the following general Hamiltonian

$$H(\phi, J, \lambda) = \tilde{\gamma}(\lambda) J + \hat{\alpha}(\lambda) J^2 + \epsilon\sqrt{J(1 - J)} \sin\phi \,, \tag{7.54}$$

where also in this case $\tilde{\gamma}(\lambda)$ incorporates a constant term α_{ab} with respect to the original definition used in (7.42).

The parameter $\alpha(\lambda)$ (or $\hat{\alpha}(\lambda)$) has a fundamental impact on the phase-space topology as, when $\alpha = 0$ the Hamiltonians (7.23) or (7.42) have only two elliptic fixed points, whereas when $\alpha \neq 0$ an additional pair of one elliptic and one hyperbolic fixed point might be generated (see Ref. [64]). The conditions for the existence of these additional fixed points are discussed in Appendix 7.c. Indeed, the presence of a hyperbolic fixed point implies the existence of a separatrix, which introduces a singularity in the phase-space structure and hence
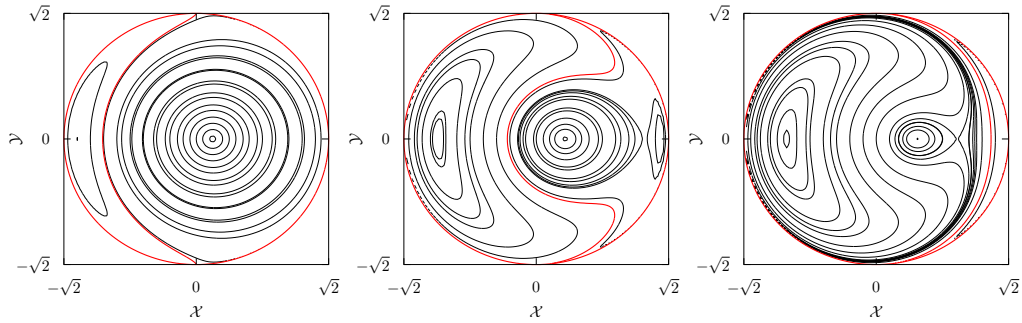
FIGURE 7.3 – Phase portraits of the Hamiltonian (7.52) with $\alpha_{aa} = 1$, $\alpha_{ab} = 0$, $q = 0.25$, $J_b = 1$ at $\delta = -1$ (left), $\delta = -0.58$ (center), $\delta = -0.44$ (right), in Cartesian $(\mathcal{X}, \mathcal{Y})$ co-ordinates. The orbits that pass through $\mathcal{X} = 0$, $\mathcal{Y} = \pm\sqrt{2}$ are shown in red.

alters the character of the dynamics. Examples of phase-space portraits for different values of δ are shown in Fig. 7.3, and the hyperbolic fixed points are clearly visible.

In particular, the nice property about the exponentially small change of J, linked to the analyticity of the dynamics of (7.42), is lost. From the discussion presented in the Appendix 7.C it follows that when α_{aa} is sufficiently small, no extra fixed point is present and the phase-space topology is unchanged with respect to (7.23) with no separatrix present and hence an exponentially small bound on the variation of the invariant change during the resonance-crossing process.

7.5 | Two-way crossing of the coupling resonance

So far, the focus has been on the analysis of the adiabaticity properties of the crossing of the coupling resonance for a linear and nonlinear system. However, another process is possible and is interesting to consider, namely the two-way crossing of the resonance. Such a process would allow studying the reversibility of the resonance-crossing process and, in particular, the impact on the phase variable, as that on the action variable is already fully covered by the considerations made in the previous sections. The treatment proposed in [4] is used to deal with the two-way resonance crossing. The starting point is the Hamiltonian (7.54) in which the parameter $\gamma(\lambda)$ is supposed to describe a closed curve when $\lambda \in [0, 1]$, corresponding to $t \in [0, 1/\epsilon]$. The change in the phase of the action-angle variables when the system moves along the closed curve can

be evaluated by [4]

$$\phi\left(\frac{1}{\epsilon}\right) - \phi(0) = \chi_{\text{dyn}} + \chi_{\text{geom}} + \chi_{\text{rem}}, \qquad (7.55)$$

where the three terms can be generically computed, assuming the Hamiltonian is given as $H = H_0(J, \gamma(\tau)) + \epsilon H_1(\phi, J, \tau)$, according to

$$\chi_{\text{dyn}} = \frac{1}{\epsilon} \int_0^1 \frac{\partial H_0(J(\frac{\tau}{\epsilon}), \gamma(\tau))}{\partial J} \, d\tau$$

$$\chi_{\text{geom}} = \int_0^1 \frac{\partial \mathcal{H}_1(J(0), \tau)}{\partial J} \, d\tau, \quad \mathcal{H}_1 = \langle H_1 \rangle_\phi \qquad (7.56)$$

$$\chi_{\text{rem}} = \epsilon \int_0^{1/\epsilon} \frac{\partial H_1(\phi(\eta), J(\eta), \epsilon\eta)}{\partial J} \, d\eta - \chi_{\text{geom}}.$$

The first term, χ_{dyn}, takes into account the dynamical change of the phase and is relevant in the adiabatic regime, i.e. when $\epsilon \ll 1$ and depends only on the form of H_0. The second term, χ_{geom}, depends on the angular average of H_1 and is the so-called Berry phase [20, 21] or Hannay angle [43]. The third term, χ_{rem}, is relevant in the non-adiabatic regime and depends only on H_1.

These general definitions can be specialized to the case of the Hamiltonian (7.54) and one obtains

$$\chi_{\text{dyn}} = \frac{1}{\epsilon} \int_0^1 \gamma(\tau) \, d\tau$$

$$\chi_{\text{geom}} = 0 \qquad (7.57)$$

$$\chi_{\text{rem}} = \frac{\epsilon}{2} \int_0^{1/\epsilon} \frac{1 - 2J(\eta)}{\sqrt{(1 - J(\eta)) J(\eta)}} \sin\phi(\eta) \, d\eta,$$

where $\chi_{\text{geom}} = 0$ is due to the special form of H_1, which is zero when averaged over the angle ϕ. Note that χ_{dyn} is independent on the action variable, whereas it depends on ϵ. It is worth noting that geometrically, χ_{dyn} represents the area enclosed by the closed curve described by $\gamma(\tau)$, and such an area is zero in case resonance is crossed in the same way in each of the two directions. χ_{rem} depends on the action-angle variables. This means that in the adiabatic regime the phase is affected by an ϵ-dependent shift, only, whereas in the non-adiabatic case the shift depends also on the action-angle variables. Therefore, in the adiabatic case the distribution of initial conditions is rigidly rotated, i.e. by an amplitude-independent angle, in a two-way crossing of the coupling resonance (the action variable is only very weakly affected), while in

the non-adiabatic case the initial distribution undergoes a nonlinear deformation by a two-way resonance-crossing process.

It is worth stressing that the rigid rotation of the initial distribution in case of a two-way crossing of the coupling resonance in the adiabatic regime is a consequence of the special form of H_0, which is linear in the action variable. Indeed, whenever amplitude detuning is considered, H_0 is no longer a linear function of J and, hence, even in the adiabatic regime, the initial distribution will be rotated by an amplitude-dependent quantity. This means that a two-way crossing of the resonance is never a fully reversible process for a nonlinear system. Hence, a periodic crossing of the coupling resonance, even if it occurs adiabatically, will always distort the distribution, with an adverse effect on the preservation of the linear invariants. In physical terms, this is the situation for a circular accelerator operated with nonzero chromaticity and close to the coupling resonance, which can be crossed due to the tune modulation induced by the chromaticity.

7.6 | The map model

A system made of a FODO cell and a skew quadrupole, which is interpolated by the phase flow of the Hamiltonian (7.6), is described by the one-turn map given by

$$x_{n+1} = M_{\text{FODO}} M_{\text{Skew}} x_n \tag{7.58}$$

where

$$M_{\text{Skew}} = \begin{pmatrix} 1 & 0 & 0 & 0 \\ 0 & 1 & \hat{q} & 0 \\ 0 & 0 & 1 & 0 \\ \hat{q} & 0 & 0 & 1 \end{pmatrix}. \tag{7.59}$$

Using the steps detailed in the Appendix 7.D, it is possible to recast Eq. (7.58) as a Hénon-like map as

$$\begin{pmatrix} X \\ X' \\ Y \\ Y' \end{pmatrix}_{n+1} = \begin{pmatrix} R(\omega_x) & 0 \\ & \\ 0 & R(\omega_y) \end{pmatrix} \begin{pmatrix} X \\ X' + qY \\ Y \\ Y' + qX \end{pmatrix}_n \tag{7.60}$$

and this is the map used in the numerical simulations presented in Section 7.7.

As an example, the resonance-crossing process is shown in Fig. 7.4, where a distribution of initial conditions with variable $J_{\text{a,i}}$ value and a constant $J_{\text{b}} = 2 \times 10^{-4}$ evolves through the resonance from a negative value of δ (left), a zero one (center), and a positive one (right) using the map (7.60). The color scale
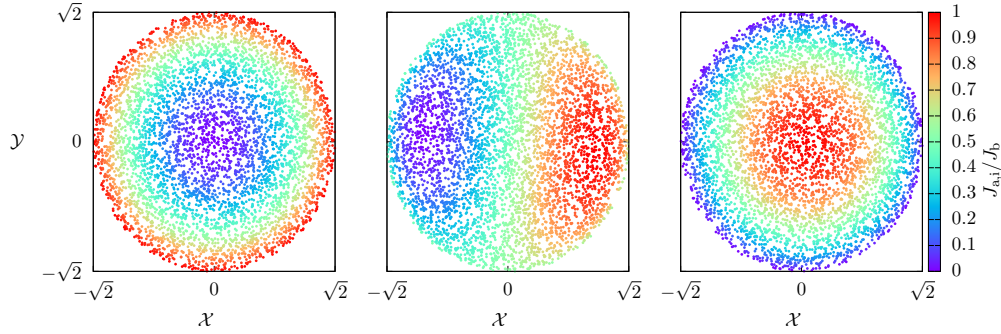
FIGURE 7.4 – Distribution of particles in $(\mathcal{X}, \mathcal{Y})$ space from simulation of map (7.60) for $\delta = -0.1$ (left), $\delta = 0$ (center), and $\delta = 0.1$ (right), for a set of initial conditions at fixed $J_b = 2 \times 10^{-4}$. The colors encode the value of the initial action $J_{a,i}$, and show how particles exchange their action values $J_{a,f}$ at the end of the process.

is used to encode the value of J_a and it is clearly visible how the conditions exchange the J_a value between beginning and end of the crossing process. In fact, the conditions around the origin of phase space at the end of the crossing have the same action values as those in the outer part of phase space at the beginning.

The analysis of the impact of the amplitude detuning has been studied by modifying the map (7.60) including the effect of a angular frequency variation on the amplitude in phase space. In this case, in Eq. 7.60 we substitute ω_x with $\tilde{\omega}_x(X, X', Y, Y')$ and ω_y with $\tilde{\omega}_y(X, X', Y, Y')$, where

$$
\begin{aligned}
\tilde{\omega}_x &= \omega_x + \alpha_{xx}(X^2 + X'^2) + \alpha_{xy}(Y^2 + Y'^2) \,, \\
\tilde{\omega}_y &= \omega_y + \alpha_{xy}(X^2 + X'^2) + \alpha_{yy}(Y^2 + Y'^2) \,.
\end{aligned}
\tag{7.61}
$$

Here α_{xx}, α_{xy}, α_{yy} are the terms introduced in (7.49) to describe the variation of the angular frequency with amplitude in the two transverse planes. This model satisfies the requirements mentioned earlier of simulating an angular frequency variation with amplitude, but without exciting resonances other than the coupling one.

7.7 | Results of numerical simulations

Numerical simulations have been performed using both the Hamiltonian and the map models. However, based on the fact that the results obtained are the same, only those obtained with the map will be presented here.

7.7.1 | Linear map model

As a first step, numerical simulations have been carried out to evaluate the dependence of the emittance-exchange phenomenon on the adiabaticity of the resonance-crossing process. In the simulations, ω_y has been changed while keeping ω_x constant. Thus, $\delta(\lambda) = \omega_x - \omega_y(\lambda)$ is changed from a negative to a positive value passing through zero. As a figure of merit, we used the function P_{na}, introduced in [1], which is defined as

$$P_{\mathrm{na}} = 1 - \frac{\langle I_{x,\mathrm{f}} \rangle - \langle I_{x,\mathrm{i}} \rangle}{\langle I_{y,\mathrm{i}} \rangle - \langle I_{x,\mathrm{i}} \rangle}\,, \tag{7.62}$$

where $I_{z,\mathrm{i}}$ and $I_{z,\mathrm{f}}$ are the initial and final linear action variables, respectively. Therefore, P_{na}, is zero when a perfect exchange is attained and one when no exchange occurs.

The evolution of a set of initial conditions, representing a beam exponentially distributed in I_x, i.e. $\rho(I_x) = (N_0/\langle I_x \rangle) \exp(-I_x/\langle I_x \rangle)$, has been computed by means of the map (7.60), while varying ω_y in the fixed interval $\omega_{y,\mathrm{i}} = 2.5$ and $\omega_{y,\mathrm{f}} = 2.7$ over a given time interval N. According to the Hamiltonian theory presented in the previous sections, we expect that $\langle I_x \rangle$ becomes $\langle I_y \rangle$ after the resonance crossing. What we observe in Fig. 7.5 is a clear exponential dependence of P_{na} as a function of $1/\epsilon$, in evident agreement with the findings of Ref. [1], and also in perfect agreement with the discussion carried out previously.

The exponential behavior of P_{na} features a clear dependence on q, and an oscillatory behavior is also observed. We have been studying this effect by means of dedicated numerical simulations, in which the evolution of P_{na} at large number of turns has been probed.

Figure 7.6 (top left) shows these oscillations, whose amplitude and angular frequency are shown in the top-right and center-left plots, respectively. The oscillations of P_{na} are characterized by an angular frequency, which has been determined by using refined techniques based on FFT [8, 9], that for small q-values corresponds to $(\omega_{y,\mathrm{f}} - \omega_x)/2$. The sudden jump visible in the inset is due to the q-value being too small for the ϵ-value used to preserve the resonance-crossing process. This is similar to what can be observed in the center-right plot of the same figure. The residual for $q \to 0$ is given by $(\omega_{y,\mathrm{f}} - \omega_x)/4$, as shown by the analysis in Appendix 7.E.

In the center-right part of Fig. 7.6 a zoom of the behavior of the average P_{na} for small $|q|$ values is shown and the characteristic scaling with q^2 is clearly visible, which is linked to the neglected terms that are affecting the preservation of the invariants. Note the rapid increase of P_{na} towards 1 when $|q| \to 0$, which
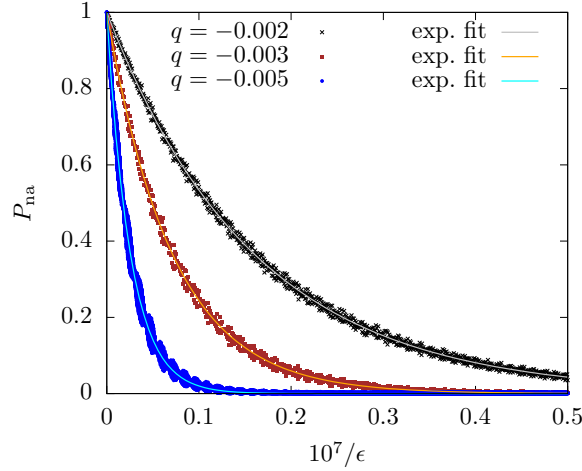
FIGURE 7.5 – Evolution of P_{na} as a function of $1/\epsilon$ for an exponential distribution of initial conditions, and different values of q. Exponential fits are also presented. The map (7.60) has been used, with parameters $\omega_x = 2.602$, $\omega_{y,\text{i}} = 2.5$, $\omega_{y,\text{f}} = 2.7$, and a set of initial conditions with $\langle I_{x,\text{i}} \rangle = 10^{-4}$, $\langle I_{y,\text{i}} \rangle = 4 \times 10^{-4}$.

originates from the linear coupling being too small for the exchange of the invariants to occur.

Another important point to stress is that these scaling laws are not connected to the features of the distribution of initial conditions, as the theoretical results clearly indicate that these properties are linked to the individual orbits of the Hamiltonian system. Indeed, this can be seen in Fig. 7.7.

In fact, when plotting $\langle J_{\text{a,f}} \rangle$ as a function of $J_{\text{a,i}}$ (left), we observe a linear difference between $(J_{\text{b}} - J_{\text{a,i}})$ and $\langle J_{\text{a,f}} \rangle$ when the adiabatic parameter ϵ is very small. This difference decreases exponentially when we vary the adiabaticity of the resonance-crossing process (right), i.e. $\Delta J_{\text{a}} = \kappa \exp\left[-\xi(\omega_{y,\text{f}} - \omega_{y,\text{i}})/\epsilon\right]$. Note that also in this case oscillations appear when ϵ decreases as the actions $J_{a,b}$ are not the correct adiabatic invariant due to the value of q used in the simulations.

The dependence of the exponential fit parameters κ and ξ can be fully determined by means of numerical simulations. If we perform the same analysis on different values of the initial action (using a set of initial conditions $\delta(J_a - J_{\text{a,i}})$ uniformly distributed w.r.t. the angular variable) and we apply the same exponential fit we see that $\kappa \propto J_{\text{a,i}}$ whereas ξ remains constant (Fig. 7.8, left).

Therefore, the value of $\xi = (1.9544 \pm 0.0007) \times 10^{-4}$ (obtained by fitting the data with a constant) is independent on the initial radial distribution and is indeed retrieved in the fit of Fig. 7.5 for $q = -0.005$ where we get $\xi =$
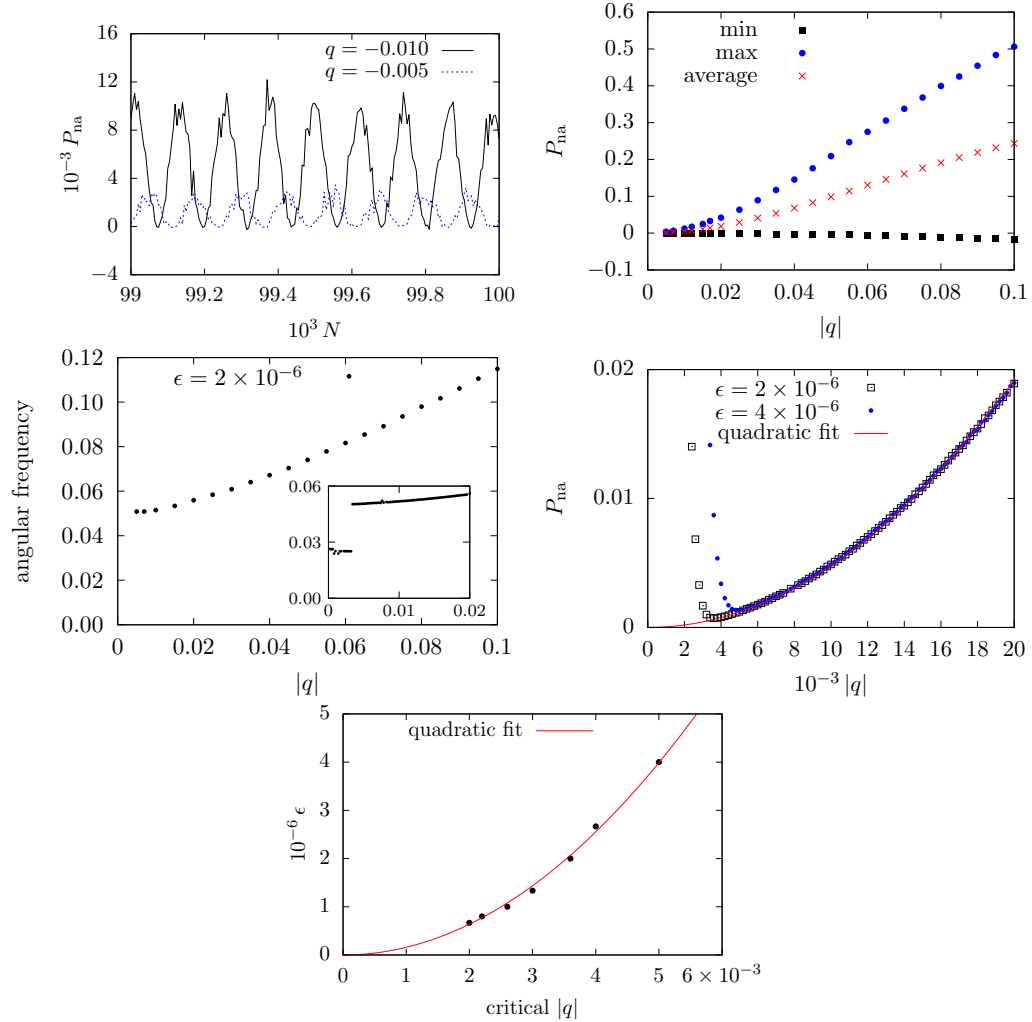
FIGURE 7.6 – Top left: Oscillations of P_{na} at large values of turns N for different values of q. Top right: Minimum, average, and maximum value of P_{na} for $9 \times 10^4 \leq N \leq 1 \times 10^5$ for different values of q. Center right: zoom in the small q region of the average value of P_{na} with a quadratic fit. Note that for small $|q|$ values the emittance exchange breaks down, which is indicated by P_{na} growing towards 1 and the q-value corresponding to the break down is ϵ-dependent. Center left: main angular frequency of the oscillations of P_{na} obtained by a refined FFT as a function of q. Bottom: relation between the critical value of $|q|$, for which the break down of P_{na} is observed, and ϵ. A quadratic fit to the data is also shown, which confirms the scaling law (7.63). The map (7.60) has been used, with parameters $\omega_x = 2.602$, $\omega_{y,\mathrm{i}} = 2.5$, $\omega_{y,\mathrm{f}} = 2.7$, and a set of initial conditions with $\langle I_{x,\mathrm{i}} \rangle = 10^{-4}$, $\langle I_{y,\mathrm{i}} \rangle = 4 \times 10^{-4}$.
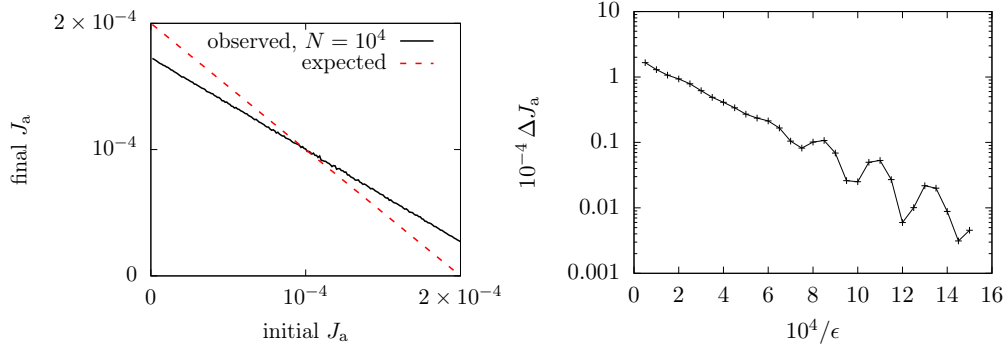
FIGURE 7.7 – Left: computed, ($\langle J_{a,f} \rangle$, black line) and expected, ($J_b - J_{a,i}$, red, dashed) final value of the invariant as a function of $J_{a,i}$ after a resonance-crossing procedure. To each $J_{a,i}$ value is associated a uniform distribution of angles in $[0, 2\pi]$. Right: amplitude of the difference between the two lines in the left plot for $J_{a,i} = 0$ (close to the fixed-point position) as a function of $1/\epsilon$. The map (7.60) has been used, with parameters $q = -0.005$, $\omega_x = 2.602$, $\omega_{y,i} = 2.5$, $\omega_{y,f} = 2.7$, and a set of initial conditions with $J_b = 2 \times 10^{-4}$.
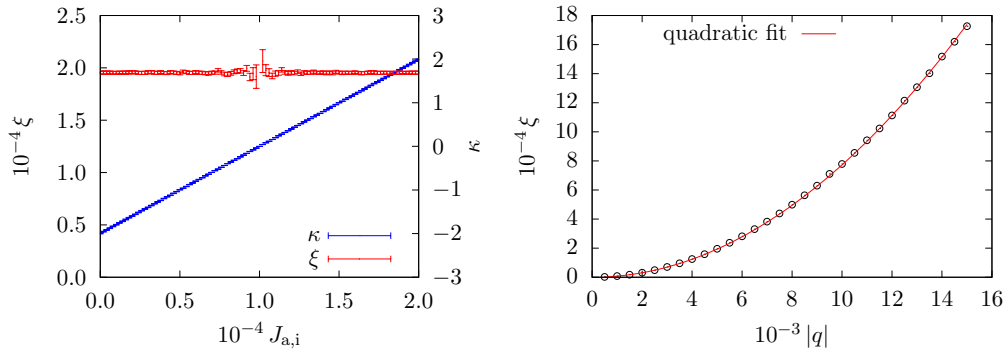
FIGURE 7.8 – Left: Parameters of the exponential fit to the formula $\Delta J_a = \kappa \exp\left[-\xi(\omega_{y,f} - \omega_{y,i})/\epsilon\right]$ for distributions with constant $J_{a,i}$ as in the bottom plot of Fig. 7.7 as a function $J_{a,i}$. The oscillations of the value of ξ when $J_{a,i}$ is close to $J_b/2$ is linked to the increase of the uncertainty on the exponential fit parameter at small values of $|\kappa|$. Right: Dependence of the parameter of the exponential ξ on the q (a quadratic fit is also presented). The map (7.60) has been used with parameters $q = -0.005$ (for the left plot), $\omega_x = 2.602$, $\omega_{y,i} = 2.5$, $\omega_{y,f} = 2.7$, and a set of initial conditions with $J_b = 2 \times 10^{-4}$.

$(1.9563 \pm 0.0015) \times 10^{-4}$. Finally, as predicted in Section 7.3, we observe (Fig. 7.8, right) that ξ depends quadratically on the linear coupling strength q, as found also in [1].

It is key to stress that the scaling law $\Delta J_a = \kappa \exp\left(-\hat{\xi}\, q^2/\epsilon\right)$, which has been justified theoretically in the previous sections, is essential in establishing a link between the two parameters q and ϵ that are governing the dynamics of the system under consideration. Indeed, whenever the following is satisfied

$$\epsilon = \text{const.} \times q^2 \tag{7.63}$$

the variation of J_a is left unchanged. This means that when q is decreased, ϵ should be reduced even further to maintain the character of the dynamics unaffected. This aspect is clearly appreciated in Fig. 7.6 (center right) where the curves corresponding to two values of ϵ are shown: a reduction of ϵ allows moving forward the break down behavior observed. This phenomenon has been studied in detail, and the results are shown in the bottom plot of Fig. 7.6, where the relationship between the break-down value q and the corresponding ϵ value is shown. The points lie on a quadratic curve, in perfect agreement with the scaling law reported in Eq. (7.63). It is evident that in the case of a resonance crossing that is nonlinear in λ, as discussed earlier, the relationship (7.63) reads

$$\epsilon = \text{const.} \times q^{\frac{2n+2}{2n+1}}\,, \tag{7.64}$$

where $2n+1$ is the power of λ with which the resonance is crossed.

The distribution of the action jumps during the resonance-crossing process for a set of initial conditions with the same value of $J_{a,i}$ and the phase uniformly distributed in $[0, 2\pi]$, is shown in Fig. 7.9.

It is worth noting that when ϵ decreases the average of the jump of the invariant tends to zero (see the right plot in Fig. 7.12) and the extent of the support of the distribution of ΔJ_a shrinks. At the same time, the distribution becomes more symmetrical and it flattens out.

7.7.2 | Map model with amplitude detuning

As described in Section 7.4, we studied also the impact of amplitude detuning on the adiabaticity of the emittance exchange using the map model given in (7.60) with the frequencies of Eq. (7.61) and simulating the resonance-crossing process in the same way as in the absence of detuning. The map with detuning depends on three parameters that describe how the frequencies vary with the amplitude in phase space. In the numerical simulations presented in the following a single parameter α is varied, which is related with the others by $\alpha = 2\alpha_{xx} = 2\alpha_{yy} = -4\alpha_{xy}$. This choice is made to mimic the amplitude
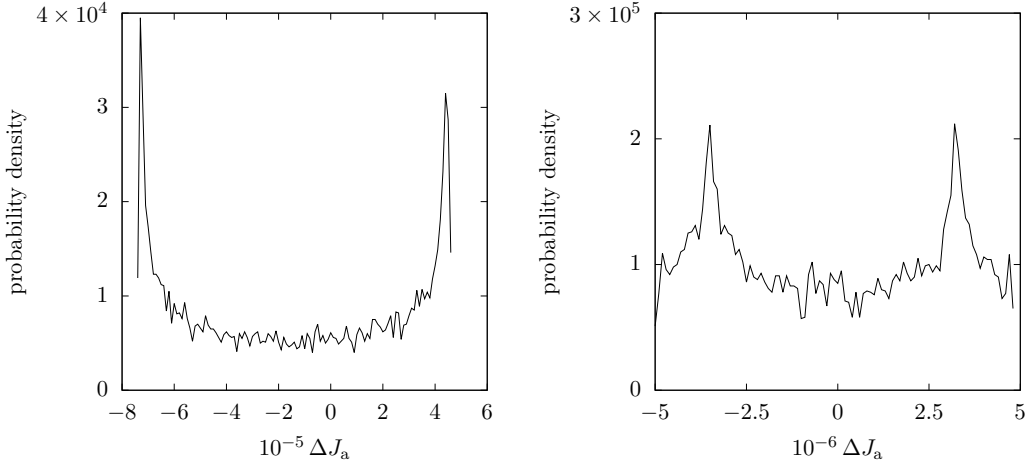
FIGURE 7.9 – Distribution of the jump of the invariant (difference between $J_{a,f}$ and the expected one $J_b - J_{a,i}$) for particles at $J_{1,i} = 5 \times 10^{-5}$. Left: $N = 10^4$, i.e. $\epsilon = 2 \times 10^{-5}$, Right: $N = 5 \times 10^4$, i.e. $\epsilon = 4 \times 10^{-6}$. The map (7.60) has been used, with parameters $q = -0.005$, $\omega_x = 2.602$, $\omega_{y,i} = 2.5$, $\omega_{y,f} = 2.7$, $J_b = 2 \times 10^{-4}$.

detuning generated by a system including a single octupole in thin lens approximation [17].

For Gaussian distributions of initial conditions corresponding to different emittances in x and y, P_{na} has been evaluated for different values of α and the results are shown in Fig. 7.10.

Two behaviors, depending on the value and sign of α, are clearly visible. For $\alpha > 0$ and α small in absolute value, P_{na} is essentially zero, which indicates that even when amplitude detuning is present, a perfect emittance exchange occurs. Such a behavior is hardly seen for $\alpha < 0$, even in the neighborhood of zero. Rather, a sharp rise of P_{na} is visible. Globally, outside a small interval around zero for α, P_{na} is always different from zero, indicating that the emittance exchange is not perfect.

Note that the position of the new fixed points either on the right or on the left of the coupling arc is linked to the sign of α. Therefore, the presence of new detuning-related fixed points has a different impact on the final distribution of initial conditions, and hence on the emittance exchange, depending on where they are located in the phase space. In this specific case, when $0 < \alpha < 15$ even if α is positive the effect on P_{na} is negligible: this is compatible with the theoretical predictions that small enough values of α do not generate new fixed points and do not affect the emittance exchange.

The essential difference between the linear case and that with amplitude detuning is clearly visible when investigating the dependence of P_{na} on the adi-
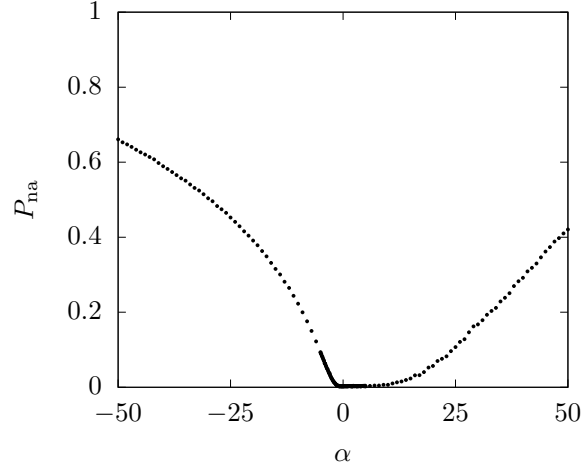
FIGURE 7.10 – P_{na} as a function of the detuning coefficient α. The map (7.61) has been used with parameters $q = -0.008$, $\omega_x = 2.602$, $\omega_{y,\mathrm{i}} = 2.5$, $\omega_{y,\mathrm{f}} = 2.7$, $N = 10^5$, and a set of initial conditions with $\langle I_{x,\mathrm{i}} \rangle = 10^{-4}$, $\langle I_{y,\mathrm{i}} \rangle = 4 \times 10^{-4}$.

abatic parameter ϵ. This is shown in Fig. 7.11 (top left). The exponential behavior is lost and is replaced by a power-law function for P_{na}.

The two values of α have been selected to provide cases in which more than two fixed points are present. The dependence on α is shown in the top-right plot, where the dependence of the fit parameters is reported together with the behavior of the reduced χ^2, which is depicted for the power- and exponential-law cases. The behavior of the reduced χ^2 for the two fit models shows clearly that while the exponential dependence is the most suitable one for α close to zero, the power-law best describes the data outside of this interval of α. This is in full agreement with the theoretical discussion carried out in the previous section. Finally, the dependence of the fit parameters for some values of α is shown as a function of q in the bottom plots of Fig. 7.11.

Additionally, in the presence of amplitude detuning, it is possible to derive a scaling law linking q and ϵ. It is very easy to conclude that P_{na} is linked to the change of the invariants during the crossing process. Therefore, the scaling law $P_{\mathrm{na}} = a\epsilon^{b(\alpha,q)} + c(\alpha,q)$, which has been analyzed in Fig. 7.11, gives rise to the following relationship

$$\ln \epsilon = \frac{\mathrm{const.} + c(\alpha,q)}{a\,b(\alpha,q)} \,, \tag{7.65}$$

which should be fulfilled in order to keep constant the change of the invariant. The essential difference with respect to what has been found in the absence of nonlinear detuning is apparent.
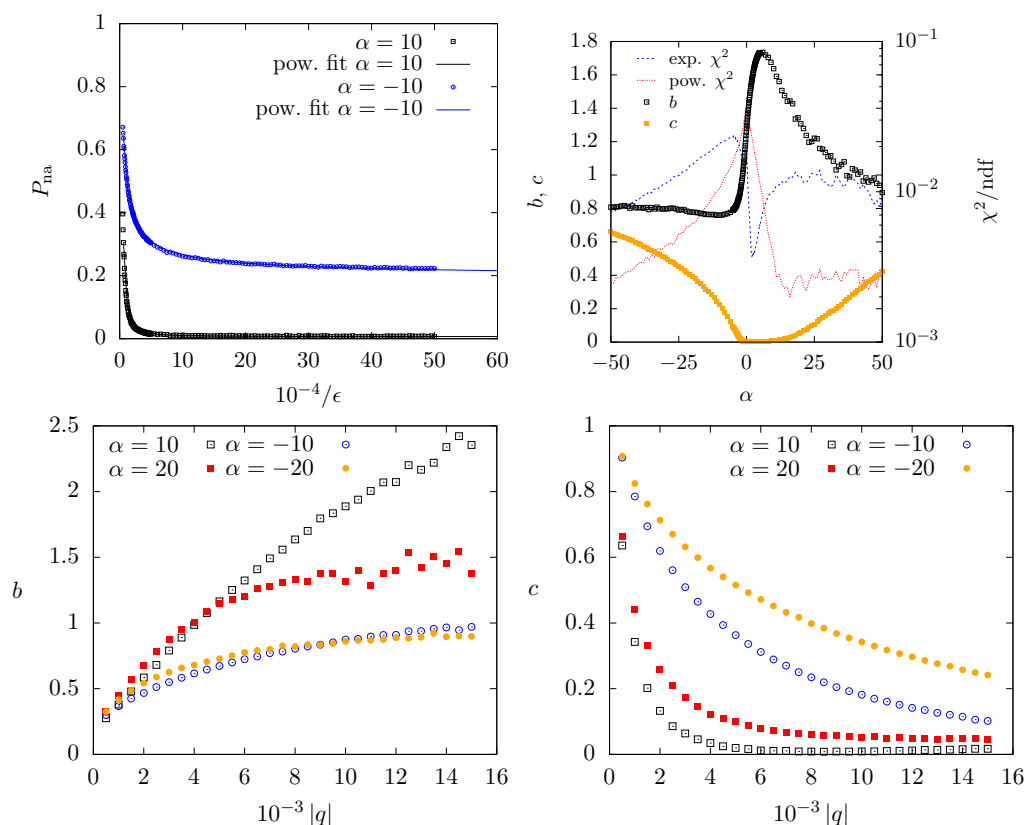
FIGURE 7.11 – Top left: Dependence of P_{na} on ϵ for $\alpha = 10$ and $\alpha = -10$. A power-law dependence $P_{na} = a\epsilon^b + c$, is fitted and the results are also shown ($b = -1.61 \pm 0.01$ for $\alpha = 10$ and $b = -0.642 \pm 0.006$ for $\alpha = -10$). Top right: Dependence of the power-law exponent b and c (left axis) and reduced χ^2 for the power- and exponential-law fits (right axis) as a function of α. Bottom: dependence of power-law exponent b (left) and c (right) on q, for some values of α. The map (7.61) has been used, with parameters $q = -0.008$ (top plots), $\omega_x = 2.602$, $\omega_{y,i} = 2.5$, $\omega_{y,f} = 2.7$, $N = 10^5$, $\epsilon = 2 \times 10^{-6}$, and a set of initial conditions with $\langle I_{x,i} \rangle = 10^{-4}$, $\langle I_{y,i} \rangle = 4 \times 10^{-4}$.
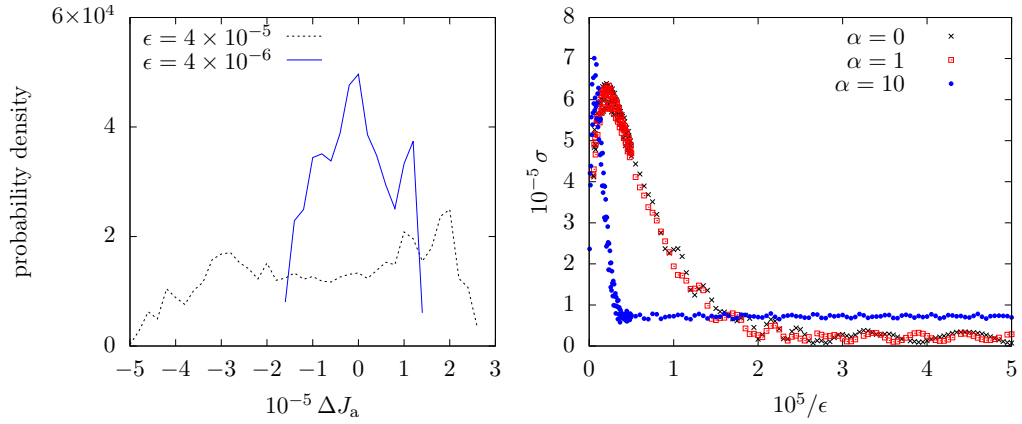
Figure 7.12 – Left: Distribution of the jump of the invariant (difference between $J_{a,f}$ and the expected one $J_b - J_{a,i}$) for $\alpha = 10$, for $N = 5 \times 10^3$, i.e. $\epsilon = 4 \times 10^{-5}$ and $N = 5 \times 10^4$, i.e. $\epsilon = 4 \times 10^{-6}$. Right: Standard deviation σ of the jumps distribution for $\alpha = 0, 1, 10$ at different values of ϵ. The map (7.61) has been used, with parameters $q = -0.008$, $\omega_x = 2.602$, $\omega_{y,i} = 2.5$, $\omega_{y,f} = 2.7$, and a set of initial conditions with $J_{a,i} = 5 \times 10^{-5}$, $J_b = 2 \times 10^{-4}$.

Finally, Fig. 7.12 shows the features of the distribution of the jumps of the invariants in the case with amplitude detuning.

In the left plot, the distribution of J_a, i.e. the difference between the observed and the expected value of $J_{a,f}$, for $\alpha = 10$ for initial conditions at a given fixed $J_{a,i}$ and J_b, is shown for two values of ϵ. The distributions look completely different from the ones obtained in the linear case and shown in Fig. 8.6. Although these distributions tend to be centered around zero as ϵ decreases, their standard deviation σ as a function of ϵ might tend to a finite limit for $\epsilon \to 0$. This is visible in the right plot, where the evolution of the standard deviation of the distribution of the action jump is depicted as a function of ϵ. Three values of α are shown, namely, 0, 1, 10. The asymptotic behavior is clearly different: while for the first two values it tends to zero, the case $\alpha = 10$ features a nonzero limiting value. Note that the first two values correspond to $P_{na} = 0$, i.e. a perfect emittance exchange occurs. These results and observations indicate that the invariant is indeed experiencing a finite jump even when the adiabatic regime is reached when α is large enough. This is a direct consequence of the presence of a separatrix linked to additional fixed points, as

found in [52, 73].

7.8 | Conclusions

In this Chapter, the Hamiltonian theory of the dynamic crossing of the coupling resonance has been presented and discussed in detail, considering not only the linear, but also the case with nonlinear dependence of the frequencies on the phase-space amplitude.

The main focus has been the analysis of the so-called emittance exchange process, which arises from the resonance crossing. The detail of the mechanism has been considered, both in standard phase space as well as considering the normal modes, which provide the correct description of the system behavior. In particular, this framework allows considering the interplay between the two small parameters of the problem, namely the adiabaticity parameter and the strength of the linear coupling. It is worth stressing that, while the true invariants are exactly exchanged, the linear actions feature only a partial exchange. This is because they are not the true invariants of the system and that a projection effect from the space of the invariants to the physical space has to be taken into account. All this should be carefully considered when translating these observations to circular accelerators, in which the physical planes are normally the reference concepts used to interpret the phenomena linked to the crossing of the coupling resonance. Otherwise, the system undergoes periodic variations of the transverse emittances as a function of ϵ^{-1}. This is a simple consequence of the fact that, whenever the coupling strength is not small, the uncoupled emittances are no longer the correct invariants of the system. Furthermore, it has been shown how the dynamical properties of the system under consideration can be best appreciated by looking at the dynamics on a sphere, rather than the standard flat phase space.

It has been discussed how the presence of a real separatrix in phase space is the key feature that distinguishes the behavior of the crossing of the coupling resonance for a linear and nonlinear system. The origin of such a difference is connected with the breaking down of the analytical properties of the dynamical system whenever a separatrix is present.

Detailed numerical simulations have been carried out to provide a full characterization of the rich spectrum of behaviors. It is worth stressing that the observed exponential dependence on the adiabaticity parameter of the emittance exchange is a natural consequence of the analyticity properties of the system under consideration. To the best of our knowledge, for the first time, the behavior of a nonlinear system has been probed while crossing the coupling resonance and, in excellent agreement with the theory presented, a power law, instead of an exponential one, has been observed for the emittance exchange process.

A fundamental relationship between the key system parameters q and ϵ has been derived for the case with and without amplitude detuning. Such a link describes how the crossing of the coupling resonance should be performed in order to keep it adiabatic as a function of the value of the linear coupling. It is evident that such a relationship is of paramount importance in applications and, to the best of our knowledge, this is a novel result.

Finally, a digression has been made, considering the features of a two-way crossing of the coupling resonance. By applying the adiabatic theory, it has been shown that the reversibility of the resonance crossing process is not granted in the nonlinear case, even in the adiabatic limit. This is a rather interesting and thoughtful result for its implications in the domain of accelerator physics applications, e.g. in the case of periodic resonance crossing induced by finite chromaticity, for which a non-negligible impact on the beam distribution is to be expected, no matter the speed of the resonance crossing.

Appendices

7.A | On the equations of motion of Hamiltonian (7.23)

Let us consider a Hamiltonian $H(\phi, J)$ and the scaled Hamiltonian

$$\tilde{H}(\phi, J) = \lambda(J)(H(\phi, J) - E_0), \tag{7.66}$$

where $H(\phi_0, J_0) = E_0$. We explicitly compute (in this context f' stands for the derivative of f with respect to J)

$$
\begin{aligned}
\frac{\partial \tilde{H}}{\partial J} &= \lambda(J)\frac{\partial H}{\partial J} + \lambda'(J)(H(\phi, J) - E_0) \\
\frac{\partial \tilde{H}}{\partial \phi} &= \lambda(J)\frac{\partial H}{\partial \phi}
\end{aligned}
\tag{7.67}
$$

so that given the initial conditions (ϕ_0, J_0) and E_0 the solution of the Hamiltonian system

$$
\begin{aligned}
\frac{\mathrm{d}\phi}{\mathrm{d}\tau} &= \frac{\partial \tilde{H}}{\partial J} \\
\frac{\mathrm{d}J}{\mathrm{d}\tau} &= -\frac{\partial \tilde{H}}{\partial \phi}
\end{aligned}
\tag{7.68}
$$

with initial energy $\tilde{H}(\phi, J) = 0$, we obtain the system

$$\frac{1}{\lambda(J)}\frac{\mathrm{d}\phi}{\mathrm{d}\tau} = \frac{\partial H}{\partial J}$$
$$\frac{1}{\lambda(J)}\frac{\mathrm{d}J}{\mathrm{d}\tau} = -\frac{\partial H}{\partial \phi} \tag{7.69}$$

and if we introduce the scaled time $\lambda(J)\mathrm{d}\tau = \mathrm{d}t$, we recover the solution of the initial Hamiltonian. Of course, the phase-space structure of both Hamiltonian systems is the same.

Using this approach, the solutions of the equations of motion of the Hamiltonian (7.23) can be associated with those of the Hamiltonian

$$\tilde{H}(\phi, J, \lambda) = \frac{1}{\sqrt{(1-J)J}}\left\{[\delta(\lambda)J - E_0] + q\sqrt{(1-J)J}\sin\phi\right\}$$
$$= \frac{\delta J - E_0}{\sqrt{(1-J)J}} + q\sin\phi \tag{7.70}$$

in the scaled time $\sqrt{(1-J)J}\,\mathrm{d}t = \mathrm{d}\tau$, where E_0 is the value of the initial energy, namely

$$E_0 = \delta(\lambda)J_0 + q\sqrt{(1-J_0)J_0}\cos\phi_0 . \tag{7.71}$$

Therefore, we consider the orbit with zero energy $H' = 0$ and the equations of motion give the solution of the initial Hamiltonian system in the scaled time. However, the phase space has the same structure for both Hamiltonians. In the Hamiltonian H', E_0 is a parameter.

Starting from the Hamiltonian (7.23) and using the expression given in Eq. (7.71) for E_0 we get the equation of motion (see [59])

$$\ddot{J} + (\delta^2 + q^2)J = \delta E_0 + \frac{q^2}{2} \tag{7.72}$$

that can be explicitly solved in the form of

$$J(t) = \sqrt{\left(\delta E_0 + \frac{q^2}{2}\right) - \frac{E_0^2}{\delta^2 + q^2}}\cos\left(\sqrt{\delta^2 + q^2}\,t\right) +$$
$$+ \delta E_0 + \frac{q^2}{2} \tag{7.73}$$

that is a sinusoidal function, whose period is given by

$$T = \frac{2\pi}{\sqrt{\delta^2 + q^2}} \tag{7.74}$$

and that is independent on the initial energy.

7.B | Analysis of the dynamics using normal modes: details

Let us start from the Hamiltonian (7.6) with the goal of studying the dynamics considering the normal modes. Let us denote $\omega = (\omega_1, \omega_2)$ the vector of the normal modes and $\boldsymbol{R}(\lambda)$ the orthogonal matrix built using the components of the eigenvectors, then the normal variables $\boldsymbol{X}$ are defined

$$x = \boldsymbol{R}(\lambda)\,\boldsymbol{X} \tag{7.75}$$

A generating function for the transformation $F_2(x, \boldsymbol{P}, \lambda)$ can be written in the form

$$F_2(x, \boldsymbol{P}, \lambda) = \boldsymbol{P}^\top \boldsymbol{R}(\lambda)^\top x \tag{7.76}$$

and the new Hamiltonian reads

$$H(\boldsymbol{X}, \boldsymbol{P}, \lambda) = \frac{P_1^2 + P_2^2}{2} + \frac{\omega_1^2(\lambda)X_1^2 + \omega_2^2(\lambda)X_2^2}{2} + \\ + \epsilon \boldsymbol{P}^\top \frac{\partial \boldsymbol{R}^\top}{\partial \lambda}\boldsymbol{R}\,, \tag{7.77}$$

where the last term is generated by the time derivative of the generating function. Furthermore, it can be verified that the matrix

$$\boldsymbol{\Xi}(\lambda) = \frac{\partial \boldsymbol{R}^\top}{\partial \lambda}\boldsymbol{R} \tag{7.78}$$

is anti-symmetric and has the form

$$\boldsymbol{\Xi}(\lambda) = \begin{pmatrix} 0 & \xi(\lambda) \\ -\xi(\lambda) & 0 \end{pmatrix}, \tag{7.79}$$

where

$$\begin{aligned} \xi(\lambda) &= -2q\frac{\omega_x(\lambda)\,\omega_x'(\lambda) - \omega_y(\lambda)\,\omega_y'(\lambda)}{\left(\omega_x^2(\lambda) - \omega_y^2(\lambda)\right)^2 + 4q^2} \\ &= -q\frac{\delta_2'(\lambda)}{\delta_2^2(\lambda) + 4q^2} \end{aligned} \tag{7.80}$$

and we obtain a term analogous to the Coriolis potential in the Hamiltonian. Note that $\xi(\lambda) = 0$ when $\delta'(\lambda) = 0$ and $\xi(\lambda^*) \propto -(2q)^{-1} \gg 1$ when $\delta(\lambda^*) = 0$, however, in this case $\delta'(\lambda^*) = \mathbb{O}(1)$.

We evaluate

$$\frac{\omega_1}{\omega_2} = \frac{1}{2}\left(\frac{\omega_1^2 + \omega_2^2}{\omega_1\omega_2}\right)\left[1 + \frac{\omega_1^2 - \omega_2^2}{\omega_1^2 + \omega_2^2}\right] \tag{7.81}$$

so that we get the estimates

$$
\sqrt{\frac{\omega_1}{\omega_2}} \simeq \sqrt{\frac{1}{2}\left(\frac{\omega_1^2 + \omega_2^2}{\omega_1 \omega_2}\right)}\left[1 + \frac{1}{2}\frac{\omega_1^2 - \omega_2^2}{\omega_1^2 + \omega_2^2}\right]
$$

$$
= \sqrt{\frac{1}{2}\left(\frac{\omega_x^2 + \omega_y^2}{\sqrt{\omega_x^2 \omega_y^2 - q^2}}\right)}\left[1 + \frac{1}{2}\frac{\sqrt{\delta_2^2(\lambda) + 4q^2}}{\omega_x^2 + \omega_y^2}\right] \tag{7.82}
$$

$$
\sqrt{\frac{\omega_2}{\omega_1}} \simeq \sqrt{\frac{1}{2}\left(\frac{\omega_x^2 + \omega_y^2}{\sqrt{\omega_x^2 \omega_y^2 - q^2}}\right)}\left[1 - \frac{1}{2}\frac{\sqrt{\hat{\delta}^2(\lambda) + 4q^2}}{\omega_x^2 + \omega_y^2}\right].
$$

Finally we define the quantities

$$
\xi_1(\lambda) = \xi(\lambda)\sqrt{\frac{1}{2}\left(\frac{\omega_x^2 + \omega_y^2}{\sqrt{\omega_x^2 \omega_y^2 - q^2}}\right)} \tag{7.83}
$$

$$
\xi_2(\lambda) = \xi(\lambda)\sqrt{\frac{1}{8}\frac{\delta_2^2(\lambda) + 4q^2}{\sqrt{(\omega_x^2 \omega_y^2 - q^2)(\omega_x^2 + \omega_y^2)}}}, \tag{7.84}
$$

and we observe that $\xi_2 = \mathcal{O}(q)$ when $\delta(\lambda) \to 0$.

By introducing the scaled variables

$$
\tilde{X} = (X_1/\sqrt{\omega}_1,\ X_2/\sqrt{\omega}_2), \qquad \tilde{P} = (P_1\sqrt{\omega}_1,\ P_2\sqrt{\omega}_2) \tag{7.85}
$$

and the matrix $\mathbf{\Omega} = \mathrm{diag}(\omega_1, \omega_2)$ we get the Hamiltonian

$$
H(\tilde{X}, \tilde{P}, \lambda) = \omega_1(\lambda)\frac{X_1^2 + P_1^2}{2} + \omega_2(\lambda)\frac{X_2^2 + P_2^2}{2} +
$$

$$
+ \epsilon \tilde{P}^\top \mathbf{\Omega}\,\mathbf{\Xi}\,\mathbf{\Omega}^{-1}\tilde{X} + \epsilon \tilde{X}^\top \frac{\mathrm{d}\mathbf{\Omega}}{\mathrm{d}\lambda}\mathbf{\Omega}^{-1}\tilde{P}, \tag{7.86}
$$

where the last term is generated by the time derivative of the generating function of the coordinate transformation and

$$
\frac{\mathrm{d}\mathbf{\Omega}}{\mathrm{d}\lambda}\mathbf{\Omega}^{-1} = \begin{pmatrix} \omega_1'(\lambda)/\omega_1(\lambda) & 0 \\ 0 & \omega_2'(\lambda)/\omega_2(\lambda) \end{pmatrix}. \tag{7.87}
$$

The Hamiltonian (7.86) can be cast in the following form by using the linear action angle variables

$$
\begin{aligned}
H(\boldsymbol{\theta},\boldsymbol{I},\lambda) = {} & \omega_1(\lambda)I_1 + \omega_2(\lambda)I_2 + 2\epsilon\xi\sqrt{I_1 I_2}\times \\
& \times\left(\sqrt{\frac{\omega_2}{\omega_1}}\sin\theta_1\cos\theta_2 - \sqrt{\frac{\omega_1}{\omega_2}}\cos\theta_1\sin\theta_2\right) + \\
& + \epsilon\frac{\omega_1'}{\omega_1}I_1\sin\theta_1\cos\theta_1 + \epsilon\frac{\omega_2'}{\omega_2}I_2\sin\theta_2\cos\theta_2\,.
\end{aligned}
\tag{7.88}
$$

Both actions $I_{1,2}$ are adiabatic invariants as the resonant conditions $\omega_1 \pm \omega_2 = 0$ are never satisfied, and we define

$$
\begin{aligned}
\hat{\delta}(\lambda) = {} & \omega_1(\lambda) - \omega_2(\lambda) \\
= {} & \delta(\lambda)\frac{\omega_x(\lambda) + \omega_y(\lambda)}{\omega_1(\lambda) + \omega_2(\lambda)} - \frac{1}{\omega_1(\lambda) + \omega_2(\lambda)}\left(\delta_2(\lambda) + \sqrt{\delta_2^2(\lambda) + 4q^2}\right)
\end{aligned}
\tag{7.89}
$$

so that $\hat{\delta}(\lambda) \geq \mathbb{O}(q)$ and there is a quasi-resonant condition only if $q \ll 1$. Hence, we introduce the slow angle $\phi_1 = \theta_1 - \theta_2$, and we define $\phi_2 = \theta_2$ and J_1, J_2 are the corresponding actions, so that the new Hamiltonian is

$$
\begin{aligned}
H(\boldsymbol{\phi},\boldsymbol{J},\lambda) = {} & \hat{\delta}(\lambda)J_1 + \omega_2(\lambda)J_2 + \\
& + 2\,\epsilon\sqrt{(J_2 - J_1)J_1}\,[\xi_1(\lambda)\sin\phi_1 + \xi_2(\lambda)\sin(\phi_1 + 2\phi_2)] + \\
& + \frac{\epsilon}{2}\left[\frac{\omega_1'}{\omega_2}J_1\sin 2(\phi_1 + \phi_2) + \frac{\omega_2'}{\omega_2}(J_2 - J_1)\sin 2\phi_2\right]\,.
\end{aligned}
\tag{7.90}
$$

If $\omega_2 \sim 1$ one can average on the angle ϕ_2 and the Hamiltonian reduces to

$$
H(\boldsymbol{\phi},\boldsymbol{J},\lambda) = \hat{\delta}(\lambda)J_1 + \omega_2(\lambda)J_2 + 2\,\epsilon\,\xi_1(\lambda)\sqrt{(J_2 - J_1)J_1}\sin\phi_1\,.
\tag{7.91}
$$

We remark that $\xi_1(\lambda) = \mathbb{O}(q^{-1})$ and $\hat{\delta}(\lambda) = \mathbb{O}(q)$ when $\delta_2(\lambda) \to 0$. Therefore, using a time scaling, the previous Hamiltonian is equivalent to

$$
H(\boldsymbol{\phi},\boldsymbol{J},\lambda) = \gamma(\lambda)J_1 + \epsilon\sqrt{(J_2 - J_1)J_1}\sin\phi_1\,,
\tag{7.92}
$$

where J_2 is an integral of motion whereas J_1 changes when $\gamma(\lambda) \ll 1$, $\gamma(\lambda) = \hat{\delta}(\lambda)/(2\,\xi_1(\lambda)) = \mathbb{O}(q^2)$ when $\delta_2 \to 0$.

7.C | Additional fixed points for the Hamiltonian in the presence of detuning

The determination of the fixed points of the Hamiltonian (7.53) is done by imposing that $\dot{\phi} = 0$ and $\dot{J} = 0$, i.e.

$$\cos\phi = 0$$

$$\tilde{\delta} + 2\alpha J \pm \frac{q}{2}\frac{1 - 2J}{\sqrt{J(1-J)}} = 0 \,, \tag{7.93}$$

where the first equation gives $\phi = \pi/2, 3\pi/2$ and the second one the following quartic equation

$$16\,\alpha^2 J^4 + 16\,\alpha(\tilde{\delta} - \alpha)J^3 + 4(q^2 + \tilde{\delta}^2 - 4\alpha\tilde{\delta})J^2 +$$
$$- 4(q^2 + \tilde{\delta}^2)J + q^2 = 0 \,, \tag{7.94}$$

where it is immediate to observe that the coefficients of the terms J^4, J, and the constant term have a fixed sign, which is positive, negative, and positive, reflectively. On the other hand, the coefficients of the terms J^3 and J^2 do not have a fixed sign, but when $\tilde{\delta} \ll 1$ the first is negative and the latter is positive.

For our purpose, we want to determine when Eq. (7.94) has two real solutions, which occurs if the discriminant Δ is negative. By direct computation, one obtains

$$\Delta = -65536\,\alpha^2 q^2(\alpha + \tilde{\delta})^2[27\alpha^4 q^2 + \alpha^3(8\tilde{\delta}^3 + 54\tilde{\delta}q^2) +$$
$$+\alpha^2(12\tilde{\delta}^4 + 39\tilde{\delta}^2 q^2) + 6\alpha\tilde{\delta}(\tilde{\delta}^2 + q^2)^2 + (\tilde{\delta}^2 + q^2)^3] \tag{7.95}$$
$$= -65536\,\alpha^2 q^2(\alpha + \tilde{\delta})^2 f(\alpha)$$

and this implies that $f(\alpha)$ should always be positive. Note that $f(\alpha)$ is also represented by a quartic polynomial and its sign can be studied by considering its discriminant, $\hat{\Delta}$, which reads

$$\hat{\Delta} = 314928\,q^4(q^4 - \tilde{\delta}^4)^3(\tilde{\delta}^4 + 4q^4)^2 \tag{7.96}$$

and whose sign is easily determined

$$\hat{\Delta} > 0 \qquad \text{if} \qquad -q < \tilde{\delta} < q \,. \tag{7.97}$$

Therefore, considering also the following properties

$$f(0) > 0$$
$$f'(0) > 0 \qquad \text{if} \qquad \tilde{\delta} > 0 \tag{7.98}$$

one has that

$$\text{if} \quad \tilde{\delta} < -q \quad \text{or} \quad \tilde{\delta} > q \quad \text{then} \quad \hat{\Delta} < 0$$

hence

$$f(\alpha_i) = 0 \quad i = 1, 2 \quad \alpha_i \in \mathbb{R}$$

and

$$\tilde{\delta} < -q \quad 0 < \alpha_1 < \alpha_2$$
$$\tilde{\delta} > q \quad \alpha_1 < \alpha_2 < 0$$

hence

$$f(\alpha) > 0 \quad \text{for} \quad \alpha < \alpha_1 \quad \text{or} \quad \alpha > \alpha_2 \,. \tag{7.99}$$

Note that during the resonance-crossing process $\tilde{\delta} \to 0$ with constant q and therefore $\hat{\Delta}$ will eventually change sign.

Whenever $\hat{\Delta} > 0$ four or no real roots are possible and this depends on the conditions on two additional quantities, namely

$$\text{if} \quad -q < \tilde{\delta} < q \quad \text{then} \quad \hat{\Delta} > 0$$

hence if

$$16\,\tilde{\delta}^6 + 27\,\tilde{\delta}^2 q^4 > 0$$

and

$$-64\,\tilde{\delta}^{12} + 8019\,\tilde{\delta}^4 q^8 - 216\,\tilde{\delta}^8 q^4 + 6561\,q^{12} < 0$$

there are four distinct roots

$$\text{else, if} \tag{7.100}$$

$$16\,\tilde{\delta}^6 + 27\,\tilde{\delta}^2 q^4 < 0$$

or

$$-64\,\tilde{\delta}^{12} + 8019\,\tilde{\delta}^4 q^8 - 216\,\tilde{\delta}^8 q^4 + 6561\,q^{12} > 0$$

there are no real roots

from which the conclusion on the number of real solutions of the equation $f(\alpha) = 0$ depends only upon the study of the sign of the polynomial

$$g(\tilde{\delta}) = -64\,\tilde{\delta}^{12} - 216\,\tilde{\delta}^8 q^4 + 8019\,\tilde{\delta}^4 q^8 + 6561\,q^{12} \tag{7.101}$$

that is even, i.e. $g(\tilde{\delta}) = g(-\tilde{\delta})$ and $g(\tilde{\delta}) \to -\infty$ for $\tilde{\delta} \to \pm\infty$. $g(\tilde{\delta})$ can be considered as a cubic polynomial in the variable $\tilde{\delta}^4$ and one can verify that the discriminant is always positive, thus ensuring that there are three real and distinct roots of the equation $g(\tilde{\delta}) = 0$. Moreover, their product is positive, thus imposing that they are all positive or one positive and two negative. It turns out

that indeed only one is positive and the solution of the initial equation is given only by

$$\tilde{\delta}^4 = \mu q^4 \quad \text{i.e.} \quad \tilde{\delta} = \pm\mu^{1/4}|q|, \quad \mu \approx 17.9085 \times \frac{9}{16}. \tag{7.102}$$

Therefore

$$g(\tilde{\delta}) > 0 \quad \text{if} \quad -\mu^{1/4}q < \tilde{\delta} < \mu^{1/4}q \tag{7.103}$$

and a fortiori it is positive in the interval $[-q, q]$, which shows that on that interval $f(\alpha) = 0$ has four real and distinct roots. It is easy to verify that an even number of roots can be negative and such a number does not depend on the sign of $\tilde{\delta}$.

On the other hand, looking at the extrema of $f(\alpha)$, one finds three real and distinct extrema and the product of the values $\alpha_{i,\text{ext}}, i = 1, 2, 3$ for which the extremum is reached satisfies $\text{sgn}(\alpha_{1,\text{ext}}\alpha_{2,\text{ext}}\alpha_{3,\text{ext}}) = -\text{sgn}(\tilde{\delta})$, which shows that for $\tilde{\delta} > 0$ an odd number of extrema is negative, whereas for $\tilde{\delta} < 0$ an even number is negative.

It is then clear that as the sign of the solutions of $f(\alpha) = 0$ does not depend on the sign of $\tilde{\delta}$ while the sign of $\alpha_{i,\text{ext}}$ does, only two solutions α_i are positive and the number maxima with negative position varies from two for $\tilde{\delta} < 0$ to one for $\tilde{\delta} > 0$. In summary, the following holds

$$\text{if} \quad -q < \tilde{\delta} < q \quad \text{then} \quad \hat{\Delta} > 0$$

hence

$$f(\alpha_i) = 0 \quad i = 1, 2, 3, 4 \quad \alpha_i \in \mathbb{R}$$

and

$$\alpha_1 < \alpha_2 < 0 < \alpha_3 < \alpha_4$$

hence

$$f(\alpha) > 0 \quad \text{if} \quad \alpha < \alpha_1 \quad \text{or} \quad \alpha_2 < \alpha < \alpha_3 \quad \text{or} \quad \alpha > \alpha_4$$

$$\tag{7.104}$$

and this shows that it is indeed possible to have only two fixed points in phase space with a nonzero amplitude detuning.

7.D | Computation of the map used in the numerical simulations

The matrix $\boldsymbol{M}_{\text{FODO}}$ can be transformed in Jordan form via the transformation $\boldsymbol{T}$, so that $\boldsymbol{T}^{-1}\boldsymbol{M}_{\text{FODO}}\boldsymbol{T} = \boldsymbol{R}(\omega_x, \omega_y)$, where $\boldsymbol{R}(\omega_x, \omega_y)$ is the 4D rotation matrix for the frequencies ω_x and ω_y, i.e.

$$\boldsymbol{R}(\omega_x, \omega_y) = \boldsymbol{R}(\omega_x) \otimes \boldsymbol{R}(\omega_y) = \begin{pmatrix} \boldsymbol{R}(\omega_x) & \boldsymbol{0} \\ \boldsymbol{0} & \boldsymbol{R}(\omega_y) \end{pmatrix}, \tag{7.105}$$

where $R(\omega_z)$ is a standard 2D rotation matrix. This transformation induces a new set of co-ordinates $X = (X, X', Y, Y')$ defined as $X = T^{-1}x$ where T is well-known and reads

$$T = \begin{pmatrix} T_x & \mathbf{0} \\ \mathbf{0} & T_y \end{pmatrix} \quad \text{where} \quad T_z = \begin{pmatrix} \sqrt{\beta_z} & 0 \\ -\alpha_z/\sqrt{\beta_z} & 1/\sqrt{\beta_z} \end{pmatrix}. \tag{7.106}$$

The map then reads

$$\begin{aligned} X_{n+1} &= \left(T^{-1}x_{n+1}\right) \\ &= \left(T^{-1}M_{\text{FODO}}T\right)\left(T^{-1}M_{\text{Skew}}T\right)\left(T^{-1}x_n\right) \\ &= R(\omega_x, \omega_y)\left(T^{-1}M_{\text{Skew}}T\right)X_n, \end{aligned} \tag{7.107}$$

where

$$\hat{M}_{\text{Skew}} = T^{-1}M_{\text{Skew}}T = \begin{pmatrix} 1 & Q \\ Q & 1 \end{pmatrix} \tag{7.108}$$

and

$$Q = \begin{pmatrix} 0 & 0 \\ q & 0 \end{pmatrix}, \qquad q = \sqrt{\beta_x\beta_y}\hat{q} \tag{7.109}$$

so that

$$X_{n+1} = R(\omega_x, \omega_y)\hat{M}_{\text{Skew}} = \begin{pmatrix} R(\omega_x) & Q_x \\ Q_y & R(\omega_y) \end{pmatrix} X_n \tag{7.110}$$

having defined

$$Q_z = q \begin{pmatrix} \sin\omega_z & 0 \\ \cos\omega_z & 0 \end{pmatrix}. \tag{7.111}$$

7.E | On the residual frequency of P_{na} as $q \to 0$

At the end of the emittance exchange process, a residual frequency can be observed for P_{na} as function of N (center-left plot of Fig. 7.6). This is due to the only variable term in the expression of P_{na}, which is $J_x = (x^2 + p_x^2)/2$. A residual frequency is observed also for $q \to 0$, as it is visible in the zoomed sub-plot in the same Figure. It is possible to compute this quantity approximating the evolution of map of Eq. 7.60 at first order in q.

The map of Eq. 7.60 can be written as

$$M_1 = \begin{pmatrix} R(\omega_x) & qB_1 \\ qC_1 & R(\omega_y) \end{pmatrix}. \tag{7.112}$$

where

$$B_1 = \begin{pmatrix} \sin\omega_x & 0 \\ \cos\omega_x & 0 \end{pmatrix}, \qquad C_1 = \begin{pmatrix} \sin\omega_y & 0 \\ \cos\omega_y & 0 \end{pmatrix}, \tag{7.113}$$

and ω_y is dependent on the turn number n, according to the linear law $\omega_{y,i} = \omega_{y,0} + i\Delta_y/N$. We set Δ_y as the difference between the final and the initial ω_y, while N is the total number of turns.

At order q, the combination of two matrix M_1, with two different values of ω_y, namely ω_y and ω_y', reads

$$M_1' M_1 = \begin{pmatrix} R(2\omega_x) & q[R(\omega_x)B_1 + B_1 R(\omega_y)] \\ q[C_1' R(\omega_x) + R(\omega_y')C_1] & R(\omega_y + \omega_y') \end{pmatrix} + \mathcal{O}(q^2), \tag{7.114}$$

and, in general, being $M_{1,i} = M_1(\omega_y = \omega_{y,i}$ and $M_n = M_{1,n}M_{1,n-1}\cdots M_{1,0}$:

$$M_n = \begin{pmatrix} R(n\omega_x) & qB_n \\ qC_n & R\left(\sum_{i=0}^{n}\omega_{y,i}\right) \end{pmatrix} + \mathcal{O}(q^2). \tag{7.115}$$

We are only interested in J_x, therefore we only need to study the first two rows of M_n. The succession B_n can be written in recursive form as

$$B_{n+1} = R(\omega_x)B_n + B_1 R\left(\sum_{i=1}^{n-1}\omega_{y,i}\right) \tag{7.116}$$

and the general formula for solving first-order recurrence equation can be employed, using the fact that 2D rotation matrices are commutative. We get, at turn N

$$B_N = R((N-1)\omega_x)\times$$
$$\left[B_1 + \sum_{m=1}^{N-1}\begin{pmatrix} \sin((1-m)\omega_x) & 0 \\ \cos((1-m)\omega_x) & 0 \end{pmatrix}\begin{pmatrix} \cos\sum_{i=1}^{m}\omega_{y,i} & \sin\sum_{i=1}^{m}\omega_{y,i} \\ 0 & 0 \end{pmatrix}\right]. \tag{7.117}$$

Now, without loss of generality, we can choose a particle whose initial conditions are $x = x_0$, $p_x = 0$, $y = y_0$, $p_y = 0$. In that case, the action J_x at turn N is

$$J_{x,N} = \frac{x_N^2 + p_{x,N}^2}{2} = \frac{x_0^2}{2} + qx_0 y_0\left(\cos N\omega_x B_{N,11} - \sin N\omega_x B_{N,21}\right) + \mathcal{O}(q^2) \tag{7.118}$$

and the two components of the $\boldsymbol{B}_N$ matrix read:

$$B_{N,11} = \sin N\omega_x + \sum_{m=1}^{N-1} \sin(N-m)\omega_x \cos\left(m\omega_{y,0} + \frac{m(m-1)}{2}\frac{\Delta_y}{N}\right) \qquad (7.119)$$

$$B_{N,21} = \cos N\omega_x + \sum_{m=1}^{N-1} \cos(N-m)\omega_x \cos\left(m\omega_{y,0} + \frac{m(m-1)}{2}\frac{\Delta_y}{N}\right), \quad (7.120)$$

where we write the sum of the $\omega_{y,i}$ according to the sum of an arithmetic progression.

Substituting the expressions for $B_{N,11}$ and $B_{N,21}$, one finds

$$\Delta J = J_x - J_{x_0} = -qx_0 y_0 \sum_{m=1}^{N-1} \sin m\omega_x \cos\left(m\omega_{y,0} + \frac{m(m-1)}{2}\frac{\Delta_y}{N}\right). \qquad (7.121)$$

The oscillating behavior is given by the sum. The amplitude is controlled by q, and disappears when $q \to 0$, but the frequency, at first order, is not dependent on q. We observe that the sum, for $N \gg 1$, is well approximated by the integral

$$I = \int_0^N dm \, \sin m\omega_x \cos\left(m\omega_{y,0} + \frac{m(m-1)}{2}\frac{\Delta_y}{N}\right) =$$

$$= \frac{1}{2}\int_0^N dm \left[\sin\left(m\left(\omega_x + \omega_{y,0} - \frac{\Delta_y}{2N}\right) + \frac{\Delta_y}{2N}m^2\right)\right.$$

$$\left. + \cos\left(m\left(\omega_x - \omega_{y,0} + \frac{\Delta_y}{2N}\right) - \frac{\Delta_y}{2N}m^2\right)\right] =$$

$$= \frac{1}{2}\int_0^N dm \left[\sin\left(am + bm^2\right)\cos\left(cm - bm^2\right)\right] =$$

$$
= \frac{1}{2}\sqrt{\frac{\pi}{2b}} \left\{ -\sin\left(\frac{a^2}{4b}\right)\left[C\left(\frac{a+2bN}{\sqrt{2\pi b}}\right) - C\left(\frac{a}{\sqrt{2\pi b}}\right)\right] \right.
$$

$$
+ \cos\left(\frac{a^2}{4b}\right)\left[S\left(\frac{a+2bN}{\sqrt{2\pi b}}\right) - S\left(\frac{a}{\sqrt{2\pi b}}\right)\right]
$$

$$
+ \cos\left(\frac{c^2}{4b}\right)\left[C\left(\frac{2bN-c}{\sqrt{2\pi b}}\right) + C\left(\frac{c}{\sqrt{2\pi b}}\right)\right]
$$

$$
\left. + \sin\left(\frac{c^2}{4b}\right)\left[S\left(\frac{2bN-c}{\sqrt{2\pi b}}\right) + S\left(\frac{c}{\sqrt{2\pi b}}\right)\right]\right\} \quad (7.122)
$$

where $S(x)$ and $C(x)$ are Fresnel integrals.

When $x \gg 1$, we can approximate $S(x) = C(x) = 1/2 + \mathcal{O}(1/x)$, and we are left with

$$
I = \frac{1}{2}\sqrt{\frac{\pi}{2b}}\sin\left(\frac{c^2}{4b} + \frac{\pi}{4}\right) + \mathcal{O}\left(\frac{1}{\sqrt{N}}\right) \tag{7.123}
$$

and, substituting b and approximating $c^2/(4b)$ as

$$
\frac{c^2}{4b} = \frac{(\omega_x - \omega_{y,0})^2}{2}\frac{N}{\Delta_y} + \frac{\omega_x - \omega_{y,0}}{4\Delta_y} + \mathcal{O}\left(\frac{1}{N}\right) \tag{7.124}
$$

one finds

$$
I \approx \frac{1}{2}\sqrt{\frac{\pi N}{\Delta_y}}\sin\left(\frac{(\omega_x - \omega_{y,0})^2}{2\Delta_y}N + \text{phase}\right) \tag{7.125}
$$

and the oscillation frequency reads

$$
\omega_{\text{osc}} = \frac{(\omega_x - \omega_{y,0})^2}{2\Delta_y} \,. \tag{7.126}
$$

For a symmetric variation of ω_y, i.e. $|\omega_x - \omega_{y,0}| = \Delta = 2\Delta_y$ gives $\omega_{\text{osc}} = \Delta/4$, in accordance with the residual frequency observed in Fig. 7.6 for very small values of q.

8 | Emittance sharing: non-linear resonances

The content of this chapter, with the due adaptations, has resulted in the article by A. Bazzani, F. C., M. Giovannozzi *"Manipulation of transverse emittances in circular accelerators by crossing non-linear 2D resonances"*, which has been made available as a preprint on arXiv in February 2022 (Ref. [11]). The manuscript has been accepted in May 2022 for publication in Eur. Phys. Jour. Plus.

8.1 | Introduction

In the last chapter, we analysed the emittance exchange effect that happens when the 1 : 1 coupling resonance is crossed, explaining it in terms of adiabatic invariant conservation theory. The natural extension of this approach, which we devote this chapter to, is to consider the adiabatic crossing of a non-linear 2D coupled difference resonance. This should provide a control of the emittances in the horizontal and vertical planes: one can imagine that a sort of exchange between the two directions still applies. We call this phenomenon *emittance sharing*.

As we discussed in Section 2.3, under linear motion in circular particle accelerators, the transverse emittances are invariant, which are conserved if radiation effects can be neglected, and time-dependent effects are absent. When non-linear resonances and time-dependent effects are introduced in the system, the invariance of the transverse emittances is broken, which implies a potential harmful impact on the accelerator performance due to the diffusion of orbits in phase space [18, 54, 74, 77]. There are, however, also some advantages that we would like to highlight and promote. Indeed, the lack of invariance for the transverse emittances implies a degraded accelerator performance in terms, e.g. of emittance growth and particle loss. On the other hand, one could devise appropriate beam manipulations in which the transverse emittances are acted upon in a controlled way.

For example, experience with Multi-Turn Extraction (Chapter 3 shows that the beam splitting, achieved when particles are trapped inside the stable islands, induces a reduction of the horizontal emittance only, i.e. the emittance of each of the five generated beamlets is smaller than that of the initial single-Gaussian beam. This is related to the 1D character of the resonance used. In this context a manipulation technique which could redistribute the emittance between the two directions would be welcome.

<center>❖</center>

Crossing a non-linear 2D resonance provides extended capabilities in terms of control and manipulation of transverse emittances and could be pursued both from the theoretical and experimental point of view. The source of inspiration is the analysis of the impact of crossing the Walkinshaw, i.e. $\omega_x - 2\omega_y = 0$, resonance [32, 61], and the $2\omega_x - \omega_y$ resonance [53]. However, the focus of the analysis performed in Ref. [61] was to estimate the emittance growth due to the resonance crossing, whereas our aim is to manipulate the transverse emittances.

In this chapter, we propose a general approach to emittance sharing based on adiabatic invariance and separatrix-crossing theory. Differently from the case of coupling resonance, when non-linear resonances are employed, real separatrices have to be crossed by particles to experience a change in the value of their adiabatic invariant which leads to the emittance sharing.

When the linear frequencies are slowly modulated so to cross the selected resonance, the area of the phase space enclosed by the separatrix changes and particles can jump between different phase-space regions, which results in a change of their adiabatic invariant. The statistical analyses show that, starting from a Gaussian distribution of initial conditions with emittances $\varepsilon_{x,\mathrm{i}}$, $\varepsilon_{y,\mathrm{i}}$, at the end of the resonance crossing process the emittances are given by $\varepsilon_{x,\mathrm{f}} \propto \varepsilon_{y,\mathrm{i}}$ and $\varepsilon_{y,\mathrm{f}} \propto \varepsilon_{x,\mathrm{i}}$, with factors depending on the order of the crossed resonance.

The approach presented in this chapter has been assessed by means of a detailed analysis of the phase-space topology of simple Hamiltonian systems, which is the basis for applying the adiabatic theory. The technique is then probed using more realistic map models. Extensive numerical simulations have been performed to determine the dependence of the beam manipulation on the various system's parameters.

The plan of the chapter is the following: in Section 8.2 the models are introduced, the phase-space topology of the Hamiltonians described is studied in detail, including considerations on some specific low-order resonances, which are useful for applications. The results of extensive numerical simulations are presented and discussed in Section 8.3, while some conclusions are drawn in

Section 8.4. Moreover, a discussion on which type of magnet excites a given resonance is given in Appendix 8.A, while a short digression on the motion in the resonant condition is reported in Appendix 8.B.

8.2 | Theoretical framework

8.2.1 | General considerations

The starting point is the choice of the model used for our analyses, which is the Hénon-like [44] 4D symplectic map that describes the transverse betatron motion in a FODO cell with nonlinearities [17]. Such a map is composed by rotations of frequencies ω_x and ω_y and a $2(r+1)$-polar kick, i.e.

$$
\begin{pmatrix} x' \\ p_x' \\ y' \\ p_y' \end{pmatrix} = R(\omega_x, \omega_y) \begin{pmatrix} x \\ p_x + \sqrt{\beta_x}\,\mathrm{Re}\left[\left(\dfrac{K_r + i J_r}{r!}\right)\left(\sqrt{\beta_x}\,x + i\sqrt{\beta_y}\,y\right)^r\right] \\ y \\ p_y - \sqrt{\beta_y}\,\mathrm{Im}\left[\left(\dfrac{K_r + i J_r}{r!}\right)\left(\sqrt{\beta_x}\,x + i\sqrt{\beta_y}\,y\right)^r\right] \end{pmatrix}, \quad (8.1)
$$

where $R(\omega)$ is a 2D rotation matrix and $R(\omega_x, \omega_y) = \mathrm{diag}\big(R(\omega_x), R(\omega_y)\big)$, while K_r and J_r are the normal and the skew integrated strength of the $2(r+1)$-polar magnet, respectively. They are obtained by considering the following expression for the transverse magnetic field

$$
B_y + i B_x = B\rho \sum_{r=1}^{M} (k_r + i j_r)\, \frac{(x + iy)^r}{r!}\,, \quad (8.2)
$$

where $B\rho$ is the beam magnetic rigidity and $K_r = k_r \ell$, $J_r = j_r \ell$, where ℓ is the length of the magnetic element.

In certain situations, it is interesting to introduce an explicit amplitude-detuning effect in the map of Eq. (8.1) that models the case where a magnetic multipole excites the resonance, whereas the effect of other magnetic elements, not modelled as kicks in the map, is to generate an amplitude-dependent detuning. In this case, the rotation matrix in Eq. (8.1) is replaced by a rotation matrix $R(\omega_x + \alpha_{xx} J_x + \alpha_{xy} J_y, \omega_y + \alpha_{xy} J_x + \alpha_{yy} J_y)$, where the linear actions $J_x = (x^2 + p_x^2)/2$, and $J_y = (y^2 + p_y^2)/2$ have been used, which defines an amplitude-dependent 4D rotation.

We say that ω_x, ω_y satisfy a (m, n) resonance condition if the following holds

$$m\omega_x - n\omega_y = 2\pi k \qquad m, n \in \mathbb{N}, k \in \mathbb{Z}, \tag{8.3}$$

and the resonance order is given by $m + n$.

Normal Form theory applied to the map of Eq. (8.1) close to a (m, n) resonance condition allows a resonant Normal Form to be built, from which an quasi-resonant interpolating Hamiltonian can be derived [17]. The analysis focuses on the resonances of orders 3 and 4 that are possible to excite using common magnetic elements (the details about which magnet type can excite a given resonance are given in Appendix 8.A) according to the following scheme

- $(1, 2)$ resonance: normal sextupole $(j_2 = 0)$;

- $(2, 1)$ resonance: skew sextupole $(k_2 = 0)$;

- $(3, 1)$ resonance: skew octupole $(k_3 = 0)$;

- $(1, 3)$ resonance: skew octupole $(k_3 = 0)$.

We remark that this correspondence between magnet type and resonance is valid for the case of a single kick, i.e. for a map of the form of Eq. (8.1). In the case of a system with two non-linear kicks, the fourth-order resonances can also be excited by using a combination of normal and skew sextupoles.

8.2.2 | Phase-space topology of the Hamiltonian model

The Normal Form Hamiltonian in the resonant case, written in action-angle variables reads

$$\begin{aligned}
\mathcal{H}(\phi_x, J_x, \phi_y, J_y) &= \omega_x J_x + \omega_y J_y + \alpha_{xx} J_x^2 + 2\alpha_{xy} J_x J_y + \alpha_{yy} J_y^2 \\
&\quad + G J_x^{m/2} J_y^{n/2} \cos(m\phi_x - n\phi_y),
\end{aligned} \tag{8.4}$$

where the amplitude-detuning parameters $\alpha_{xx}, \alpha_{xy}, \alpha_{yy}$ have been introduced and the resonance condition is given by $m\,\omega_x - n\,\omega_y \approx 0$. The resonance-strength parameter G is directly proportional to the magnet strength k_r or j_r, as one can verify by computing the resonant Normal Form Hamiltonian for map (8.1) using, e.g. software presented in Ref. [15].

The canonical transformation (see [4, p. 410])

$$\begin{aligned}
J_x &= m J_1, & \phi_1 &= m\phi_x - n\phi_y, \\
J_y &= J_2 - n J_1, & \phi_2 &= \phi_y,
\end{aligned} \tag{8.5}$$

introduces the fast and slow phases and casts the Hamiltonian into the form

$$
\begin{aligned}
\mathcal{H}(\phi_1, J_1) = {} & \delta J_1 + \alpha_{12} J_1 J_2 + \alpha_{11} J_1^2 \\
& + G(m J_1)^{\frac{m}{2}} (J_2 - n J_1)^{\frac{n}{2}} \cos \phi_1 + \left[\omega_y J_2 + \alpha_{22} J_2^2 \right],
\end{aligned}
\tag{8.6}
$$

where $\delta = m \omega_x - n \omega_y$ is the resonance-distance parameter, and the new constants α_{11}, α_{12}, and α_{22} are functions of α_{xx}, α_{xy} and α_{yy} according to

$$
\begin{aligned}
\alpha_{11} &= m^2 \alpha_{xx} - 2m\,n\,\alpha_{xy} + n^2 \alpha_{yy}\,, \\
\alpha_{12} &= 2(m\,\alpha_{xy} - n\,\alpha_{yy})\,, \\
\alpha_{22} &= \alpha_{yy}\,.
\end{aligned}
\tag{8.7}
$$

We remark that the term in square brackets of Eq. (8.6) can be discarded as it is a function of J_2 only, which is an integral of motion since $\partial \mathcal{H}/\partial \phi_2 = 0$. Hence, it represents a constant additive term of the Hamiltonian. Furthermore, we remark that the term α_{12} induces a shift in the resonance crossing, which occurs for $\delta + \alpha_{12} J_2 = 0$, thus making the resonance-crossing process dependent on the value of J_2 (that is a constant in time). We remark also that the condition $J_y > 0$ constrains the motion within the circle $J_1 < J_2/n$, which we call the *allowed circle*.

To study the phase-space structure, it is convenient to express Eq. (8.6) using the rescaled variable $\tilde{J}_1 = J_1/J_2$, that gives the Hamiltonian

$$
\tilde{\mathcal{H}}(\phi_1, \tilde{J}_1) = \frac{\delta}{G J_2^{\frac{m+n-2}{2}}} \tilde{J}_1 + \frac{\alpha_{12}}{G J_2^{\frac{m+n-4}{2}}} \tilde{J}_1 + \frac{\alpha_{11}}{G J_2^{\frac{m+n-6}{2}}} \tilde{J}_1^2 + (m \tilde{J}_1)^{\frac{m}{2}} (1 - n \tilde{J}_1)^{\frac{n}{2}} \cos \phi_1\,.
\tag{8.8}
$$

It appears that the resonance-crossing process is actually governed by the parameter

$$
\eta = \frac{\delta}{G J_2^{\frac{m+n-2}{2}}}\,.
\tag{8.9}
$$

Therefore, there is an interplay between the distance from resonance, δ, the multipole strength, proportional to G, and the invariant action J_2. We also remark that the coefficients α_{12}, α_{11} are rescaled by the quantity $1/(G J_2^{\frac{m+n-6}{2}})$.

The equations of motion for the Hamiltonian of Eq. (8.6) are

$$
\begin{aligned}
\dot{\phi}_1 &= \frac{\partial \mathcal{H}}{\partial J_1} = \delta + 2\alpha_{11} J_1 + \alpha_{12} J_2 + \\
& \qquad + \frac{m}{2} G(m J_1)^{\frac{m}{2}-1} (J_2 - n J_1)^{\frac{n}{2}-1} \left[m J_2 - n(m+n) J_1 \right] \cos \phi_1\,, \\
\dot{J}_1 &= -\frac{\partial \mathcal{H}}{\partial \phi_1} = G\,(m J_1)^{\frac{m}{2}} (J_2 - n J_1)^{\frac{n}{2}} \sin \phi_1\,,
\end{aligned}
\tag{8.10}
$$

and the phase-space topology that is originated by them depends both on m and n, although some features do not.

The knowledge about the existence of the fixed points of Eq. (8.10) and their stability is essential for understanding the phase-space topology. The solutions of the equation $\partial \mathcal{H}/\partial \phi_1 = 0$ that satisfy the condition $J_2 - n J_1 = 0$, are particularly relevant for our study, since they lie on the border of the allowed circle, and for this reason, these solutions have to be unstable fixed points and are computed by solving

$$\cos \phi_1 = \frac{2(\delta + 2\alpha_{11} J_1 + \alpha_{12} J_2)}{G m^{m/2} \left[n^2 J_1 - m(J_2 - n J_1) \right] J_1^{\frac{m}{2}-1} (J_2 - n J_1)^{\frac{n}{2}-1}} \,. \tag{8.11}$$

When imposing the condition $J_1 - n J_2 = 0$, the r.h.s. of Eq. (8.11) is not singular only if $n = 1$ or $n = 2$ (the exactly resonant case will be discussed later).

The separatrix that passes through the unstable fixed points on the border of the allowed circle is called *coupling arc* (as in Ref. [61]), and is found by solving the equation

$$\mathcal{H}(\phi_1, J_1) = \delta \frac{J_2}{n} + \left(\frac{\alpha_{11}}{n} + \frac{\alpha_{12}}{n} \right) J_2^2 \,, \tag{8.12}$$

which can be rewritten as

$$n\delta + \alpha_{11} n^2 (J_2 + n J_1) + n \alpha_{12} J_2 = G m^{m/2} J_1^{m/2} (J_2 - n J_1)^{\frac{n}{2}-1} \cos \phi_1 \,. \tag{8.13}$$

For $n = 1$, the term $(J_2 - n J_1)^{1/2}$ appears in the numerator of Eq. (8.11) with a positive power, and when $J_1 = J_2$, i.e. on the allowed circle, $\cos \phi_1 = 0$, so $\phi_1 = \pm \pi/2$. With no amplitude detuning, the equation of the coupling arc reads

$$\delta (J_2 - J_1)^{1/2} = G m^{m/2} J_1^{m/2} \cos \phi_1 \,, \tag{8.14}$$

and the existence of solutions requires $\delta \cos \phi_1 > 0$. If $\delta > 0$ the coupling arc lies in the right semicircle, while for $\delta < 0$ it lies in the left one. Furthermore, for large values of $|\delta|$ the coupling arc is very close to the allowed circle, as it can be seen from the equation in the limit $|\delta| \to +\infty$.

For $n = 2$, the term $(J_2 - 2 J_1)$ disappears from the denominator of Eq. (8.11), and the coupling-arc intersections are found for

$$\cos \phi_1 = 2^{\frac{m}{2}-1} \frac{\delta + (\alpha_{11} + \alpha_{12}) J_2}{G m^{m/2} J_2^{m/2}} \,, \tag{8.15}$$

which exist as long as $|\cos \phi_1| \leq 1$, and they do not depend on J_1. In this case, in the absence of amplitude detuning, we obtain a simple expression for the coupling arc

$$J_1 = \left(\frac{\delta}{2 G m^{m/2} \cos \phi_1} \right)^{2/m} \,. \tag{8.16}$$

Once recast the Hamiltonian of Eq. (8.6) in Cartesian coordinates ($X = \sqrt{2J_1}\cos\phi_1$, $Y = \sqrt{2J_1}\sin\phi_1$), one can observe that the other fixed points, which could be associated to the presence of other separatrices, can be found only on the X axis due to symmetry reasons.

First of all, we remark that the origin ($X = 0$, $Y = 0$) is a fixed point only if $m > 1$. In this case, we can study the isoenergetic surface of the origin from the equation $\mathscr{H}(\phi_1, J_1) = 0$, i.e.

$$J_1\left(\delta + \alpha_{11}J_1 + \alpha_{12}J_2 + Gm^{m/2}J_1^{m/2-1}(J_2 - nJ_1)^{n/2}\cos\phi_1\right) = 0\,, \qquad (8.17)$$

which is solved for $J_1 = 0$ or for

$$\delta + \alpha_{12}J_2 = -\alpha_{11}J_1 - Gm^{m/2}J_1^{m/2-1}(J_2 - nJ_1)^{n/2}\cos\phi_1\,. \qquad (8.18)$$

For $m = 2$, we can solve analytically the case without amplitude-detuning terms, as the equation becomes

$$\delta = -2G(J_2 - nJ_1)^{n/2}\cos\phi_1\,. \qquad (8.19)$$

A solution $J_1(\phi_1)$ that passes through the origin when $\mathrm{acos}\left(\delta/(2GJ_2^{n/2})\right)$ exists, i.e. for $|\delta| \le 2GJ_2^{n/2}$. The condition on the signs shows that the solution lies in the positive-X domain if $\delta < 0$, and in the negative one if $\delta > 0$. For $m > 2$, the origin is a genuine fixed point and the Hamiltonian can be linearized around the origin using the coordinates X, Y. One obtains a simple rotator Hamiltonian, i.e. $\mathscr{H}_{\mathrm{lin}} = \delta(X^2 + Y^2)/2$, which shows that the origin is an elliptic fixed point.

Finally, additional fixed points might exist on the axis $Y = 0$, and they should be solutions of $\partial\mathscr{H}/\partial X = 0$, having set $Y = 0$. The equation reads

$$\delta + \alpha_{11}X^2 + \alpha_{12}J_2 +$$
$$+ \frac{G}{2}\left(\frac{m}{2}\right)^{\frac{m}{2}}\left(J_2 - \frac{n}{2}X^2\right)^{\frac{n}{2}-1}X^{m-2}\left[2mJ_2 - 2 - n(m+n)X^2\right] = 0\,. \qquad (8.20)$$

The number of real solutions of Eq. (8.20) that lie inside the allowed circle depends on the degree of the resulting polynomial in X, which is determined by the order of the resonance condition. Therefore, the topology of the phase space of higher-order resonances can be very complicated, and its detail is a crucial element for the feasibility of emittance sharing. A specialised discussion on fixed points on the $Y = 0$ axis is carried out for each resonance taken into consideration in our study in Section 8.2.3.

We remark that when $\delta + \alpha_{12}J_2 = 0$, i.e. the resonance condition is met, and $\alpha_{11} = 0$, nontrivial solutions of Eq. (8.20) are given by

$$2mJ_2 - n(m+n)X^2 = 0\,, \qquad \text{or} \qquad X = \pm\sqrt{\frac{2mJ_2}{n(m+n)}}\,. \qquad (8.21)$$

The two symmetrical solutions are both stable fixed points. For the origin, the previous discussion holds, having set $\delta = 0$. Moreover, the coupling arc equation at resonance becomes $\cos\phi_1 = 0$, and the coupling arc is reduced to the diameter of the allowed circle passing through $\phi_1 = \pm\pi/2$, for any value of m and n. Separatrices that are not coupling arcs approximate the behaviour of a coupling arc close to the resonance (see, e.g. the top-right phase-space portrait of Fig. 8.3).

In general, at resonance, the allowed circle is symmetrically divided in two regions. Hence, whatever the resonance is crossed, if $\alpha_{11} = 0$ there is always a neighbourhood of the resonant condition $\delta + \alpha_{12}J_2 = 0$ where the phase space is divided into two regions. This is the ideal condition to perform emittance sharing, as it will be shown in Section 8.2.4.

In the following, we analyse some resonances that can be excited using magnetic elements commonly installed in particle accelerators.

8.2.3 | Motion close to low-order resonances

We now compute the most important features of the phase space of the resonant Normal Form Hamiltonian for low-order resonances excited by sextupole or octupole magnets. The theory of emittance sharing relies on separatrix crossing, therefore we need to know which fixed points exist in the phase space, their stability, and where separatrices exist. In general, we will search for unstable fixed points on the allowed circle, which give rise to a coupling arc, for stable fixed points on $\phi_1 = 0$ or $\phi_1 = \pi$, and for possible extra separatrices.

Resonance $(1, 2)$

Resonance $(1, 2)$ Hamiltonian in (ϕ_1, J_1) coordinates, corresponding to the resonant Normal Form of a Hénon-like map with a normal sextupolar kick, reads [32, 61],

$$\mathcal{H}(\phi_1, J_1) = \delta J_1 + \alpha_{11}J_1^2 + \alpha_{12}J_1 J_2 + G J_1^{1/2}(J_2 - 2J_1)\cos\phi_1 . \quad (8.22)$$

The phase space features an allowed circle given by $J_1 < J_2/2$, and a coupling arc. From Eq. (8.11) one obtains the unstable fixed points as solutions of

$$\cos\phi = \frac{\delta + (\alpha_{11} + \alpha_{12})J_2}{G\sqrt{2J_2}} \quad (8.23)$$

and a coupling arc (see Eq. (8.13)) that, expressed in Cartesian coordinates, reads

$$4\alpha_{11}(X^2 + Y^2) - \frac{G}{\sqrt{2}}X + 2(\delta + \alpha_{12}J_2 + 2\alpha_{11}J_2) = 0 . \quad (8.24)$$

This represents a circumference that crosses the allowed circle when

$$\left| \frac{\delta + (\alpha_{11} + \alpha_{12})J_2}{G\sqrt{2J_2}} \right| \leq 1 \tag{8.25}$$

dividing it in two regions. When $\alpha_{11} = 0$, the coupling arc reduces to the straight line

$$X = \frac{\sqrt{2}(\delta + \alpha_{12}J_2)}{2G} \tag{8.26}$$

that sweeps through the phase space if δ is varied, defining two equal regions when $\delta = -\alpha_{12}J_2$. The equation of the stable fixed points for $\phi_1 = 0$ or $\phi_1 = \pi$ reads

$$(\delta + 2\alpha_{11}J_1 + \alpha_{12}J_2)J_1^{1/2} \pm G(J_2 - 6J_1) = 0 \,, \tag{8.27}$$

and we obtain two real solutions inside the allowed circle, one for each side of the coupling arc. Therefore, the phase space is always divided into no more than two regions.

Resonance $(2, 1)$

The starting point is the Hénon-like 4D map with a skew sextupole kick and the resonant Normal Form provides an interpolating Hamiltonian up to order 3 of the form

$$\mathcal{H}(\phi_1, J_1) = \delta J_1 + \alpha_{11}J_1^2 + \alpha_{12}J_1 J_2 + 2G J_1\sqrt{J_2 - J_1}\cos\phi_1 \,, \tag{8.28}$$

and the motion is limited to the allowed circle $J_1 < J_2$. The fixed points on the allowed circle are given by $\cos\phi_1 = 0$, i.e. $\phi_1 = \pm\pi/2$, whereas the expression of the coupling arc is obtained by solving $\mathcal{H}(J_1, \phi_1) - \mathcal{H}(J_1 = J_2, \phi_1 = \pm\pi/2)$, i.e.

$$(\delta + \alpha_{11}(J_2 + J_1) + \alpha_{12}J_2)\sqrt{J_2 - J_1} = 2G J_1 \cos\phi_1 \,, \tag{8.29}$$

which is easily solved when $\alpha_{11} = 0$:

$$J_1(\phi_1) = -\frac{\hat{\delta}^2 - \hat{\delta}\sqrt{16G^2 J_2 \cos(\phi_1)^2 + \hat{\delta}^2}}{8G^2 \cos(\phi_1)^2} \qquad \text{with} \qquad \hat{\delta} = \delta + \alpha_{12}J_2 \,. \tag{8.30}$$

We remark that if $\hat{\delta} > 0$ we must have $\cos\phi_1 > 0$, i.e. the coupling arc lies in the positive domain of X, whereas for $\hat{\delta} < 0$ in the negative one. Moreover, for $\hat{\delta} = 0$ the coupling arc reduces to a line that evenly divides the allowed circle. On the other hand, we can look for solutions when $\phi_1 = 0$ and $\phi_1 = \pi$, and when $\alpha_{11} = 0$, the equation reads

$$\hat{\delta}\sqrt{J_2 - J_1} \pm G(2J_2 - 3J_1) = 0 \,. \tag{8.31}$$

Assuming $G > 0$, we need to impose conditions on the existence of the solutions before squaring: for $\phi_1 = 0$ and $\hat{\delta} > 0$, the condition $2J_2/3 < J_1 < J_2$ holds, while for $\hat{\delta} < 0$ we require $J_1 < 2J_2/3$. For $\phi_1 = \pi$ the conditions are reversed. Finally, we obtain the solutions

$$J_1^{\pm} = \frac{2}{3}J_2 \pm \frac{\hat{\delta}}{18G^2}\left(\sqrt{12G^2 J_2 + \hat{\delta}^2} \mp \hat{\delta}\right). \tag{8.32}$$

No matter the sign, the quantity inside the brackets is always positive, which implies $J_1^+ > 2J_2/3$ if $\hat{\delta} > 0$ and $J_1^+ < 2J_2/3$ if $\hat{\delta} < 0$, and this solution is acceptable only for $\phi_1 = 0$. Conversely, $J_1^- > 2J_2/3$ if $\hat{\delta} < 0$ and $J_1^- < 2J_2/3$ if $\hat{\delta} > 0$. This solution is only acceptable when $\phi_1 = \pi$. Finally, we always have a solution in the positive X semi-axis and one in the negative one, as long as the solution for J_1 inside the allowed circle, but, as $J_1^+ \to J_2$ when $\hat{\delta} \to \infty$, and $J_1^- \to J_2$ as $\hat{\delta} \to -\infty$, this never occurs.

Let us study the trajectory of a point whose initial condition is at the origin. We have to solve the equation $\mathcal{H}(\phi_1, J_1) = 0$, i.e.

$$J_1\left(\delta + 2G\sqrt{J_2 - J_1}\cos\phi_1\right) = 0, \tag{8.33}$$

and we have the solutions $J_1 = 0$ and $\delta + 2G\sqrt{J_2 - J_1}\cos\phi_1 = 0$. The latter can only be solved for $\cos\phi_1 < 0$ if $\delta > 0$, and $\cos\phi_1 > 0$ if $\delta < 0$. Therefore, there is only one trajectory passing through the origin: it does not alter the topology of the phase space introducing new islands (see Fig. 8.1), and the allowed circle is always divided into two regions, thus making the emittance sharing possible.

We remark that in Fig. 8.1 and in general in the phase-space portraits of the Hamiltonian functions discussed in this paper, we used large values of δ and J_2, compared to those chosen for the numerical simulations that will be later discussed. This is justified by the fact that the Hamiltonian models depend on the unique parameter $\eta = \delta/(G\sqrt{J_2})$, for third order resonances, and $\eta = \delta/(GJ_2)$, for fourth-order ones (see Eq. 8.9), hence it is perfectly justified to choose conditions with $\eta \sim 1$.

Resonance $(1, 3)$

For the $(1, 3)$ resonance, which is excited using a skew octupole, we have the quasi-resonant Hamiltonian

$$\mathcal{H}(\phi_1, J_1) = \delta J_1 + \alpha_{12}J_1 J_2 + \alpha_{11}J_1^2 + GJ_1^{1/2}(J_2 - 3J_1)^{3/2}\cos\phi_1. \tag{8.34}$$

If we set $\alpha_{11} = \alpha_{12} = 0$, which is the case when the resonance is excited without sextupolar kicks, we have fixed points for $\phi_1 = 0$ or for $\phi_1 = \pi$ that are the
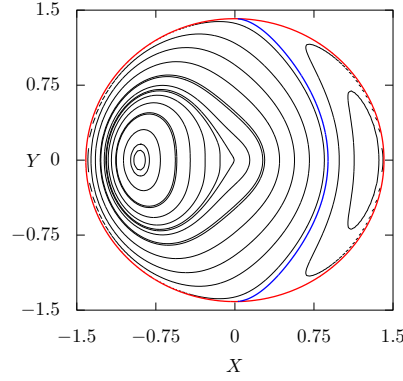
FIGURE 8.1 – Phase space portrait of Eq. (8.28) with $\delta = G = J_2 = 1$. The red line delimits the allowed circle, the blue line is the coupling arc.

solutions of

$$\frac{\partial \mathcal{H}}{\partial J_1}\bigg|_{\phi_1 = 0, \pi} = \delta \pm \frac{G}{2}\left(J_1^{-1/2}(J_2 - 3J_1)^{3/2} - 9J_1^{1/2}(J_2 - 3J_1)^{1/2}\right) = 0 \,, \quad (8.35)$$

that gives

$$\delta J_1^{1/2} = \pm \frac{G}{2}\left(9J_1(J_2 - 3J_1)^{1/2} - J_1^{1/2}(J_2 - 3J_1)^{3/2}\right) . \quad (8.36)$$

The r.h.s. of Eq. 8.36 is positive when $\pm G\left(J_1 - \frac{J_2}{12}\right) > 0$, and we will compare it to the sign of δ. Let us choose $G > 0$. For $\phi_1 = 0$, we have solutions for $\delta > 0$ and $J_2/12 < J_1 < J_2/3$, or for $\delta < 0$ and $0 < J_1 < J_2/12$. For $\phi = \pi$ the conditions are reversed. By squaring the equation, which gives a cubic polynomial, we compute its roots, taking into account all conditions. The solutions are given in Fig. 8.2. There are the following possibilities:

- if $\delta/(GJ_2) > 1$, there exists only one stable fixed point for $\phi_1 = \pi$ that tends to the origin when $\delta/(GJ_2) \gg 1$;

- if $0 < \delta/(GJ_2) < 1$, there are two fixed points on $\phi_1 = 0$ and one on ϕ_π. The inner solution on $\phi_1 = 0$ (J_1^+) and the solution on $\phi_1 = \pi$ (J_1^-) are stable, while the outer fixed point on $\phi_1 = 0$ is unstable, and generates a separatrix. The phase space is divided into three regions: $S^\pm$ around $J_1^\pm$, and $\hat{S}$ that is the area between the separatrix which crosses $\hat{J}_1$ and the allowed circle. Portraits with $\delta/(GJ_2) = 0.1$ and $\delta/(GJ_2) = 0.8$ are shown in Fig. 8.3;
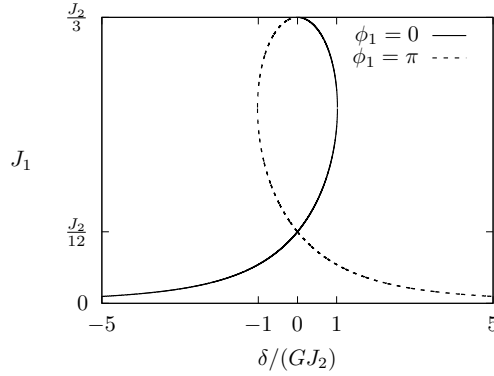
FIGURE 8.2 – Fixed points of Eq. (8.34) ($\alpha_{11} = \alpha_{12} = 0$) for $\phi_1 = 0$ (solid line) and $\phi_1 = \pi$ (dashed line) as a function of δ.

- if $\delta = 0$, two fixed points are present in $J_2/12$, at $\phi_1 = 0$ and $\phi_1 = \pi$. The separatrix degenerates to the diameter of the allowed circle.

- if $\delta < 0$, one has the same situation as for $\delta > 0$, but exchanging $\phi_1 = 0$ and $\phi_1 = \pi$.

Resonance $(3, 1)$

From the general properties stated before, the allowed circle is $J_1 < J_2$ and the coupling arc intersects the border of the allowed circle at $\phi_1 = \pm\pi/2$. Then, we have the origin that, being $m > 2$, is a stable fixed point.

For what concerns the fixed points on the X axis, we initially consider the case with $\alpha_{11} = \alpha_{12} = 0$. For $\phi_1 = 0$ or $\phi_1 = \pi$, the equation $\partial H/\partial J_1 = 0$ reads

$$2\delta\sqrt{J_2 - J_1} = \pm 3\sqrt{3}G J_1^{1/2}(4J_1 - 3J_2). \tag{8.37}$$

Assuming $G > 0$, for $\delta > 0$ we can accept solutions on $\phi_1 = 0$ for $J_1 < 3J_2/4$ and on $\phi_1 = \pi$ for $3J_2/3 < J_1 < J_2$, and the opposite for $\delta < 0$. By squaring, we obtain the cubic equation

$$4\delta^2(J_2 - J_1) = 27G^2 J_1(4J_1 - 3J_2)^2 \tag{8.38}$$

whose roots can be studied by rewriting the equation as

$$\frac{4\delta^2}{27G^2} = \frac{J_1(4J_1 - 3J_2)^2}{J_2 - J_1} = f\left(\frac{J_1}{J_2}\right), \tag{8.39}$$

and by studying $f(J_1/J_2)$ as a function of J_1 in $[0, J_2]$. This function has zeroes in $J_1 = 0$ and $J_1 = 3J_2/4$ and diverges to $+\infty$ as $J_1 \to J_2$. From its
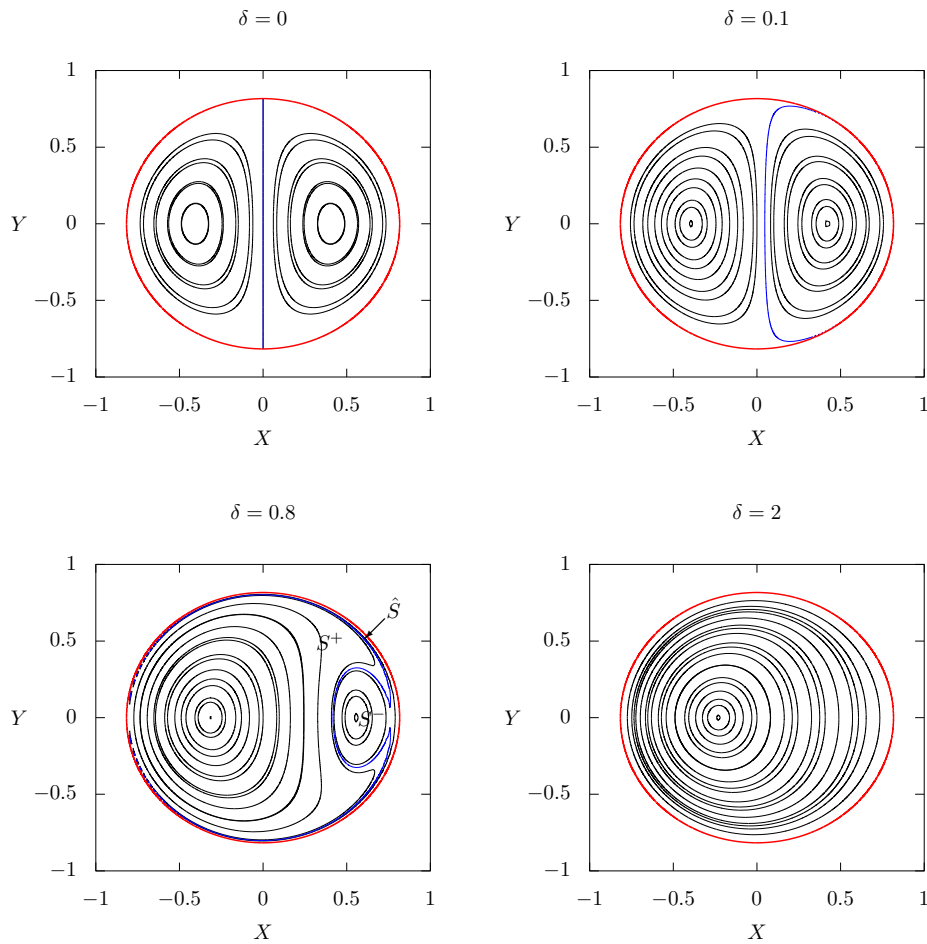
FIGURE 8.3 – Phase space of Eq. (8.34) for different values of δ with $G = 1$ and $J_2 = 1$. The red line delimits the allowed circle, while the blue line is the separatrix. In the bottom-left plot, the extended region on the left is S^+, the one inside the separatrix on the right is S^- while the small region between the separatrix and the allowed circle is $\hat{S}$.
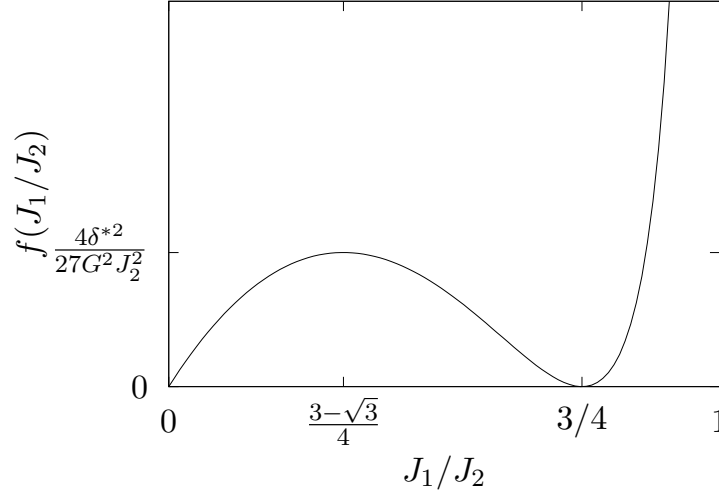
Figure 8.4 – Plot of $f(J_1/J_2) = \dfrac{(J_1/J_2)(4J_1/J_2 - 3)^2}{1 - J_1/J_2}$, which corresponds to the r.h.s. of Eq. (8.39). The real solutions of the equation are found as $f(J_1/J_2) = 4\delta^2/(27G^2 J_2)$.

derivative, we find that a local maximum exists for $J_1 = (3 - \sqrt{3})J_2/4$ and the corresponding value of δ is (see Eq. (8.39))

$$\delta^* = \pm\frac{9G}{2}\sqrt{2\sqrt{3} - 3}\, J_2 \approx \pm 3.1 G J_2\,. \qquad (8.40)$$

The plot of $f(J_1/J_2)$ is shown in Fig. 8.4. Considering the sign conditions on the solution, one has the following possibilities (some examples of phase-space portraits are shown in Fig. 8.5):

- if $\delta > \delta^*$, there are a stable fixed point at the origin and a stable fixed point at the right of the coupling arc for $\phi_1 = 0$ and $J_1 > 3J_2/4$ (see Fig. 8.5, right);

- if $0 < \delta < \delta^*$, a stable fixed point at the origin, an unstable fixed point for $\phi_1 = \pi$, $0 < J_1 < (3 - \sqrt{3})J_2/4$, and a stable fixed point for $\phi_1 = \pi$ and $(3 - \sqrt{3})J_2/4 < J_1 < 3J_2/4$, plus a stable fixed point at the right of the coupling arc, for $\phi_1 = 0$ and $J_1 > 3J_2/4$. The separatrix that passes through the unstable fixed point is the green line in Fig. 8.5 (centre) de-limiting the regions S_1 and S_2;

- if $\delta = 0$, two stable fixed points at $J_1 = 3J_2/4$; the coupling arc is a line that passes through the origin (see Fig. 8.5, left);
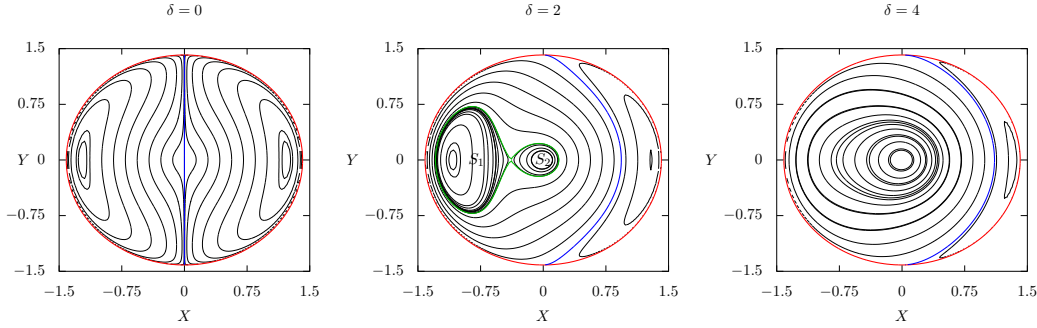
FIGURE 8.5 – Phase space of Hamiltonian of Eq. (8.6), with $m = 3$, $n = 1$, expressed in ($X = \sqrt{2J_1}\cos\phi_1$, $Y = \sqrt{2J_1}\sin\phi_1$) coordinates, for three values of δ, having set $G = J_2 = 1$ and the amplitude detuning coefficients to zero. The red line delimits the allowed circle while the blue line is the coupling arc. In plot for $\delta = 2$, the green line is the extra separatrix which delimits the regions S_1 and S_2.

- if $-\delta^* < \delta < 0$, a stable fixed point at the origin, an unstable fixed point for $\phi_1 = 0$, $0 < J_1 < (3 - \sqrt{3})J_2/4$, and a stable fixed point for $\phi_1 = 0$ and $(3 - \sqrt{3})J_2/4 < J_1 < 3J_2/4$, plus a stable fixed point at the left of the coupling arc, for $\phi_1 = \pi$ and $J_1 > 3J_2/4$. The topology is the same of Fig. 8.5 (centre), but horizontally reversed;

- $\delta < -\delta^*$: a stable fixed point at the origin and a stable fixed point at the left of the coupling arc for $\phi_1 = \pi$ and $J_1 > 3J_2/4$. Once more, the topology is mirrored w.r.t. the rightmost plot of Fig. 8.5.

8.2.4 | Emittance-sharing process

General considerations

Let us consider a process described by the Hamiltonian of Eq. (8.4), with either ω_x or ω_y, or both, slowly changing as a function of time to cross the (m, n) resonance. According to the transformations that led to Eq. (8.6), this is modelled varying δ from a case where $\hat{\delta} = \delta + \alpha_{12}J_2 \gg 0$ to one where $\hat{\delta} \ll 0$, i.e. $\hat{\delta}$ is adiabatically changed from $+\delta_{\max}$ to $-\delta_{\max}$ during a time interval T. The variation of $\hat{\delta}$ changes the position of the coupling arc, that sweeps the disk $J_1 < J_2/n$ within which the dynamics is constrained.

A particle starts its orbit far from the resonance, with an action $J_{1,i} = J_{x,i}/m$, where, the only fixed point is close to the origin and the particle orbit is almost a circle, of area $2\pi J_{1,i}$. This area is an adiabatic invariant, and it is conserved

when $\hat{\delta}$ is slowly varied. As $\hat{\delta}$ is decreased, the moving coupling arc reduces the extent of the region the particle is orbiting in, dividing the allowed circle in two parts that have equal area when $\hat{\delta} = 0$. When the area of the initial region is equal to $2\pi J_{1,\mathrm{i}}$, according to separatrix crossing theory (1.5), the particle will cross the coupling arc and enter the other phase-space region with an action corresponding to the area of the arrival region at the jump time divided by 2π.

Since the allowed circle has an area $2\pi J_2/n$, the resulting action will be

$$J_{1,\mathrm{f}} = \frac{J_2}{n} - J_{1,\mathrm{i}} , \tag{8.41}$$

and, transforming back to the initial actions

$$J_{x,\mathrm{f}} = m J_{1,\mathrm{f}} = m\left(\frac{J_{y,\mathrm{i}} + n J_{x,\mathrm{i}}/m}{n} - \frac{J_{x,\mathrm{i}}}{m}\right) = \frac{m}{n} J_{y,\mathrm{i}} \tag{8.42}$$

and

$$J_{y,\mathrm{f}} = \frac{n}{m} J_{x,\mathrm{i}} . \tag{8.43}$$

As δ continues decreasing, the area of the region containing the particle orbit increases and, at the end of the variation of δ (far from the resonance), the orbit is a circle around the origin whose area corresponds to the new action.

For each particle, this process realises an *action sharing* between the two degrees of freedom. The product $J_x J_y$ remains constant, but the two values are, at the end of the process, reallocated according to a n/m ratio. Note that for the case of the linear coupling resonance, i.e. $n = m = 1$, this corresponds to the well-known emittance exchange process we describe in Chapter 7. It is essential to stress that the analysis outlined before holds true only when the phase space is exactly divided into two regions by the coupling arc, and no other separatrices are present. Otherwise, a different analysis is needed to assess whether the additional phase-space regions interfere with the trapping process leading to the emittance sharing, and in this case how to mitigate such effects: a discussion is carried out in Section 8.2.4. If the action sharing is successful, it is possible to verify what happens in the presence of a set of initial conditions that are Gaussian distributed in both planes (x, p_x) and (y, p_y), i.e. an exponential distribution in J_x and J_y. Using the standard definition, i.e. $\varepsilon_x = \langle J_x \rangle$, $\varepsilon_y = \langle J_y \rangle$, the initial distribution reads

$$\rho_{\mathrm{i}}(J_x, J_y) = \frac{1}{\varepsilon_x \varepsilon_y} \exp\left(-\frac{J_x}{\varepsilon_x} - \frac{J_y}{\varepsilon_y}\right) \tag{8.44}$$

and, after the exchange process using Eqs. (8.42, 8.43), we obtain the final distribution

$$\rho_{\mathrm{f}}(J_x, J_y) = \frac{1}{\varepsilon_x \varepsilon_y} \exp\left(-\frac{m}{n}\frac{J_y}{\varepsilon_x} - \frac{n}{m}\frac{J_x}{\varepsilon_y}\right) . \tag{8.45}$$

The new averages are given by the integrals

$$\varepsilon_{x,\mathrm{f}} = \langle J_{x,\mathrm{f}} \rangle = \int_0^\infty \mathrm{d}J_x \int_0^\infty \mathrm{d}J_y \, J_x \, \rho_\mathrm{f}(J_x, J_y) \quad = \frac{m}{n} \langle J_{y,\mathrm{i}} \rangle = \frac{m}{n} \varepsilon_{y,\mathrm{i}}$$

$$\varepsilon_{y,\mathrm{f}} = \langle J_{y,\mathrm{f}} \rangle = \int_0^\infty \mathrm{d}J_x \int_0^\infty \mathrm{d}J_y \, J_y \, \rho_\mathrm{f}(J_x, J_y) \quad = \frac{n}{m} \langle J_{x,\mathrm{i}} \rangle = \frac{n}{m} \varepsilon_{x,\mathrm{i}} \,,$$

(8.46)

and it is evident that an *emittance sharing* occurred.

It is also possible to compute the initial distributions in terms of J_1 and J_2

$$\rho_1(J_1) = \int_0^\infty \mathrm{d}J_y \, \rho_\mathrm{i}(m J_1, J_y) = \frac{1}{\varepsilon_x} \exp\left(-\frac{m J_1}{\varepsilon_x}\right)$$

$$\rho_2(J_2) = \int_0^{\frac{m}{n} J_2} \mathrm{d}J_x \, \rho_\mathrm{i}\left(J_x, J_2 - \frac{n}{m} J_x\right)$$

$$= \frac{m}{m \varepsilon_x - n \varepsilon_y} \left[\exp\left(-\frac{J_2}{\varepsilon_y}\right) - \exp\left(-\frac{m J_2}{n \varepsilon_x}\right)\right].$$

(8.47)

Then, given the dependence of the phase-space topology on the conserved parameter J_2, it is useful to consider the initial Gaussian distribution in J_x and J_y as an ensemble of distributions in J_1 dependent on the parameter J_2 distributed as $\rho_2(J_2)$: the distribution of J_1 for a given J_2 reads

$$\rho_{12}(J_1|J_2) = \frac{\rho(m J_1, J_2 - n J_x/m)}{\rho_2(J_2)} = \frac{m \varepsilon_y - n \varepsilon_x}{m \varepsilon_x \varepsilon_y} \frac{\exp\left(\frac{n-m}{\varepsilon_x} J_1\right)}{1 - \exp\left(\frac{n \varepsilon_x - m \varepsilon_y}{n \varepsilon_x \varepsilon_y} J_2\right)}$$

(8.48)

where the normalisation

$$\int_0^\infty \mathrm{d}J_2 \, \rho_2(J_2) \int_0^{J_2/n} \mathrm{d}J_1 \, \rho_{12}(J_1|J_2) = 1$$

(8.49)

holds.

During the emittance-sharing process, δ is varied between $\pm\delta_\mathrm{max}$, and correspondingly, η (see Eq. (8.9)) varies between $\pm\eta_\mathrm{max}$, where $\eta_\mathrm{max} = \eta(\delta_\mathrm{max})$. For any pair $(J_{1,\mathrm{i}}, J_{2,\mathrm{i}})$, there exists a value η^* for which the area of the phase-space region $A_{J,2}(\eta)$ satisfies $2\pi J_{1,\mathrm{i}} = A_{J_{2,\mathrm{i}}}(\eta^*)$, and whenever the phase space is divided into two regions, $A_{J_{2,\mathrm{i}}}(\eta)$ is a monotonic decreasing function of η (and of δ) during the resonance-crossing process. Therefore, the function $J_1(\eta^*) = A(\eta^*)/(2\pi)$ is monotonic as well. During the resonance crossing, the fraction τ of particles that effectively undergoes emittance sharing is given by all particles for which $\eta^* \in [-\eta_\mathrm{max}, \eta_\mathrm{max}]$ and it can be obtained by

$$\tau = \int_0^\infty \mathrm{d}J_2 \, \rho_2(J_2) \int_{J_1(-\eta_\mathrm{max})}^{J_1(\eta_\mathrm{max})} \mathrm{d}J_1 \, \rho_{12}(J_1) \,.$$

(8.50)

The sharing fraction τ will also be a monotonic function of $\eta_{\max}$. The parameter $\eta_{\max}$ determines the effectiveness of the emittance sharing due to geometrical reasons: under the assumption that the initial beam distributions are Gaussian, one can define the following parameter

$$\kappa_{\mathrm{geom}} = \frac{\delta_{\max}}{G \left\langle J_{2,\mathrm{i}} \right\rangle^{(m+n-2)/2}} \,, \tag{8.51}$$

as the relevant quantity to study the performance of the emittance-sharing process.

The phase-space geometry is certainly important in the emittance-sharing process, but the efficiency is also influenced by the adiabaticity of the resonance-crossing process. A form for the adiabaticity parameter should therefore be determined. For this purpose we remark that the Hamiltonian of Eq. (8.6) can be written, while δ is varied, as

$$\mathcal{H} = \epsilon t J_1 + H_0(J_1) + G H_1(\phi_1, J_1) \,, \tag{8.52}$$

where $\epsilon = 2\delta_{\max}/T$, and H_0, H_1 represent the amplitude-dependent and resonant terms, respectively, that appear in the equations of motion

$$\begin{aligned}
\dot{J}_1 &= -G \, \frac{\partial H_1}{\partial \phi} \\
\dot{\phi}_1 &= \epsilon t + \frac{\partial H_0}{\partial J} + G \, \frac{\partial H_1}{\partial J} \,.
\end{aligned} \tag{8.53}$$

We now perform the same rescaling that we introduced in Eq. 7.27. If $\bar{t} = Gt$, one obtains the equations

$$\begin{aligned}
\frac{\partial J_1}{\partial \bar{t}} &= -\frac{\partial H_1}{\partial \phi} \\
\frac{\partial \phi_1}{\partial \bar{t}} &= \frac{\epsilon}{G^2} \bar{t} + \frac{1}{G} \frac{\partial H_0}{\partial J} + \frac{\partial H_1}{\partial J} \,.
\end{aligned} \tag{8.54}$$

Therefore, the appropriate adiabaticity parameter is given by ϵ/G^2, i.e. one obtains the same emittance sharing if G scales as $G \sim \sqrt{\epsilon}$, while the amplitude-detuning terms are rescaled by a factor G. Parenthetically, as discussed in the previous chapter, it is possible to improve the adiabaticity of the resonance-crossing process by using $\delta \sim (\epsilon t)^p$ with $p > 1$. If ϵ is kept constant and the sharing efficiency is evaluated for different values of $\delta_{\max}$, then the parameter that controls the emittance sharing, including the dynamical effects, is given by

$$\kappa_{\mathrm{dyn}} = \frac{\sqrt{\delta_{\max}}}{G \left\langle J_{2,\mathrm{i}} \right\rangle^{(m+n-2)/2}} \,. \tag{8.55}$$

We remark that $\kappa_{\mathrm{geom}}/\kappa_{\mathrm{dyn}} = \sqrt{\delta_{\max}}$.

Note that an effective resonance strength, which corresponds to the inverse of the parameter κ_{dyn} defined above, was introduced in Ref. [61] and [32] as the unique parameter needed to describe the emittance sharing due to the crossing of the resonance $(1, 2)$. Our discussion shows that the purely phenomenological choice can be explained by means of rigorous mathematical arguments.

Effect of phase-space topology on emittance sharing

A general assumption on emittance sharing requires that the allowed circle is divided by the coupling arc in two regions. From the considerations reported in Section 8.2.3, this is always true for third-order resonances. However, for fourth-order resonances, such as $(1, 3)$ and $(3, 1)$, the situation is more complex. Indeed, close to the resonance $(1, 3)$, an extra phase-space region is present (see Fig. 8.3), although it does not affect the emittance sharing.

Let us follow the evolution of the system from a state when $\delta \gg G J_2$ and one with $\delta \ll -G J_2$. At the beginning, only a fixed point is present, around which the particle orbits. When $\delta < G J_2$, the region $\hat{S}$ appears (see Fig. 8.3) and particles orbiting outside the new separatrix are automatically captured into that region, without any jump in J_1, since the area they enclose within their orbit remains the same.

While δ further decreases, however, $\hat{S}$ is pushed towards the outer circle. Particles inside it are then captured into S^+, for which $\Theta^+ = \mathrm{d}A(S^+)/\mathrm{d}\delta > 0$, with the expected change in the adiabatic invariant. However, since in the crossing of the outer separatrix no change of adiabatic invariant occurs, the passage from $\hat{S}$ to S^- is perfectly equivalent to the passage between S^+ and S^-. Once δ reaches zero, the situation is perfectly symmetric, with two stable fixed points and a separatrix dividing the allowed circle in two equal parts.

We then continue reducing δ in the negative domain. A new unstable fixed point appears at $\phi_1 = \pi$, and a topology akin to the third plot of Fig. 8.3, although mirrored, appears. The problem is whether the new outer region will trap particles, and this turns out not to be possible. The outer region is maximal at $\delta = -G J_2$, and the unstable fixed point is at $J_1 = J_2/4$ and $\phi_1 = \pi$. We can thus estimate the area of the outer region as the difference between the outer circle at $J_1 = J_2/3$, and the circle at $J_1 = J_2/4$, which gives $\pi J_2/6$. On the contrary, particles inside $\hat{S}$ have a minimum action of $J_2/4$, i.e. their orbit area is at least $\pi J_2/2$. Hence, since the area of $\hat{S}$ is always smaller than $\pi J_2/2$, no particle can reach the minimum action required when crossing from S^+ to $\hat{S}$. Thus, $\hat{S}$ remains void until, at $\delta = -G J_2$ it disappears completely.

Finally, the extra fixed point does not affect the emittance exchange process, as all particles pass from S^- to S^+, which results, according to our previous

generic analysis, in an emittance exchange.

In the case of the resonance $(3, 1)$, the presence of extra stable fixed points (see Fig. 8.5) translates in an extra (and unavoidable) phase-space region that can, in principle, trap particles, thus spoiling the emittance sharing. Nevertheless, numerical observations discussed in Section 8.3) show that emittance sharing is still feasible, although with some reduction in performance due to the particles trapped in the extra region.

8.3 | Results of numerical simulations

To assess the performance of the emittance-sharing process for different resonances, we compute the evolution of a Gaussian distribution of initial conditions $\rho(J_x, J_y)$ under the dynamics generated by the map of Eq. (8.1) iterated N times, with or without amplitude-detuning terms, where ω_x is kept constant while ω_y is linearly varied between an initial value $\omega_{y,i} = m\omega_x/n + \delta_{\max}$ and the final one $\omega_{y,f} = m\omega_x/n - \delta_{\max}$, to cross the (m, n) resonance. The initial and final emittance values are then compared, and a figure of merit is introduced to evaluate how well the emittance sharing occurred. To do so, we adapt the definition of P_{na}, introduced in Eq. 7.62 for the $(1, 1)$ resonance crossing leading to emittance exchange, to retain its properties when a (m, n) resonance is crossed, and emittance sharing occurs, and the generalised definition is

$$P_{\mathrm{na}} = 1 - \frac{\langle J_{x,\mathrm{f}} \rangle - \langle J_{x,\mathrm{i}} \rangle}{(m/n)\langle J_{y,\mathrm{i}} \rangle - \langle J_{x,\mathrm{i}} \rangle} \,, \tag{8.56}$$

which is 1 when no emittance sharing is achieved and zero when the sharing is perfect, i.e. according to the Eq. (8.46).

Note that in Ref. [61] a different figure of merit is introduced, the so-called fractional emittance growth (FEG), defined as

$$\mathrm{FEG} = \left| \frac{\langle J_{x,\mathrm{f}} \rangle}{\langle J_{x,\mathrm{i}} \rangle} - 1 \right| + \left| \frac{\langle J_{y,\mathrm{f}} \rangle}{\langle J_{y,\mathrm{i}} \rangle} - 1 \right| \,, \tag{8.57}$$

which is 0 when no exchange is performed and $\left| \dfrac{m\langle J_{y,\mathrm{i}} \rangle}{n\langle J_{x,\mathrm{i}} \rangle} - \dfrac{n\langle J_{x,\mathrm{i}} \rangle}{m\langle J_{y,\mathrm{i}} \rangle} \right|$ for a perfect emittance sharing. The reason of this definition is that the goal of [61] is to avoid emittance sharing, and therefore to reduce the FEG, whereas our goal is the opposite, as we are looking for performing the emittance sharing, and hence P_{na} is the best choice for our study.

When not stated differently, we set $\beta_x = \beta_y = 1$, $\langle J_{x,i} \rangle = \langle J_{y,i} \rangle = 1 \times 10^{-4}$, $\omega_x = 2.602$, and $\alpha = 0$, generating distributions of initial conditions with $N_p = 1 \times 10^4$ particles. For the $(1, 2)$ and $(2, 1)$ resonances we use $\delta_{\max} = 0.1$, k_2 (or j_2) equal to 1, $N = 1 \times 10^6$. For the $(1, 3)$ and $(3, 1)$ resonances we set $\delta_{\max} = 0.01$, $j_3 = 10$, $N = 1 \times 10^7$.

The initial and final distributions of x, y, p_x, p_y for the four resonances are plotted in Fig. 8.6, and they show clearly the effectiveness of the emittance sharing in standard conditions. Fits of Gaussian distributions with zero average are performed for the final distributions of the phase-space variables. The excellent agreement between the numerical results and the fitted functions shows that the emittance-sharing process preserves the Gaussian nature of the beam, acting only on the standard deviation.

We proceed with the quantitative evaluation of the performance of the proposed technique by analysing how P_{na} changes as a function of the parameters. In particular, we have concentrated our analyses on the dependence of P_{na} on: *(i)* the excursion of ω_y, i.e. $\delta_{\max}$; *(ii)* the strength of the non-linear magnets j_2, k_2, and j_3, depending on the resonance crossed; *(iii)* the number of map iterations (turns) N; *(iv)* the detuning parameter α (that has been chosen as $\alpha = \alpha_{xx} = \alpha_{yy} = -2\alpha_{xy}$ to mimic the amplitude detuning generated by normal octupoles as done in the previous chapter; *(v)* the initial values of $\langle J_x \rangle$ and $\langle J_y \rangle$; *(vi)* the ratio between $\langle J_{y,i} \rangle$ and $\langle J_{x,i} \rangle$. It is worth stressing that in our numerical investigation of the 4D parameter space, the dependence of P_{na} is probed by changing one parameter at a time while keeping the others set to their nominal values.

Figure 8.7 (left) shows the plot of P_{na} as a function of $\delta_{\max}$ whereas in the right part the dependence on the strength of the non-linear magnets is reported for the various resonances considered. A difference between the behaviour of the third- and fourth-order resonances is clearly seen. While for the former it is possible to determine the optimal value of $\delta_{\max}$, or the strength of the non-linear magnets, such that $P_{na} = 0$, i.e. the emittance sharing is perfect, this is not the case for the latter resonances, for which P_{na} reaches a non-zero minimum value.

We remark that when $\delta_{\max}$ approaches 0, P_{na} does not converge to 1. This is due to the fact that, when $\delta \approx 0$, the motion of all particles is very close to resonant conditions, and all particles revolve around one of the two stable fixed points in the phase space. Taking the average of the coordinate J_1 along the orbit, allows estimating the value of P_{na} when $\delta_{\max} \to 0$ (the details are found in Appendix 8.B).

Other effects need to be taken into account, e.g. the adiabaticity of the system. Weak non-linear coupling, which corresponds to a small value of G in the Hamiltonian of Eq. (8.6), means a faster resonance crossing. For instance,
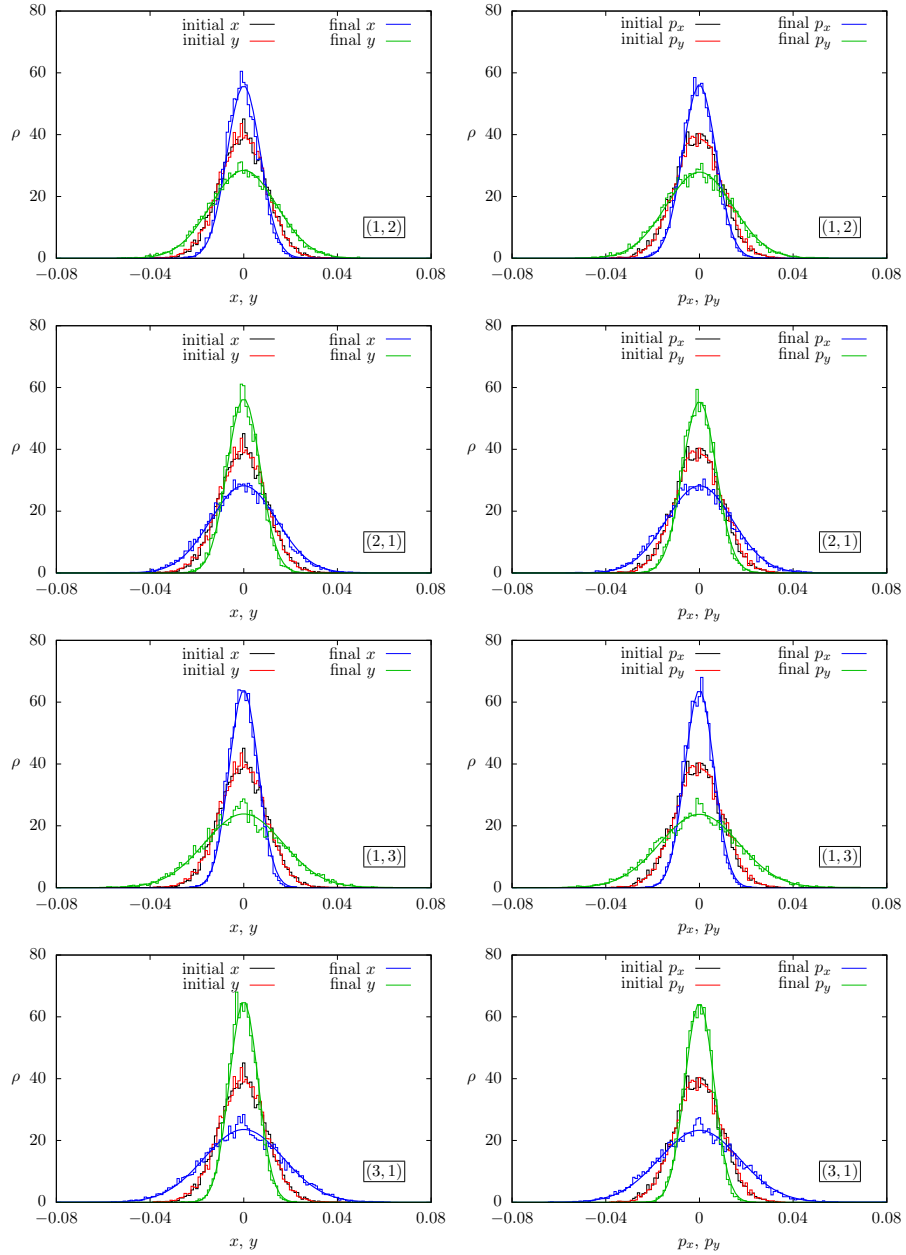
FIGURE 8.6 – Histograms of the initial and final distribution of x, y (left plots) and p_x, p_y (right plots) after the resonance-crossing process for the four resonances under study. The initial distribution is Gaussian, with a standard deviation $\langle J_{x,\mathrm{i}} \rangle = \langle J_{y,\mathrm{i}} \rangle = 0.01$. The map of Eq. (8.1) has been used, with parameters $\delta_{\max} = 0.1$, $j_2 = 1$ or $k_2 = 1$, $N = 10^6$, $\alpha = 0$ for the third-order resonances; $\delta_{\max} = 0.01$, $j_3 = 10$, $N = 10^7$, $\alpha = 0$ for the fourth-order ones. The thick blue and green lines represent the Gaussian fits with zero average of the final distributions.
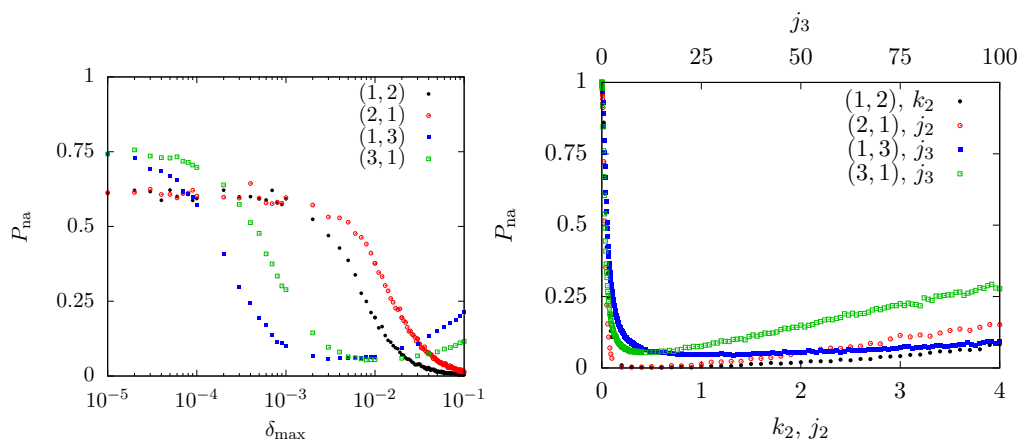
FIGURE 8.7 – Left: P_{na} as a function of the excursion ω_y, i.e. $\delta_{\max}$. Right: P_{na} as a function of the strength of the non-linear magnets (k_2, j_2 or j_3 depending on the resonance used). In both plots the map (8.1) has been used, setting $\alpha = 0$, and $N = 10^6$ (for the third-order resonances) and $N = 10^7$ (for the fourth-order ones), and using initial distributions with $\langle J_{x,\mathrm{i}} \rangle = \langle J_{y,\mathrm{i}} \rangle = 0.01$. In the left plot, depending on the resonance, we set either $k_2 = 1$, $j_2 = 1$, or $j_3 = 10$. In the right plot, $\delta_{\max} = 0.1$ has been chosen for $(1, 2)$ and $(2, 1)$ while $\delta_{\max} = 0.01$ for $(1, 3)$ and $(3, 1)$.

for a particle moving close to the $(1, 2)$ resonance, the coupling arc, given by the line of equation $X = \delta/(\sqrt{2}G)$, moves, over one map iteration, by $\delta X = \delta_{\max}/(\sqrt{2}GN)$. This means that the adiabaticity condition is not met when the strength of the non-linear magnets is small, and for this reason P_{na} goes to 1. The same effect accounts for the lower sharing efficiency at large $\delta_{\max}$, when N is kept constant.

We remark that when the strength of the non-linear magnets becomes large, the quasi-resonant Hamiltonian may be no longer a good approximation of the dynamics generated by the map as the higher-order terms cannot be neglected anymore. This observation will be particularly relevant when we will discuss the results shown in Figs. 8.9 later in this Section.

Figure 8.8 shows the dependence of P_{na} on the initial emittance values and the ratio between vertical and horizontal emittances. On the left plot, we keep $\langle J_{x,\mathrm{i}} \rangle = \langle J_{y,\mathrm{i}} \rangle$ and we change their value, while on the right plot we keep $\langle J_{x,\mathrm{i}} \rangle = 1 \times 10^{-4}$ and we vary $\langle J_{y,\mathrm{i}} \rangle$ from 1×10^{-6} to 1×10^{-2}. As observed before, the behaviour for the third- and fourth-order resonances are different. The first type of resonances features a virtually zero P_{na} over a rather wide range of parameters under consideration. On the other hand, the fourth-order resonances feature a non-zero minimum for P_{na}, and that is achieved for well-defined values of the parameters under consideration.

Furthermore, for all the four resonances P_{na} increases (therefore that the emittance sharing is less effective) for large values of the initial emittances. This is due to a lower number of particle effectively performing the adiabatic jump. It also increases for small values of the initial action, as this translate to a more difficult onset of adiabatic conditions. It is also observed that achieving emittance sharing for fourth-order resonances is far more difficult than for the third-order ones when $\langle J_{y,\mathrm{i}} \rangle \neq \langle J_{x,\mathrm{i}} \rangle$. In particular, we remark that for $(1, 3)$ and $(3, 1)$ the situation is reversed, as emittance sharing fails for $(1, 3)$ when $\langle J_{y,\mathrm{i}} \rangle \ll \langle J_{x,\mathrm{i}} \rangle$, whereas this occurs for $\langle J_{y,\mathrm{i}} \rangle \gg \langle J_{x,\mathrm{i}} \rangle$ in the case of the $(3, 1)$ resonance. This fact will be discussed later.
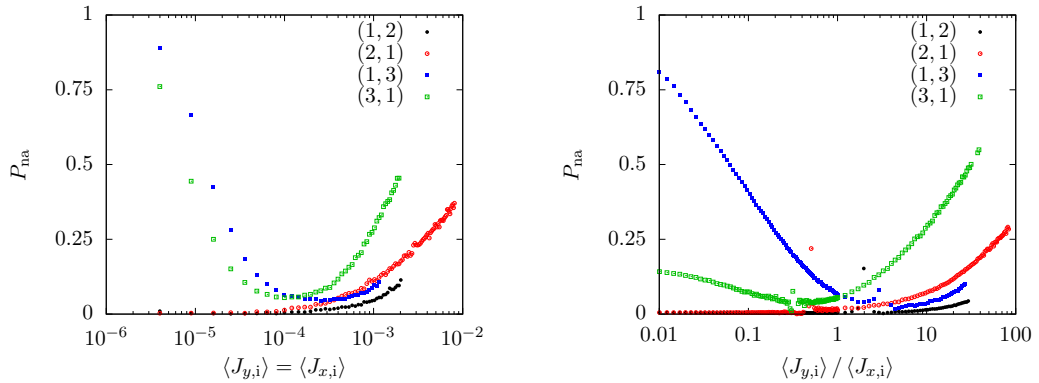
FIGURE 8.8 – Left: P_{na} as a function of the initial $\langle J_{x,\mathrm{i}} \rangle$ (chosen to be equal to $\langle J_{y,\mathrm{i}} \rangle$), for the four resonances. Right: P_{na} as a function of the ratio between $\langle J_{y,\mathrm{i}} \rangle$ and $\langle J_{x,\mathrm{i}} \rangle$, using $\langle J_{x,\mathrm{i}} \rangle = 0.01$. In both plots the map (8.1) has been used, setting $\alpha = 0$, and $\delta_{\max} = 0.1$, $j_2 = 1$ or $k_2 = 1$, $N = 10^6$ (for the third-order resonances) and $\delta_{\max} = 0.01$, $j_3 = 10$, $N = 10^7$ (for the fourth-order ones).

Some common observations can be drawn from Figs. 8.7 and 8.8. First of all, it is clear that, in general, third-order resonances achieve smaller values of P_{na}, than fourth-order ones. In the observed conditions, the best results for resonances $(1, 2)$ and $(2, 1)$ correspond to $P_{\mathrm{na}} \approx 0.01$, while for $(1, 3)$ and $(3, 1)$ the best performance corresponds to $P_{\mathrm{na}} \approx 0.06$. This is explained by the fact, as can be seen from the higher values of P_{na} at low initial action in the left plot of Fig. 8.8, that fourth-order resonances are more affected than third-order ones by adiabaticity (note that the numerical simulations for fourth-order resonances were performed with a number of turns an order of magnitude higher than those of the third-order resonances).

In Fig. 8.9, we combine data from both plots of Fig. 8.7 and the left plot
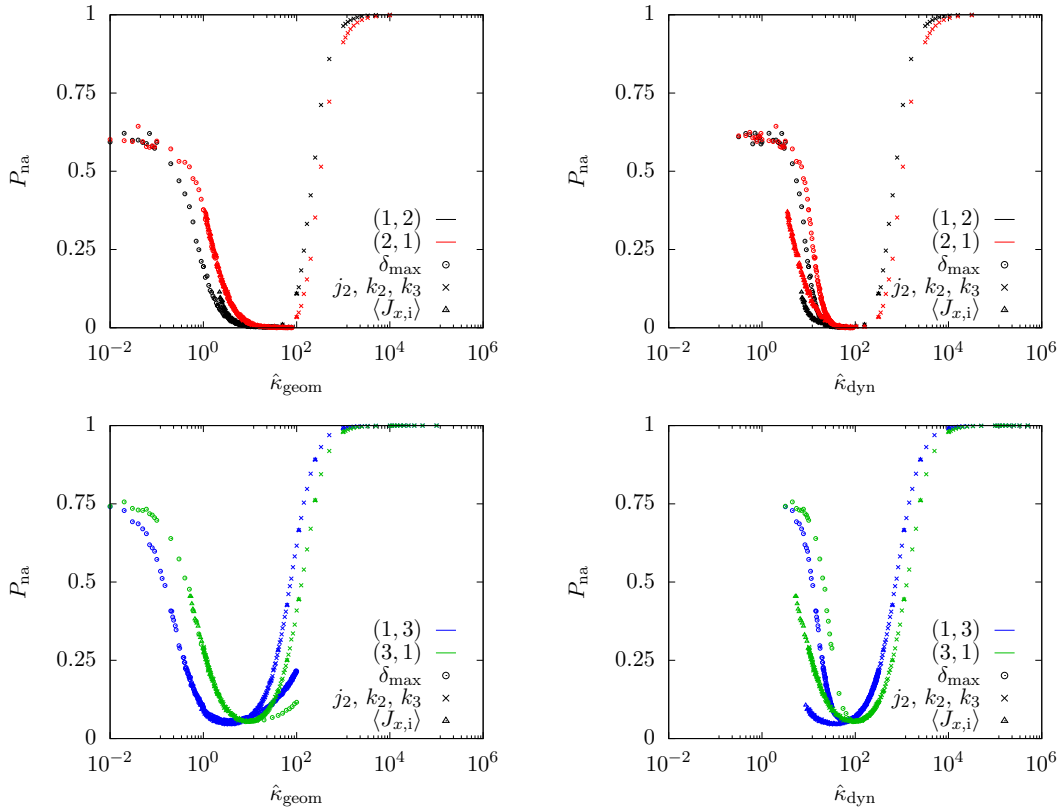
FIGURE 8.9 – Plots obtained by combining the numerical data presented in Fig. 8.7 (left and right) and in Fig. 8.8 (left), using, as independent variable, $\hat{\kappa}_{\text{geom}}$, introduced in Eq. (8.58a), for the left plots, and $\hat{\kappa}_{\text{dyn}}$, from Eq. (8.58b), for the right ones. The top plots refer to third-order while the bottom plots to fourth-order resonances. The colours encode the resonance considered, while the different point styles the variable that is varied in the data set, namely δ_{max}, the strength of the non-linear magnets or the initial distribution width.

of Fig. 8.8, using, as independent variables one of the two

$$\hat{\kappa}_{\text{geom}} = \frac{\delta_{\max}}{g\sqrt{\langle J_{x,\text{i}}\rangle^{m+n-2}}} \tag{8.58a}$$

$$\hat{\kappa}_{\text{dyn}} = \frac{1}{g}\sqrt{\frac{\delta_{\max}}{\langle J_{x,\text{i}}\rangle^{m+n-2}}}\,, \tag{8.58b}$$

where g stands for the generic strength of the non-linear magnets, which, according to the resonance, is k_2, j_2 or j_3. The two new parameters differ from those introduced in Eqs. (8.51) and (8.55) only for their adaptation to the configuration of the numerical simulations that feature initial distributions where $\langle J_{x,\text{i}}\rangle = \langle J_{y,\text{i}}\rangle$. The goal of this analysis is to identify in which regime these global parameters are the relevant quantities to describe the emittance-sharing process: in that case, the data obtained by varying each parameter entering in the expression of the global parameters should lie on the same curve.

It is clearly visible that, when $\hat{\kappa}_{\text{geom}}$ and $\hat{\kappa}_{\text{dyn}}$ are small (i.e. $\delta_{\max}$ is small, the strength of the non-linear magnets is large, and the distribution of initial conditions is wide), P_{na} depends primarily on $\hat{\kappa}_{\text{geom}}$: the performance of the emittance sharing is only limited by the fact that the tune is varied only over a finite range.

The disagreement between the data collected while varying $\delta_{\max}$ and the other quantities is visible when considering the resonance $(1, 2)$, but it can be understood by considering that when transforming the map (8.1) with a normal sextupole to a resonant normal form, and truncating at second order in the action variables, contributions to the amplitude detuning are present, even in the absence of an octupolar term. Indeed, the coefficients α_{11} and α_{12} are proportional to k_2^2. As $\alpha_{12} \neq 0$, the separatrix crossing in $[\delta_{\max}, -\delta_{\max}]$ is no longer symmetric, and a lower number of particles undergoes emittance sharing.

For large values of the two parameters, $\hat{\kappa}_{\text{dyn}}$ captures the correct scaling, as in this regime, corresponding to large $\delta_{\max}$, low g, and small initial emittance with constant value of $1/N$, the emittance sharing effectiveness is limited by the degree of adiabaticity of the process.

We remark that the scaling $g\langle J_{x,\text{i}}\rangle^{(r-2)/2}$ always holds, since the strength of the non-linear magnets, for the model considered in this paper that features a single multipole, can always be normalised to unity under a convenient coordinate rescaling, therefore changing the average value of $J_{x,\text{i}}$.

In Fig. 8.10 (top-left) the role of the amplitude-detuning parameter α is probed. Very different behaviours are observed depending on the resonance order. For the case of third-order resonances, a rather broad minimum of
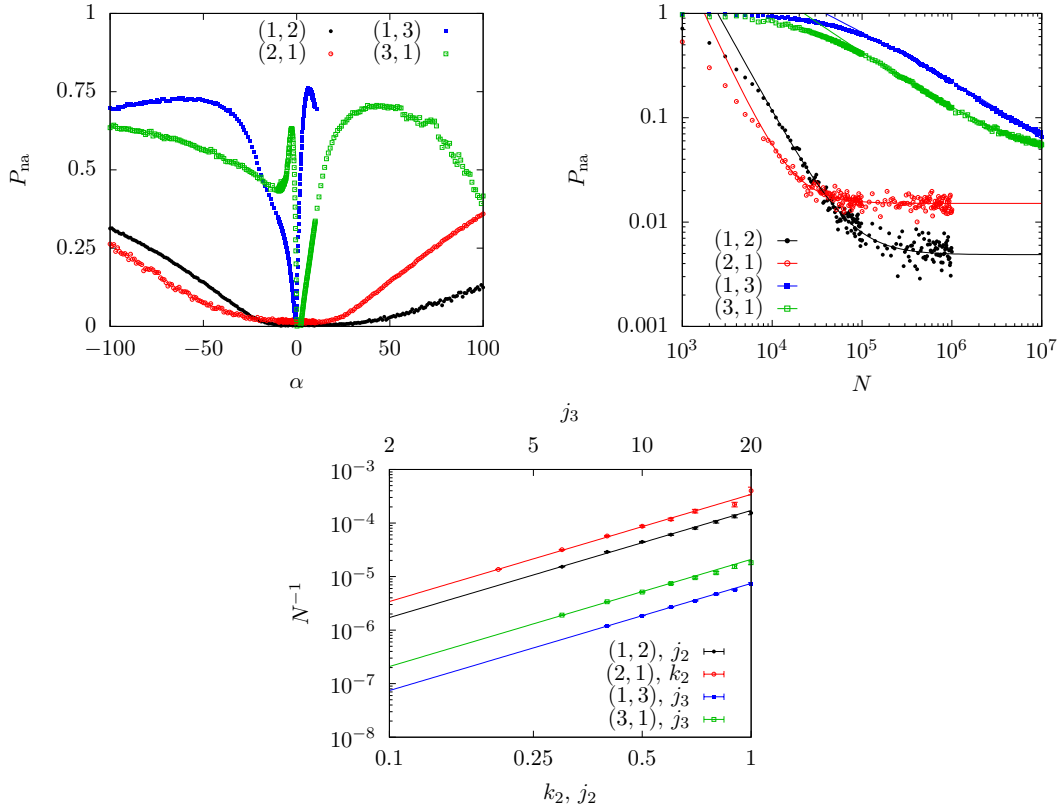
FIGURE 8.10 – Top-left: P_{na} as a function of the amplitude-detuning parameter α, for the four resonances. Top-right: P_{na} as a function of the number of turns N. Power-law fits $P_{\text{na}} = a_{m,n}N^{-b_{m,n}} + c_{m,n}$ are provided for each (m, n) resonance. Bottom: the inverse of the number of turns for which P_{na} reaches the value $P_{\text{na}} = 0.2$ (for third-order resonances) and $P_{\text{na}} = 0.3$ (for fourth-order ones) as a function of the strength of the non-linear magnets. Quadratic fit between N^{-1} and the strength of the non-linear magnets are presented, confirming the scaling of Eq. (8.54). The parameters used for the plots are: $\langle J_{x,\text{i}} \rangle = 0.01$, $\delta_{\text{max}} = 0.1$ for resonance $(1, 2)$ and $(2, 1)$ and $\delta_{\text{max}} = 0.01$ for $(1, 3)$ and $(3, 1)$. For the top-left plot $N = 10^6$, $k_2 = 1$ or $j_2 = 1$ (for third-order resonances), $N = 10^7$, $j_3 = 10$ (for fourth-order ones) are used. The same values for the strength of the non-linear magnets are used in the top-right plot. Both the top-right and the bottom plots use $\alpha = 0$.

P_{na} is observed around $\alpha = 0$, which indicates that the presence of amplitude-detuning effects does not spoil the emittance sharing process. The situation is radically different for the case of the fourth-order resonances, where the presence of a non-zero amplitude detuning changes the number and the stability type of the fixed points of the systems under consideration. This is indicated by the presence of a very sharp minimum of P_{na} around $\alpha = 0$ with a steep increase in the close neighbourhood.

In the top-right plot of Fig. 8.10, the dependence of P_{na} on the number of turns N is shown. A fit using a power law $P_{\text{na}} = a_{m,n} N^{-b_{m,n}} + c_{m,n}$ provides an excellent agreement with the numerical data. This observation is crucial, as it reveals the intrinsic difference between the behaviour of the crossing of these non-linear 2D resonances with respect to that of the linear $(1, 1)$ resonance studied in Ref. [12]. For the case of the linear coupling resonance, an exponential law for P_{na} was found in the absence of amplitude detuning. The difference can be explained since the Hamiltonian describing the crossing of the linear coupling resonance is analytic, as the unstable fixed points in the action-angle coordinates are only a pathology of the coordinate system, while the Hamiltonian describing the 2D non-linear resonances features real unstable fixed points. The separatrices related with these unstable fixed points introduce an error in the action, which is the adiabatic invariant of the system, after the jump from one region to the other one of the phase space. Such a jump in the value of the adiabatic invariant has a power-law dependence on the number of turns. The values of the exponent of the fit law for P_{na} are: $b_{1,2} = 1.56 \pm 0.02$, $b_{2,1} = 1.84 \pm 0.08$, $b_{1,3} = 0.43 \pm 0.01$ and $b_{3,1} = 0.60 \pm 0.01$, which reveal that they are strongly model dependent.

The bottom plot of Fig. 8.10 shows the scaling between the strength of the non-linear magnets and the inverse of the number N of turns, which is a direct measurement of the adiabaticity of the emittance sharing process. The data show, for different values of k_2, j_2 and j_3 (depending on the resonance considered), the value of N for which one obtains a small value for P_{na}, i.e. $P_{\text{na}} = 0.2$ for third-order resonances and $P_{\text{na}} = 0.3$ for fourth-order ones. The curves represent quadratic functions that fit in an excellent way the numerical data, thus confirming the quadratic scaling found in Eq. (8.54), which is independent on m and n.

Finally, in Fig. 8.11 we analyse the emittance sharing process by generating uniform distributions of 10^4 initial conditions at a fixed value of $J_{x,\text{i}}$, in the range $0 \leq J_{x,\text{i}} \leq m J_2 / n$, having fixed $J_2 = 1 \times 10^{-4}$. In the plots in the left column, we compare, for each resonance (m, n), $\langle J_x \rangle$ at the end of the process with the expected value from the theory, namely

$$J_{x,\text{f}} = \frac{m}{n} J_2 - J_{x,\text{i}} \, , \tag{8.59}$$
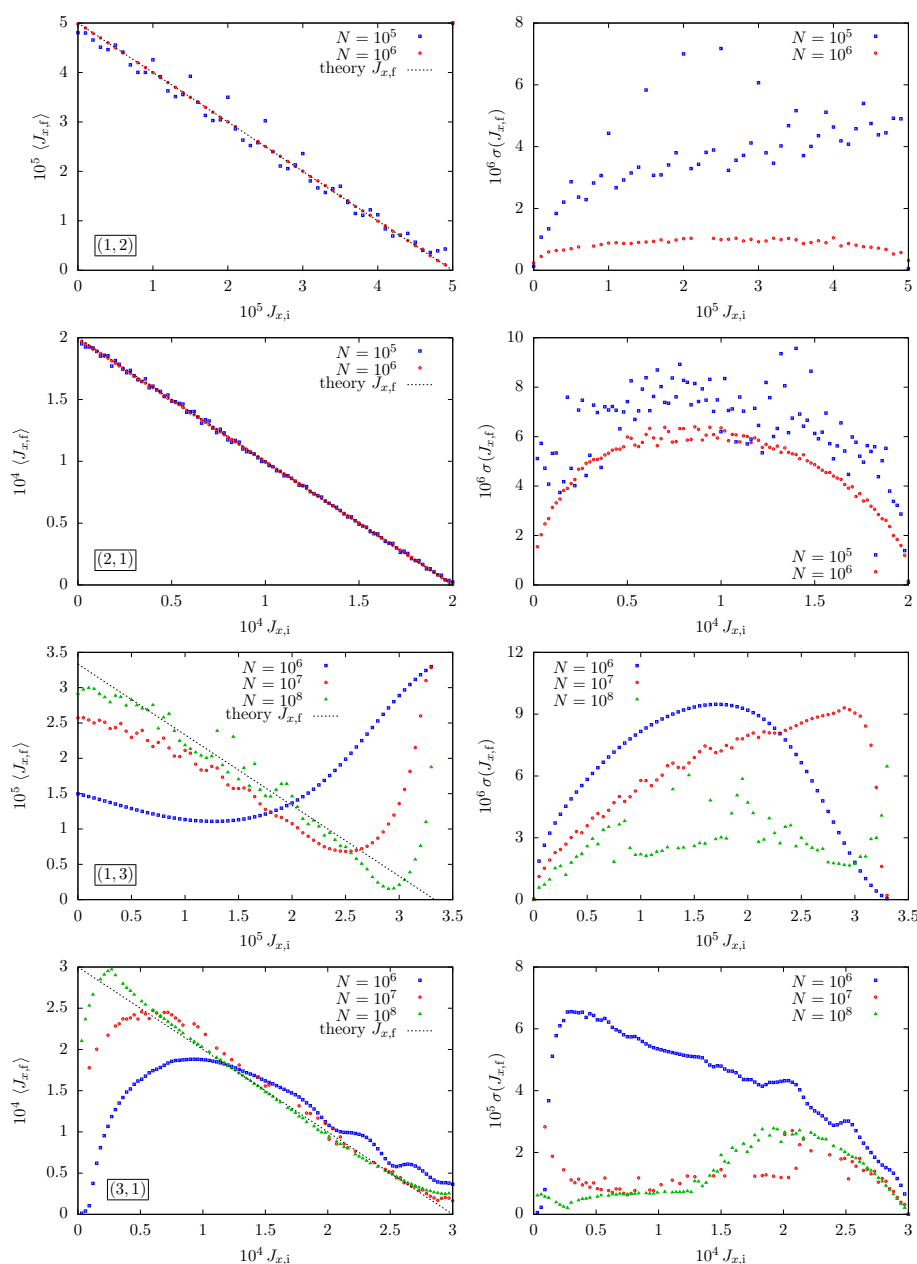
FIGURE 8.11 – Average (left column) and variance (right column) of $J_{x,\mathrm{f}}$, from initial uniform distributions at fixed $J_{x,\mathrm{i}}$ chosen in the allowed interval $0 \leq J_{x,\mathrm{i}} \leq J_{2,\mathrm{i}}/n$, having fixed $J_2 = 1 \times 10^{-4}$. The average of $J_{x,\mathrm{f}}$ is compared to the theoretical value $J_{x,\mathrm{f}} = m J_2/n - J_{x,\mathrm{i}}$. The map (8.1) has been used with no amplitude-detuning terms, using different numbers of turns N. For the third-order resonances, $\delta_{\max} = 0.1$, $j_2 = 1$ or $k_2 = 1$ have been used, whereas for the fourth-order ones $\delta_{\max} = 0.01$, $j_3 = 10$ have been used.

computed for the case of a perfect emittance-sharing process. The results of numerical simulations are presented for different number of turns N (for $N = 1 \times 10^8$, only 10^3 initial conditions have been used due to constraints on the available CPU time). In the plots in the right column, the standard deviation of the values of $J_{x,\mathrm{f}}$ is shown. The rows correspond to the various resonances considered. When increasing the number of turns, the average jump becomes closer to the theoretical expectation. For the resonances $(1, 2)$ and $(2, 1)$ we remark that the data oscillate around the expected value, in a similar fashion to what was observed in Ref. [12] for an analogous situation with linear coupling. For the fourth-order resonances, the effects of the more complicated phase-space topology are clearly visible. For instance, resonance $(1, 3)$ suffers from a slow convergence of the the data towards the expected values for large $J_{x,\mathrm{i}}$, while for resonance $(3, 1)$ the same occurs, but rather at low values of $J_{x,\mathrm{i}}$. This is consistent with what found when analysing initial conditions with $\langle J_{x,\mathrm{i}} \rangle \neq \langle J_{y,\mathrm{i}} \rangle$: resonance $(1, 3)$ fails at high values of $J_{x,\mathrm{i}}$, while $(3, 1)$ at small ones. In the latter case, also, a variance bump is observed for $J_{x,\mathrm{i}} > 1.5 \times 10^{-4}$ also at high adiabaticity: this is an effect of the presence of extra regions in the phase space. Finally, the plots of fourth-order resonances show how slowly the emittance sharing converges to the expected value when the number of turns is increased, which explains the lower performance for emittance sharing for fourth-order resonances.

8.4 | Conclusions

In this chapter, a novel beam manipulation technique is presented, based on the crossing of a 2D non-linear resonance to induce a sharing of the transverse emittances. The foundations of this technique have been discussed using Hamiltonian models and the adiabatic theory applied to resonance crossing. The performance of this manipulation has been assessed by means of detailed numerical simulations using map models, which are more realistic than the Hamiltonian ones. The results of the numerical simulations indicate that it is indeed possible to control the proposed process so to achieve a sharing of the transverse emittances. The final distributions of initial conditions retain the Gaussian character of the initial ones, which is an excellent feature. Scans of the various system parameters have been performed, thus achieving a good understanding of the details of the proposed mechanism.

Differences in the behaviour and performance of the emittance-sharing process have been found and when comparing third- and fourth-order resonances, although these observations can be fully understood and explained in terms of the phase-space topology linked with each of the resonances under

study.

As far as applications are concerned, the analysis shows clearly the theoretical feasibility of an emittance sharing process where the target emittance is met at up to $\approx 99\%$, using third-order resonances, and up to $\approx 90\%$, using fourth-order ones. These results are extremely encouraging, also in consideration of the fact that the resonances under consideration can be excited by widespread magnetic elements, such as normal and skew sextupoles, or skew octupoles (that can also be substituted by pairs of normal and skew sextupoles).

In summary, the novel beam manipulation passed successfully through theoretical and numerical tests and it is now ready for experimental validation.

Appendices

8.A | Magnets and resonances: analysis using Normal Forms

The goal of this appendix is to compute, using Normal Form theory, which resonance can be excited by a certain non-linearity in an Hénon-like map as the one of Eq. (8.1).

We start the analysis by considering which monomial appears in the complex representation of the generic polynomial map. When dealing with 4D complex coordinates (z_1, z_1^*, z_2, z_2^*), we use the vector notation $(\ell_1, m_1, \ell_2, m_2)$ to identify a monomial $z_1^{\ell_1} z_1^{*m_1} z_2^{\ell_2} z_2^{*m_2}$, and we indicate a 4D complex function as $\mathbf{F} = (F_1, F_1^*, F_2, F_2^*)$.

Starting from an Hénon-like map, we replace the real variables with complex ones, defined according to $z_1 = x - ip_x$, $z_2 = y - ip_y$, together with the corresponding complex conjugate relationships, and we obtain, expanding all

binomials, the following complex map

$$
\begin{aligned}
z_1' = e^{i\omega_1} &\Bigg[z_1 + \sqrt{\beta_x} \frac{k_r \beta_x^{\frac{r}{2}}}{2^r r!} \sum_{q \le r/2} \sum_{\ell=0}^{r-2q} \sum_{p=0}^{2q} (-1)^q \left(\frac{\beta_y}{\beta_x} \right)^q \binom{r}{2q} \binom{r-2q}{\ell} \times \\
&\times \binom{2q}{p} z_1^{r-2q-\ell} z_1^{*\ell} z_2^{2q-p} z_2^{*p} + \\
&- \sqrt{\beta_y} \frac{j_r \beta_x^{\frac{r}{2}}}{2^r r!} \sum_{q \le (r-1)/2} \sum_{\ell=0}^{r-2q-1} \sum_{p=0}^{2q+1} (-1)^q \left(\frac{\beta_y}{\beta_x} \right)^q \binom{r}{2q+1} \times \\
&\times \binom{r-2q-1}{\ell} \binom{2q+1}{p} z_1^{r-2q-\ell-1} z_1^{*\ell} z_2^{2q-p+1} z_2^{*p} \Bigg]
\end{aligned}
\tag{8.60}
$$

and

$$
\begin{aligned}
z_2' = e^{i\omega_2} &\Bigg[z_2 - \frac{\beta_y}{\sqrt{\beta_x}} \frac{k_r \beta_x^{\frac{r}{2}}}{2^r r!} \sum_{q \le (r-1)/2} \sum_{\ell=0}^{r-2q-1} \sum_{p=0}^{2q+1} (-1)^q \left(\frac{\beta_y}{\beta_x} \right)^q \binom{r}{2q+1} \times \\
&\times \binom{r-2q-1}{\ell} \binom{2q+1}{p} z_1^{r-2q-1-\ell} z_1^{*\ell} z_2^{2q+1-p} z_2^{*p} \\
&- \sqrt{\beta_y} \frac{j_r \beta_x^{\frac{n}{2}}}{2^r r!} \sum_{q \le r/2} \sum_{\ell=0}^{r-2q} \sum_{p=0}^{2q} (-1)^q \left(\frac{\beta_y}{\beta_x} \right)^q \binom{r}{2q} \binom{r-2q}{\ell} \times \\
&\times \binom{2q}{p} z_1^{r-2q-\ell} z_1^{*\ell} z_2^{2q-p} z_2^{*p} \Bigg],
\end{aligned}
\tag{8.61}
$$

and we express the map action as $\mathbf{z}' = \mathbf{F}(\mathbf{z})$. F_1 includes the following monomials

- for a normal multipole k_r, the generic term $(r-2q-\ell,\ \ell,\ 2q-p,\ p)$ with

$$
0 \le q \le \frac{r}{2}, \qquad 0 \le \ell \le r - 2q, \qquad 0 \le p \le 2q;
$$

- for a skew multipole j_r, the generic term $(r-(2q+1)-\ell,\ \ell,\ 2q+1-p,\ p)$ with

$$
0 \le q \le \frac{r-1}{2}, \qquad 0 \le \ell \le r - (2q+1), \qquad 0 \le p \le 2q+1;
$$

while for F_2 we obtain

- for a normal multipole k_r, the generic term $(r-(2q+1)-\ell,\ \ell,\ 2q+1-p,\ p)$ with

$$0 \le q \le \frac{r-1}{2}, \qquad 0 \le \ell \le r - (2q+1), \qquad 0 \le p \le 2q+1 \ ;$$

- for a skew multipole j_r, the generic term $(r - 2q - \ell,\ \ell,\ 2q - p,\ p)$ with

$$0 \le q \le \frac{r}{2}, \qquad 0 \le \ell \le r - 2q, \qquad 0 \le p \le 2q \ ,$$

and we remark that the form of the monomials for the normal and skew components exchanges between F_1 and F_2.

As introduced in Section 1.7, the Normal Form map $\mathbf{U}$ contains all the terms that are needed to solve the functional equation $\mathbf{F} \circ \mathbf{\Phi} = \mathbf{\Phi} \circ \mathbf{U}$, and, at order k, we have the functional equation

$$\Delta[\mathbf{\Phi}]_k(\zeta) + [\mathbf{U}]_k(\zeta) = [\mathbf{Q}]_k(\zeta) \tag{8.62}$$

where $[\mathbf{Q}]_k = [\mathbf{F} \circ \mathbf{\Phi}]_k$, the symbol $[\cdot]_k$ indicates the truncation of the homogeneous polynomial at order k, while $\mathbf{U}$ contains all monomials that are in the kernel of the Normal-Form operator Δ, defined as $\Delta\mathbf{\Phi}(\zeta) = e^{i\omega}\mathbf{\Phi}(\zeta) - \mathbf{\Phi}(e^{i\omega}\zeta)$, which, following [17, p. 128], occurs for monomials satisfying

$$\begin{aligned} F_1 : & \quad \omega_x(\ell_1 - m_1) + \omega_y(\ell_2 - m_2) = \omega_x \ , \\ F_2 : & \quad \omega_x(\ell_1 - m_1) + \omega_y(\ell_2 - m_2) = \omega_y \ . \end{aligned} \tag{8.63}$$

For a $(m,\ n)$ resonance (with $m,\ n$ coprimes), we can rewrite the previous relations as

$$F_1 : \qquad \ell_1 - m_1 + \frac{m}{n}(\ell_2 - m_2) = 1 \ , \tag{8.64a}$$

$$F_2 : \qquad \frac{n}{m}(\ell_1 - m_1) + \ell_2 - m_2 = 1 \ . \tag{8.64b}$$

A condition for the resonant terms to be present in the interpolating Hamiltonian is that the corresponding monomials in the kernel of Δ are present in either F_1 or F_2 at order r.

To satisfy the condition for F_1, we need

$$\ell_2 - m_2 \equiv 0 \pmod{n} \ , \tag{8.65}$$

which for a normal multipole translates to

$$2(q - p) \equiv 0 \pmod{n} \ , \tag{8.66}$$

while for a skew one to

$$2(q - p) + 1 \equiv 0 \quad (\mathrm{mod}\ n)\,. \tag{8.67}$$

The condition is always satisfied when $\ell_2 = m_2$ and in this case $\ell_1 = m_1 + 1$ and the form of the corresponding monomial is

$$\left(\frac{m + n}{2} - p,\ \frac{m + n}{2} - p - 1,\ p,\ p\right), \tag{8.68}$$

which is a valid solution only if m and n are both odd.

Solutions are also found whenever $\ell_2 - m_2 = s\,n$ with $s \neq 0$. For a normal multipole, $2(m-p) \leq 2(m+p) \leq r$ and we can restrict s to $0 < s \leq (m-1)/n+1$.

If $m < n$, then only $s = 1$ is possible and if n is odd, no other solution can be found. If n is even, we have $2(q - p) = n$ for which the resonant condition (8.64a) becomes $m - p - \ell = 1$ and the form of the generic monomial reads $(-p,\ m - p - 1,\ p + n,\ p)$, from which we can only choose $p = 0$, so that the solution for n even and $m < n$ reads

$$(0,\ m - 1,\ n,\ 0)\,. \tag{8.69}$$

If $m > n$, again two cases should be considered. If n is odd, then s must be even and the resonant condition (8.64a) is

$$m + n + s(m - n) = 2(1 + p + \ell) \tag{8.70}$$

and m must be odd. Let $m = 2m' + 1$, $n = 2n' + 1$ and $s = 2s'$. Substituting, we get the relation $p + \ell = m' + n' + 2s'(m' - n')$, and ℓ_1 becomes $\ell_1 = m'(1 - 2s') + n'(1 - 2s') - p + 1 - 2s'$. Since $s' > 0$, ℓ_1 is always negative and no solution can be found.

If, on the other hand, n is even, then m has to be odd, and from Eq. (8.70), s is necessarily odd. Therefore, we substitute $n = 2n'$, $m = 2m' + 1$, $s = 2s' + 1$ and we obtain $p + \ell = 2m' + 2m's' + s' - 2n's'$ and $\ell_1 = -p - 2n's' - 2m's' - s'$. The only possibility, since $\ell_1 \geq 0$, is given by $p = 0$ and $s' = 0$ (i.e. $s = 1$), which gives $\ell = 2m' = m - 1$, $2q = n$, and the general form of the resonant monomial is therefore

$$(0,\ m - 1,\ n,\ 0)\,, \tag{8.71}$$

which is the same as for the previous case (8.69)

We proceed in a similar fashion in the case of a skew multipole. The first point to note is that the special solution of Eq. (8.65) for $s = 0$ does not exist in this case. Hence, the resonant condition (8.67) $2q - 2p + 1 = s\,n$ provides a solution only if both s and n are odd. Hence, letting $n = 2n' + 1$ and $s = 2s' + 1$ and performing the usual substitutions, we get $q = 2s'n' + s' + n' + p$ and $\ell =$

$m - 2s'n' - s' - p - 1 + s'm$ and the condition $\ell_1 \geq 0$ becomes $-2s'n' - p - s'm \geq 0$, which requires $p = 0$ and $s' = 0$, and the generic skew monomial is of the form

$$(0, \ m - 1, \ n, \ 0) \,. \tag{8.72}$$

In summary, the monomials of U_1 are:

Normal multipoles:
$$\begin{cases} \left(\dfrac{m+n}{2} - p, \ \dfrac{m+n}{2} - p - 1, \ p, \ p \right), \quad 0 \leq p \leq \dfrac{r-1}{2} \\ \qquad\qquad \text{if} \quad m, n \text{ are odd,} \\[2mm] \\ (0, \ m - 1, \ n, \ 0) \qquad \text{if} \quad n \text{ is even}, \end{cases}$$

Skew multipoles: $\quad (0, \ m - 1, \ n, \ 0) \qquad \text{if} \quad n \text{ is odd.}$
$$\tag{8.73}$$

Thus far, only Eq. (8.64a) has been considered. For F_2, we proceed in the same way. We need to apply the resonant condition (8.64b), which requires $\ell_1 - m_1 \equiv 0 \pmod{m}$, i.e.

$$\frac{n}{m}(\ell_1 - m_1) = s \, n \,. \tag{8.74}$$

For a normal multipole, the divisibility condition and the resonant correspond to

$$\begin{cases} m(1 - s) + n & = 2(q + \ell + 1) \\ 2(q - p) & = s \, n \,, \end{cases} \tag{8.75}$$

and solving for ℓ and q, and substituting in ℓ_1 we obtain $\ell_1 = \frac{1}{2}(m+n)(1+s)-1-p$. We have $0 \leq \ell_1 \leq r = m + n - 1$, because $(m + n)(1 + s) \geq 2(p + 1) \geq 0$ implies $s \leq 0$, and $(m + n)(1 + s) \leq 2(r + 1 + p)$ implies $1 + s \leq 2(1 + r/(r - 1)) \leq 2$, therefore $s \leq 1$. This means that we can restrict s to the two values $s = 0$ or $s = 1$.

For $s = 0$, we obtain the solution

$$\left(\frac{m+n}{2} - p - 1, \ \frac{m+n}{2} - p - 1, \ p + 1, \ p \right) \qquad \text{for} \quad 0 \leq p \leq r/2 \,, \tag{8.76}$$

which only exists if $m + n$ is even, so both m and n must be odd, while, for $s = 1$

$$(m + n - p - 1, \ n - p - 1, \ p - n + 1, \ p) \,. \tag{8.77}$$

The only way to ensure both $m_1 \geq 0$ and $\ell_2 \geq 0$ is setting $m_1 = \ell_2 = 0$, so $p = n - 1$, whence we obtain the resonant solution

$$(m, \ 0, \ 0, \ n - 1) \tag{8.78}$$

In the case of a skew multipole, we have the equations

$$\begin{cases} m + n - 1 - 2q - 2\ell & = sm \\ 2q & = 1 + 2p - sn \end{cases} \tag{8.79}$$

and the same condition for ℓ_1, which imposes as before, $s = 0$ or $s = 1$. For $s = 0$, we have the same solution (if m and n are odd)

$$\left(\frac{m + n}{2} - p - 1, \ \frac{m + n}{2} - p - 1, \ p + 1, \ p \right), \tag{8.80}$$

while, for $s = 1$, as before

$$(m, \ 0, \ 0, \ n - 1). \tag{8.81}$$

Now, if we substitute $\ell_1 = m$, $m_1 = \ell_2 = 0$ and $m_2 = n - 1$ in the generic Normal Form term in U_2, we need $2q = n-2$, so $q = (n-2)/2$, which is possible only if n is even. In the skew case, on the other hand, we have $2q = n-1$, which is solved only for odd n. Thus, summarising:

$$\text{Normal multipoles:} \begin{cases} \left(\dfrac{m + n}{2} - p - 1, \ \dfrac{m + n}{2} - p - 1, \ p + 1, \ p \right) & m, n \text{ odd} \\[2ex] (m, \ 0, \ 0, \ n - 1) & n \text{ even}, \end{cases} \tag{8.82}$$

$$\text{Skew multipoles:} \begin{cases} \left(\dfrac{m + n}{2} - p - 1, \ \dfrac{m + n}{2} - p - 1, \ p + 1, \ p \right) & m, n \text{ odd} \\[2ex] (m, \ 0, \ 0, \ n - 1) & n \text{ odd}, \end{cases} \tag{8.83}$$

The next step is to consider how the resonant monomials in the Normal Form $\mathbf{U}$ contribute to the interpolating Hamiltonian. The first point consists in showing that monomials of type

$$\left(\frac{m + n}{2} - p, \ \frac{m + n}{2} - p - 1, \ p, \ p \right) \tag{8.84}$$

do not contribute to the resonant part of the interpolating Hamiltonian. In fact, given a 4D Normal Form $\mathbf{U}(\boldsymbol{\zeta}, \boldsymbol{\zeta}^*) = (U_1, U_1^*, U_2, U_2^*)$, and writing polynomials as:

$$A(\zeta_1, \zeta_1^*, \zeta_2, \zeta_2^*) = \sum_{\ell_1, m_1, \ell_2, m_2} A(\ell_1, \ m_1, \ \ell_2, \ m_2) \zeta_1^{\ell_1} \zeta_1^{*m_1} \zeta_2^{\ell_2} \zeta_2^{*m_2}, \tag{8.85}$$

the construction of the interpolating Hamiltonian of order r is done as follows:

$$\mathcal{H}(\ell_1 + 1, m_1, \ell_2, m_2) = -\frac{1}{\ell_1 + 1} U_1^*(\ell_1, m_1, \ell_2, m_2) \quad (\ell_1 + m_1 + \ell_2 + m_2 = r),$$

$$\mathcal{H}(0, m_1 + 1, \ell_2, m_2) = \frac{1}{m_1 + 1} U_1(0, m_1, \ell_2, m_2) \quad (m_1 + \ell_2 + m_2 = r),$$

$$\mathcal{H}(0, 0, \ell_2 + 1, m_2) = -\frac{1}{\ell_2 + 1} U_2^*(0, 0, \ell_2, m_2) \quad (\ell_2 + m_2 = r),$$

$$\mathcal{H}(0, 0, 0, r + 1) = \frac{1}{r + 1} U_2(0, 0, 0, r).$$

The monomials in U_1^* and U_2^* are the same in U_1 and U_2, but with the exchanges $\ell_1 \leftrightarrow m_1$ and $\ell_2 \leftrightarrow m_2$. Hence, the U_1 terms can be $(0, m - 1, n, 0)$ or $(\ell_2 + 1, \ell_2, m_1, m_1)$ and in U_1^* we will have either $(m - 1, 0, 0, n)$ or $(\ell_2, \ell_2 + 1, m_1, m_1)$. If this latter form is present in U_1^*, it gives rise to the Hamiltonian coefficient $\mathcal{H}(\ell_2 + 1, \ell_2 + 1, m_1, m_1)$, and by performing the transformation to the action-angle coordinates $(\boldsymbol{J}, \boldsymbol{\phi})$, i.e. $\zeta_1 = \sqrt{J_x} e^{i\phi_x}$, $\zeta_2 = \sqrt{J_y} e^{i\phi_y}$, the angular parts of these terms vanish, and we obtain a $J_x^{\ell_2/2} J_y^{m_1/2}$ monomial, which is clearly non resonant.

For what concerns the second component of the map, we see from the construction of the interpolating Hamiltonian that we need to restrict our search to monomials with $\ell_1 = m_1 = 0$. We can have terms in U_2 of the form

$$\left(0, \ 0, \ \frac{r + 1}{2}, \ \frac{r - 1}{2} \right) \tag{8.86}$$

owing to the resonant condition $\ell_2 - m_2 = 1$ with $\ell_2 + m_2 = r$. Since such a term contributes to the Hamiltonian via U_2^*, it gives rise to the Hamiltonian term $\mathcal{H}(0, 0, (r - 1)/2 + 1, (r + 1)/2) = \mathcal{H}(0, 0, (r + 1)/2, (r + 1)/2)$, and, as we discussed before, this does not give origin to a resonant term since the angular parts of ζ_2 and ζ_2^* are cancelled. Finally, we could look for monomials in U_2 of the form $(0, 0, 0, r)$, but the resonant condition would be $-r = 1$ which is never satisfied.

In conclusion, the following relationships between the parity of m and n and the type of multipole element that gives origin to quasi-resonant Hamiltonian terms:

Multipole type	m	n	U_1 non-trivial monomials	$\mathcal{H}$ resonant monomials
Normal	even	odd	no	no
	odd	odd	no	no
	odd	even	$(0, m-1, n, 0)$	$(0, m, n, 0)$ $(m, 0, 0, n)$
Skew	even	odd	$(0, m-1, n, 0)$	$(0, m, n, 0)$ $(m, 0, 0, n)$
	odd	odd	$(0, m-1, n, 0)$	$(0, m, n, 0)$ $(m, 0, 0, n)$
	odd	even	no	no

Therefore, if we restrict our search to sextupoles and octupoles ($r = 2$ or $r = 3$) we find that a normal sextupole can excite the $(1, 2)$ resonance, while a skew sextupole the $(2, 1)$ one. A skew octupole, on the other hand, is needed for both the $(1, 3)$ and $(3, 1)$ resonances.

8.B | Computation of P_{na} in resonant conditions

The motion in the resonant condition is governed by the Hamiltonian (8.6) with $\delta = 0$ (for the sake of simplicity, we neglect the amplitude-detuning terms in the following considerations). The analysis of the phase space topology shows that, independently of the resonance order, the allowed circle is symmetrically divided in two regions by the coupling arc. The trajectory of a particle with initial condition $(\phi_{1,\mathrm{i}}, J_{1,\mathrm{i}})$, in one of the two hemicircles (let us choose $\cos \phi > 0$) is given by the solution of the equation $\mathcal{H}(\phi_1, J_1) = \mathcal{H}(\phi_{1,\mathrm{i}}, J_{1,\mathrm{i}})$, i.e.

$$J_1^{m/2}(J_2 - nJ_1)^{n/2} \cos \phi_1 = J_{1,\mathrm{i}}^{m/2}(J_2 - nJ_{1,\mathrm{i}})^{n/2} \cos \phi_{1,\mathrm{i}} \qquad (8.87)$$

whose solution gives rather straightforwardly the function $\phi_1(J_1)$ given the initial conditions.

To compute P_{na} for an emittance sharing process when $\delta_{\max} \to 0$, ultimately, we should consider a motion when δ is equal to zero, and since P_{na} depends on $\langle J_{x,\mathrm{i}} \rangle$, our goal is to compute the trajectory $J_1(\phi_1)$.

For generic values of (m, n) one cannot easily invert analytically $\phi_1(J_1)$ from Eq. (8.87), yet this task can be carried out numerically. To compute the final mean J_1 for a given initial distribution, we can use the time average of J_1

over a (long) time interval T. This is given by

$$\overline{J_1} = \frac{1}{T} \int_0^T \mathrm{d}t \, J_1(\phi_1) = \frac{1}{T} \int_{\phi_-}^{\phi_+} \mathrm{d}\phi_1 \, \frac{J_1(\phi_1)}{\dot\phi_1} = \frac{\displaystyle\int_{\phi_-}^{\phi_+} \mathrm{d}\phi_1 \left(J_1(\phi_1)/\dot\phi_1 \right)}{\displaystyle\int_{\phi_-}^{\phi_+} \mathrm{d}\phi_1 \, (1/\dot\phi_1)},$$

(8.88)

where $\phi_\pm$ are the inversion points of the trajectory and $\dot\phi_1$ is taken from the equations of motion with $\delta = 0$. Note that the strength G of the resonant term never appears in the integral.

Then, the averaging of the result of $\overline{J_1}$ over the initial conditions $(\phi_{1,i}, J_{1,i})$ provides the expected value of $\langle J_{x,i} \rangle$ as $\delta \to 0$, and therefore of P_{na}.

For resonance $(1, 2)$, if the Cartesian coordinate X is used instead of the angle ϕ_1 to parametrise the motion, $J_1(X)$ can be written as

$$J_1 = \frac{1}{2} \left(J_2 - \frac{X_i(J_2 - X_i^2)}{X} \right)$$

(8.89)

and the time average $\overline{J_1}$

$$\overline{J_1} = \frac{J_2}{2} + \frac{C_i}{2} \frac{\displaystyle\int_{X_-}^{X_+} \mathrm{d}X \, \frac{1}{X^2\sqrt{J_2 - X^2 + C_i/X}}}{\displaystyle\int_{X_-}^{X_+} \mathrm{d}X \, \frac{1}{X\sqrt{J_2 - X^2 + C_i/X}}}$$

(8.90)

where $C_i = X_i\sqrt{X_i^2 - J_2}$ and the inversion points are $X_- = X_i = \sqrt{2J_{1,i}} \cos\phi_{1,i}$, $X_+ = -\left(X_i + \sqrt{4J_2 - 3X_i^2} \right)/2$.

A numerical evaluation of this integral, averaged on a Gaussian distribution for $(\phi_{1,i}, J_{1,i})$ with $\langle J_{x,i} \rangle = 1 \times 10^{-4}$ gives $\overline{J_1} = 8.115 \times 10^{-5}$, which replaced into the definition of P_{na} gives a values, when $\delta \to 0$

$$P_{\mathrm{na}} = 0.623,$$

(8.91)

which is consistent with the value observed in Fig. 8.7 (left). This procedure can be used to explain the values observed for other resonances, too.

Conclusions

In this thesis, we started from 2D or 4D Hamiltonian formulation of particle dynamics in circular hadron accelerators in the presence of time-dependent and/or non-linear perturbations, with the goal of proposing a variety of possible techniques whose outcome, when some parameters are slowly modulated, is a controlled modification of the beam transverse distribution.

These effects have been theoretically explained using the theory of adiabatic invariance and separatrix crossing, and the findings have been tested against numerical simulations of the original models. For each studied model we established scaling laws of the main parameters, in view of optimizing the machine performance.

In particular, we proved possible, at least in the limits of our 2D models, to perform beam splitting in stable islands generated using a resonant oscillating exciter (dipolar or higher-order field), and to reduce the emittance of an annular beam by trapping and transporting particles towards the centre of the phase space thanks to an island generated by a resonant AC dipole.

For a method of beam splitting which employs a resonant tune together with a second resonance given by the frequency of an external exciter, some preliminary studies showed a break of the symmetry between the stable islands.

Considering 4D models, we studied the emittance exchange between the x and y transverse directions when the coupling resonance is excited by skew quadrupoles. The well-known properties of this process have been fully described by the Hamiltonian theory of adiabatic processes. For higher-order resonances, generated by specific non-linear magnetic elements, we have shown the possibility of performing emittance sharing, i.e. the emittance values are exchanged between x and y, but multiplied (or divided) by a factor depending on the resonance order. In this way, the emittance sharing can be controlled by selecting the resonance order that is crossed.

It is, however, clear that the line of research presented in this thesis is not fully accomplished, yet. As we discussed in the Introduction, the studies here reported correspond, for each proposed manipulation, to the first step — the theoretical feasibility — of the process that transforms a mathematical model

into an operational routine. In the close future, we will tackle the goal of studying prototypical machine configurations that implement the proposed beam shaping methods. Such configurations will be carefully scrutinised by means of detailed numerical simulations in view of experimental validation in the CERN Proton Synchrotron. Nevertheless, knowing that simulations of Multi-Turn Extraction on realistic models of the Proton Synchrotron, taking also into account longitudinal motion, did not show great deviations from the predictions of the original 2D Hénon map model of MTE [51], we are confident that our techniques can hold up in more advanced numerical simulations.

Furthermore, other extensions of the proposed models shall be investigated, such as the possibility to perform emittance exchange crossing the $2\omega_x - 2\omega_y = \ell$ resonance in the presence of non-linear elements such as normal octupoles. Such a resonance has been the subject of intense investigations in the past, in particular in the domain of space charge effects, under the name of Montague resonance. As for the case of emittance sharing due to crossing the $\omega_x - \omega_y = \ell$ resonance, we are confident that the Hamiltonian theory of adiabatic process will provide the correct framework to describe in detail the observed phenomena. Beam splitting in lepton machines has been considered from the experimental standpoint and detailed numerical work has been carried out. We shall include the synchrotron radiation damping in the framework describing the adiabatic process, extending the theory in a direction useful for applications.

Bibliography

[1] M. Aiba and J. Kallestrup. "Theory of emittance exchange through coupling resonance crossing". *Phys. Rev. Accel. Beams* 23 (4 Apr. 2020), p. 044003. doi: 10.1103/PhysRevAccelBeams.23.044003.

[2] V. I. Arnol'd and A. Avez. *Problèmes Ergodiques de la Mécanique Classique*. Paris: Gauthier-Villars, 1967.

[3] V. Arnol'd. *Méthodes mathématiques de la mécanique classique*. Moscou: Editions MIR, 1976.

[4] V. Arnol'd, V. Kozlov, and A. Neishtadt. *Mathematical aspects of classical and celestial mechanics. Dynamical systems III; 3rd rev. version*. Encyclopaedia of mathematical sciences. Heidelberg: Springer, 2006. doi: 10.1007/978-3-540-48926-9.

[5] V. I. Arnol'd. "Small denominators and problems of stability of motion in classical and celestial mechanics". *Uspekhi Mat. Nauk* 18(6) (1963), pp. 91–192. doi: 10.1070/RM1963v018n06ABEH001143.

[6] M. Bai. "Beam manipulation with an RF dipole". *Proceedings of the 1999 Particle Accelerator Conference (Cat. No. 99CH36366)*. Vol. 1. IEEE. 1999, pp. 387–391.

[7] J. Barranco García and S. Gilardoni. "Simulation and optimization of beam losses during continuous transfer extraction at the CERN Proton Synchrotron". *Phys. Rev. ST Accel. Beams* 14 (3 Mar. 2011), p. 030101. doi: 10.1103/PhysRevSTAB.14.030101.

[8] R. Bartolini *et al.* "Precise measurement of the betatron tune". *Part. Accel.* 55 (1996), pp. 1–10.

[9] R. Bartolini *et al.* "Tune evaluation in simulations and experiments". *Part. Accel.* 52 (1995), pp. 147–177.

[10] A. Bazzani, F. Capoani, and M. Giovannozzi. "Analysis of adiabatic trapping phenomena for quasi-integrable area-preserving maps in the presence of time-dependent exciters". In preparation.

[11] A. BAZZANI, F. CAPOANI, and M. GIOVANNOZZI. "Manipulation of transverse emittances in circular accelerators by crossing non-linear 2D resonances" (2022). arXiv: 2202.04559 [physics.acc-ph].

[12] A. BAZZANI, F. CAPOANI, M. GIOVANNOZZI, and A. I. NEISHTADT. "Adiabaticity of emittance exchange due to crossing of the coupling resonance". *Phys. Rev. Accel. Beams* 24 (9 Sept. 2021), p. 094002. DOI: 10.1103/PhysRevAccelBeams.24.094002.

[13] A. BAZZANI, F. CAPOANI, M. GIOVANNOZZI, and R. TOMÁS. "Nonlinear cooling of an annular beam distribution" (2022). arXiv: 2205.03290 [physics.acc-ph].

[14] A. BAZZANI, C. FRYE, M. GIOVANNOZZI, and C. HERNALSTEENS. "Analysis of adiabatic trapping for quasi-integrable area-preserving maps". *Phys. Rev. E* 89 (4 2014), p. 042915. DOI: 10.1103/PhysRevE.89.042915.

[15] A. BAZZANI, M. GIOVANNOZZI, and E. TODESCO. "A Program to compute Birkhoff normal forms of symplectic maps in $\mathbb{R}^4$". *Comput. Phys. Commun.* 86 (1995), pp. 199–207. DOI: 10.1016/0010-4655(94)00140-W.

[16] A. BAZZANI, S. MARMI, and G. TURCHETTI. "Nekhoroshev estimate for isochronous non resonant symplectic maps". *Celestial Mechanics and Dynamical Astronomy* 47(4) (1989), pp. 333–359. DOI: 10.1007/BF00051010.

[17] A. BAZZANI, G. SERVIZI, E. TODESCO, and G. TURCHETTI. *A normal form approach to the theory of nonlinear betatronic motion*. CERN Yellow Reports: Monographs. Geneva: CERN, 1994. DOI: 10.5170/CERN-1994-002.

[18] A. BAZZANI, S. SIBONI, and G. TURCHETTI. "Diffusion in Hamiltonian systems with a small stochastic perturbation". *Physica D: Nonlinear Phenomena* 76(1) (1994), pp. 8–21. ISSN: 0167-2789. DOI: 10.1016/0167-2789(94)90246-1.

[19] A. BAZZANI *et al.* "Advances on the modeling of the time evolution of dynamic aperture of hadron circular accelerators". *Phys. Rev. Accel. Beams* 22 (10 Oct. 2019), p. 104003. DOI: 10.1103/PhysRevAccelBeams.22.104003.

[20] M. BERRY. "Classical adiabatic angles and quantal adiabatic phase". *J. Phys. A: Math. Gen.* 18 (1985), pp. 15–27. DOI: 10.1088/0305-4470/18/1/012.

[21]   M. Berry. "Quantal phase factors accompanying adiabatic changes". *Proc. R. Soc. Lond. A* 392 (1984), pp. 45–57. DOI: 10.1098/rspa.1984.0023.

[22]   N. Biancacci and R. Tomás. "Using ac dipoles to localize sources of beam coupling impedance". *Phys. Rev. Accel. Beams* 19 (5 May 2016), p. 054001. DOI: 10.1103/PhysRevAccelBeams.19.054001.

[23]   G. Birkhoff. "Proof of Poincaré's geometric theorem". *Transactions of the American Mathematical Society* (1913), pp. 14–22.

[24]   J. Borburgh et al. "First implementation of transversely split proton beams in the CERN Proton Synchrotron for the fixed-target physics programme". *EPL* 113(3) (2016), p. 34001. DOI: 10.1209/0295-5075/113/34001.

[25]   C. Bovet et al. "The fast shaving ejection for beam transfer from the CPS to the CERN 300 GeV machine". *IEEE Trans. Nucl. Sci.* 20 (1973), pp. 438–41. DOI: 10.1109/TNS.1973.4327144.

[26]   J. M. Burgers. "Adiabatic invariants of mechanical systems". *The London, Edinburgh, and Dublin Philosophical Magazine and Journal of Science* 33(198) (1917), pp. 514–520. DOI: 10.1080/14786440608635665.

[27]   J. Candy and W. Rozmus. "A symplectic integration algorithm for separable Hamiltonian functions". *Journal of Computational Physics* 92(1) (1991), pp. 230–256. ISSN: 0021-9991. DOI: 10.1016/0021-9991(91)90299-Z.

[28]   R. Cappi and M. Giovannozzi. "Multiturn extraction and injection by means of adiabatic capture in stable islands of phase space". *Phys. Rev. ST Accel. Beams* 7 (2 2004), p. 024001. DOI: 10.1103/PhysRevSTAB.7.024001.

[29]   R. Cappi and M. Giovannozzi. "Novel Method for Multiturn Extraction: Trapping Charged Particles in Islands of Phase Space". *Phys. Rev. Lett.* 88 (10 2002), p. 104801. DOI: 10.1103/PhysRevLett.88.104801.

[30]   F. Carlier, R. Tomás, E. Maclean, and T. Persson. "First experimental demonstration of forced dynamic aperture measurements with LHC ac dipoles". *Phys. Rev. Accel. Beams* 22 (3 Mar. 2019), p. 031002. DOI: 10.1103/PhysRevAccelBeams.22.031002.

[31]   A. Chao et al. "Experimental Investigation of Nonlinear Dynamics in the Fermilab Tevatron". *Phys. Rev. Lett.* 61 (24 Dec. 1988), pp. 2752–2755. DOI: 10.1103/PhysRevLett.61.2752.

[32] H.-C. Chao. "Emittance evolution in crossing Walkinshaw resonance and envelope dynamics simulations". PhD thesis. Indiana University, 2015.

[33] P. Ehrenfest. "Over adiabatische veranderingen van een stelsel in verband met e theorie de quanta". *Verslagen Kon. Akad. Amsterdam* 25 (1916), pp. 412–433.

[34] A. Franchi, S. Gilardoni, and M. Giovannozzi. "Progresses in the studies of adiabatic splitting of charged particle beams by crossing nonlinear resonances". *Phys. Rev. ST Accel. Beams* 12 (2009), p. 014001. DOI: 10.1103/PhysRevSTAB.12.014001.

[35] A. Franchi and M. Giovannozzi. "Split or unsplit electron beams?" (2022). arXiv: 2202.04684 [physics.acc-ph].

[36] A. Franchi, E. Métral, and R. Tomás. "Emittance sharing and exchange driven by linear betatron coupling in circular accelerators". *Phys. Rev. ST Accel. Beams* 10 (6 June 2007), p. 064003. DOI: 10.1103/PhysRevSTAB.10.064003.

[37] S. Gilardoni et al. "Experimental evidence of adiabatic splitting of charged particle beams using stable islands of transverse phase space". *Phys. Rev. ST Accel. Beams* 9 (10 2006), p. 104001. DOI: 10.1103/PhysRevSTAB.9.104001.

[38] S. Gilardoni, M. Giovannozzi, and C. Hernalsteens. "First observations of intensity-dependent effects for transversely split beams during multiturn extraction studies at the CERN Proton Synchrotron". *Phys. Rev. Spec. Top. Accel. Beams* 16 (2013), p. 051001. DOI: 10.1103/PhysRevSTAB.16.051001.

[39] M. Giovannozzi and J. Morel. "Principle and analysis of multiturn injection using stable islands of transverse phase space". *Phys. Rev. ST Accel. Beams* 10 (3 Mar. 2007), p. 034001. DOI: 10.1103/PhysRevSTAB.10.034001.

[40] M. Giovannozzi, D. Quatraro, and G. Turchetti. "Generating unstable resonances for extraction schemes based on transverse splitting". *Phys. Rev. ST Accel. Beams* 12 (2 Feb. 2009), p. 024003. DOI: 10.1103/PhysRevSTAB.12.024003.

[41] P. Goslawski et al. *Technical Design Study BESSY VSR*. Tech. rep. Berlin: Helmholtz-Zentrum Berlin für Materialien und Energie GmbH, June 2015. DOI: 10.5442/R0001.

[42] G. Guignard. *The general theory of all sum and difference resonances in a three-dimensional magnetic field in a synchrotron.* CERN Yellow Reports: Monographs. Geneva: CERN, 1976. DOI: 10.5170/CERN-1976-006.

[43] J. Hannay. "Angle variable holonomy in adiabatic excursion of an integrable Hamiltonian". *J. Phys. A: Math. Gen.* 18 (1985), pp. 221–230. DOI: 10.1088/0305-4470/18/2/011.

[44] M. Hénon. "Numerical study of quadratic area-preserving mappings". *Q. Appl. Math.* 27 (1969), p. 291. DOI: 10.1090/qam/253513.

[45] J. Henrard. "The Adiabatic Invariant in Classical Mechanics". *Dynamics Reported: Expositions in Dynamical Systems.* Ed. by C. K. R. T. Jones, U. Kirchgraber, and H. O. Walther. Berlin/Heidelberg: Springer, 1993, pp. 117–235. ISBN: 978-3-642-61232-9. DOI: 10.1007/978-3-642-61232-9_4.

[46] W. Herr and E. Forest. "Non-linear Dynamics in Accelerators". *Particle Physics Reference Library : Volume 3: Accelerators and Colliders.* Ed. by S. Myers and H. Schopper. Cham: Springer International Publishing, 2020, pp. 51–104. ISBN: 978-3-030-34245-6. DOI: 10.1007/978-3-030-34245-6_3.

[47] G. W. Hill. "On the part of the motion of the lunar perigee which is a function of the mean motions of the sun and moon". *Acta Mathematica* 8(none) (1900), pp. 1–36. DOI: 10.1007/BF02417081.

[48] A. Huschauer *et al.* "Advancing the CERN proton synchrotron multi-turn extraction towards the high-intensity proton beams frontier". *Phys. Rev. Accel. Beams* 22 (10 Oct. 2019), p. 104002. DOI: 10.1103/PhysRevAccelBeams.22.104002.

[49] A. Huschauer *et al.* "Approaching the High-Intensity Frontier Using the Multi-Turn Extraction at the CERN Proton Synchrotron". *Proc. 61st ICFA Advanced Beam Dynamics Workshop (HB'18)* (Daejeon, South Korea, June 17–22, 2018). ICFA Advanced Beam Dynamics Workshop 61. Geneva: JACoW Publishing, July 2018, pp. 231–236. ISBN: 978-3-95450-202-8. DOI: 10.18429/JACoW-HB2018-WEA1WA02.

[50] A. Huschauer *et al.* "Transverse beam splitting made operational: Key features of the multiturn extraction at the CERN Proton Synchrotron". *Phys. Rev. Accel. Beams* 20 (6 2017), p. 061001. DOI: 10.1103/PhysRevAccelBeams.20.061001.

[51] A. Huschauer. "Beam Dynamics Studies for High-Intensity Beams in the CERN Proton Synchrotron". PhD thesis. Technischen Universität Wien, May 2016. URL: https://cds.cern.ch/record/2194332.

[52]   A. Itin, A. Vasiliev, G. Krishna, and S. Watanabe. "Change in the adiabatic invariant in a nonlinear two-mode model of Feshbach resonance passage". *Physica D: Nonlinear Phenomena* 232 (Dec. 2006), pp. 108–115. doi: 10.1016/j.physd.2007.06.001.

[53]   J. Kallestrup and X. Gu. "Possible Application of Round-to-Flat Hadron Beam Creation Using 3rd Order Coupling Resonances for the Electron-Ion Collider". *Proc. IPAC'21* (Campinas, Brazil). 12th International Particle Accelerator Conference. Geneva: JACoW Publishing, Aug. 2021, pp. 99–102. isbn: 978-3-95450-214-1. doi: 10.18429/JACoW-IPAC2021-MOPAB019.

[54]   H. Kandrup, C. Siopis, G. Contopoulos, and R. Dvorak. "Diffusion and scaling in escapes from two-degrees-of-freedom Hamiltonian systems." *Chaos* 9 (2 1999), pp. 381–392. doi: 10.1063/1.166415.

[55]   F. Kramer *et al.* "Characterization of the second stable orbit generated by transverse resonance island buckets (TRIBs)". *Proc. 9th Int. Particle Accelerator Conf. (IPAC'18)* (Vancouver, Canda). Geneva: JACoW Publishing, May 2018, p. 1656. doi: 10.18429/JACoW-IPAC2018-TUPML052.

[56]   L. Landau and E. Lifshitz. *Meccanica.* Corso di Fisica teorica 1. Mosca/Roma: MIR/Editori riuniti, 1975.

[57]   P. Langevin and L. de Broglie, eds. *La théorie du rayonnement et les quanta.* Solvay conference (Bruxelles, 1911). Paris: Gauthier-Villars, 1912.

[58]   J. Laskar. "Introduction to Frequency Map Analysis". *Hamiltonian Systems with Three or More Degrees of Freedom.* Ed. by C. Simó. Springer. Dordrecht: Springer, 1999, pp. 134–150. doi: 10.1007/978-94-011-4673-9.

[59]   S. Y. Lee. *Accelerator physics; 4th ed.* Singapore: World Scientific, 2019. doi: 10.1142/11111.

[60]   S. Y. Lee. "Beam dynamics experiments at the IUCF cooler ring". *AIP Conference Proceedings* 326(1) (1995), pp. 12–51. doi: 10.1063/1.47311.

[61]   S. Y. Lee, K. Y. Ng, H. Liu, and H. C. Chao. "Evolution of Beam Distribution in Crossing a Walkinshaw Resonance". *Phys. Rev. Lett.* 110 (9 2013), p. 094801. doi: 10.1103/PhysRevLett.110.094801.

[62]   A. Lenard. "Adiabatic invariance to all orders". *Annals of Physics* 6(3) (1959), pp. 261–276. issn: 0003-4916. doi: https://doi.org/10.1016/0003-4916(59)90082-X.

[63] T. Levi-Civita. "Sugli invarianti adiabatici". *Resoconto del Congresso Nazionale dei Fisici* (Como-Pavia-Roma, Sept. 11–20, 1927). Vol. II. Bologna: N. Zanichelli, 1928, pp. 475–513.

[64] J. Y. Liu *et al.* "Determination of the linear coupling resonance strength using two-dimensional invariant tori". *Phys. Rev. E* 49 (3 Mar. 1994), pp. 2347–2352. doi: 10.1103/PhysRevE.49.2347.

[65] P. Lochak and C. Meunier. *Multiphase averaging for classical systems: with applications to adiabatic theorems*. Vol. 72. New York: Springer-Verlag, 1988. doi: 10.1007/978-1-4612-1044-3.

[66] M. Giovannozzi, N. Carmignani, and A. Franchi. "Could synchrotron light sources benefit from the experience at CERN with beams split in horizontal phase space?" *Proc. Nonlinear Dynamics and Collective Effects NOCE 2017 in Particle Beam Physics, Arcidosso, Italy*. World Scientific 2017, ISBN: 978-981-3279-61-2, 2017. url: https://www.worldscientific.com/worldscibooks/10.1142/11257.

[67] M. Ries *et al.* "Transverse resonance island buckets at the MLS and BESSY II". *Proc. 6th International Particle Accelerator Conf. IPAC2015)*. JACoW Publishing, 2015, pp. 138–140. url: http://accelconf.web.cern.ch/IPAC2015/papers/mopwa021.pdf.

[68] L. I. Mandel'shtam. *Collected works*. Moskva: Akad. Nauk sssr, 1948, pp. 297–304.

[69] Maxim (https://math.stackexchange.com/users/491644/maxim). *Asymptotic expansion of $\int_0^{2\pi} d\theta \sqrt{k^2 \cos^2 \theta - \cos \theta + 1}$ as $k \to 0$.* Mathematics Stack Exchange, https://math.stackexchange.com/questions/4167778/asymptotic-expansion-of-int-02-pi-mathrmd-theta-sqrtk2-cos2-theta#comment8640217_4167778. Accessed: 2021-06-10. 2021.

[70] E. Métral. *Simple theory of emittance sharing and exchange due to linear betatron coupling*. Tech. rep. CERN-PS-2001-066-AE. Geneva: CERN, 2001. url: https://cds.cern.ch/record/529690.

[71] R. Miyamoto, S. Kopp, A. Jansson, and M. Syphers. "Parametrization of the driven betatron oscillation". *Phys. Rev. ST Accel. Beams* 11 (8 Aug. 2008), p. 084002. doi: 10.1103/PhysRevSTAB.11.084002.

[72] A. I. Neishtadt. "Probability phenomena due to separatrix crossing". *Chaos: An Interdisciplinary Journal of Nonlinear Science* 1(1) (1991), pp. 42–48. doi: 10.1063/1.165816.

[73] A. Neishtadt. "Change of an Adiabatic Invariant at a Separatrix". *Fiz. Plasmy* 12(992) (1986).

[74] A. Neishtadt. "On mechanisms of destruction of adiabatic invariance in slow–fast Hamiltonian systems". *Nonlinearity* 32(11) (Oct. 2019), R53–R76. doi: 10.1088/1361-6544/ab2a2c.

[75] A. Neishtadt. "On the accuracy of conservation of the adiabatic invariant". *Journal of Applied Mathematics and Mechanics* 45(1) (1981), pp. 58–63. issn: 0021-8928. doi: 10.1016/0021-8928(81)90010-1.

[76] A. Neishtadt. "Passage through a separatrix in a resonance problem with a slowly-varying parameter". *Journal of Applied Mathematics and Mechanics* 39(4) (1975), pp. 594–605. issn: 0021-8928. doi: 10.1016/0021-8928(75)90060-X.

[77] A. Neishtadt and A. Vasiliev. "Destruction of adiabatic invariance at resonances in slow-fast Hamiltonian systems". *Nucl. Instrum. Meth. A* 561(2) (2006). Proceedings of the Workshop on High Intensity Beam Dynamics, pp. 158–165. issn: 0168-9002. doi: 10.1016/j.nima.2006.01.008.

[78] A. Neishtadt, A. Vasiliev, and A. Artemyev. "Capture into resonance and escape from it in a forced nonlinear pendulum". *Regular and Chaotic Dynamics* 18(6) (2013), pp. 686–696. issn: 1468-4845. doi: 10.1134/S1560354713060087.

[79] P. Goslawski *et al.* "Two orbit operation at BESSY II during a user test week". *Proc. 10th International Particle Accelerator Conf. (IPAC2019).* Geneva: JACoW Publishing, 2019, pp. 3419–3421. url: http://accelconf.web.cern.ch/ipac2019/papers/thyyplm2.pdf.

[80] Y. Papaphilippou. "Detecting chaos in particle accelerators through the frequency map analysis method". *Chaos: An Interdisciplinary Journal of Nonlinear Science* 24(2) (2014), p. 024412. doi: 10.1063/1.4884495.

[81] S. Peggs and C. Tang. *Nonlinear diagnostics using an AC dipole.* Report No. RHIC/AP/159. Brookhaven National Laboratories, 1998. url: https://www.rhichome.bnl.gov/RHIC/RAP/rhic_notes/RHIC-AP-1-177/RHIC-AP-159.pdf.

[82] H. Poincaré. *Les méthodes nouvelles de la mécanique céleste.* Vol. 2. Paris: Gauthier-Villars et fils, 1893.

[83] G. Russo, G. Franchetti, and M. Giovannozzi. "New Techniques to Compute the Linear Tune". *Proc. IPAC'21* (Campinas, SP, Brazil). International Particle Accelerator Conference 12. Geneva: JACoW Publishing, Aug. 2021, pp. 4142–4145. isbn: 978-3-95450-214-1. doi: 10.18429/JACoW-IPAC2021-THPAB189.

[84] G. Servizi *et al.* "GIOTTO: a code for the nonlinear analysis of area-preserving mappings". *International Journal of Modern Physics C* 06(05) (1995), pp. 651–661. doi: 10.1142/S0129183195000551.

[85] G. J. Sussman and J. Wisdom. *Structure and interpretation of classical mechanics*. 2nd ed. Cambridge: The MIT Press, 2015. isbn: 9780262028967.

[86] J. L. Tennyson, J. R. Cary, and D. F. Escande. "Change of the Adiabatic Invariant due to Separatrix Crossing". *Phys. Rev. Lett.* 56 (20 1986), pp. 2117–2120. doi: 10.1103/PhysRevLett.56.2117.

[87] R. Tomás. "Adiabaticity of the ramping process of an ac dipole". *Phys. Rev. ST Accel. Beams* 8 (2 Feb. 2005), p. 024401. doi: 10.1103/PhysRevSTAB.8.024401.

[88] R. Tomás. "Normal form of particle motion under the influence of an ac dipole". *Phys. Rev. ST Accel. Beams* 5 (5 2002), p. 054001. doi: 10.1103/PhysRevSTAB.5.054001.

[89] R. Tomás *et al.* "Measurement of global and local resonance terms". *Phys. Rev. ST Accel. Beams* 8 (2 Feb. 2005), p. 024001. doi: 10.1103/PhysRevSTAB.8.024001.

[90] G. Turchetti. *Dinamica classica dei sistemi fisici*. Bologna: Zanichelli, 1998. isbn: 9783540489269.

[91] S. White, E. Maclean, and R. Tomás. "Direct amplitude detuning measurement with ac dipole". *Phys. Rev. ST Accel. Beams* 16 (7 July 2013), p. 071002. doi: 10.1103/PhysRevSTAB.16.071002.

[92] H. Wiedemann. *Particle accelerator physics*. Springer Nature, 2015.

[93] E. Wilson. "Nonlinear resonances" (May 1986). doi: 10.5170/CERN-1987-003-V-1.41.

Acknowledgements

Cui dono lepidum novum libellum
arida modo pumice expolitum?

<div style="text-align: right">Catull., i, 1–2.</div>

A three-year-long PhD work is never the result of an individual endeavour. This thesis, and the research results it reports, would have never been possible without the help and the guidance of many people. Among them — first and foremost — I want to thank my two supervisors: Prof. Armando Bazzani at Bologna University and Dr. Massimo Giovannozzi at CERN. My gratitude is due to them not only for their constant support, their availability and their patience during these years of PhD, but also for having encouraged and assisted me in multiple roles during many years (from the tutorship at Collegio Superiore to the advisorship in Bachelor and Master's theses and the supervision during periods spent at CERN) and for giving me the opportunity to join this research field. In short, quoting the same ode by Catullus, thanks for *"meas esse aliquid putare nugas"*. I also thank them both for having read, revised, and corrected the drafts of this thesis — the usual disclaimer on remaining mistakes of course applies.

I also want to thank the other people which co-authored the articles that resulted from my PhD work, Prof. Anatoly I. Neishtadt and Dr. Rogelio Tomás García, for their contribution in terms of discussions, ideas and proposals. Furthermore, I thank my CERN section and group leaders, Dr. Stefano Redaelli and Dr. Yannis Papaphilippou for the review of our manuscripts — and the anonymous referees of our article [12] for the suggestions received.

As an addition to this page before submitting the final version of the thesis, I am grateful to Dr. Elias Métral and Prof. Mauro Migliorati who reviewed the preliminary edition of this thesis, for having carefully read the work and for their useful comments and corrections.